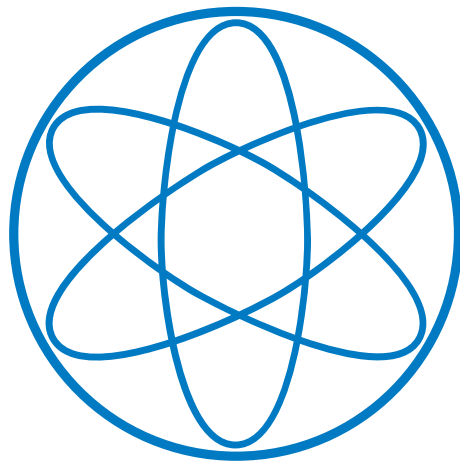# Probing New Physics with Big Bang Nucleosynthesis

Tests neuer Physik mit primordialer Nukleosynthese

Victor Fernando Maura Breick

Department of Physics
Technical University Munich

Master thesis presented for the degree
M. Sc. in Physics

Supervised by
Prof. Dr. Alejandro Ibarra

Submitted on 1st September 2023

Abstract

Big Bang Nucleosynthesis (BBN) describes a crucial period in the early stages of our Universe. According to this theory, in a matter of minutes, the primordial distribution of light nuclei is determined and was instrumental in the development of modern Cosmology due to its success in predicting the observational abundances of light nuclei. Since its birth, striking progress has been made, both from a theoretical point of view leading to a prediction of light nuclei abundances with an accuracy at the percent level, as well as on the experimental side, mainly due to equally precise measurements of the primordial abundances.

Remarkably, BBN theory still broadly agrees with observations and, highly non-trivially, with the rest of the Standard Model of Cosmology as a whole, so any elements of new physics that influence the primordial nucleosynthesis are very severely constrained. Thus, BBN has become one of the most powerful cosmological probes and can be used to test theories beyond the Standard Model, opening up a window into the Universe at the earliest time and highest energies presently accessible to us.

The goal of this thesis is to do precisely that. First, given the strong sensitivity of the Helium abundance on the Neutron lifetime τ_n and the long standing Neutron Lifetime anomaly (NLA), we will derive constraints on τ_n providing an independent measurement competitive with other current experiments. Additionally, we will derive BBN constraints on dark decays of the neutron proposed to resolve the NLA.

Furthermore, motivated by a novel measurement of the Helium abundance by the EMPRESS collaboration, which is in tension with the standard prediction from BBN theory by about 3σ, we will focus on elements of new physics which might be able to alleviate it. Concretely, we will perform an exhaustive global analysis using different sets of BBN and CMB data, both independently and combined, for three different scenarios.

First, we allow for a non-standard expansion history of the Universe by allowing the effective number of neutrino species N_{eff} to deviate from its SM value, which will require $\Delta N_{\text{eff}} < 0$. We will provide a possible interpretation of this as a hint of a time variation of the gravitational constant G_N. Motivated by this hint, we will also explore how a time variation of the Higgs vacuum expectation value affects BBN, updating and improving upon previous constraints. However, we will argue that perhaps the simplest explanation for the tension is the presence of a lepton asymmetry several orders of magnitude larger than the baryon asymmetry, so we will derive current constraints and explore the future sensitivity of BBN and CMB data on primordial lepton asymmetries.

Declaration

I hereby declare that the thesis submitted is my own unaided work. All direct or indirect sources used are acknowledged as references.

Ich versichere hiermit, dass ich die von mir eingereichte Abschlussarbeit selbstständig verfasst und keine anderen als die angegebenen Quellen und Hilfsmittel benutzt habe.

Munich,

Acknowledgements

First and foremost, I would like to express my sincerest gratitude to my supervisor, Alejandro Ibarra, for his invaluable guidance and mentorship not only over the course of this thesis, but the last three years. His incessant curiosity and contagious fascination for any aspect of phsyics is truly an inspiration for me. I am forever thankful for all the knowledge you have shared with me, for believing in me and giving me invaluable opportunities. I hope and am certain that this is not the last time our paths will cross.

This thesis, among so many other things, would not have been possible without Miguel Escudero, whose enthusiasm for physics and unique outlook on life, but most importantly his optimistic personality and sincere friendship has helped me overcome many obstacles over the last three years. I am happy to call you not only a colleague and mentor, but, most importantly, a friend.

Another friend who has accompanied me ever since I started my journey in Munich almost 5 years ago is Christoph. Through long nights doing exercises for class, cramming for exams in the Deutsches Museum, or sharing moments watching and playing tennis, you have always been there in one way or another and I am very thankful for that.

I also want to thank Heidi and Achim, for welcoming me into your family without even blinking an eye and taking care of me as if I was just another one of your children.

None of this would have been possible without the unconditional love and support of my mother, Nadi. Thank you for always being there for me and believing in me, lending me an ear when I need it, and sharing your immense wisdom with me. The same goes for my father, Emilio, who is an inspiration to me in so many ways. I am extremely glad to be a Maura Breick.

Last, but not least, I would like to thank Melina. I cannot even fathom where I would be right now if not for you. Thank you for your honest and unwavering love, for always being there for me.

List of Abbreviations

ΛCDM Standard model of Cosmology

BAU Baryon Asymmetry of the Universe

BBN Big Bang Nucleosynthesis

BE Bose-Einstein

BSM Beyond the Standard Model

CMB Cosmic Microwave Background

EFT Effective Field Theory

FD Fermi-Dirac

FLRW Friedman-Lemaitre-Robertson-Walker

GR General Relativity

NLA Neutron Lifetime Anomaly

NSE Nuclear Statistical Equilibrium

SBBN Standard Big Bang Nucleosynthesis

SM Standard Model

vev Vacuum Expectation Value

Contents

Chapter 1

Introduction

In the seminal book, *"The Structure of Scientific Revolutions"*, published in 1962 by Thomas S. Kuhn [1], science is described as a collaborative endeavour where progress is made in a cumulative fashion within an established framework, also known as a *"paradigm"*, in a process he denominated *"normal science"*. This period of rapid development within a given framework aims at exploring the boundaries of the paradigm.

As a result of this exploration, inconsistencies and problems are revealed over time, both from a theoretical and an experimental point of view. At first, it is uncertain whether these merely demonstrate the community's lack of understanding or if they indicate a problem within the paradigm itself. Generally, these paradigms have previously shown great success during the period of *normal science*, so only when these inconsistencies start to accumulate and become more significant does this get taken seriously as a problem.

Science enters a state of crisis, *normal science* continues to accumulate anomalies, and faith is lost in the previously well-established paradigm. The search for a new framework within which to conduct research, the endeavor of *"revolutionary science"*, begins. During this period, the paradigm is scrupulously reevaluated and, with the anomalies and tensions as guideposts, new theories are put forward. Once one of these theories emerges as successful, a *"paradigm shift"* in that field of science takes place and the winner establishes itself as the new framework future development will be based upon. One could argue that the fields of Cosmology and Particle Physics are currently on the verge of precisely this period of crisis.

In Particle Physics, the Standard Model (SM) has established itself as the most precise theory in the history of physics ([2]), its culmination being the discovery of the Higgs Boson in 2012 ([3]), the last particle missing to complete the particle spectrum of the theory. It is the paradigm within which most research in Particle Physics is conducted.

The Standard model of Cosmology (ΛCDM), on the other hand, assumes an isotropic and homogeneous Universe expanding according to the laws of General Relativity (GR) comprised of the particle content of the SM and two additional (and dominant) ingredients: a large component (73%) of Dark Energy Λ and 23% of cold, non-baryonic dark matter. This model has been extremely successful up to now, its crowning achievements being the prediction and description of an isotropic and

homogeneous Cosmic Microwave Background [4] and the synthesis of light elements during Big Bang Nucleosynthesis (BBN).

Despite their respective successes, both models face severe challenges from laboratory experiments as well as Cosmological Observations and are theoretically inconsistent in certain ways. Some of them need to be addressed by modifying the SM or the ΛCDM, while some may be addressed by both.

The SM cannot accommodate the fact that neutrinos are massive and, especially, that their masses are so light. Additionally, there are some long-standing and more recent experimental anomalies ([5]) that challenge the SM, like measurements of the anomalous magnetic moment of the muon and the mass of the W bosons, as well as theoretical inconsistencies, most notably the problem of naturalness [6].

The ΛCDM model, too, is extremely challenged by some very precise measurements, most notably the Hubble [7] and the S_8 [8] tensions and, in the context of BBN the Lithium Problem [9]. Additionally, while the ΛCDM model can manually add the Dark components, it does not explain them in any way, they are simply treated as variable parameters, the SM does not contain a consistent candidate for Dark Matter, and the only way to produce a constant vacuum energy via the Higgs Vacuum Expectation Value is many orders of magnitude away from the observed magnitude of this constant.

Last, but definitely not least, we know that we are living in a Universe with slightly more matter than antimatter. This is either a problem that highlights the incompleteness of the SM, as the amount of CP violation generated in the SM is not enough to generate the Baryon Asymmetry of the Universe (BAU) within the current cosmological framework, or that the rather simple picture of the ΛCDM model is incorrect.

Thus, while the claim of Particle Physics and Cosmology being in crisis may be too bold for some, there is irrefutable evidence, and a wide consensus, that these theories need to be modified and extended. The time for *revolutionary science* has come.

The aim of this thesis, however, is not to revolutionize our understanding of the world. Rather, it aims at highlighting the importance and usefulness of Big Bang Nucleosynthesis as a probe of new physics. Concretely, this means how anomalies and constraints derived from this crucial epoch in the development of our Universe can be used as guideposts for developing new paradigms and challenge those who modify the physics during this epoch, both for the field of particle physics as well as Cosmology.

This is motivated by a novel measurement of the Helium abundance by the EMPRESS collaboration [10], which, using an extended catalogue of extremely metal poor systems, reported a value which is in a 3σ tension with the standard BBN scenario. However, in order not to be wholly dependent on just one measurement, the standard PDG value [11] will also be used, highlighting the importance of this choice on the constraints derived.

In light of this, the structure of the thesis will be as follows. First, in Ch. 2 we will review the experimental status of the observations of primordial abundances and introduce the statistical methods, as well as the different measurements, we will use throughout the thesis. Then, in Ch. 3, we will review the Standard theory of BBN

(SBBN) with the aim of presenting it in such a way that the different assumptions that go into it become apparent, so that we may later relax them when studying elements of new physics.

After having reviewed the Standard paradigm (Ch. 4), we will begin to analyze the different constraints usually derived from BBN, starting with the, in principle, only free parameters of the theory, the baryon density, as well as the neutron lifetime, which is generally treated as an input to the theory, but given the sensitivity of the Helium abundance to this value, can also be constrained from BBN directly, providing an independent measurement on τ_n, perhaps crucial in order to resolve the long standing Neutron Lifetime Anomaly. We will then depart from SBBN and allow for a non-standard expansion history of the Universe, as parametrized by the effective number of neutrino species N_{eff}, a topic of intense study in the context of Nucleosynthesis in the last years.

For the EMPRESS prior we find that a resolution in terms of a modification of N_{eff} requires it to be smaller than its SM prediction. A possible explanation of this is a time variation of the gravitational constant, G_N, which is why in Ch. 5 we will focus on this topic and study the impact of a time variation of G_N, as well as the Higgs vacuum expectation value v, on Nucleosynthesis and derive constraints on their respective time dependence.

After having studied the effects of a non-standard expansion history of the Universe, we shift our attention to modifications of the weak rates. A possible solution to the NLA, proposed in [12] is the existence of a dark sector to which the neutron can decay. First, in Ch. 6, we derive a model-independent constraint on the neutron lifetime and its branching ratio to dark sector particles.

Lastly, after a study of general modifications to the weak rates, we find (Ch.7) that the simplest modification allowing for the low value of the primordial Helium abundance measured by the EMPRESS survey is the presence of a large lepton asymmetry at the epoch of BBN. In light of that, we undertake a comprehensive analysis of primordial lepton asymmetries using BBN and CMB data, deriving constraints for current experiments and determining the reach of future experiments.

Chapter 2

Experimental Status

Nucleosynthesis describes the process whereby in a very short period of time at about 300 s after the supposed beginning of the Universe all nuclei that will eventually form the matter that we are made of and surrounded by were formed from an initial abundance of neutrons and protons. As we will see in the next chapter, after this process was complete, the Universe was mostly composed of protons and Helium-4, with trace amounts of Deuterium, Helium-3, Tritium, and Lithium-7. As carbon-based lifeforms, who breathe oxygen obtained from an atmosphere mostly made of nitrogen, it is not hard to see that this cannot be the full story, and, indeed, this was only beginning.

As the Universe cooled down, the nuclei were able to form electrically neutral, stable, bound systems with free electrons, also known as atoms, at the era of recombination about 380 000 years after the formation of these primordial nuclei. As the Universe continued to cool down and structure began to form, these primordial atoms became the fuel for the first generation of stars that lit up the Universe about 100 million years later. These stars burnt their fuel comparatively quickly and ejected their contents back to the Universe in a violent explosions, releasing the heavier stable elements that had been created in the stellar burning process into the Universe once again only to be used as fuel by further stars. This cycle of the life and death of stars has been ongoing ever since.

Thus, as time passes and the Universe expands, ever more stars are formed that continuously pollute the pristine gas of protons and Helium comprising most baryonic matter in the Universe after nucleosynthesis with astrophysical metals, that is elements heavier than Helium-4. While this pollution is essential for our existence, it also raises a crucial question we need to answer before concerning ourselves with the actual theory of nucleosynthesis. Can we even measure the primordial abundances?

Sadly, the answer is no, we cannot measure them directly, but we can infer it from different astrophysical observations. This, generally consists of finding the youngest systems possible, measuring the abundance of different nuclei in these systems and hope that we can accurately extrapolate to even younger systems until we eventually reach a plateau that corresponds to the primordial abundances. We will now highlight the most important aspects of these measurements that will be of importance for us later on, but refer to, e.g. [13, 11] for reviews on this topic.

2.1 Helium

Helium is one of the first elements that can be produced in stars from Hydrogen burning. Additionally, stars can also use Helium as a fuel to produce heavier nuclei. Thus, Helium is both copiously produced and destroyed during stellar evolution already very early on. In order to obtain the primordial abundance, we therefore need to find regions that are only marginally chemically evolved. Since nucleosynthesis does not abundantly produce metals, a proxy for the age or amount of chemical evolution of a certain galactic region can be obtained by measuring its metallicity, that is, essentially the amount of oxygen or nitrogen it contains. By measuring the Helium abundance for a large amount of galaxies and extrapolating to zero metallicity, one can obtain the primordial abundance. This is actually the most common method to determine the primordial helium abundance [14, 15, 16, 17, 18].

Obtaining the abundance of Helium, by itself, regardless of the metallicity of the system, is already a challenge. Generally, this requires measuring the intensity of emission lines caused by the recombination of Hydrogen and Helium ions, from which the neutral hydrogen and Helium column densities can be inferred. The presence of further ionized nuclei not visible through this method is accounted for by running photo-ionisation simulations. From this, we can now obtain the full Helium-to-Hydrogen ratio y. From this, the "primordial" Helium mass fraction at the given metallicity can be obtained:

$$Y = \frac{4y}{1 + 4y} \tag{2.1}$$

All that is left now is to plot the different values for Y as a function of metallicity obtained from as many systems as possible and extrapolate to the primordial helium abundance present at zero metallicity. This is shown on the left panel of Fig. 2.1. As we can see, the determination of both metallicity and primordial Helium mass fraction leaves a lot to wish for. In fact, this approach has been historically prone to many different sources of systematic errors, so that different groups obtain many different results.

As an example, the authors of [19] find $Y_P = 0.2551 \pm 0.0022$, whereas the authors of [14] find $Y_P = 0.2453 \pm 0.0034$, which amounts to a 2.5σ tension. Recent measurements appeared to be converging toward this lower determination of the Helium abundance, as can be seen on Fig. 2.1, causing the PDG to recommend the following weighted average[11]:

$$Y_P = 0.245 \pm 0.003 \qquad [\text{PDG} - 22] \tag{2.2}$$

which from now on we will refer to as the PDG-22 determination of Y_P. On the other hand, fairly recently the EMPRESS survey [10] increased the sample of extremely metal poor galaxies (EMPGs). Assuming these measurements are correct, this would imply that the extrapolation to zero metallicity from this experiment is more reliable, as it includes in principle more pristine systems that are closer to the primordial state of the Universe. Interestingly, the inclusion of these EMPGs lead them to report a value of the Helium abundance:

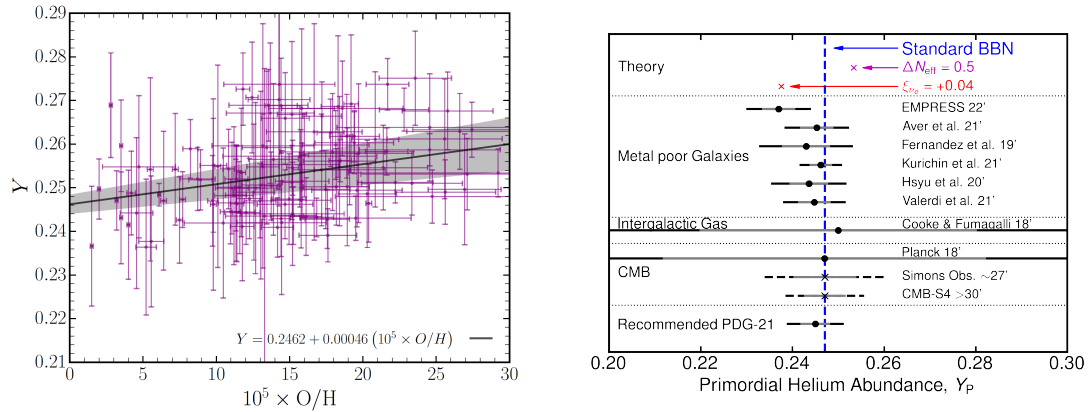$$Y_P = 0.2370 \pm 0.0034 \qquad [\text{EMPRESS}] \tag{2.3}$$

Figure 2.1: **Left:** Determinations of the Primordial Helium mass fraction Y as a function of the oxygen to hydrogen ratio. The grey line shows the best fit of the data, with the grey band corresponding to the 68% CL. Figure from [23] **Right**:Current status in the measurements and the theoretical determinations of the primordial helium abundance, and forecasts for the upcoming Simons Observatory and CMB-S4, Figure from [24]

This measurement is only mildly in tension with previous measurements, but is 3σ smaller than the value predicted by the Standard Model [20]. In the absence of a systematic error in the measurement, such a low value hints at the presence of new physics modifying the expansion of the Universe at the epoch of BBN.

While this method is the most common and precise, it is not the only method by which to infer the primordial Helium abundance. As shown in [21], the helium abundance could be inferred from the absorption lines of the light of a background quasar when passing through a near-pristine intergalactic gas cloud. This method yields:

$$Y = 0.250^{+0.033}_{-0.025} \tag{2.4}$$

which is in agreement with both the EMPRESS and PDG-22 proposed values, but is not nearly as precise. However, this measurement is currently dominated by statistics and has the potential of reaching a sensitivity that is competitive with them, providing an invaluable independent measurement of Y_P.

Additionally, much like most processes in the Early Universe, primordial Helium affects the power spectrum of the CMB. Ionized Helium, at the time of recombination, affects the number of free electrons, thus leaving an imprint in the CMB temperature and polarization power spectra at small angular scales. An analysis of Planck observations of the CMB [4, 22] yields:

$$Y_P = 0.245 \pm 0.018 \tag{2.5}$$

which improves upon measurements of [21], but is still not competitive with measurements of the emission line spectra in metal poor galaxies. A summary of recent determinations is shown in Fig. 2.1, and show a fairly good agreement with the Standard Model expectations.
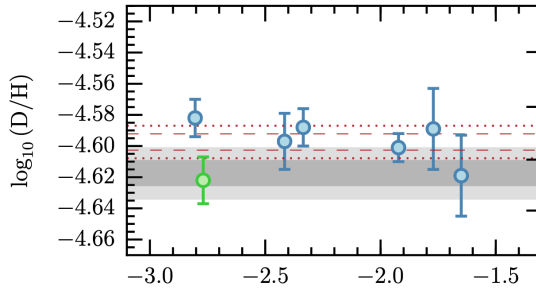
Figure 2.2: Determinations of the Deuterium to Hydrogen ratio from measurements of the absorption lines of pristine interstellar gas clouds fulfilling the criteria from [25] as a function of the oxygen to hydrogen ratio. The red dashed (dotted) lines correspond to the 68% (95%) CL from the weighted mean of all the data, whereas the grey line shows the Standard BBN prediction assuming a CMB prior on the baryon density at the same CLs. Figure from [26]

2.2 Deuterium

Deuterium is also very efficiently burned during the stellar process. Unlike Helium, though, it is much less abundant and there are in principle no astrophysical sources capable of significantly producing Deuterium [13]. Thus, in principle, any detection of deuterium is of primordial origin, but since it can be burned in stars, it is only a lower limit on its primordial abundance and, the more pristine the target of the observations, the more likely this is to correspond to the actual primordial abundance.

The most common method to determine the Deuterium abundance is to measure the absorption lines of pristine gas clouds against a source of background light, typically quasars. If these systems fulfil certain additional criteria, as pointed out in [25], many of the systematic uncertainties limiting the precision of previous experiments can be avoided and extremely precise measurements can be made.

Currently, only 7 such systems have been detected [26], whose abundance as a function of metallicity is shown on Fig. 2.2. As we can see, the inferred deuterium abundance from these systems are all in very good agreement with each other and exhibit a clear plateau, hinting at its primordial origin. Largely based on these measurements, the PDG recommends a value for the Primordial Deuterium abundance, usually quoted as the ratio of primordial deuterium to primordial hydrogen[11]:

$$D/H|_P = (2.547 \pm 0.025) \times 10^{-5} \qquad [\text{PDG} - 22] \qquad (2.6)$$

with a precision of 1%, comparable to the precision of the Helium abundance. Unlike Helium, this precision is mainly controlled by statistics, as we only have 7 systems fulfilling the strong requirements from [26], but there is very little disagreement on the precision of this measurement, unlike with Helium.

2.3 Lithium

Lithium has three main astrophysical sources. It can be created during BBN, through nuclear reactions between cosmic rays and the intergalactic medium and in
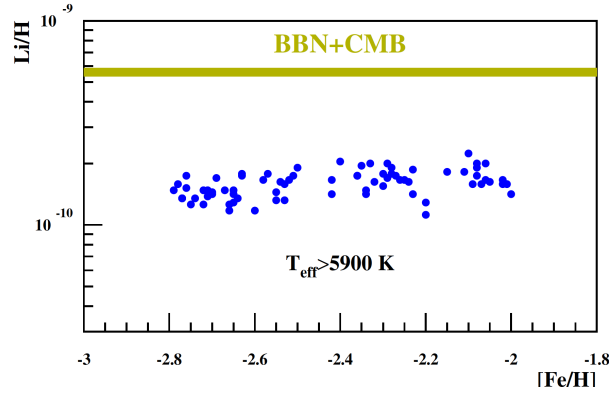
Figure 2.3: Observations of the Lithium to Hydrogen (blue points) ratio as a function of metallicity showing the features of the Spite plateau compared to the Standard model prediction (green band). Figure form [20]

stars. Thus, Lithium can both be produced and destroyed as the Universe expands. Interestingly, some of the best sources from which to infer the Lithium abundance are extremely old stars in the halo of our own galaxy. Already in the 1980s the first measurements appeared [27] from precisely such stars, reporting a metallicity independent plateau, the "Spite Plateau", which just like with Deuterium can be interpreted as a strong indication for a primordial origin of the measured abundance.

More recent results are shown on Fig. 2.3, along with a green band corresponding to the prediction from cosmology. Needless to say this is a severe problem, as the measured abundance is lower than the predicted one by a factor of 3! This so-called Lithium problem is one of the biggest challenges the standard theory of nucleosynthesis faces and needs to be addressed. Indeed, a lot of work has gone into resolving this issue, both from the experimental side trying to find any systematic errors in the measurement, as well as from the theoretical side with different proposals as to what type of new physics could yield such a low value of Lithium.

However, there is still no consensus as to what is the solution to this long-standing problem, whether it is a theoretical problem or an astrophysical one. In light of that, in what follows we choose not to use a prior on the Lithium abundances to constrain new physics with BBN. This is unfortunate, as this reduces slightly the predictive power of BBN as we can now constrain one parameter less, but it avoids the introduction of unnecessary tension into the data. Nonetheless, one should always keep in mind that this is still a problem when praising the beautiful agreement between standard nucleosynthesis and data on the observational abundances.

While in principle one can predict the primordial abundance up to even different isotopes of nitrogen, measurements, astrophysical observations on their primordial abundances either cannot be made or they are too inaccurate. The most promising candidate in this respect is Helium-3, but currently measurements only provide an upper limit on the Primordial abundance.

2.4 Statistical Methods

Motivated by the recent result by the EMPRESS survey, we will undertake a comprehensive study of current constraints on standard nucleosynthesis, as well as different scenarios of new physics through its effect on the production of primordial abundances by comparing the predictions to the observational abundance from BBN and CMB data independently and combined. For the statistical analysis, we will adopt a freqeuentist approach using a χ^2 statistic, instead of a Bayesian one[1]. Since we only really have one Universe to test our theories, the latter may perhaps be the more consistent approach, but it has been shown that when data dominate the analysis, both methods yield the same results, which is the case here.

Regardless of the actual dataset, we will proceed in an analogous way for all analyses. Let us assume that we have N parameters θ_i in our theory, whose interpretation will depend on the actual cosmological scenario we are testing. We will assume Gaussian distributions for all measurements we include in the analysis. Assuming that $\vec{y}$ corresponds to our measurements, we can simply build our χ^2 as follows:

$$\chi^2(\vec{\theta}) = (\vec{y} - \hat{y}(\theta_1, ..., \theta_N)) \cdot \Sigma^{-1} \cdot (\vec{y} - \hat{y}(\theta_1, ..., \theta_N)) \tag{2.7}$$

where Σ is the Gaussian covariance matrix for the measurements. Since the actual dependence of $\vec{y}(\theta_1, ..., \theta_N)$ is highly non-trivial, in order to minimize this distribution we will simply generate an N-dimensional grid Θ for a given range of each parameter[2] and calculate $\chi^2(\theta_1, ..., \theta_N)$ for each point on that grid. The best fit estimate of our parameters $\hat{\theta}$ is then simply found as

$$\hat{\theta} = \underset{\vec{\theta} \in \Theta}{\arg \min} \; \chi^2(\vec{\theta}) \tag{2.8}$$

and the minimal value of χ^2 is obtained analogously. Subsequently, one can construct the $\Delta\chi^2 = \chi^2(\vec{\theta}) - \chi^2_{\min}$. This is now a multi-dimensional χ^2 distribution centered around the best-fit value. From this distribution, we construct isocontours that correspond to different confidence levels. Assuming that there is only one parameter θ, then $\Delta\chi^2 = n^2$ corresponds to a $n \cdot \sigma$ confidence level. In that case, by finding the values of θ corresponding to $\Delta\chi^2 = 1$, we find an estimator for the uncertainty on our best fit parameter. If we are constraining two parameters at once, then we obtain isocontour ellipses for a given confidence level. Generally, we will only be interested in the 1σ and 2σ contours, corresponding to $\Delta\chi^2 = 2.3$ and $\Delta\chi^2 = 6.18$ respectively.

However, there are cases where we have more than two parameters and even for two we want to be able to find an estimator for the uncertainty on our best-fit parameters. Thus, we need to be able to treat nuisance parameters in some way. For this purpose, we will use the profile likelihood ratio, which is actually quite simple. Let us say that we are only interested in one parameter θ and the other $N-1$ parameters are just nuisance parameters ν_i, such that $\vec{\theta} = (\theta, \nu_1, ..., \nu_{N-1})$.

---

[1]We will only briefly cover the most important aspects of our analysis, but we very closely follow the methods described in [11]

[2]This grid needs to be sufficiently fine grained. Depending on the number of parameters, this may pose a computational challenge, but we have made sure that the spacing between points is at least ten times as small as the uncertainty on that parameter, so that this will not affect any conclusions.

In order to obtain the χ^2 distribution as a function of only θ, we will simply choose values for ν_i that minimize the χ^2. We will call this process marginalizing over the parameter ν_i. The marginalized distribution is then simply defined as:

$$\chi^2(\theta) = \min_{\vec{\nu}} \chi^2(\theta, \vec{\nu}) \tag{2.9}$$

This can be used to find the uncertainty for any parameter in the same way as discussed before. This procedure will likewise allow us to obtain confidence-level ellipses for distributions with more than two parameters.

BBN Data

All that is left now is to discuss the different priors and combinations we will use in the analysis. We will mainly focus on the implications of the recent helium measurement by EMPRESS [10]:

$$Y_\mathrm{P}|_\mathrm{EMPRESS} = 0.2370 \pm 0.0034 \,. \tag{2.10}$$

However, we will also consider, for comparison and in order to simply update some constraints that have only been obtained previously with outdated measurements of the observational abundances, the recommended PDG-22 value [28]:

$$Y_\mathrm{P}|_\mathrm{PDG-22} = 0.245 \pm 0.003 \,. \tag{2.11}$$

We will also include the measurement of the primordial deuterium abundance, which is typically used to constrain the baryon energy density. The PDG recommended value reads [28]:

$$\mathrm{D/H_P}|_\mathrm{PDG-21} = (2.547 \pm 0.025) \times 10^{-5} \,, \tag{2.12}$$

which is largely based on the analysis of [26]. Apart from the experimental uncertainty, the theoretical prediction also has some uncertainties from the value of the neutron lifetime, as well as the nuclear reaction rates. We also take this theoretical uncertainty into account by, quite simply, adding in quadrature to the observational and theoretical uncertainties. Concretely, for helium we take $\sigma_\mathrm{Theo}(Y_\mathrm{P}) = 0.00017$ [20]. For Deuterium, as we will see later on, different groups obtain different results, depending on some, in theory, trivial choices that should yield equivalent results, but given poor data actually do not. For the deuterium to hydrogen ratio we take $\sigma_\mathrm{Theo}(\mathrm{D/H}|_\mathrm{P}) = 0.07 \times 10^{-5}$ when using the nuclear reaction rates from [29] (PArthENoPE rates), and $\sigma_\mathrm{Theo}(\mathrm{D/H}|_\mathrm{P}) = 0.04 \times 10^{-5}$ when using those from [30] (PRIMAT rates).

We will assume that these measurements are statistically independent, so that the covariance matrix of the BBN prior is just the sum of the respective χ^2 distributions, namely:

$$\chi^2(\vec{\theta}) = \chi^2(\vec{\theta})|_{Y_P} + \chi^2(\vec{\theta})|_{D/H|_P}$$
$$= \frac{\left(Y_P^\mathrm{obs} - Y_P^\mathrm{th}(\vec{\theta})\right)^2}{\sigma_{Y,\,\mathrm{obs}}^2 + \sigma_{Y,\,\mathrm{th}}^2} + \frac{\left(D/H|_P^\mathrm{obs} - D/H|_P^\mathrm{th}(\vec{\theta})\right)^2}{\sigma_{D/H,\,\mathrm{obs}}^2 + \sigma_{D/H,\,\mathrm{th}}^2} \tag{2.13}$$

where for Y_P we can either choose the EMPRESS prior (Eq.2.10) or the PDG-22 prior (Eq. 2.11).

CMB Data

Lastly, we will also use results from Planck CMB observations [4]. These provide independent determinations of the baryon density, $\Omega_b h^2$, $Y_{\rm P}$, and the effective number of neutrino species $N_{\rm eff}$, which we will introduce later on. Concretely, assuming the standard cosmological model, the Planck collaboration reports a baryon energy density

$$\Omega_b h^2|_{\rm Planck} = 0.02242 \pm 0.00014 \,, \tag{2.14}$$

from combining the full temperature and polarization data, together with CMB lensing and baryon acoustic oscillations. Since $\Omega_b h^2$ is one of the parameters that determine the final abundance, we can quite simply construct the χ^2 distribution as:

$$\chi^2(\Omega_b h^2) = \left(\frac{\Omega_b h^2 - \Omega_b h^2|_{\rm Planck}}{\sigma_{\Omega_b h^2}} \right)^2 \tag{2.15}$$

However, the baryon density measurement from the CMB is actually correlated with Y_P, as the primordial Helium abundance will affect the CMB power spectrum through its effect on the number of free electrons at recombination. Therefore, the Planck collaboration has also made an analysis of the CMB data allowing for a non-standard primordial helium abundance, so it is more consistent to use this as a prior when combining BBN and CMB data to constrain the primordial abundances. Thus, we need to use the full correlation matrix to define the Planck χ^2 in Eq. 2.7, which requires the knowledge of the correlation parameter ρ between Y_P and $\Omega_b h^2$, as well as the uncertainty on each parameter individually, which reads [22]:

$$\Omega_b h^2|_{\rm Planck} = 0.02239 \pm 0.00018 \,, \tag{2.16a}$$
$$Y_{\rm P}|_{\rm Planck} = 0.242 \pm 0.012 \,, \tag{2.16b}$$
$$\rho(\Omega_b h^2, Y_{\rm P}) = 0.663 \,. \tag{2.16c}$$

Lastly, we will also look at the situation where we will allow the effective number of neutrino species $N_{\rm eff}$ to vary, which allows us to constrain scenarios with a non-standard expansion history of the Universe with one simple parameter, which makes it a very important piece of evidence for Cosmology. The Planck collaboration has analyzed the CMB data allowing also for variations in $N_{\rm eff}$. For this scenario, the determination of $\Omega_b h^2$, $Y_{\rm P}$ and $N_{\rm eff}$ with their corresponding correlation coefficients read:

$$\text{Planck}$$
$$\Omega_b h^2|_{\rm Planck} = 0.02238 \pm 0.00019 \,, \tag{2.17a}$$
$$Y_{\rm P}|_{\rm Planck} = 0.245 \pm 0.018 \,, \tag{2.17b}$$
$$N_{\rm eff} = 2.97 \pm 0.29 \,, \tag{2.17c}$$
$$\rho(\Omega_b h^2, Y_{\rm P}) = +0.273 \,, \tag{2.17d}$$
$$\rho(\Omega_b h^2, N_{\rm eff}) = +0.270 \,, \tag{2.17e}$$
$$\rho(N_{\rm eff}, Y_{\rm P}) = -0.686 \,. \tag{2.17f}$$

In order to combine BBN and CMB measurements, we will assume that they are statistically independent and simply add the χ^2 distributions for different priors

together. In principle, we now have all the information we need to constrain the observational abundances except for one slight detail, namely how the primordial Helium and Deuterium abundances depend on the parameters we would like to constrain.

Chapter 3

Theory of Big Bang Nucleosynthesis

Before introducing elements of new physics, we need to first understand the standard picture of Big Bang Nucleosynthesis that has established itself as one of the pillars of modern Cosmology. It describes an extremely important moment in the evolution of our Universe, crucial to our own personal existence, a process whereby, within the Hot Big Bang theory of our Universe, the earliest nuclei were formed. It is from this primordial matter that the first stars were made, eventually leading to the formation of all the baryonic matter that surrounds.

If things had happened ever so slightly differently, we may not even exist. Thus, nucleosynthesis answers, at least partly, a question that is innate to our human curiosity, namely where the matter we are made of actually comes from. As such, it is not a wonder that the theory of nucleosynthesis marks one of the earliest developments in what we could today consider modern Cosmology.

3.1   A Brief History of Big Bang Nucleosynthesis

Although the history of how this theory came to be is rather confusing [32], it is clear that the idea emerged in the mid 1940s, with G. Gamow being widely credited as the first to take a step in the right direction. He was concerned with explaining the observed abundances of all nuclear elements in the Universe, as shown in Fig. 3.1. Previously, it had been proposed that the exponential decrease in the observed abundance should be due to an equilibrium process taking place in the Early Universe, only dependent on the temperature of the Universe at that time and the qualities describing a nucleus like binding energy and mass number.

In a paper published in 1946 [33], however, Gamow argued that this would not explain the plateau the curve on Fig. 3.1 exhibited for larger mass nuclei and, perhaps more importantly, that the conditions required for this equilibrium state were only present for too short a period of time. Instead, he stated that a much more likely explanation involved "some kind of unequilibrium process taking place during a limited interval of time"[33].

This process required a dense gas of neutrons as primordial matter which, by virtue of the rapid expansion of the Universe, at some point stopped interacting with
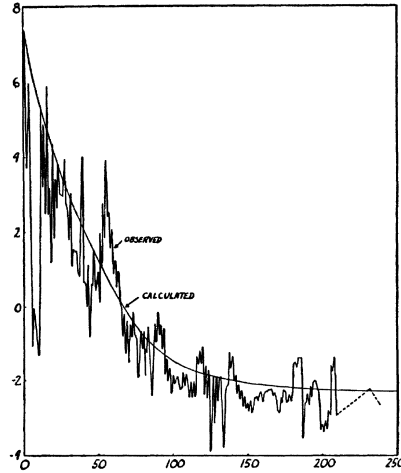
Figure 3.1: Logarithm of the observed relative abundance of the chemical elements as a function of their nuclear mass number compared to the predicted abundance by R.A. Alpher, H.A. Bethe and G. Gamow according to their neutron-capture theory of the formation of elements [31].

each other and decayed freely into protons and electrons through β-decay. Protons and neutrons then present in $\approx 1:7$ ratio combined first to deuterium, then to heavier nuclei successively through neutron capture, with the neutron to proton ratio inside the nuclei being regulated through beta decays of neutrons inside the nucleus over time towards stable isotopes.

A refined treatment of this idea, developed as part of R.A. Alpher's doctoral dissertation [34], is put forward in the seminal "α-β-γ-paper"[31]. This paper is widely credited as one of the central papers in the development of the theory of Primordial Nucleosunthesis and Big Bang Cosmology, which is a fair assessment. Nonetheless, it made several very crucial and incorrect assumptions that differ from the standard picture nowadays: the authors of this paper assumed a matter dominated Universe and that the entire baryon density was made up of neutrons.

The first assumption led to one big problem, as was pointed out in [34]. Alpher and Herman determined the initial neutron density required to explain the observed relative abundance curve and found that value to be extremely low. A Universe contains only such a tiny amount of primordial matter, as was assumed to be the case, expands very slowly, so that this energy density, according to the Friedman equation, is only reached at a time much larger than the neutron lifetime. In such a scenario, the production of elements through neutron capture would fail as there would be no Hydrogen, the most abundant of the elements. This was solved by requiring the presence of radiation at a temperature of $T \propto \mathcal{O}(10^9 \, \mathrm{K})$ that dominated the energy density of the Universe, accelerating the expansion and shifting the time at which the neutron capture occurs to be smaller than the neutron lifetime.

This is the first mention of an overwhelmingly large presence of radiation in the early Universe at the time of BBN. In fact, as a correction to a paper published in 1948 by Gamow in Nature [35], Alpher and Herman predicted the Temperature that this background radiation, which we now know as the Cosmic Microwave Background (CMB), should have today to be $T_{CMB} = 5 \, \mathrm{K}$, which is remarkably close to the present determination $T_{CMB} = 2.73 \, \mathrm{K}$. It was this early prediction along with

the discovery of the CMB by A. Penzias and R. Wilson [36] in 1965, as well as its correct prediction of the observed Helium abundance and its conceptual simplicity, that cemented the ideas developed in these years as an integral part of any model of the Early Universe.

Furthermore, the second assumption was incorrect, or at least extremely unlikely, as was later pointed out by C. Hayashi in 1950 [37], namely that in a Universe at such high temperatures, where electrons, neutrinos and their respective antiparticles are necessarily present, neutrons and protons undergo weak reactions that interchange them. Thus, they reach an equilibrium state for temperatures higher than at least the mass of the electron in which the ratio of neutrons to protons is determined by their mass difference Q and the temperature of the plasma, namely $n_p/n_n \propto e^{Q/T}$, which is quite close to unity for the temperature range of interest.

While at first sight this might look like a big problem, it actually helped the theory which otherwise would have inevitably struggled. There are no stable nuclei with mass number 5 or 8, which meant that no elements with a mass number higher than 4 would be created. A larger presence of protons, however, allowed for an increased presence of, for example, Helium 3 which upon combination with tritium could create heavier nuclei. On the flipside, however, this realization indicated the need for the inclusion of different nuclear reaction rates, not only the neutron capture, anymore. This meant that the already complicated set of equations, that up to now had only been solved under extremely simplifying assumptions[1] , would need to be complicated further.

Alpher and Herman, along with J.W. Follin incorporated these results into the theory, summarizin them in a paper published in 1953 [39]. They focused mainly on improving the calculation by Hayashi [37] of the induced β-process rates and predicting the neutron to proton ratio In doing so, they very precisely described a timeline of events between $\approx 100\,\mathrm{MeV}$ and the end of nucleosynthesis at $\approx 1\,\mathrm{keV}$. The picture presented in this paper is that of a highly relativistic gas of photons, electrons, neutrinos, mesons and baryons, in equilibrium with each other, which cools down as the Universe expands. Neutrons and protons are kept in equilibrium through induced β-processes. Heavier nuclei are instantly dissociated because of the large amount of extremely high energy photons. The temperature continues dropping and neutrons and protons decouple from the thermal bath, so neutrons essentially decay freely now. Shortly after, nucleosynthesis begins and the process is essentially done after a couple of minutes. The crucial aspect of the formation of elements by thermonuclear reactions is left for future study in this paper, as a detailed study required correct measurements of the reaction rates and advancements in numerical computation methods.

Progress halted for a little while after this, as the theory seemed to fail in its original endeavor of explaining the genesis of all observable elements in favour of stellar production mechanisms. However, the underproduction of Helium through such mechanisms combined with the discovery of the CMB revived the theory. The first calculation of the evolution of the light elements according to the theory of

---

[1]For example, in all of the calculations in [31, 38, 33, 35], the effect of the expansion of the Universe, of paramount importance as it provides the destabilizing force that allows this process to depart from equilibrium, had been "neglected because of computational difficulties", as Alpher and Herman wrote in [38].
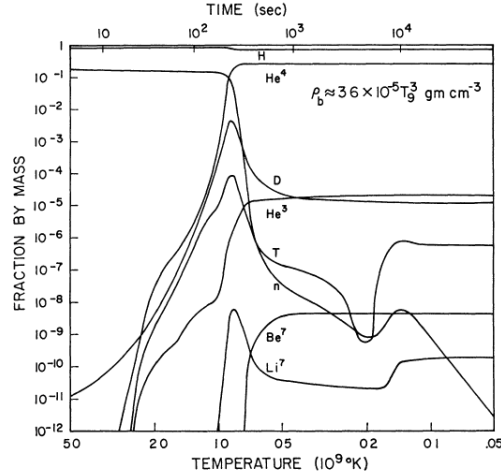
Figure 3.2: Evolution of Nuclear Mass fractions as a function of Temperature in an expanding isotropic and homogeneous Universe with low matter density, taken from [40].

Primordial Nucleosynthesis described in [39] followed shortly after, in a paper by R. Wagoner, W. Fowler and F. Hoyle in 1967, which included a full numerical treatment with more than 60 nuclear reactions and the expansion of the Universe taken into account. The result of this calculation for a Universe with similar conditions as the ones we currently believe we are living under is shown on Fig. 3.2.

3.1.1 The Current Picture

The modern theory of Primordial Nucleosynthesis is essentially based on these two papers ([39, 40]). Even though there have been significant quantitative improvements, which will be detailed throughout this chapter, the overall picture has not changed too much qualitatively:

- We start with an isotropic, homogeneous flat universe comprised of all SM particles. At the temperature range relevant for BBN $(10 - 10^{-3}\,\mathrm{MeV})$, radiation, in the form of photons, electrons, neutrinos and their respective antiparticles, dominates the energy density.

- Neutrons and protons are being interconverted through weak reactions and are roughly equal in number, with their equilibrium getting exponentially biased towards protons as temperature drops. However, at some point, the expansion rate catches up with the neutron to proton conversion rate and they depart from equilibrium at about $T = 0.8\,\mathrm{MeV}$.

- Neutrons are essentially free and start decaying to protons with a lifetime of $\tau_n = (878.4 \pm 0.5)\,\mathrm{s}$[11], further diminishing their abundance until nucleosynthesis is fully underway.

- Simultaneously, the formation of nuclei can begin as nuclear reactions now proceed faster than weak reactions. This happens not only through neutron capture, as proposed initially by Gamow [33], but through the complex system

16

of nuclear reactions described in [20]. Just after neutron proton freeze-out, the temperature is already below the binding energy of most nuclei, like Deuterium with $B_D = 2.23\,\text{MeV}$. However, due to the overwhelming overabundance of photons with respect to nucleons, there are still enough high-energetic photons in the Wien tail of the Bose-Einstein distribution that the photodissociation rate is high enough, so that the nuclear abundances remain negligibly small and neutrons continue decaying.

- The most common pathways in the system of nuclear reactions to get to higher order nuclei involve at least one deuterium nucleus. Thus, a substantial amount of deuterium is required for BBN to properly begin, even though the photodissociation rate may be negligible as Temperature drops for heavier nuclei like Helium. This is commonly known as the Deuterium bottleneck. Only when this breaks, does the synthesis of heavier nuclei really begin. This happens at $T_D \approx 0.073\,\text{MeV}$, or equivalently at $t_D = 240\,\text{s}$, which is comparable to the neutron lifetime, but small enough that there is still a substantial amount of neutrons left to be cast into heavier nuclei.

- Nucleosynthesis then proceeds astonishingly quickly. At $T \lesssim 0.04\,\text{MeV}$, that is only $\approx 600\,\text{s}$ after the deuterium bottleneck breaks, all Helium has been formed and its abundance frozen out. Other nuclei are still changing slightly by at most one order of magnitude. At $T \lesssim 0.01\,\text{MeV}$, or approximately 3 hours and 40 minutes after the beginning of the Universe, BBN is done.

- After BBN, the Universe is still mainly comprised of protons. Most free neutrons present at the onset of nucleosynthesis have been cast into Helium, making it the second most abundant nucleus. Most lighter nuclei have likewise been used up in the process of building Helium, so that only trace amounts of Deuterium, Tritium and Helium-3 are left over. Heavier nuclei, like Lithium and Beryllium, require mainly Helium and other light nuclei for their formation, so that their final abundance is even further suppressed.

After having summarized the qualitative picture of the different stages of BBN according to the ΛCDM model, we will now develop the tools necessary to describe this process more quantitatively. This will be structured in the same way as BBN, beginning with a study of the background evolution of the Universe, followed by a description of the neutron to proton freeze-out, and ending with an analysis of the reaction network leading to the formation of all heavier nuclei. Although this is a standard calculation that may be found in various places, the goal of this section is to highlight the assumptions made and present the equations in such a way that it will be clear what aspects may be modified by Beyond the Standard Model (BSM) physics and their effect on the standard outcome of BBN.

3.2 Background Evolution and Thermodynamics

The key insight that Gamow made in his first paper on the neutron capture theory [33] was recognizing that explaining the observed abundances required a departure from equilibrium. However, initially, all particles are in equilibrium. It is only due

to the expansion of the Universe that they are able to depart from it, allowing the formation of nuclei. Thus, it plays a key role in determining the final abundances and it is crucial to accurately describe it. Here, we will only summarize the most important results, with the reader being referred to appendix B for more details.

We will start by considering an expansion according to the ΛCDM model. Thus, the Universe will be assumed to be isotropic, homogeneous and flat, so that it may be described by a Friedman-Lemaitre-Robertson-Walker (FLRW) metric:

$$ds^2 = dt^2 - a(t)^2 \left(dr^2 + d\Omega \right) \tag{3.1}$$

with the scale factor $a(t)$ and cosmic time t. Einstein's General Relativity then predicts that the Universe must expand according to the Friedman equation, which can be cast into the convenient form:

$$H^2 = \left(\frac{\dot{a}}{a} \right)^2 = \frac{8\pi G_N}{3} \rho_{tot} \tag{3.2}$$

with $H(t)$ the Hubble parameter and Newton's constant $G = 6.72 \cdot 10^{-39} \, \text{GeV}^{-2}$ and $\rho_{tot}(t)$ the energy density of the Universe. At the early stages of the Universe of interest for nucleosynthesis, $\rho_{tot}(t)$ and P_{tot} contain contributions from radiation in the form of photons, electrons, positrons, neutrinos and antineutrinos, trace amounts of mesons and baryons, as well as dark matter and dark energy. In order to continue, we therefore need to find a framework that will allow us to describe the contribution of each particle species to the quantities of the cosmic fluid as a function of time in an expanding Universe where particles are constantly interacting with each other.

The best way to do this is by defining the phase-space distribution $f_i(q, p)$ for each particle species i, where q and p are its generalized coordinates. In a homogeneous and isotropic universe, these reduce to t and $p \equiv |\vec{p}|$. Essentially, f is a probability distribution function that describes the probability of the system being in a specific microstate. The macroscopic observables of interest here (see App. A.6 for more details) are obtained by taking the expectation value of specific combinations of energy and momentum in the following way:

$$
\begin{aligned}
n_i(t) &= g_i \int_0^\infty \frac{4\pi p^2 dp}{(2\pi)^3} \cdot f_i(t, p) \\
\rho_i(t) &= g_i \int_0^\infty \frac{4\pi p^2 dp}{(2\pi)^3} \cdot f_i(t, p) \cdot E(p) \\
P_i(t) &= g_i \int_0^\infty \frac{4\pi p^2 dp}{(2\pi)^3} \cdot f_i(t, p) \cdot \frac{p^2}{3E(p)}
\end{aligned}
\tag{3.3}
$$

As for the time dependence of these quantities, they can be obtained from the Boltzmann equation, which describes the time dependence of the phase space distribution. In its most general form, the Boltzmann equation can be written as follows:

$$\mathbf{L}[f] = \mathbf{C}[f] \tag{3.4}$$

The operator on the left-hand side is the Liouville operator, which describes the time-dependence of f. The operator on the right-hand side is the Collision operator.

In general, f is a vector that contains an entry for all particle species, so that this equation describes a complex system of coupled differential equations.

Essentially, what this equation is telling us, is that the change in time of the phase-space distribution of a particle is given by its collisions and interactions with other particles. We will leave the Collision term as it is for the moment and specify it later on. The Liouville operator, on the other hand, can easily be simplified[2], so that the equation 3.4 takes on the following form:

$$\frac{\partial f_i}{\partial t} - Hp\frac{\partial f_i}{\partial p} = \frac{\mathbf{C}[f]}{E(p)} \tag{3.5}$$

Obtaining the differential equations describing the time dependence of any macroscopic observable related to the phase-space density is now straightforward: you simply multiply the Boltzmann eq. with the combination of kinetic variables and phase-space density that relate f to the variable of interest and integrate over the entire phase-space. For the number density, this amounts to integrating over phase-space only:

$$\dot{n}_i + 3Hn_i = g_i \int_0^\infty \frac{4\pi p^2 dp}{(2\pi)^3} \cdot \frac{\mathbf{C}[f]}{E(p)} \equiv \mathcal{J}_i(t) \tag{3.6}$$

where $\mathcal{J}$ plays the role of a source/sink term for the particles of the species i. The significance of this is best understood if the left hand side is rewritten by multiplying it with $V = a^3$ as:

$$\frac{\mathrm{d}(N_i)}{\mathrm{d}t} = \frac{\mathrm{d}(n_i a^3)}{\mathrm{d}t} = \mathcal{J}_i(t) \tag{3.7}$$

If particles do not interact and the collision term vanishes, so does the source term. Then, there is essentially no creation or destruction of particles and they are constant inside a comoving volume $V = a^3$ and their density only gets diluted $\propto 1/V \propto a^{-3}$. If particles start to interact, then the collision term will lead to the source term being non-zero as well. Particle number is no longer constant and the amount by which they change is additionally dictated by their interactions with other particles.

A similar relation can be derived for the energy density as well, namely that:

$$\dot{\rho}_i + 3H(\rho_i + P_i) = g_i \int_0^\infty \frac{4\pi p^2 dp}{(2\pi)^3} \cdot \frac{\mathbf{C}[f]}{E(p)} E(p) \equiv \dot{q}_i \tag{3.8}$$

where $\dot{q}_i$ is defined as the volume heating rate. This equation can easily be interpreted if we recast the equation in a similar way to 3.7 with $V = a^3$:

$$\frac{\mathrm{d}(\rho_i V)}{\mathrm{d}t} = -P_i \frac{\mathrm{d}V}{\mathrm{d}t} + \dot{q}_i V \tag{3.9}$$

In the absence of collisions, $\dot{q}$ vanishes and this equation simply gives the first law of thermodynamics in an adiabatic system $dE + PdV = 0$. This implies that the fluid's energy density not only gets diluted, but actually further decreases as the universe expands proportional to the fluid's pressure. For relativistic particles, this is the well known effect of redshift, whereas for non-relativistic matter, whose pressure is negligible, it means that its energy density only gets diluted.

---

[2]See App. C.3 for details on this and all further calculations

This result should not come as a surprise, as from the conservation of the energy momentum tensor $T^{\mu\nu}$, we get a condition that

$$\frac{\mathrm{d}\rho_{tot}}{\mathrm{d}t} + 3H(\rho_{tot} + P_{tot}) = 0 \tag{3.10}$$

where the subscript *tot* means that we are looking at the total quantities that describe the cosmic fluid, not at those of one particular species. The only difference between the two equations is the volume heating rate $\dot{q}_i$. This quantity is related to the collisions of particles and describes the heat transfer between different particle species through their interactions, which will be crucial later on. Eq. 3.10 thus implies that:

$$\sum_i \dot{q}_i \overset{!}{=} 0 \tag{3.11}$$

One quantity that we have not talked about for now but which is of crucial importance is the entropy. Entropy density can be related to the phase space distribution as follows[41]:

$$s_i = -\int_0^\infty \frac{4\pi p^2 dp}{(2\pi)^3} \cdot \mathcal{S}^{\pm}(f_i),$$
$$\mathcal{S}^{\pm}(f_i) = [f_i \ln f_i \pm (1 \mp f_i) \ln(1 \mp f_i)] \tag{3.12}$$

with the upper signs holding for bosons, the lower ones for fermions. Multiplying eq. Boltzmann equation 3.5 with $\mathcal{S}^{\pm}(f_i)$, integrating over phase-spaces and using the identity:

$$\frac{\partial \mathcal{S}^{\pm}(f_i)}{\partial p} = \ln\left(\frac{f}{1 \mp f}\right)\frac{\partial f}{\partial p} \tag{3.13}$$

it can be shown that the entropy density evolves as follows:

$$\dot{s}_i + 3Hs_i = -\int_0^\infty \frac{4\pi p^2 dp}{(2\pi)^3} \cdot \frac{\mathbf{C}[f]}{E(p)} \ln\left(\frac{f}{1 \mp f}\right) \tag{3.14}$$

Its interpretation is similar to that of the evolution of number density. Again, if the particle species does not interact, its entropy inside a comoving volume is conserved! Interactions with other species, however, lead to a net entropy production or destruction [3] which is described by the source term on the right-hand side of the equation.

All of the above formulae are valid for an arbitrary phase-space distribution. In principle, in order to move forward, we would now need to solve the coupled system of differential equations to obtain the phase-space distribution as a function of time from which all other quantities can be derived, which generally requires a highly costly numerical calculation.

At the beginning of BBN, however, interactions between the relevant particles are so fast, that they are in kinetic and chemical equilibrium and can thus be described by their temperature and chemical potential, which will be crucial later on

---

[3]Since we are talking about one species that interacts with others, the system is not closed so that entropy may be destroyed, so long as the total entropy of the Universe remains constant or increases.

but neglected for now. In that case, particles can be described by a Bose-Einstein (Fermi-Dirac) distribution depending on their nature as bosons (fermions). Regardless of its quantum nature, if the particle's mass is much lower than temperature, i.e. the species is non-relativistic, these distributions approximate the Maxwell-Boltzmann distribution. After that, by relating the temperature of the Universe and the time since its beginning, we will obtain the time-evolution of any quantity we are interested in.

This greatly simplifies matters, and even analytical calculations are possible. The energy density of highly relativistic particles follows the Stefan Boltzmann law $\rho \propto T^4$, whereas in the non-relativistic regime it is Boltzmann suppressed $\rho \propto e^{-m/T}$. The exact solution interpolating these two regimes can only be obtained by numerical integration, and can contribute significantly until the temperature drops well below the particle's mass, which is very important for electrons and positrons, as shall be seen later. As for the dark sector, within the ΛCDM model, the density at that time is negligibly small as well, so their influence purely through gravitational interactions[4] can safely be ignored.

Therefore, it is enough to take into account those particles which are relativistic when BBN begins, namely photons, electrons, neutrinos and their respective antiparticles. Thus, the energy density can be parametrized using the photon temperature T as follows:

$$\rho_{tot}(T) = g_{eff}^e(T)\overline{\rho_\gamma}(T) = \frac{\pi^2}{30} \cdot g_{eff}^e(T) \cdot T^4 \qquad (3.15)$$

where we have defined $\overline{\rho_\gamma}(T)$ as the energy density of a boson with one degree of freedom and the effective degrees of freedom $g_{eff}^e(T)$ as:

$$g_{eff}^e(T) = \sum_i \frac{15}{\pi^4} g_i \left(\frac{T_i}{T}\right)^4 \int_{x_i}^\infty dz_i \frac{z_i^2 \sqrt{z_i^2 - x_i^2}}{e^{z_i} \pm 1}, \qquad (3.16)$$

where $x_i = m_i/T$, and g_i the internal degrees of freedom of the particle i.

The effective degrees of freedom take into account the effect of particles becoming non-relativistic at $T \approx m$, as well as the possibility that the different particles may contribute to the energy density with different temperatures. In general, the index i runs over all relativistic particles present at the beginning of BBN, which in the standard picture are just photons, electrons, positrons, neutrinos and antineutrinos. Thus, with eq. 3.2 and 3.15, the Hubble parameter may be written as:

$$H(T) = 1.66 \cdot \sqrt{g_{eff}^e(T)} \frac{T^2}{M_{Pl}}, \qquad (3.17)$$

with $M_{Pl} = G^{-1/2} = 1.22 \cdot 10^{19}\,\text{GeV}$.

If the system is in thermodynamic equilibrium, further simplifications can likewise be made for other quantities. Of great importance is entropy, which we will focus on now. This will allow us to relate the definition of entropy density to other thermodynamic quantities, as well as the conditions under which entropy is conserved. As a first step to derive these, it is useful to rewrite the first term of the identity

---

[4]Specific models of dark matter can have strong impacts on Nucleosynthesis through their interactions with the SM particles, but it will be assumed for now that these interactions are negligibly small.

in eq. 3.13 for the case of a Fermi-Dirac (FD) (Bose-Einstein (BE)) distribution as follows:

$$\frac{\partial \mathcal{S}^{\pm}(f_i)}{\partial p} = \ln\left(\frac{f}{1 \mp f}\right)\frac{\partial f}{\partial p} = \frac{\mu_i - E_i}{T} \tag{3.18}$$

After integration by parts of eq. 3.12, the identity can directly be inserted. One further integration by parts to get rid of the partial derivative of the phase-space distribution, and the integrand can be identified with those of eq. 3.3. This leads to the following expression for the entropy of a species in thermodynamic equilibrium:

$$s_i = \frac{\rho_i + P_i - \mu_i n_i}{T} \tag{3.19}$$

Thus, we recover a well known result, as this is equivalent to the Gibbs-Duhem relation for a homogenous system divided by the volume.

Additionally, if the chemical potential is assumed to be negligible and we insert the equation of state for the species $w_i = P_i/\rho_i$, we find that:

$$s = (1 + w_i)\frac{\rho_i}{T} \tag{3.20}$$

so that entropy is $\propto \rho_i/T$. Thus, even though the scaling is slightly different, this equation implies that there is an equally strong hierarchy between relativistic and non-relativistic particles in the entropy as there was for the energy density at the relevant temperatures. This allows us to make a similar parametrization of entropy in terms of the effective degrees of freedom, namely:

$$\boxed{s_{tot} = \frac{2\pi^2}{45}g^s_{eff}T^3} \tag{3.21}$$

with the effective entropy degrees of freedom defined as:

$$g^s_{eff} = \sum_i \rho_i = \sum_i \frac{15}{\pi^4}g_i\left(\frac{T_i}{T}\right)^3 \int_{x_i}^{\infty} dz_i \frac{z_i^2\sqrt{z_i^2 - x_i^2}}{e^{z_i} \pm 1} \tag{3.22}$$

The entropy degrees of freedom have a similar interpretation than those for the energy density and, for the most part, they are interchangeable. However, they have a different scaling in terms of the temperature ratio of the particle species i and the photons, so if there is a relativistic species that is decoupled from the plasma, the two will differ.

We can now also insert the identity from eq. 3.18 into the equation for the time evolution of entropy, eq. 3.14, from which we can easily derive the following equation:

$$\dot{s}_i + 3Hs_i = \frac{\dot{q}_i}{T} - \frac{\mu_i}{T}\left(\dot{n}_i + 3Hn_i\right) \tag{3.23}$$

or, equivalently for the entropy inside a comoving volume S:

$$T\dot{S}_i = \dot{q}_i V - \mu_i \dot{N}_i \tag{3.24}$$

This means that entropy inside a comoving volume for one particle species is conserved if there is either no heat exchange $\dot{q}_i = 0$, i.e. there are no interactions, if

the chemical potential vanishes or if particle number is conserved, either because there are no interactions or the particle is in equilibrium and source and sink terms cancel each other. As entropy is an extensive quantity, the total entropy is the sum of the individual entropies for each species. From the conservation of the energy momentum tensor we know that there is no absolute heat generation, i.e. $\sum_i \dot{q}_i = 0$. Thus, for the total entropy we have that:

$$T\dot{S}_{tot} = -\sum_i \mu_i \dot{N}_i \tag{3.25}$$

Thus, the total entropy density is conserved in thermodynamic equilibrium if the chemical potentials vanishes or the particle number is conserved for all species. If we assume that chemical potentials are neglected, and insert the parametrization for the entropy density from eq. 3.21, the conservation of total entropy gives us:

$$a^3 \cdot g_{eff}^s(T) \cdot T^3 = const. \tag{3.26}$$

This allows us to obtain the scale factor as a function of temperature $a(T)$. All that is needed for that is a reference temperature for which we know the scale factor and the assumption that entropy is conserved until that moment. Taking, for example, the temperature of the CMB today $T_0 = 2.73\,\text{K}$ and the scale factor today $a_0 = 1$, we get:

$$a(T) = \left(\frac{g_{eff}^s(T_0)}{g_{eff}^s(T)} \right)^{\frac{1}{3}} \cdot \frac{T_0}{T} \tag{3.27}$$

If the entropy for a single particle species is conserved, then a similar relation holds, although T then corresponds to the species' temperature, not necessarily equal to that of photons and the effective degrees of freedom vanish. This should not come as a surprise as this is simply the well known effect of redshift.

While this relation is extremely useful and important, there is one crucial element still missing in our considerations, namely the relation between time and temperature, which is of extreme importance as it directly influences the amount of time the neutrons are allowed to free-stream and decay. However, we already have all the necessary ingredients to derive it. We start with the derivative of time with respect to temperature, which using the chain rule can be rewritten as:

$$\frac{\mathrm{d}t}{\mathrm{d}T} = \frac{\mathrm{d}t}{\mathrm{d}a} \cdot \frac{\mathrm{d}a}{\mathrm{d}T} \tag{3.28}$$

From the definition of the Hubble parameter, we know that:

$$\frac{\mathrm{d}t}{\mathrm{d}a} = \frac{1}{a(T)H(T)} \tag{3.29}$$

while the derivative of eq. 3.27 is:

$$\frac{\mathrm{d}a}{\mathrm{d}T} = -\frac{a(T)}{T} \cdot \left(1 + \frac{1}{3} \frac{T}{g_{eff}^s(T)} \frac{\mathrm{d}g_{eff}^s(T)}{\mathrm{d}T} \right) \tag{3.30}$$

Thus, we find that:

$$\frac{\mathrm{d}t}{\mathrm{d}T} = -\frac{1}{HT} \left(1 + \frac{1}{3} \frac{T}{g_{eff}^s(T)} \frac{\mathrm{d}g_{eff}^s}{\mathrm{d}T} \right) \equiv -\frac{1 + \Delta}{HT} \tag{3.31}$$

In order to obtain $t(T)$, we now only need to integrate this equation from a starting time t_0 until t. However, as the Universe expands and cools down extremely quickly at the beginning, if we choose t_0 early enough, the integral between $t = 0$ and $t = t_0$ will contribute very little to the result and we can put it to 0 in the integral. If, additionally, the effective degrees of freedom remain constant during the interval, then the integral can be obtained analytically:

$$t = \frac{1}{2H(T)} \simeq 0.3 \cdot \frac{M_{Pl}}{\sqrt{g_{eff}^e(T)}} \cdot \frac{1}{T^2} \qquad (3.32)$$

However, electrons and positrons become non-relativistic shortly after neutrons and protons freeze-out, so that it is incorrect to assume that the effective degrees of freedom remain constant, leading to corrections to the relation of $\approx 20 - 30\%$. On top of that, this happens during the time where neutrons are free-streaming, so that BBN is especially susceptible to any change in the time-temperature relation. Thus, while eq. 3.32 is extremely useful for an order of magnitude estimate and we will indeed use it, for precise calculations a numerical integration of 3.31 is necessary.

3.2.1 Neutrino Decoupling

With this, we now have essentially all the tools to describe the expansion of the Universe. A key assumption in our description is the fact that we only need to take into account the particles that are relativistic at the beginning of BBN, namely photons, electrons, positrons, neutrinos, and antineutrinos. This allows us to solve for the expansion of the Universe first and then solve the equations describing the abundane of nuclei assuming with the cosmolofical evolution to be in the background and greatly influence BBN, but not vice-versa. This amounts to neglecting the energy density in the form of baryons and the entropy produced in weak reactions in the form of neutrinos. This is all justified because of the overwhelming overabundance of photons, namely that $\eta_B \ll 1$.

The description of electrons and photons is actually quite simple, since they are very tightly coupled because of electromagnetic interactions up to temperatures $T \lesssim 1\,\text{eV} \ll T_{BBN}$ and can be described as a plasma in equilibrium at a temperature T using the simple techniques of equilibrium thermodynamics described in section A.6. The only challenge comes from the fact that that pair production stops being efficient at Temperatures close to the electron mass and thus all of the energy and entropy stored in $e^{\pm}$ gets converted into photons, slowing down the cool-down of the Universe, although more commonly referred to as reheating. This effect, however, is taken into account in the effective degrees of freedom and the time temperature relation of eq. 3.31, so that no further adjustments are necessary to first order. There are, of course, corrections to this from finite temperature QFT, for example QED corrections for the plasma thermodynamics like a shift of the electron and photon mass dependent on temperature. These effects have been calculated and taken into account in the up-to date BBN-codes used throughout this thesis[20, 42, 43, 44, 45].

Already to first order, the situation is more involved for neutrinos. At higher temperatures, they are kept in thermodynamic equilibrium with the plasma mainly

through the following neutral as well as charged current weak force interactions:

$$
\begin{aligned}
\nu + \bar{\nu} &\longleftrightarrow e^+ + e^- \\
\nu + e^\pm &\longleftrightarrow \nu \ + e^\pm \\
\nu + \bar{\nu} &\longleftrightarrow e^+ + e^-
\end{aligned}
\tag{3.33}
$$

Neutron to proton conversion is also mediated by the weak force, so the reaction rate is comparable to those above. Thus, already from this consideration, we see that the moment when neutrinos decouple from the plasma will be around the same time when neutrons and protons do so. Neutrinos being additionally directly involved in the conversion reactions, this inevitably means that neutrino decoupling will greatly influence the events that lead to the formation of nuclei.

In order to determine when the decoupling happens, we can first assume that the process happens instantaneously at the moment when the reaction rate drops below the expansion rate of the Universe, namely:

$$
\Gamma \lesssim H
\tag{3.34}
$$

In order to obtain the reaction rate, we need to look at the electroweak sector of the SM after the Higgs phase transition. As the energies relevant for BBN $T \lesssim \mathcal{O}(10\,\mathrm{MeV})$ are orders of magnitude below the electroweak scale, the effective field theory where the degrees of freedom of the massive bosons have been integrated out is a good approximation given our precision goal. The coupling constant that regulates the strength of interactions is, then, Fermi's constant $G_F = 1.16 \cdot 10^{-5}\,\mathrm{GeV}^{-2}$.

The reaction rate Γ has to be $\propto G_F^2$, which has dimensions of GeV^{-4}, which has to be compensated by a dependence on $E^5 \approx T^5$. Thus, a simple dimensional analysis gives that the rate for these reactions is:

$$
\Gamma \simeq G_F^2 T^5
\tag{3.35}
$$

Compared to the Hubble rate from eq. 3.17 with $g_{eff}^e = 10.75$, this gives:

$$
T_{\nu,f} \simeq \left(\frac{1.66 \sqrt{g_{eff}^e}}{G_F^2 M_{Pl}} \right)^{\frac{1}{3}} \simeq 1.5\,\mathrm{MeV}
\tag{3.36}
$$

The assumption of instantaneous decoupling is that the particles follow their equilibrium distribution until this point, after which interactions are set to zero and particles free-stream. This implies that the source term $\mathcal{J}_i$ in eq. 3.6 and the heating rate $\dot{q}_i$ from eqs. 3.8 vanish. Particle Number is conserved inside a comoving volume and energy only gets redshifted because of the expansion after this point. Additionally, this also leads to entropy being conserved. Thus, for $T_\nu \leq T_{\nu,f}$:

$$
\begin{aligned}
n_\nu(T_\nu) &= n_\nu a^3 \big|_{T_{\nu,f}} \cdot a(T_\nu)^{-3} \\
\rho_\nu(T_\nu) &= \rho_\nu a^4 \big|_{T_{\nu,f}} \cdot a(T_\nu)^{-4} \\
s_\nu(T_\nu) &= s_\nu a^3 \big|_{T_{\nu,f}} \cdot a(T_\nu)^{-3}
\end{aligned}
\tag{3.37}
$$

In principle, this is also the same dependence on the scale factor they would have if they had remained in equilibrium. We can therefore define a brightness temperature for the neutrinos T_ν, which is the temperature neutrinos would have if they were still described by a FD distribution. This implies that:

$$a(T_{\nu,f})T_{\nu,f} = a(T_\nu)T_\nu \tag{3.38}$$

which is similar to the relation between scale factor and photon temperature we obtain from total entropy conservation 3.26. In fact, as long as the effective degrees of freedom do not change, that is, as long as there is no reheating due to pair production freezing out, the two equations are equivalent and neutrinos evolve with the same temperature as photons.

After the temperature drops below $T \leq m_e$, electron-positron pairs annihilate producing a constant stream of photons with $E > T$. These slow down the cooling of the plasma with the expansion. Neutrinos, however, are not produced, so they do not partake in the reheating and their brightness temperature becomes smaller than that of photons.

This effect is already taken into account in the definition of the effective degrees of freedom, since we have allowed the different species to contribute to the energy and entropy density with different temperatures. All we need is to find the ratio between the two temperatures. In order to avoid confusion when deriving it, we will explicitly write which species the temperature corresponds to. We define $T = T_\gamma = T_\nu > T_{\nu,f}$ and $T'_\gamma, T'_\nu < T_{\nu,f}$. All we need now is to relate these two regimes using conservation of entropy for the entire Universe (eq. 3.26) and for neutrinos separately 3.38, which may be rewritten as:

$$\begin{aligned}
g^s_{eff}(T_\gamma)a(T_\gamma)^3 T_\gamma^3 &= g^s_{eff}(T'_\gamma)a(T'_\gamma)^3 T'^3_\gamma \\
a(T_\nu)T_\nu &= a(T'_\nu)T'_\nu
\end{aligned} \tag{3.39}$$

Both T'_ν and T'_γ refer to the same moment in the expansion of the Universe and, thus, to the same scale factor $a(T'_\nu) = a(T'_\gamma)$. For the temperature range relevant here, the effective degrees of freedom are simply:

$$g^s_{eff}(T_\gamma) = g_\gamma + \frac{7}{8}(g_{e^-}(T_\gamma) + g_{e^+}(T_\gamma)) + N_\nu \cdot \frac{7}{8}(g_\nu + g_{\bar\nu})\left(\frac{T_\nu}{T}\right)^3 \tag{3.40}$$

where $N_\nu = 3$ stands for the number of neutrinos in the SM. We can now solve the equation to obtain:

$$\frac{T'}{T'_\nu} = \left(\frac{g^{s,\,no\,\nu}_{eff}(T_\gamma)}{g^{s,\,no\,\nu}_{eff}(T'_\gamma)}\right)^{\frac{1}{3}} \tag{3.41}$$

The superscript $no\nu$ indicates that the neutrino degrees of freedom are not taken into account. The $e^\pm$ degrees of freedom $g_{e^-}(T) = g_{e^+}(T)$ are temperature dependent and change from 2 to 0 over the course of BBN, so that $g^{s,\,no\,\nu}_{eff}(T_\gamma) = 2 + \frac{7}{8}\cdot 4 = \frac{11}{2}$ and after $e^\pm$-annihilation $g^{s,\,no\,\nu}_{eff}(T'_\gamma) = 2$, leading to the canonical value for the neutrino to photon temperature ratio:

$$\frac{T}{T_\nu} = \left(\frac{11}{4}\right)^{\frac{1}{3}} \simeq 1.401 \tag{3.42}$$

which is only valid for temperatures far below the electron mass. Eq. 3.39 is valid for all temperatures, so that we may define $\frac{T_\nu}{T}$ as a function of T, in order to bridge the gap between the two regimes, taking into account the fact that the contribution of electrons varies with temperature.

3.2.2 Baryon to Photon Ratio

A similar relation can be derived for the Baryon to photon ration η_b. This is, as we will see, a crucial quantity for BBN and, in the standard picture, its only unconstrained parameter. As indicated by its name, it is defined as:

$$\eta_B = \frac{n_B}{n_\gamma} \tag{3.43}$$

The baryon number is conserved inside a comoving volume, so $n \propto a^{-3}$, just like for photons, which we can recast in terms of Temperature using Eq. 3.27. For temperatures $\gg 1\,\mathrm{MeV}$, the baryons in the form of nucleons are in equilibrium with the photons, such that $T_B = T_\gamma$. As we will see, baryons decouple from the plasma at $T \approx 0.8\,\mathrm{MeV}$. Thus, they do not partake in the reheating of the bath and, just like with neutrinos, the ratio of baryon to photon temperature departs from one. The derivation of the temperature ratio is analogous to the case of neutrinos, so we find:

$$\frac{T'}{T'_B} = \left(\frac{g^s_{eff}(T_\gamma)}{g^s_{eff}(T'_\gamma)} \right)^{\frac{1}{3}} \tag{3.44}$$

or, defining η_B^0 as the baryon to photon ratio at $T_0 = T_{\mathrm{CMB}}$:

$$\frac{\eta_B}{\eta_B^0} = \frac{g^s_{eff}(T_\gamma)}{g^s_{eff}(T_0)} \tag{3.45}$$

This implies that, for higher temperatures, the baryon to photon ratio increases by a factor of ≈ 2.75 compared to the CMB measured value. However, for $T = T_{\mathrm{BBN}} \approx 0.073\,\mathrm{MeV}$, the ratio is almost one, so that we expect the CMB and BBN to measure the same baryon to photon ratio or, equivalently, the same baryon density.

3.2.3 Incomplete Neutrino Decoupling

Even though the treatment of neutrino decoupling presented above is quite simple, it does allow for a description of the background thermodynamics which leads to predictions accurate to $\propto 2-3\%$. With current measurements of the primordial helium abundance having reached sub-percent precision [18], a better treatment of this crucial aspect of nucleosynthesis has become imperative. This topic has therefore been extensively studied in the last 40 years and seen substantial improvements. Discussing all of these aspects in detail lies beyond the scope of this thesis. However, the most important effects will briefly be reviewed with the reader being referred to [46] and references therein for more details.

The first modification to our treatment is, of course, the simplest and most important one. We have assumed that neutrino decoupling happens instantaneously at

temperatures much higher than the electron mass, when it is clear neither of those assumptions is correct. In reality, neutrino decoupling is a gradual process which extends far beyond the temperatures where electron positron annihilation begins. Thus, in a way, not all neutrinos have decoupled from the thermal bath at temperatures when $e^{\pm}$-reheating begins, so that a part of neutrinos get reheated, leading to an increase in the neutrino energy density and modifying the ratio of photon to neutrino temperature to be slightly below the standard value. Additionally, this leads to spectral distortions in the phase-space distribution of neutrinos that modify the weak rates.

Also the QED corrections to the pressure discussed before influence the neutrino energy density evolution as well, as solving for the neutrino evolution requires a solution of the full coupled Boltzmann equation.

Furthermore, we have treated neutrino species as if they had no flavour and were indistinguishable from each other in their interactions. We also know that neutrinos are not massless and undergo oscillations. From the measured values of the mass differences and the mixing angles, one obtains that neutrinos start oscillating at $T \propto 5 - 10 \, \mathrm{MeV}$. Both of these effects can be taken into account in the solution of the Boltzmann equation. Even though they further enhance the energy density of neutrinos, the main contribution of neutrino oscillations is to equilibrate the phase space distributions of the different flavours and thus weak rates.

Lastly, the key reactions that dictate the process of neutrino decoupling 3.33 have up to now only been calculated at tree level in most computations of BBN. A recent study [46], however, calculated them at NLO and found that this actually decreases the energy density of neutrinos by an amount similar to neutrino oscillations.

All of these effects influence nucleosynthesis in two ways, namely it affects the energy density, and with it the neutrino temperature, and it distorts the phase-space distribution, so that it departs from a FD distribution. The latter effect was found in [20] to be negligible with the current precision aim, while the former effect is the dominant one. It affects the weak reaction rates while simultaneously enhancing the energy density and thus the expansion rate. The increase in the expansion rate means that the Universe is younger when nucleosynthesis starts, so that neutrons have less time to decay, leading to an increased ^{4}He abundance. However, the weak rates are likewise modified in two ways. An increase in the neutrino energy density means tyhat there are simply more neutrinos for neutrons and protons to interact with, leading to an enhancement of the weak rates, so that particles decouple at a lower temperature. With a Boltzmann suppressed distribution, this implies that there are less neutrons available at the end of nucleosynthesis, which comes with a decrease in Helium production. Nevertheless, the increase in neutrino energy comes from a decrease in the plasma energy, which allows nucleosynthesis to happen at higher temperatures, which counteracts the aforementioned effect. It was actually found in [47] that these two effects cancel out, so that the main influence on nucleosynthesis from this is actually purely the change in the time temperature relation from partial neutrino reheating.

It is useful, for a number of reasons that shall become clearer over the course of this thesis, to attribute this increase in energy density to the presence of a non-integer effective number of neutrinos N_{eff}. Since this parameter will be time-dependent and it influences the CMB, it is customary to define it by its value at $T_0 = T_{CMB}$.

Without taking incomplete neutrino decoupling into account, the neutrino energy density in Standard Big Bang Nucleosynthesis (SBBN) is:

$$\rho_\nu(T_0) = \frac{7}{8} \cdot 2 \cdot N_\nu \left(\frac{4}{11}\right)^{\frac{4}{3}} \overline{\rho_\gamma}(T_0) \tag{3.46}$$

The effective description proposed here is obtained by simply allowing N_ν to be different from three by substituting it with N_{eff}. From this, it is simple to define N_{eff}. We will write it in a slightly more cumbersome, yet more widely applicable way as follows:

$$N_{\text{eff}} = \frac{8}{7} \left(\frac{11}{4}\right)^{\frac{4}{3}} \left(\frac{\rho_{rad} - \rho_\gamma}{\rho_\gamma}\right)\bigg|_{T_0} \tag{3.47}$$

In SBBN, the only form of radiation present other than photons are neutrinos. If we further assume that spectral distortions are negligible, their energy density can be characterized by the temperature only, so that N_{eff} may be written as:

$$N_{\text{eff}} = N_\nu \left(\frac{11}{4}\right)^{\frac{4}{3}} \left(\frac{T_\nu}{T}\right)^4 \bigg|_{T_0} \tag{3.48}$$

In the case of instantaneous neutrino decoupling, this will give us the expected result $N_{\text{eff}} = N_\nu = 3$, whereas incomplete decoupling effects will modify the neutrino to photon temperature ratio to be above the standard value and increase N_{eff}. Its value for SBBN has been extensively studied and the most precise calculation to date [46] gives:
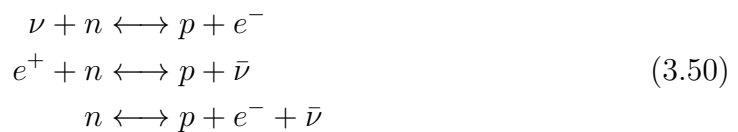
$$N_{\text{eff}} = 3.043 \tag{3.49}$$

This value, as expected, is quite close to three, but nevertheless differs from it by more than 1% and indeed appreciably modifies BBN.

3.3 Neutron Proton Freeze-Out

Now that we know how to describe the expanding Universe in the background and how it affects the events of BBN, we have laid out our canvas and can begin to paint the picture of nucleosynthesis. This picture, of course starts with a description of the first baryons from which all nuclei are formed: neutrons and protons.

In the very early stages of the Universe, the primordial plasma contains essentially free quarks and gluons. As the temperature drops to $T_{QCD} \sim 160\,\text{MeV}$, these quarks and gluons hadronize to produce all sorts of baryons and mesons, including nucleons. These are kept in equilibrium with the plasma and each other through weak reactions that interchange neutrons and protons, namely:

$$\begin{aligned}
\nu + n &\longleftrightarrow p + e^- \\
e^+ + n &\longleftrightarrow p + \bar\nu \\
n &\longleftrightarrow p + e^- + \bar\nu
\end{aligned} \tag{3.50}$$

As long as these reactions are fast enough, no elements can form from neutrons and protons as they are not free for a long enough period of time. Thus, the first

step in describing the formation of elements is the freeze-out of the weak reactions interconverting nucleons. A precise treatment of this non-equilibrium process will necessarily involve a study of the Boltzmann equation 3.4. In general, this would require us to solve a coupled system of equations for all particles involved. Nevertheless, we know from the previous section the phase-space distribution of electrons and neutrinos, and the reactions conserve the overall number of neutrons and protons, so it suffices to only look at the Boltzmann equation for neutrons and from conservation of baryon number obtain the proton density. For concreteness, we will focus first on the forward reaction $n + \nu \longrightarrow p + e^-$.

Our starting point is the Boltzmann equation in the following form:

$$\dot{n}_n + 3Hn_n = \frac{g_n}{(2\pi)^3} \int \frac{d^3\vec{p}_n}{E_n} \, \mathbf{C}[f] \tag{3.51}$$

which in appendix C.3 is shown to be equivalent to:

$$\dot{n}_n + 3Hn_n = -\int d\Pi_e \int d\Pi_\nu \int d\Pi_n \int d\Pi_p \, (2\pi)^4 \delta^4(p_n + p_\nu - p_p - p_e)$$
$$\overline{|M|}^2 \cdot f_n f_\nu (1 - f_p)(1 - f_e) \tag{3.52}$$

We have suppressed the dependencies of the phase-space distribution and used the shorthand notation for the integral over the lorentz invariant phase-space $d\Pi_i = \frac{d^3\vec{p}}{(2\pi)^3 2E_i}$. In general, f is function of Energy, temperature and chemical potential in equilibrium $f = f(E_i, T_i, \mu_i)$. In SBBN, the chemical potential is assumed to be negligible, as both μ_ν, μ_e depend on the baryon chemical potential, whose value can be related to the Baryon Asymmetry making it negligibly small compared to the Energy of the particles. We will relax that assumption later on and explain why that is justified, but for now we will assume both to be zero.

Before BBN begins, the nucleons are in equilibrium, and their abundances Boltzmann-suppressed. Thus, the Pauli-blocking factor $(1 - f_p) \approx 1$, which already simplifies the equation. As for the blocking factor for electrons and neutrinos, the following identity for a FD distribution:

$$1 - f(E) = f(-E) \tag{3.53}$$

is helpful to simplify the expression. Additionally, we can now integrate over the proton phase-space using the delta distribution for three-momentum, which amounts to simply enforcing in the following expressions that:

$$\vec{p}_p = \vec{p}_n + \vec{p}_\nu - \vec{p}_e \tag{3.54}$$

With these simplifications and making the dependencies of the phase-space densities explicit, the equation now looks as follows:

$$\dot{n}_n + 3Hn_n = -\int d\Pi_e \int d\Pi_\nu \int d\Pi_n \, \frac{\pi}{E_p} \delta(E_n + E_\nu - E_p - E_e)$$
$$\overline{|M|}^2 \cdot f_n(E_n, \mu_n) f_\nu(E_\nu) f_e(-E_e) \tag{3.55}$$

3.3.1 Fermi Theory of the Weak Rates

In order to continue, we need to have a closer look at the matrix element $\overline{|M|}^2$, which for the energies of interest can be calculated to satisfactory precision from Fermi theory, which is the low-energy Effective Field Theory (EFT) of the electroweak interaction with protons and neutrons, not quarks and gluons, as the fundamental one-particle states. The Fermi theory describes how nucleons interact with the standard model leptons. The interaction Lagrangian contains the V-A structure of the SM weak sector, with a term that describes the neutral current interactions mediated by the Z-boson, as well as charged current interactions mediated by the W-bosons. The latter is the reaction we will focus on now as the weak reactions interchanging nucleons are of this type.

The interaction Lagrangian for this theory has the following form:

$$\mathcal{L}_{\mathrm{I}} = -\frac{G_F}{\sqrt{2}} \left(\left[J_{ij}^{CC} \right]_{\mu}^{\dagger} \left[J_{lk}^{CC} \right]^{\mu} \right) \tag{3.56}$$

where there is one charged current associated to each $SU(2)$-doublet of the Standard model. Of interest for us will be those of the nucleons as well as electrons and neutrinos, which look as follows:
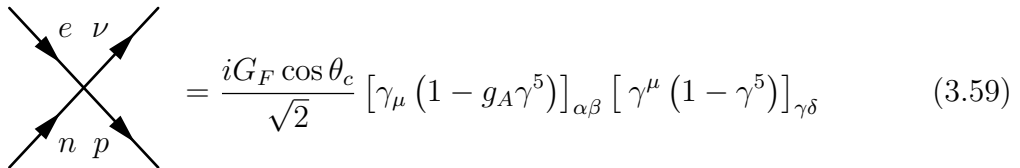
$$\begin{aligned} \left[J_{np}^{CC} \right]^{\mu} &= \cos\theta_c \cdot \overline{n} \, \gamma^{\mu} \left(1 - g_A \gamma^5 \right) p \\ \left[J_{\nu e}^{CC} \right]^{\mu} &= \overline{\nu} \, \gamma^{\mu} \left(1 - \gamma^5 \right) e \end{aligned} \tag{3.57}$$

where, as expected, the neutrino charged current exhibits full parity violation, whereas the charged current of the nucleon doublet is only partially violated as parametrized by the axial coupling g_A. Additionally, the Cabbibo angle $\cos\theta_c$ from the CKM matrix appears, accounting for the fact that the u, d valence-quarks that make up the nucleons are not the states that interact with the W bosons.

The interaction of interest is then described by the following Lagrangian:

$$\mathcal{L}_{\mathrm{I}} = -\frac{G_F}{\sqrt{2}} \cos\theta_c \overline{p} \, \gamma_{\mu} \left(1 - g_A \gamma^5 \right) n \overline{\nu} \, \gamma^{\mu} \left(1 - \gamma^5 \right) e \tag{3.58}$$

from which we can obtain the following rule for the four fermion interaction:

 $$= \frac{iG_F \cos\theta_c}{\sqrt{2}} \left[\gamma_{\mu} \left(1 - g_A \gamma^5 \right) \right]_{\alpha\beta} \left[\gamma^{\mu} \left(1 - \gamma^5 \right) \right]_{\gamma\delta} \tag{3.59}$$

All that is left to obtain the matrix-element for the process is to multiply this vertex with the correct initial and final state polarization spinors $u(s,p)$, $v(s,p)$ that come from the general solution to the free Dirac equation, depending on which reactions are of interest. For the case of $n + \nu \longleftrightarrow p + e^-$, we therefore find:

$$M = \frac{iG_F \cos\theta_c}{\sqrt{2}} \left[\overline{u}_p \gamma_{\mu} \left(1 - g_A \gamma^5 \right) u_n \right] \left[\overline{u}_e \gamma^{\mu} \left(1 - \gamma^5 \right) u_{\nu} \right] \tag{3.60}$$

The quantity that enters the collision term is the spin-averaged absolute value squared of the matrix element, which in our case, since neutrinos only have one spin polarization, gives:

$$\overline{|M|}^2 = \frac{1}{2} \sum_{s_i} |M|^2 = \frac{1}{2} \sum_{s_i} \frac{G_F^2 \cos^2 \theta_c}{2} \left[\overline{u}_p \gamma_\mu \left(1 - g_A \gamma^5 \right) u_n \right] \left[\overline{u}_n \gamma_\nu \left(1 - g_A \gamma^5 \right) u_p \right]$$
$$\left[\overline{u}_e \gamma^\mu \left(1 - g_A \gamma^5 \right) u_\nu \right] \left[\overline{u}_\nu \gamma^\nu \left(1 - g_A \gamma^5 \right) u_e \right] \quad (3.61)$$

where the sum is over the spins of all particles. Using the completeness relation for a particle of mass m and momentum p:

$$\sum_s u_\alpha(p, s) \overline{u}_\beta(p, s) = \not{p} + m \quad (3.62)$$

and with some standard manipulations, we find that:

$$\overline{|M|}^2 = \frac{G_F^2 \cos^2 \theta_c}{4} \mathrm{Tr} \left[\gamma_\mu \left(1 - g_A \gamma^5 \right) \left(\not{p}_n + m_n \right) \gamma_\nu \left(1 - g_A \gamma^5 \right) \left(\not{p}_p + m_p \right) \right]$$
$$\cdot \mathrm{Tr} \left[\gamma^\mu \left(1 - \gamma^5 \right) \not{p}_\nu \gamma^\nu \left(1 - \gamma^5 \right) \left(\not{p}_e + m_e \right) \right] \quad (3.63)$$

All that is left now is to simplify the trace using some straight-forward, yet slightly tedious, algebra with gamma matrices, which can also be left to a computer algebra system, giving:

$$\overline{|M|}^2 = 16 G_F^2 \cos^2 \theta_c \left[\left(g_a^2 - 1 \right) m_n m_p \left(p_\nu \cdot p_e \right) + \left(g_a - 1 \right)^2 \left(p_n \cdot p_\nu \right) \left(p_p \cdot p_e \right) \right.$$
$$\left. + \left(g_a + 1 \right)^2 \left(p_n \cdot p_e \right) \left(p_\nu \cdot p_p \right) \right] \quad (3.64)$$

which, without specifying the momentum of the particles is the best we can do. This result can now be inserted into eq. 7.9.

This has been derived only for one specific reaction, namely $n + \nu \rightarrow p + e^-$. However, all six reactions in eq. 3.50 have the same matrix element. The reason is that, first of all, forward reactions involving a neutron can be obtained from crossing symmetry of electrons and neutrinos. Crossing symmetry, in this case [48], amounts to $p_\nu \rightarrow -p_\nu$ and an overall minus sign in the matrix element for neutrinos, and the same for electrons. Inserting this into eq. 3.64, it is trivial to see that the matrix element is invariant under this symmetry. Additionally, the backward reaction is obtained through time reversal or, equivalently, through CP conjugation. CP is conserved at this level, so the matrix element likewise remains invariant for the proton reactions. Thus, all that changes are the kinematics of the integral in the Boltzmann equation as well as the weighting by the phase-space distribution.

3.3.2 Born Approximation

We return to eq. 7.9. In principle, all that is left is to perform the integration, which is not easy for a 9-D integral. It may be reduced to 8-D with the Dirac distribution, and isotropy of the neutrino and electron distribution functions allows us to perform the integral over all angular dimensions but one, leaving us with an, overall, 5-D integral in the end. This is the method followed in, e.g. [49]. However,

it is simpler and faster to make use of the special kinematic situation at hand. Let us assume we are in the rest frame, so that

$$m_n + E_\nu = E_p + E_e$$

We have an interaction that involves nucleons with mass $m_n \sim 939\,\text{MeV}$ and thermal neutrinos whose energy is $E \sim T \ll m_n$. Expanding the proton energy in the non-relativistic limit, one finds:

$$\frac{p_p^2}{2m_p} \lesssim Q + T - E_e \sim \mathcal{O}(1\,\text{MeV}) \ll m_p$$

That is, the maximal momentum transferred to the proton will be orders of magnitude smaller than its rest mass, so $E_p \approx m_p$ or, equivalently:

$$E_e - E_\nu \simeq m_n - m_p = Q$$

This allows us to significantly simplify the integral. One can, as a next step, make a Fokker-Planck expansion of the energy difference in terms of $\frac{T}{m_N}$ and calculate corrections to this approximation. For now, we will start with the lowest order and postpone a discussion of the impact of these corrections to later on and stay in the so-called Born approximation.

This allows us to significantly simplify eq. 3.64, as the momentum of nucleons can be neglected compared to their mass. Thus, the dot-products involving nucleons simplify to:

$$p_{n/p} \cdot p_{\nu/e} = m_{n/p} E_{\nu/e} \tag{3.65}$$

such that the matrix element becomes:

$$\overline{|M|}^2 = 16 G_F^2 \cos^2 \theta_c \left[\left(1 + 3g_A^2\right) m_n m_p E_\nu E_e + \left(g_a^2 - 1\right) m_n m_p E_\nu p_e \cos\theta \right] \tag{3.66}$$

with θ the angle between the incoming neutrino and the outgoing electron momentum. This is already a massive simplification, as now the matrix element contains two terms: one that is only dependent on E_ν and E_e and another that also has an angular dependence. Nevertheless, it is an odd function of $\cos\theta$, which will be integrated over a symmetric interval, so the contribution vanishes. Now, we can insert this into the Boltzmann equation to find:

$$\dot{n}_n + 3H n_n = -\int d\Pi_e \int d\Pi_\nu \int d\Pi_n \frac{\pi}{m_p} \delta(E_e - E_\nu - Q) \cdot 16 G_F^2 \cos^2 \theta_c \left(1 + 3g_A^2\right)$$
$$m_n m_p E_\nu E_e \cdot f_n(E_n, \mu_n) f_\nu(E_\nu) f_e(-E_e) \tag{3.67}$$

The factor $m_n m_p E_\nu E_e$ cancels with the normalization of $d\Pi_i$, so the only dependence on the neutron momentum is in the phase-space density, which integrated over phase-space gives the number density (eq. 3.3). Thus, we find:

$$\dot{n}_n + 3H n_n = -n_n \Gamma_{n\nu \to pe} \tag{3.68}$$

where we have defined the reaction rate $\Gamma_{n\nu \to pe}$ as everything that remains after factoring out n_n, that is:

$$\Gamma_{n\nu \to pe} \equiv 2\pi G_F^2 \cos^2 \theta_c \left(1 + 3g_A^2\right) \int \frac{d^3\vec{p}_e}{(2\pi)^3} \int \frac{d^3\vec{p}_\nu}{(2\pi)^3} \, \delta(E_e - E_\nu - Q) \cdot f_\nu(E_\nu) f_e(-E_e) \tag{3.69}$$

We can now proceed to writing the differential in spherical coordinates $d^3\vec{p} = p^2 dp d\Omega$ and integrate over the solid angle, which for a homogeneous function gives simply a factor of $(4\pi)^2$ leaving us with:

$$\Gamma_{n\nu \to pe} = \frac{G_F^2 \cos^2 \theta_c}{2\pi^3} \left(1 + 3g_A^2\right) \int_0^\infty p_e^2 dp_e \int_0^\infty p_\nu^2 dp_\nu \; \delta(E_e - E_\nu - Q) \cdot f_\nu(E_\nu) f_e(-E_e) \tag{3.70}$$

We now have a double integral over the momenta of the electron and neutron over a functions whose natural variable is actually the energy, rather than momentum. Thus, it is sensible to make a change of variables using the energy-momentum relation $E^2 = m^2 + p^2$, which gives $pdp = EdE$ and adjusting the limits of integration. This leaves us with:

$$\Gamma_{n\nu \to pe} = \frac{G_F^2 \cos^2 \theta_c}{2\pi^3} \left(1 + 3g_A^2\right) \int_{m_e}^\infty dE_e \int_0^\infty dE_\nu \; \delta(E_e - E_\nu - Q) \cdot p_e E_e E_\nu E_\nu \cdot f_\nu(E_\nu) f_e(-E_e) \tag{3.71}$$

It is trivial now to perform the integral over the neutrino energy because of the Dirac distribution by simply setting $E_\nu = E_e - Q$ whenever the condition inside it is met, i.e. when $E_e \geq Q$. This leaves us with:

$$\Gamma_{n\nu \to pe} = \frac{G_F^2 \cos^2 \theta_c}{2\pi^3} \left(1 + 3g_A^2\right) \int_Q^\infty dE_e \; (E_e - Q)^2 \, E_e \sqrt{E_e^2 - m_e^2} \cdot f_\nu(E_e - Q) f_e(-E_e) \tag{3.72}$$

In principle, this is as far as we can go, since this integral does not have an analytic solution. In order to simplify the numerical integration, it is best to work with dimensionless variables. We therefore define:

$$\epsilon = \frac{E_e}{m_e}, \quad q = \frac{Q}{m_e} \tag{3.73}$$

which after performing the change of variables gives us the final version of the reaction rate :

$$\Gamma_{n\nu \to pe} = \frac{G_F^2 \cos^2 \theta_c}{2\pi^3} \left(1 + 3g_A^2\right) m_e^5 \int_q^\infty d\epsilon \; \epsilon \, (\epsilon - q)^2 \, \sqrt{\epsilon^2 - 1} \cdot f_\nu(\epsilon - q) f_e(-\epsilon) \tag{3.74}$$

This is only one of the six weak reactions that maintain neutrons and protons in equilibrium with the bath. Nevertheless, all other reactions can be obtained in an analogous matter with the result for the Boltzmann equation being a sum of all contributions. We will start with the reactions involving a neutron in the initial state. The matrix element is the same for all reactions, so only two modifications to do with the thermal average of the energies and the conservation of energy are necessary, concretely:

1. The phase-space density of $e^\pm$, assuming a thermal distribution, only gets modified as $f_e = f_e(\alpha_e E)$, where $\alpha_e = 1$ for an e^+ initial state and $\alpha_e = -1$ for an e^- final state. The same holds for neutrinos if their chemical potential is negligible.

2. The second modification is to the kinematics. Using the same definitions for α_ν, α_e, it is easy to show from energy conservation that, in the Born approximation, $Q + \alpha_e E_e + \alpha_\nu E_\nu = 0$, which is the condition the δ-distribution enforces, dictating the neutrino energy upon integration as well as the limits of integration for E_e.

With these two modifications, the Boltzmann equation has the same form for all reactions and we just have to sum over them, so it now looks as follows:

$$\dot{n}_n + 3Hn_n = -n_n \left(\Gamma_{n\nu \to pe} + \Gamma_{ne \to p\nu} + \Gamma_{n \to pe\nu} \right) \tag{3.75}$$

with the reaction rates taking the following form:

$$\Gamma_{n\nu \to pe} = K \int_q^\infty d\epsilon \, \epsilon \, (\epsilon - q)^2 \sqrt{\epsilon^2 - 1} \cdot f_\nu(\epsilon - q) f_e(-\epsilon)$$

$$\Gamma_{n \to pe\nu} = K \int_1^q d\epsilon \, \epsilon \, (\epsilon - q)^2 \sqrt{\epsilon^2 - 1} \cdot f_\nu(\epsilon - q) f_e(-\epsilon) \tag{3.76}$$

$$\Gamma_{ne \to p\nu} = K \int_1^\infty d\epsilon \, \epsilon \, (\epsilon + q)^2 \sqrt{\epsilon^2 - 1} \cdot f_\nu(-(\epsilon + q)) f_e(\epsilon)$$

$$\text{with } K \equiv \frac{G_F^2 \cos^2 \theta_c \left(1 + 3g_A^2\right) m_e^5}{2\pi^3}$$

We define the sum of all reaction rates converting neutrons to protons, since it will be useful later on, as:

$$\Gamma_{n \to p} = K \int_1^\infty d\epsilon \, \epsilon \sqrt{\epsilon^2 - 1} \left[(\epsilon - q)^2 f_\nu(\epsilon - q) f_e(-\epsilon) + (\epsilon + q)^2 f_\nu(-(\epsilon + q)) f_e(\epsilon) \right] \tag{3.77}$$

It is now quite straightforward to obtain the reaction rates for backward reactions. Nothing changes in the derivation except that we factor out the proton number density and the fact that the signs of the energy in the neutrino and electron phase-space densities flip, leading to:

$$\Gamma_{pe \to n\nu} = K \int_q^\infty d\epsilon \, \epsilon \, (\epsilon - q)^2 \sqrt{\epsilon^2 - 1} \cdot f_\nu(-(\epsilon - q)) f_e(\epsilon)$$

$$\Gamma_{pe\nu \to n} = K \int_1^q d\epsilon \, \epsilon \, (\epsilon - q)^2 \sqrt{\epsilon^2 - 1} \cdot f_\nu(-(\epsilon - q)) f_e(\epsilon) \tag{3.78}$$

$$\Gamma_{p\nu \to ne} = K \int_1^\infty d\epsilon \, \epsilon \, (\epsilon + q)^2 \sqrt{\epsilon^2 - 1} \cdot f_\nu(\epsilon + q) f_e(-\epsilon)$$

One can likewise define the sum of all rates converting protons to neutrons as $\Gamma_{p \to n}$. It is easy to see by comparing eqs. 3.77 and 3.78 that the two are related by:

$$\Gamma_{p \to n} = \Gamma_{n \to p}(-q) \tag{3.79}$$

One thing we have not paid too close attention to is the factor in front of the rates. This factor is determined by the numerical value of Fermi's constant and the Cabbibo angle. These can be related to the value of the neutron lifetime as measured in experiments. It turns out that the precision on τ_n is greater than the

combined error that would come from using the independent measurement of both quantities. Thus, it is customary to write K in terms of τ_n instead of G_F and $\cos\theta_c$. The inverse of the neutron lifetime corresponds to $\Gamma_{n\to pe\nu}$ at zero temperature:

$$\frac{1}{\tau_n} = K \int_1^q d\epsilon \, \epsilon \, (\epsilon - q)^2 \sqrt{\epsilon^2 - 1} \equiv K\lambda_0 \tag{3.80}$$

where $\lambda_0 \simeq 1.636$. From this, one can obtain that

$$K = \frac{1}{\lambda_0 \tau_n} \tag{3.81}$$

It should be noted that this calibration through the neutron lifetime has a caveat, namely that there is currently an unresolved tension in the experimental value measured in two different types of experiments by more than 4σ, see [50] for a review of this problem and its influence for BBN. We will postpone a discussion to the end of this chapter and, throughout the thesis, use the mean value proposed by the PDG $\tau_n = (878.4 \pm 0.5)\,\text{s}$ [28] unless explicitly stated otherwise.

With this, we have now derived the contribution to the Boltzmann equation governing the evolution of neutrons and protons in the early Universe in the Born Approximation at early times as:

$$\dot{n}_n + 3Hn_n = \Gamma_{p\to n}n_p - \Gamma_{n\to p}n_n \tag{3.82}$$

One can factor out the dilution effect due to the expansion of the Universe by defining the quantity $X_{n,p} = \frac{n_{n,p}}{n_B}$, where we have used the fact that Baryon number is conserved. Additionally, since at the early stages of BBN neutrons and protons are the only abundant baryons, we have that $n_B = n_n + n_p$, or equivalently $X_n + X_p = 1$. Equation 3.82 can therefore be recast as:

$$\dot{X}_n = \Gamma_{p\to n}\left(1 - X_n\right) - \Gamma_{n\to p}X_n \tag{3.83}$$

The final result has the simple form of a master equation that one would have naively expected from such a process; that is, the net change in particle number inside a comoving volume is only dependent on the difference between the creation and destruction rate.

There is one aspect that is not apparent in this equation, namely the role the expansion of the Universe plays in this, which we know should be crucial. The phase-space distributions are a function of temperature, whereas we are integrating over time. The expansion is disguised in the time-dependence of the photon temperature. Temperature, or rather its inverse ratio $y = \frac{m_e}{T}$ with respect to a reference value (here the electron mass), is a better quantity to describe the evolution of the Universe, so we will solve for $X_n(y)$ and then, if needed, find its time dependence through eq. 3.32. All we need to do is rewrite the differential using the chain rule and eq. 3.31, which results in:

$$\frac{dX_n}{dy} = \frac{1 + \Delta}{Hy}\left[\Gamma_{p\to n}\left(1 - X_n\right) - \Gamma_{n\to p}X_n\right] \tag{3.84}$$

Thus, as expected, the ratio between the reaction and expansion rate dictates the evolution of the neutron abundance, especially when the particles depart from equilibrium, that happens when $\Gamma/H \ll 1$.
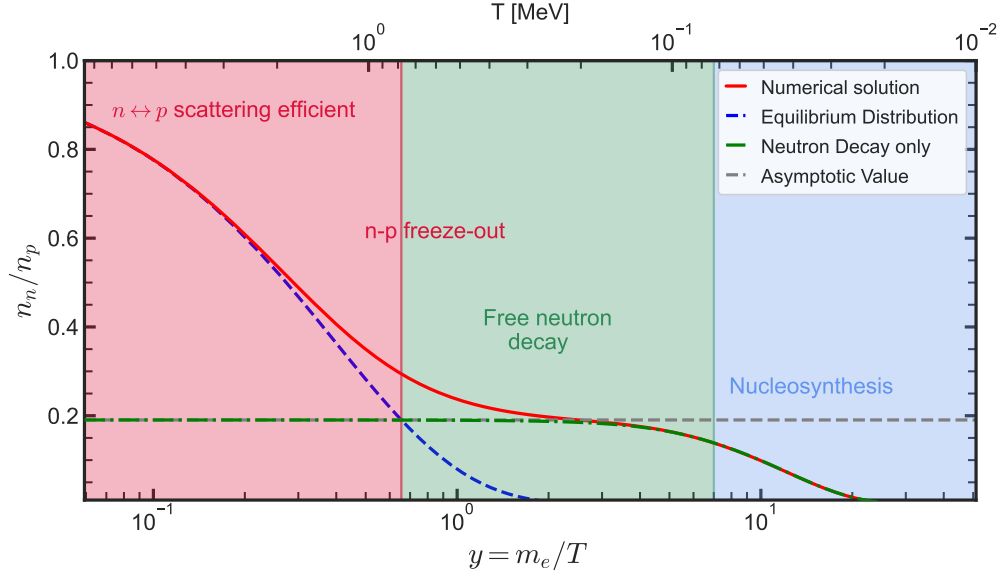
Figure 3.3: Evolution of the neutron to proton ratio obtained as a solution of eq. 3.84, highlighting the contributions from different reactions. The solid red line is the full numerical solution, the dashed blue line is the equilibrium distribution, while the dash-dotted green line describes the free neutron decay $\propto e^{-t/\tau_n}$ of the asymptotic value of n_n/n_p if the neutron would not decay, which is also shown as the grey-dashed line.

This equation can be solved numerically to obtain the evolution of the neutron mass fraction X_n, from which the neutron-to-proton ratio can be obtained. The evolution of $\frac{n_n}{n_p}$ as a function of y is shown as the red line on Fig. 3.3. This figure is extremely useful to explain the three stages that neutrons and protons go through before being cast into nuclei and explain to what their ratio is most sensitive.

At high energies, the reaction rate is much larger than the expansion rate. The system is extremely responsive and very quickly adapts to a change in temperature to remain in thermodynamic equilibrium following a Maxwell Boltzmann distribution. As we have assumed that the neutrino and electron chemical potentials are negligible, this implies that $\mu_n = \mu_p$. If we neglect effects $\sim \mathcal{O}\frac{Q}{T}$, the neutron to proton ratio is then:

$$\frac{n_n}{n_p} = e^{-\frac{Q}{T}} \tag{3.85}$$

which is what is shown as the blue dashed line on fig. 3.3. We can clearly see that X_n indeed follows an equilibrium distribution for high temperatures. Here, the only important quantity is the mass difference and how long they actually remain in equilibrium.

This is dictated by the $n \longleftrightarrow p$-scattering reactions. As the Universe expands and cools down, the scattering reactions freeze-out. The ratio between reaction and expansion rate drops below unity at

$$T_f \simeq 0.8 \, \text{MeV} \tag{3.86}$$

Before that moment, neutrons essentially follow an equilibrium distribution and the

neutron to proton ratio has the following value:

$$\left.\frac{n_n}{n_p}\right|_{T_f} = e^{-\frac{Q}{T_f}} \simeq 0.16 \tag{3.87}$$

Thus, the n-p ratio at this stage is exponentially sensitive to any change in the strength of the interactions, either through modifications of the of e, ν phase-space distributions, the normalization of the overall rates, effectively modifying the neutron lifetime, or simply by adding corrections to the weak rates calculated here.

After decoupling, neutrons are free and only efficiently decay, so that the evolution follows an exponential decay:

$$\frac{n_n}{n_p}(t) = \left.\frac{n_n}{n_p}\right|_{T_f} e^{-\frac{t}{\tau_n}} \tag{3.88}$$

This evolution is shown as the green dash-dotted line, while the grey dashed line shows the asymptotic value of $X_n = 0.16$. This indeed very closely approximates the numerical solution for later times. There is an interval between those two regimes where only the numerical solution gives the right behavior. However, it is safe to say that the qualitative picture presented here and that helped develop nucleosynthesis in the early 1950s is quite accurate for this epoch of BBN.

If this were the whole story, we would not be here today. At some point, nucleosynthesis begins. The time between the onset of BBN and the freeze-out determines how many neutrons are available to be cast into nuclei. There are, therefore, two main effects that influence the ratio here: the neutron lifetime and the time difference between the onset of nucleosynthesis and the decoupling. This last part is dictated by the t-T relation, that is, by the thermodynamics of the Universe's background expansion. Additionally, the onset of nucleosynthesis is influenced by the rate of dissociation of heavier nuclei. In principle, this would mean that, once we drop below the binding energy formation begins. However, there are way too many photons present. Thus, it is at this stage where the importance of the baryon to photon ratio shows up for the first time.

All in all, this highlights the complex interplay of particle physics and cosmology that makes the accurate prediction already of the neutron to proton ratio only such an amazing accomplishment and the potential it has to constrain new physics because of its extreme sensitivity to any effect that modifies either aspect in the chain of events presented here.

3.3.3 Corrections to the Weak Rates

The treatment presented here in the Born Approximation at tree level is already accurate to a few percent. However, just as with the decoupling of neutrinos and the background evolution in general, in order to obtain a prediction that matches the accuracy of experiments, we must predict the neutron to proton ratio with much better precision. Likewise, extensive research has been undertaken to correct the above treatment of the neutron to proton decoupling. Calculating these corrections lies beyond the scope of this thesis, but the reader is referred to [20] for a review on this topic. Additionally, in the state of the art codes PRIMAT and PArthENoPE used in this thesis, these corrections have been implemented.
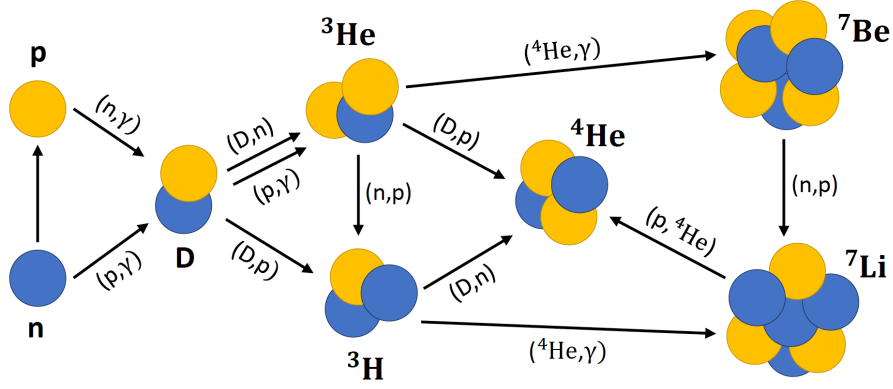
Figure 3.4: Diagram of a simplified nuclear reaction network for nuclei up to ^7Be including the most important reactions only. The arrows indicate the direction of the reactions. The brackets, along with the nuclei at the beginning and the end of the reaction are commonly used as a shorthand notation, where X(a,b)Y is equivalent to $X + a \rightarrow Y + b$. Some photodissociation reactions that are important at the early stages only are missing. Figure from [23]

3.4 Nuclear Reactions

Once neutron to proton conversion rates freeze out, nucleons are finally free and can be cast into heavier nuclei. This happens through a complex network of nuclear reactions. A significantly simplified version of this, involving only the most abundant nuclei D, T, ^3He, ^4He, 7^Li, ^7Be, is shown on Fig. 3.4. We can see that even the formation of Helium requires the presence of lighter nuclei, particularly of deuterium. However, the overwhelming presence of highly energetic photons causes the few nuclei that are able to form to dissociate almost instantly. Through these reactions, baryons reach a state of equilibrium for high energies, called Nuclear Statistical Equilibrium Nuclear Statistical Equilibrium (NSE).

3.4.1 Nuclear Statistical Equilibrium

In principle, once nuclei are in kinetic equilibrium, that is a type of equilibrium that is maintained only through elastic scattering processes of the type $a + i \longleftrightarrow a + i$, they follow a Maxwell Boltzmann distribution. We will assume that kinetic equilibrium is maintained throughout the entire process of nucleosynthesis for nuclei as well as for neutrons and protons. This means that the abundance of an isotope i has the following form

$$n_i = g_i \left(\frac{m_i T}{2\pi} \right)^{\frac{3}{2}} e^{-\left(\frac{m_i - \mu_i}{T} \right)} \tag{3.89}$$

with $g_i = 2s_i + 1$ and s_i the particle's spin. Additionally, for Nuclear Statistical Equilibrium (NSE) to obtain, the photodissociaton reactions must be in equilibrium. These reactions are of the type:

$$Z \cdot p + (A - Z) \cdot n \longleftrightarrow {}_Z^A X + \gamma \tag{3.90}$$

where A is the mass number of the isotope, Z its atomic number, that is the number of protons, and the photon is emitted or absorbed with the nucleus' binding energy $E_\gamma = B_i$. Thus, these reactions change the nature of particles and lead to chemical equilibrium being obtained, which implies, with $N = A - Z$, that:

$$\mu_i = Z\mu_p + N\mu_n \tag{3.91}$$

so that we can obtain the chemical potential for i from that of nucleons, which we can obtain from the neutron and proton abundances, that are $\propto e^{\frac{\mu}{T}}$ as well. Thus, we find the equilibrium abundance of a nucleus i in terms of the neutron and proton abundances can be rewritten as:

$$n_i = \frac{g_i m_i^{3/2}}{2^A} \left(\frac{n_p}{m_p^{3/2}}\right)^Z \left(\frac{n_n}{m_n^{3/2}}\right)^N \left(\frac{2\pi}{T}\right)^{\frac{3(A-1)}{2}} e^{\frac{B_i}{T}} \tag{3.92}$$

where we used the following definition of the binding energy:

$$B_i = Zm_p + Nm_n - m_i \tag{3.93}$$

Just like we did for the neutron to proton abundances, we will now define a comoving quantity where the dilution due to the expansion of the Universe cancels out, the baryon fraction

$$X_i = \frac{n_i}{n_B} \tag{3.94}$$

Using $n_B = \eta_B n_\gamma$ and inserting the explicit definition for n_γ from Eq. A.17, it is straight-forward to show:

$$X_i^{NSE} = g_i \zeta(3)^{A-1} 2^{\frac{3A-5}{2}} \pi^{\frac{1-A}{2}} \left(\frac{m_i T^{A-1}}{m_p^Z m_n^N}\right)^{\frac{3}{2}} \eta_B^{A-1} X_p^Z X_n^N e^{\frac{B_i}{T}} \tag{3.95}$$

The evolution of the NSE mass fractions $Y_i = A_i X_i$ for the lightest nuclei of interest for BBN, using the result of eq 3.84 for X_n and X_p, is shown on figure 3.5. For high temperatures, we see that all abundances are many orders of magnitude below that of neutrons and protons, so the assumption that has been made in neglecting heavier nuclei is correct. This is due to the fact that the NSE abundance is $\propto \eta_B^{A-1}$, so the heavier the isotope, the further it is suppressed by the baryon-to-photon ratio, and the higher $e^{\frac{B_i}{T}}$ has to be to compensate for it.

As temperature drops, the photodissociation rate decreases and the nuclear abundances increase very rapidly to values above 1, which should be impossible because of baryon number conservation. This is a clear indication that the NSE description breaks down at some point, which is to be expected, as we have completely neglected baryon number conservation in the derivation of the NSE abundances. Thus, for example, helium gets produced very rapidly from an endless stock of neutrons and protons, which is not the case in reality, of course.

´Once the abundances depart from their NSE values and become comparable to X_n, one can say that BBN begins, as this implies there must be a significant production of nuclei. A more precise statement can be given if we look at the simplified reaction network on fig. 3.4. We see that neutrons and protons get cast
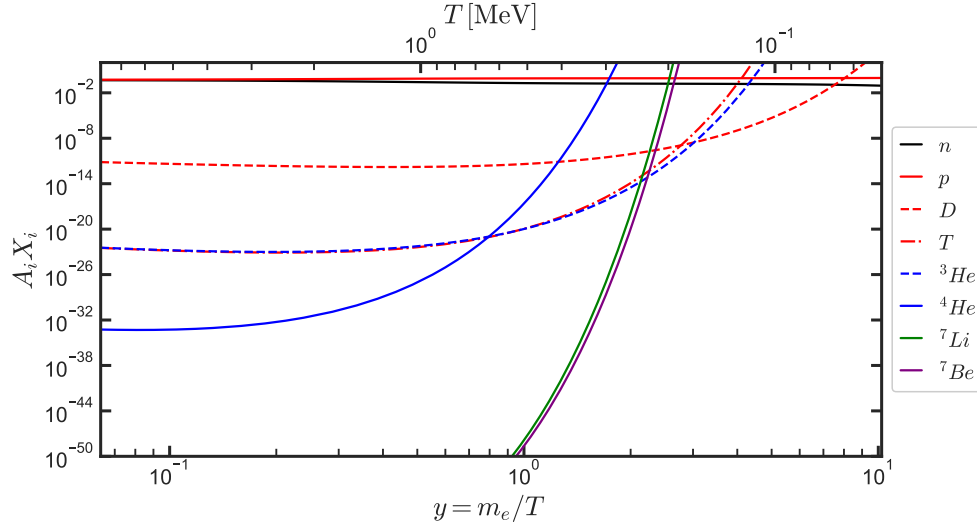
Figure 3.5: Evolution of Nuclear Statistical Equilibrium mass fractions $Y_i = A_i \cdot X_i$ according to eq. 3.95 for isotopes up to ^7Be.

directly into Deuterium. N-body reactions with $N > 2$ are highly suppressed, so the production of heavier nuclei requires at least one deuterium nucleus, if not two. BBN does not really get underway until the abundance of deuterium reaches a significant amount. This is what is commonly referred to as the deuterium Bottleneck and it is the second reason, along with the high small value of η_B, that the onset of nucleosynthesis is set back to lower temperatures and later times, allowing neutrons to decay for a longer time and decreasing the total abundance of nuclei.

For this reason, Deuterium is the central element dictating when nucleosynthesis can begin. By estimating when the NSE abundance of deuterium becomes compara-ble to X_n, NSE breaks down and BBN begins. A good estimate for the corresponding temperature T_D at which "the deuterium bottleneck breaks" can, therefore, be found by setting $X_D \simeq X_n$ in eq.3.95. This equation can be solved numerically to find:

$$
\begin{aligned}
T_D &\simeq 0.07 \, \text{MeV} \\
\Leftrightarrow t_D &\simeq 260 \, \text{s}
\end{aligned}
\tag{3.96}
$$

While it is of crucial importance that the value of $\eta_B \ll 1$ in order for T_D to be so low and allow neutrons to decay freely for a significant period of time, it is only logarithmically dependent on η_B.

After the deuterium bottleneck has been broken, nucleosynthesis proceeds ex-tremely fast, with most nuclei having been formed only seconds after that. This is an extremely complex non-equilibrium process that, of course, requires us to look at the Boltzmann equation again.

3.4.2 Boltzmann Equation for Nuclear Reaction Network

As can be seen on Fig. 3.4, the most relevant reactions for nucleosynthesis are four-body reactions. We will first look at how to derive the Boltzmann equation for a general Boltzmann equation for one single four-body reaction $a + b \rightarrow j + k$. Then

we will show how the backward reaction may be obtained. The starting point will be, just like in the previous section, the Boltzmann equation for the nucleus a in the following form:

$$\dot{n}_a + 3Hn_a = -\int d\Pi_a \int d\Pi_b \int d\Pi_j \int d\Pi_k \,(2\pi)^4\delta^4(p_a + p_b - p_j - p_k)\overline{|M|}^2 \cdot f_a f_b \tag{3.97}$$

We will assume that nuclei are still in kinetic equilibrium, so that $f_a = e^{-\frac{(E-\mu)}{T}}$, since nuclei are highly non-relativistic, so that Pauli-Blocking factors can be neglected. If this is the case, as shown in App. C, this equation can be written in terms of the thermally averaged cross section times Møller velocity:

$$\langle\sigma v\rangle_{ab\to jk} \equiv \frac{1}{n_a^{eq}n_b^{eq}}\int d\Pi_a \int d\Pi_b \int d\Pi_j \int d\Pi_k \,(2\pi)^4\delta^4(p_a + p_b - p_j - p_k)\overline{|M|}^2 \cdot e^{-\frac{E_a}{T}}e^{-\frac{E_b}{T}} \tag{3.98}$$

where $n_{a,b}^{eq}$ describes the equilibrium density without a chemical potential. The Boltzmann equation simplifies to:

$$\dot{n}_a + 3Hn_a = -\langle\sigma v\rangle_{ab\to jk}n_a n_b \tag{3.99}$$

For the backwards reaction, we will assume that CP is conserved, so that the matrix element is the same in both directions. Additionally, due to energy conservation, we have that:

$$e^{-\frac{E_a}{T}}e^{-\frac{E_b}{T}} = e^{-\frac{E_a + E_b}{T}} = e^{-\frac{E_j + E_k}{T}} = e^{-\frac{E_j}{T}}e^{-\frac{E_k}{T}} \tag{3.100}$$

This condition, commonly referred to as detailed balance condition, is fulfilled whenever the system is in kinetic equilibrium. An equivalent relation holds for the case of FD and BE distributions [51], so that the following also holds in one particle is a photon γ, which is very relevant for BBN as photodissociation rates are of this type. Detailed balance implies that it does not matter with respect to which distributions we take the thermal average, only the overall normalization differs. Combined with CP conservation, it is easy to show that:

$$\frac{\langle\sigma v\rangle_{jk\to ab}}{\langle\sigma v\rangle_{ab\to jk}} = \frac{n_a^{eq}n_b^{eq}}{n_j^{eq}n_k^{eq}} \tag{3.101}$$

Let's look, concretely, at what this means for the backward reaction if all particles involved are nuclei. Then their equilibrium number density is given by Eq. A.5. Defining the Q-value of the reaction $a + b \to j + k$ as:

$$Q_{ab\to jk} = m_a + m_b - m_j - m_k \tag{3.102}$$

with the "forward direction" of the reaction being chosen by convention such that $Q_{ab\to jk} > 0$. Then, the ratio of the forward to backward reaction has the following form:

$$\frac{n_a^{eq}n_b^{eq}}{n_j^{eq}n_k^{eq}} = \frac{g_a g_b}{g_j g_k}\left(\frac{m_a m_b}{m_j m_k}\right)^{\frac{3}{2}}e^{-\frac{Q_{ab\to jk}}{T}} \tag{3.103}$$

Typically, $Q_{ab \to jk} \sim \mathcal{O}(1\,\mathrm{MeV})$, so that the backward reaction becomes exponentially suppressed at the temperature range where BBN begins, so in general they will not play a major role, regardless of how fast the forward-reaction is. For precise calculations they, of course, need to be taken into account, but we will neglect them for now.

Detailed balance, thus, allows us to simply write the term for the backwards reaction in the Boltzmann eq. as:

$$\dot{n}_a + 3Hn_a = -\langle \sigma v \rangle_{ab \to jk} \left(n_a n_b - \frac{n_a^{eq} n_b^{eq}}{n_j^{eq} n_k^{eq}} n_j n_k \right) \tag{3.104}$$

Just as for neutrons and protons, we will rewrite the equation in terms of the Baryon number fraction X_i:

$$\dot{X}_i = -\langle \sigma v \rangle_{ab \to jk} n_B \left(X_a X_b - \frac{X_a^{eq} X_b^{eq}}{X_j^{eq} X_k^{eq}} X_j X_k \right) \tag{3.105}$$

This equation is of the same form as eq. 3.83, with the change in the comoving particle number being equal to a source term $\mathcal{J}$ that is just the difference between the creation and destruction rate of the isotope i. [5] We can now rewrite $n_B = \eta_B n_\gamma$, which shows that all nuclear reactions are $\sim \eta_B \ll 1$. Thus, all nuclear reactions are suppressed by the extremely small baryon-to-photon ratio. This reaffirms the conclusion we have come to before from the NSE abundances, that the large overabundance of photons sets nucleosynthesis back.

This derivation holds for all four-body reactions on Fig. 3.4, so all that is left to do in order to obtain the Boltzmann equation that governs the evolution of the nuclear abundances is to sum over all reactions. Factors of $1/2$ appear for reactions where the initial particle is doubled. Additionally, we have to include the weak neutron to proton conversion reactions from Eq. 3.50 that, most importantly, include the neutron decay. All of this, results in the following complex system of coupled differential equations:

$$\dot{X}_n = \langle \sigma v \rangle_{d\gamma np} n_B \eta_B^{-1} X_d + \frac{1}{2} \langle \sigma v \rangle_{dd^3hen} n_B X_d^2 + \langle \sigma v \rangle_{td\alpha n} n_B X_t X_d$$
$$\quad - \langle \sigma v \rangle_{npd\gamma} n_B X_n X_p - \langle \sigma v \rangle_{^3hentp} n_B X_{^3he} X_n - \langle \sigma v \rangle_{^7ben^7lip} n_B X_{^7be} X_n \tag{3.106a}$$
$$\quad + \Gamma_{pn} X_p - \Gamma_{np} X_n$$

$$\dot{X}_p = \langle \sigma v \rangle_{d\gamma np} n_B \eta_B^{-1} X_d + \frac{1}{2} \langle \sigma v \rangle_{ddtp} n_B X_d^2 + \langle \sigma v \rangle_{^3hentp} n_B X_{^3he} X_n$$
$$\quad + \langle \sigma v \rangle_{^3hed\alpha p} n_B X_{^3he} X_d + \langle \sigma v \rangle_{^7ben^7lip} n_B X_{^7be} X_n \tag{3.106b}$$
$$\quad - \langle \sigma v \rangle_{dp^3he\gamma} n_B X_d X_p - \langle \sigma v \rangle_{npd\gamma} n_B X_n X_p - \langle \sigma v \rangle_{^7lip\alpha\alpha} n_B X_{^7li} X_p$$
$$\quad + \Gamma_{np} X_n - \Gamma_{pn} X_p$$

$$\dot{X}_d = \langle \sigma v \rangle_{npd\gamma} n_B X_n X_p - \langle \sigma v \rangle_{d\gamma np} n_B \eta_B^{-1} X_d - \langle \sigma v \rangle_{dp^3he\gamma} n_B X_d X_p$$
$$\quad - \langle \sigma v \rangle_{dd^3hen} n_B X_d^2 - \langle \sigma v \rangle_{ddtp} n_B X_d^2 - \langle \sigma v \rangle_{^3hed\alpha p} n_B X_{^3he} X_d \tag{3.106c}$$
$$\quad - \langle \sigma v \rangle_{td\alpha n} n_B X_t X_d$$

$$\dot{X}_t = \langle \sigma v \rangle_{^3hentp} n_B X_{^3he} X_n + \frac{1}{2} \langle \sigma v \rangle_{ddtp} n_B X_d^2 + \langle \sigma v \rangle_{t\alpha^7li\gamma} n_B X_t X_\alpha$$
$$\quad - \langle \sigma v \rangle_{td\alpha n} n_B X_t X_d \tag{3.106d}$$

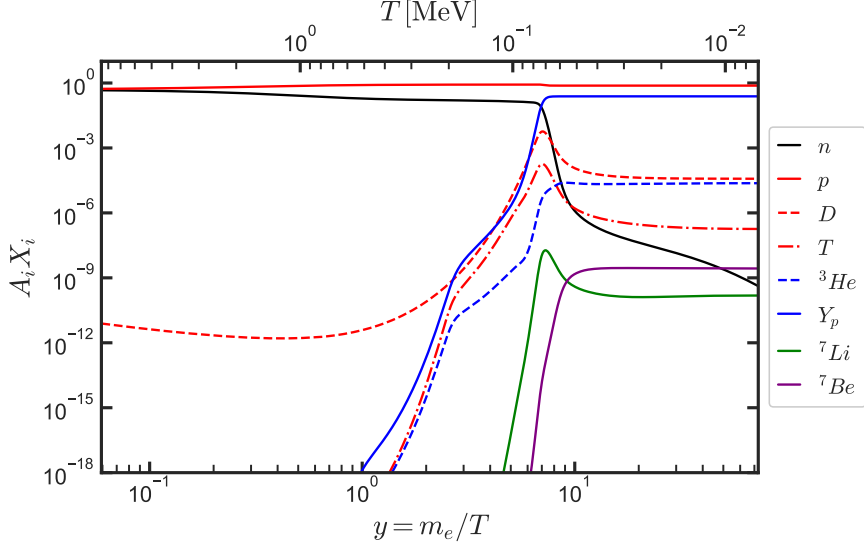[5]See App. C for a more detailed explanation of the pysical interpretation of this form of the equation.

Figure 3.6: Formation of the light elements up to ^7Be with the nuclear reaction network from 3.4 for $\eta_B = 6.14 \cdot 10^{-10}$ and $\tau_n = (878.4 \pm 0.5)\,\mathrm{s}$ [28] obtained as a solution of Eq. 3.106a.

$$
\begin{aligned}
\dot{X}_{3he} &= \langle \sigma v \rangle_{dd\,3hen}\, n_B X_d^2 + \langle \sigma v \rangle_{dp\,3he\gamma}\, n_B X_d X_p - \langle \sigma v \rangle_{3hentp}\, n_B X_{3he} X_n \\
&\quad - \langle \sigma v \rangle_{3hed\alpha p}\, n_B X_{3he} X_d - \langle \sigma v \rangle_{3he\alpha\,7be\gamma}\, n_B X_\alpha X_{3he}
\end{aligned}
\tag{3.106e}
$$

$$
\begin{aligned}
\dot{X}_\alpha &= \langle \sigma v \rangle_{3hed\alpha p}\, n_B X_{3he} X_d + \langle \sigma v \rangle_{t\alpha\,7li\gamma}\, n_B X_t X_\alpha + 2\langle \sigma v \rangle_{7lip\alpha\alpha}\, n_B X_{7li} X_p \\
&\quad + \langle \sigma v \rangle_{td\alpha n}\, n_B X_t X_d - \langle \sigma v \rangle_{3he\alpha\,7be\gamma}\, n_B X_\alpha X_{3he}
\end{aligned}
\tag{3.106f}
$$

$$
\dot{X}_{7li} = \langle \sigma v \rangle_{t\alpha\,7li\gamma}\, n_B X_t X_\alpha + \langle \sigma v \rangle_{7ben\,7lip}\, n_B X_{7be} X_n - \langle \sigma v \rangle_{7lip\alpha\alpha}\, n_B X_{7li} X_p
\tag{3.106g}
$$

$$
\dot{X}_{7be} = \langle \sigma v \rangle_{3he\alpha\,7be\gamma}\, n_B X_\alpha X_{3he} - \langle \sigma v \rangle_{7ben\,7lip}\, n_B X_{7be} X_n
\tag{3.106h}
$$

Unlike with the weak rates, where a theoretical prediction can be made with remarkable precision, there is large theoretical uncertainty in the modeling of nuclear reaction rates, so a precise value requires input from experiments. In the following, we have used the PRIMAT rates of [20]. Unfortunately, this system cannot be solved analytically, but only numerically. Just like we did for the equation for neutron to proton freeze-out (Eq. 3.83), we will not use time as the natural variable, but rather $y = \frac{m_e}{T}$.

As long as neutrons and protons are not free, the Boltzmann equations governing their evolution will be dominated by the weak rates and the nuclei will remain in NSE, as we have seen in the section before as well. Thus, only starting at temperatures $\mathcal{O}(1\,\mathrm{MeV})$ slightly above T_f does it make sense to solve the full system of equations for all nuclei. At higher temperatures, it suffices to solve the simple differential equation for X_n (eq. 3.84). The last step in the evolution and the corresponding NSE abundances can be used as initial conditions for the full solution. The resulting evolution describing the formation of nuclei up to ^7Be is shown on Fig. 3.6.

While we will mainly be interested in the final abundances and not the evolution, it is important to understand the physical processes that lead to these final abundances, especially keeping in mind that we want to use BBN as a laboratory
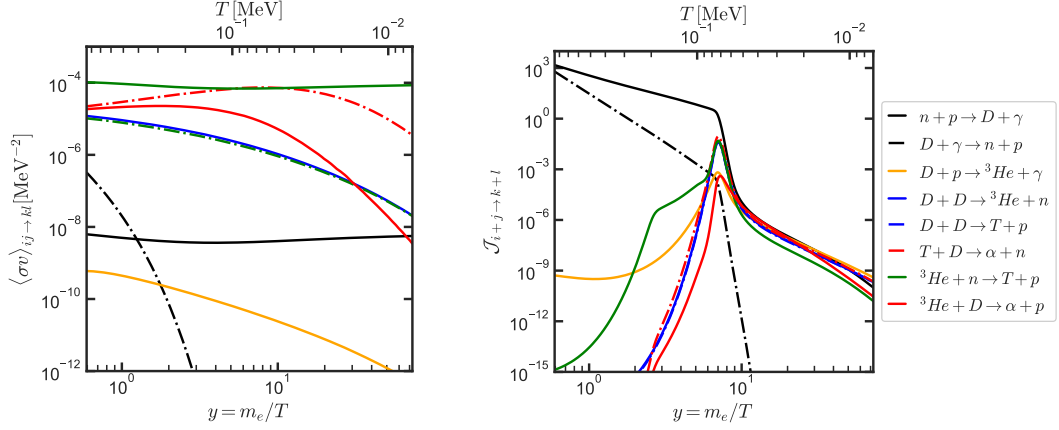
Figure 3.7: **Left:** Thermally averaged cross section times velocity in MeV^{-2} as a function of $y = \frac{m_e}{T}$ for the most important reactions from Fig. 3.4. **Right** Source term from Eq. 3.107 for the same reactions as a function of y.

for High Energy Physics and, thus, need to understand how new ingredients will influence the standard outcome of BBN.

In order to do so, it is helpful to look at the evolution of the abundances, as well as $\langle \sigma v \rangle$ and the source term

$$\mathcal{J}_{ij \to kl} = \frac{1 + \Delta}{Hy} \langle \sigma v \rangle_{ij \to kl} \eta_B n_\gamma \cdot X_i X_j \qquad (3.107)$$

corresponding to all reactions. Fig. 3.7 shows precisely these two quantities for reactions involving nuclei up to ^4He, $\langle \sigma v \rangle$ on the left and $\mathcal{J}$ on the right panel.

The source term is proportional to the by now well known ratio $\mathcal{J} \propto \frac{\Gamma}{H}$ that measures the effectiveness of the reaction. We see that almost all reactions are slower than the expansion rate of the Universe, as the source term remains far below one at those temperatures, implying that they cannot maintain nuclear statistical equilibrium, so their abundances actually remain far below that value for a long time.

An exception to this is Deuterium, since the only reaction faster than the expansion of the Universe is actually $n + p \to D + \gamma$ and its backward reaction. As can be seen from the left panel of Fig. 3.7, this is not owing to the high value of $\langle \sigma v \rangle$, but rather to the large abundance of nucleons compared to other nuclei. As a result, the deuterium abundance steadily increases, quite closely following its NSE value.

As the D-abundance slowly rises, the DD-reactions, that is, those involving two Deuterium nuclei, which form ^3He and T become increasingly efficient. These two nuclei start from the same value for the NSE abundance and $\langle \sigma v \rangle$ is quite similar for both, as can be observed from Fig. 3.7. Thus, they are produces in equal measure. However, the fastest reaction at this time (other than $n + p \leftrightarrow D + \gamma$) is the neutron capture of ^3He to create T. As a result, most ^3He ends up in Tritium, which is why its abundance surpasses that of ^3He by a couple of orders of magnitude.

As a next step, these two nuclei create ^4He through deuterium capture reactions. Since ^3He is doubly charged, the coulomb barrier that D needs to overcome is

higher and the reaction proceeds more slowly than for T. This, combined with the overabundance of T over ^3He, implies that the main pathway to form ^4He is through tritium. Thus, three deuterium nuclei are needed to form one α-particle, with one D being dissociated as a by-product of the reaction, and the reaction happens almost instantly. The starting product that determines the fate of heavier nuclei is still D, so the abundances of T and ^4He quite rapidly adapt to any change in X_D and follow its NSE evolution rather closely, as we can see from Fig. 3.6.

Meanwhile, the np reaction is still efficiently producing Deuterium and, with the DD-reactions now in action as well, there is a competition between them and the photodissociation reaction that maintains D in NSE. As soon as the source term for this reaction drops below that of DD-reactions, the situation changes dramatically and rapidly. This happens at

$$T_{BBN} = 0.08 \, \text{MeV} \tag{3.108}$$

The reservoir of frozen-out neutrons very quickly gets depleted and turned into D. This, in turn gets cast into ^4He through the aforementioned pathway almost instantly. The D and T abundances peak shortly after before being depleted just as rapidly. Because of its stability, most of the ^4He remains in that form and any reaction depleting it is negligibly small. Almost all neutrons, thus, eventually end up as ^4He. As a result, its abundance at the end of nucleosynthesis at T_e, can easily be estimated, to reasonable accuracy, as:

$$X_\alpha(T_e) = \frac{X_n(T_{BBN})}{2} = 0.063 \tag{3.109}$$

Or in terms of the usual primordial mass fraction for Helium:

$$Y_p = 2X_n(T_{BBN}) = 0.252 \tag{3.110}$$

Once the neutron reservoir has been depleted, the np-reaction ceases to be efficient, and the Helium abundance freezes out at its primordial value. The same happens for D and T which, after peaking when photodissociation stops, get depleted until they freeze out. On the contrary, the ^3He abundance actually further increases after these two peak. This is because of the alternative production channel for ^3He from D through proton capture $D + p \rightarrow {}^3He + \gamma$, which actually becomes the dominant reaction for ^3He since protons remain so abundant throughout the entire process of BBN. Once the D abundance drops below a certain threshold, this reaction also freezes out and the ^3He abundance remains constant.

We have paid little attention to elements like ^7Li and ^7Be up to now, since they only play a subdominant role in the events described. Both of them mainly get produced by a similar reaction of ^4He capture. Similar to the DD reactions, it is only the abundance of the initial products that slows down this reaction, not necessarily the actual value of $\langle \sigma v \rangle$. Thus, the abundance of ^7Li exhibits the same peak as X_T, whereas ^7Be shows a slight increase in its abundance, even after ^4He has frozen out, just like ^3He.

One final adjustment is necessary, since we know that neither ^7Be nor T are stable. ^7Be decays to ^7Li with a half-life of 53.22 d, whereas T decays to ^3He with $\tau_{1/2} = 12.32 \, \text{yr}$. Since these are much larger than the time at which nucleosynthesis

ends t_e, this amounts to setting the final abundance of ^7Li to be the sum of that of ^7Be and ^7Li, and analogously for T, leaving us with $p, ^3He, ^4He, ^7Li$ as the main elements whose abundance can be predicted with BBN.

With this, we come to the most important aspect, namely the final abundances. In order to be able to compare with experimental data, we will quote not X_A but the primordial A-to-proton ratio $A/H|_p = \frac{X_A}{X_p}$ with the exception of Helium, where it is customary to quote the primordial mass fraction Y_p. For the small network on Fig. 3.4, assuming an effective description of neutrinos with $N_{eff} = 3.043$ and computing the weak rates in the Born approximation, $\eta_B = 6.14 \cdot 10^{-10}$ and $\tau_n = (878.4 \pm 5.0)\,\mathrm{s}$, the final abundances are the following:

$$Y_p = 0.2427 \tag{3.111}$$
$$D/H|_p = 2.40 \cdot 10^{-5} \tag{3.112}$$
$$^3He/H|_p = 1.03 \cdot 10^{-5} \tag{3.113}$$
$$^7Li/H|_p = 5.66 \cdot 10^{-10} \tag{3.114}$$

In order to highlight the important physics, we have focused here on this simplified treatment of BBN. However, if we want to be as precise as observations, we not only need to leave the effective description of neutrinos and add many corrections to the weak rates, but also need to include a much larger network of reactions into our calculation. Implementing this lies beyond the scope of this thesis, but all currently up-to-date codes do. We have used the same rates as the publicly available code PRIMAT [20] used for the global analyses of Pitrou et al. Including all the effects described and with a much more extensive network of nuclear reactions, they find, for $\eta_B = 6.14 \cdot 10^{-10}$:

$$Y_p = 0.2468 \pm 0.00014 \tag{3.115a}$$
$$D/H|_p = 2.44 \pm 0.04 \cdot 10^{-5} \tag{3.115b}$$
$$^3He/H|_p = 1.04 \pm 0.01 \cdot 10^{-5} \tag{3.115c}$$
$$^7Li/H|_p = 5.5(2) \cdot 10^{-10} \tag{3.115d}$$

The theoretical uncertainty quoted here, taken from [52], is mainly due to uncertainties in the measurement of the neutron lifetime and nuclear reaction rates. This last point is actually extremely important, as we will see shortly. If we compare the outputs of this code with those of other groups performing global analyses of BBN (Pisanti et al. [29] and Yeh et al. [53]), we find good agreement for the abundances overall, with the exception of Deuterium, for which these two groups find:

$$D/H|_p = (2.48 \pm 0.08) \times 10^{-5}\,, \quad [\text{Yeh et al. 22'}] \tag{3.116a}$$
$$D/H|_p = (2.52 \pm 0.07) \times 10^{-5}\,, \quad [\text{Pisanti et al. 21'}] \tag{3.116b}$$
$$\tag{3.116c}$$

While these two determinations of deuterium agree with each other at the 1σ level, that of Pitrou et al. (Eq. 3.115) is significantly lower. We will see later the cosmological implications of this discrepancy, but we first need to understand where it comes from.

3.4.3 Importance of Nuclear Reaction Rates

In the previous section, we have seen that even the extremely simplified treatment presented there is, actually, quite complex already. An accurate prediction of the final abundances requires a sophisticated interplay of different physical phenomena at exactly the right time. Additionally, even minor modifications in the rates can have dramatic consequences for the final abundances. As with the weak rates and background thermodynamics, we require a precise knowledge of the nuclear reactions.

This is especially true for the deuterium abundance that is of paramount importance for nucleosynthesis. The deuterium abundance and its theoretical uncertainty is essentially determined by four reactions: $n(p, \gamma)D$, $D(p, \gamma)^3He$ (dpg), $D(D, p)T$ (ddp), $D(D, n)^3He$ (ddn). However, the lack of an accurate theoretical model to calculate them poses a severe challenge. It may be overcome through input from experiment by measuring $\sigma(E)$ at the energies relevant for BBN corresponding to temperatures between $10^{-2} - 1\,\text{MeV}$ and fitting the data points to obtain $\sigma(E)$.

At those temperatures, particles are not energetic enough to classically overcome the Coulomb barrier, so that they need to tunnel through them quantum-mechanically. Thus, the cross section is exponentially suppressed by the Gamow factor $\sigma(E) \propto e^{-\sqrt{E_G/E}}$, with $E_G = 2\pi^2\mu_{ij}(Z_iZ_j\alpha)^2 \sim \mathcal{O}(\text{MeV})$. In order to extract the extreme energy dependence of the Gamow factor and isolate the contribution to $\sigma(E)$ from the strong interaction, it is common in astrophysics to define the S-factor:

$$S(E) \equiv \sigma(E)Ee^{\sqrt{E_G/E}} \tag{3.117}$$

A measurement of this S-factor at BBN energies, even though essential for stellar and Big Bang nucleosynthesis, is extremely challenging and cost intensive, and dedicated experiments, rare. Thus, data points from many different experiments, with partly or even entirely non-overlapping energy ranges, and varying degrees of accuracy need to be collectively interpolated to obtain the S-factor. In doing so, the approach taken by the different authors differs in three points:

- In order to fit the data, we need to choose a functional form $S_{th}(\alpha, E)$ for S with parameters α to fit to. Assuming the reaction contains no resonances, the S-factor is a smooth function of energy, so we may essentially Taylor-expand S and fit to a polynomial function of sufficient degree. This is the approach taken by Pisanti et al. [29] and Yeh et al. [53]. Another approach is to use theoretical ab-initio calculations of the rates that give the overall energy dependence of the S-factor, leaving only the normalization as a free parameter to be determined, which is the procedure used by Pitrou et al. [20].

- Additionally, the three groups differ in their criteria for data selection. Pisanti et al. [29] take into account as much data as they can with the logic that the fit should be dominated by more precise measurements anyway. This includes data from experiments that use the indirect (or theory-dependent) Trojan Horse method [54]. Pitrou et al [20], on the other hand, perform a strict data selection where only take data from direct experiments and neglect experiments with too large uncertainties or that provide too few details and

are thus deemed unreliable. The aim is to decrease the theoretical error on deuterium under well-motivated assumptions. With their error being smaller than other determinations by a factor of two, one can say that they have succeeded in their endeavor.

- Lastly, there is a difference in the employed statistical framework. Pitrou et al. [20] advocate for a bayesian treatment, while a frequentist statistical analysis relying on minimizing a χ^2 distribution is preferred by Pisanti et al[29] and Yeh et al. [53].

Both approaches are well-motivated and consistent and there is no reason to prefer one over the other a priori. Likewise, they should, in principle, not significantly influence the outcome of nucleosynthesis if data dominates the fit. As evidenced by the discrepancy in the predicted value of $D/H|_p$, this is not the case at the moment.

A breakthrough was made in 2020 by the LUNA collaboration [55] at the underground Gran Sasso National Laboratory in Italy, which measured the reaction rate for energies between $E_{cm} = 33 - 263\,\mathrm{keV}$ that are of extreme importance for BBN with a precision of the order of 3%. This measurement significantly reduced the theoretical error of deuterium, as this was before the main contributor to its error budget, but in doing so exposed the discrepancies between the different approaches to fitting the nuclear reaction rates.

Nevertheless, the discrepancies between the different predictions do not stem from the dpg reaction LUNA measured, thanks to the precision and quality of the data, but rather from the ddp and ddn reactions [52]. This implies that when the quality of the data is good enough, it does not matter which approach one uses. Resolving the tension between the different deuterium predictions will require comparably accurate measurements for the ddn and ddp reactions, which should still take a while. In light of that, it is important to take both rates into account before coming to any conclusions from BBN.

Instead of discarding BBN as a probe altogether, it is enough to simply perform any global analysis involving BBN with the different rates whenever Deuterium is involved. In the following, we will do precisely that for two sets of rates. Given that the theoretical predictions of Pisanti et al. [29] and Yeh et al. [53] are in good agreement with each other and that they follow a similar approach overall in their determination of the rates, we will only use those from Pisanti et al. [42], which are implemented in the publicly available code `PArthENoPE-v3.0` [42, 43, 44], henceforth referred to as PArthENoPE rates. Additionally, we will use the rates of Pitrou et al. [20], which are implemented in `PRIMAT` as well. We will refer to them as PRIMAT rates.

Chapter 4

Standard Constraints from Big Bang Nucleosynthesis

We have now reviewed the standard theory leading to a prediction of the primordial abundances of the light elements. While it is a very complex process, it is only based on some very well-motivated assumptions and very consolidated aspects of physics, namely that the SM, and its low energy EFTs more precisely, include all interactions that may influence BBN, and that that the background expansion is accurately described by the ΛCDM model of Cosmology.

One of the most compelling aspects of BBN as a theory is that, given those assumptions, it makes very clear and easily falsifiable predictions. The nuclear reaction rates, as well as the neutron lifetime used to calibrate the weak rates, are taken as a fixed input parameter to the theory. They are taken into account in the theoretical uncertainty on the measurements, with σ_{τ_n} being the main contributor to the Helium uncertainty and the nuclear reaction rates dominating the error budget for Deuterium. Thus, predictions from SBBN theory are only dependent on one single cosmological parameter, the baryon to photon ratio η_B, or equivalently the baryon density $\Omega_b h^2$.

4.1 Baryon Density

The dependence of Helium (Left) and Deuterium Abundance (Right) on $\Omega_b h^2$ for $\tau_n = 878.4\,\mathrm{s}$ is shown on Fig. 4.1 for both the PArthENoPE and PRIMAT rates.

Let us first focus on the Helium Abundance. We see that, as expected, there is only a minor difference in the determination of Y_P depending on the choice of rates. This can be attributed to the fact that almost all neutrons end up in Helium at the end of Nucleosynthesis, so that the final Helium abundance is only dependent on the amount of free neutrons at the exact time of the onset of nucleosynthesis.

We saw in the previous section that this can be estimated as the moment the source term of the DD-reactions, $\mathcal{J}_{DD}$, that lead to the formation of heavier nuclei becomes larger than that of the photodissociation reaction of deuterium, $\mathcal{J}_{D\gamma}$. $\mathcal{J}_{DD} \propto \eta_B$, so an increase in the baryon density implies an increase in $\mathcal{J}_{DD}$, so that the Temperature at which they are equal increases, while $\mathcal{J}_{D\gamma}$ is not. Since $t \propto T^{-2}$, a higher value of T_{BBN} allows neutrons to decay for a shorter period of time, thus
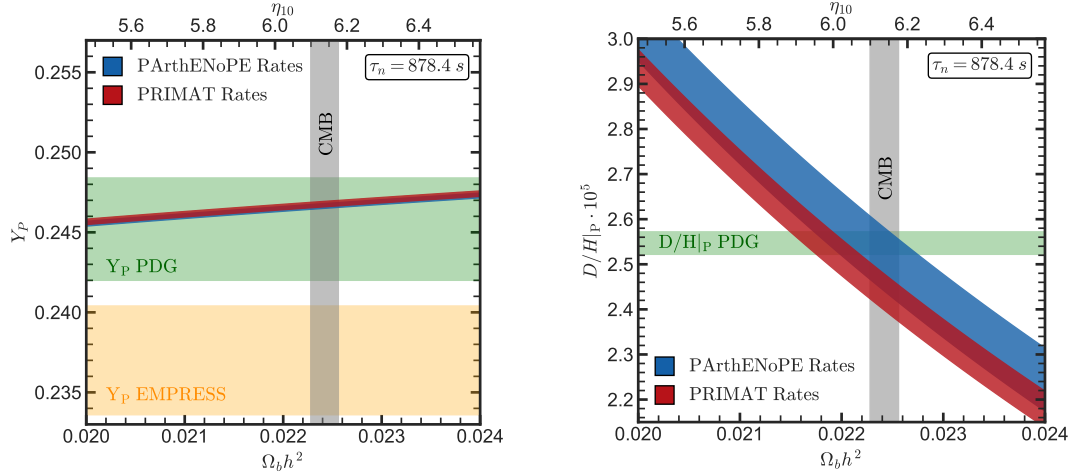
Figure 4.1: 68% CL bands for the Primordial Helium mass fraction, Y_P, (Left) and Deuterium to Hydrogen ratio, $D/H|_P$, (Right) as a function of the baryon density $\Omega_b h^2$ for both choices of nuclear rates. The green bands correspond to the PDG-22 68% CL of Y_P and $D/H|_P$, where as the yellow band corresponds to the EMPRESS prior on Y_P. The grey band shows the preferred value of $\Omega_b h^2$ from measurements of the CMB.

increasing the final Helium abundance.

However, since $\mathcal{J}_{D\gamma}$ is dominated by the exponential suppression $\propto e^{-\frac{B_D}{T}}$, T_{BBN} will only be logarithmically dependent on $\eta_B \sim \Omega_b h^2$. Thus, the Helium abundance will also only depend very weakly on $\Omega_b h^2$. In fact, we find that:

$$Y_p = Y_P|_{\mathrm{ref}} \cdot \left(\frac{\Omega_b h^2}{\Omega_b h^2|_{\mathrm{ref}}} \right)^{0.039} \tag{4.1}$$

where we have chosen $\Omega_b h^2|_{\mathrm{ref}} = \Omega_b h^2|_{\mathrm{Planck}}$ (Eq. 2.14 and the corresponding value of $Y_P|_{\mathrm{ref}} = 0.2466(0.2468)$ for the PArthENoPE (PRIMAT) rates. With an exponent of 0.039, this is indeed positively correlated and only very weakly dependent on $\Omega_b h^2$.

What can also be abstracted from that figure is the (dis)agreement between data and observations. The green and orange stripes on Fig. 4.1 are 1σ bands corresponding to the PDG-22 (Eq. 2.11) and EMPRESS 2.10 determinations of Y_P. For the PDG-22 value, we see that the prediction of SBBN for Y_P is well within 1σ of the best fit value, thus showing very good agreement between theory and observations. The picture is completely different if we use the EMPRESS determination of Y_P, as the figure quite blatantly shows the tension of SBBN with the observation. Resolving this tension purely with the baryon density would require a value as low as $\Omega_b h^2 \simeq 0.008$, which we can safely rule out. Resolving the tension with the EMPRESS measurement will therefore necessarily involve going beyond the Standard theory of nucleosynthesis.

For Deuterium, the picture is quite different. Its dependence on $\Omega_b h^2$ is shown on the right panel of Fig. 4.1. Unlike for Helium, we see that Deuterium very strongly varies with $\Omega_b h^2$. This is to be expected, since the reactions that determine its

evolution are directly proportional to this value. Since this a very sensitive system, any change will have a strong impact on the evolution and final abundance.

Additionally, the final abundance is negatively correlated with $\Omega_b h^2$. The reason for this is slightly more subtle. Take for example the $n(D, \gamma)p$ reaction. One would expect an increase in the only production channel for Deuterium to increase its final abundance. On the other hand, an increase in this reaction implies that the deuterium abundance reaches the value at which the DD reactions become efficient earlier, since D grows faster. As can be seen on Fig. 3.7, $\langle \sigma v \rangle$ decreases rapidly with temperature, so that the depletion of the Deuterium reservoir will be more efficient if it starts at lower temperatures. Thus, while X_D does increase more rapidly at the beginning, it will also be depleted more rapidly, leading to a smaller final abundance. Further increases of other reactions $\propto \Omega_b h^2$ which deplete D will have a similar effect. Parametrizing the dependence analogously to Helium, we find that for PRIMAT Rates:

$$\text{PRIMAT}: \quad D/H|_P = D/H|_{P,\text{ref}} \cdot \left(\frac{\Omega_b h^2}{\Omega_b h^2|_{\text{ref}}} \right)^{-1.632} \tag{4.2a}$$

$$\text{PArthENoPE}: \quad D/H|_P = D/H|_{P,\text{ref}} \cdot \left(\frac{\Omega_b h^2}{\Omega_b h^2|_{\text{ref}}} \right)^{-1.637} \tag{4.2b}$$

using $D/H|_{P,\text{ref}} = 2.44(2.51)$ as the reference value for PRIMAT (PArthENoPE) rates. We can also infer from this simple fit that the parametric dependence of the final abundances on $\Omega_b h^2$ is only very mildly affected by the choice of rates. What changes, however, is the face value and the theoretical uncertainty, as shown before. Nevertheless, as Fig. 4.1 very clearly shows, both determinations are in good agreement with each other within the theoretical uncertainties for all values of $\Omega_b h^2$.

The green band on this figure shows the 1σ PDG-22 determination of Deuterium (Eq. 2.12). Even though the precision of the measurement is $\sim 1\%$, only slightly more precise than that of Helium, the strong dependence on $\Omega_b h^2$ implies that this measurement allows us to put very stringent constraints on the baryon density from BBN, as theory and observations are only in agreement for a very short range where the blue(red) bands cross the green band.

$\Omega_b h^2$ can also be inferred from observations of the CMB. While $\Omega_b h^2$ is temperature dependent in general, within the ΛCDM model it remains constant between $e^{\pm}$-annihilation and the era of recombination, making BBN a parameter-free theory within this model. While the success of BBN as a theory does not necessarily depend on the evolution of the Universe after BBN, as events happening at lower temperatures might influence CMB observations, but not BBN, an agreement between the two obtained values is a crucial and highly non-trivial consistency test of the ΛCDM model. Any deviation from the baryon density inferred from the CMB will add another entry to the increasingly long list of tensions in cosmology whose resolution requires new physics.

The value reported by the Planck collaboration [56] combining CMB and BAO data is shown as the grey band. As we can see, while the choice of rates does not spoil the consistency of BBN as a theory, it forces us to draw very different conclusions regarding the health of the Standard Model of cosmology.

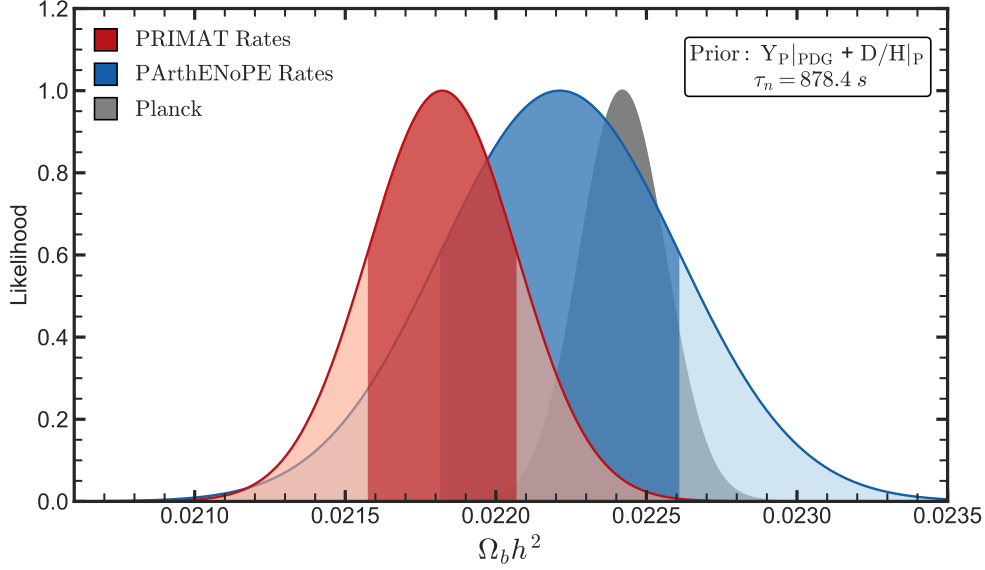In order to make this assessment more quantitative, we will now proceed to

Figure 4.2: Likelihood function for $\Omega_b h^2$ from the PDG-22 prior on both abundances, since $D/H|_P$ dominates the constraints, for PRIMAT(red) and PArthENoPE(blue) rates, as well as the independent CMB measurement (grey). The figure shows good agreement between BBN and the CMB for PArthENoPE rates and a 2.1σ tension for PRIMAT rates.

obtain constraints on the baryon density for different priors following the methods described in Chapter 2. The main results are shown on Fig. 4.2 and summarized on table 4.1.

As can be seen from Table 4.1, the constraints on the baryon density are dominated by the prior on the Deuterium Abundance. The effect of simultaneously constraining the Helium abundance is only of the order of $\sim 10^{-5}$ on the baryon density and does not increase the sensitivity, as expected given its sensitivity to $\Omega_b h^2$.

The only effect of including the prior on Helium is to increase $\chi^2_{\min}$, which serves as a measure of the goodness of fit. Regardless of the choice of nuclear reaction rates, constraining Y_P to the EMPRESS value (Eq. 2.10) causes an increase of $\Delta\chi^2_{\min} \approx 7.8$, which indicates that the measurement is in a $\sim 3\sigma$ tension with the Standard model of BBN. If, on the other hand, we choose the PDG-22 value as the prior, we find good agreement overall between observations and data and $\chi^2_{\min}$ is essentially 0. Using only $D/H|_P$ as a prior, one obtains the following constraints on the baryon density:

$$\text{PRIMAT}: \quad \Omega_b h^2 = 0.02183 \pm 0.00025 \tag{4.3a}$$
$$\text{PArthENoPE}: \quad \Omega_b h^2 = 0.02222 \pm 0.00040 \tag{4.3b}$$

In keeping with our expectations, these constraints agree with each other within 1σ, even though their best-fit value is different. As the prediction with PRIMAT rates is smaller than with PArthENoPE rates and D/H is negatively correlated with $\Omega_b h^2$, the determination from PRIMAT rates has a lower best fit value for the baryon density. Also, the sensitivity is better for this set of rates, since they report a much lower theoretical uncertainty.

Bounds and Sensitivities on the Baryon density from BBN and CMB Data

Y_P	Data Sets	Nuclear Rates	$\Omega_b h^2$	$\chi^2_{\min}$
$\times$	$D/H|_P$	PArthENoPE	0.02222 ± 0.00040	0
		PRIMAT	0.02183 ± 0.00025	0
EMPRESS	$Y_P + D/H|_P$	PArthENoPE	0.02217 ± 0.00039	7.9
		PRIMAT	0.02181 ± 0.00025	7.8
	$Y_P + D/H|_P + \Omega_b h^2|_{\text{Planck}}$	PArthENoPE	0.02239 ± 0.00013	8.2
		PRIMAT	0.02228 ± 0.00012	12.3
PDG-22	$Y_P + D/H|_P$	PArthENoPE	0.02221 ± 0.00040	0.3
		PRIMAT	0.02182 ± 0.00025	0.3
	$Y_P + D/H|_P + \Omega_b h^2|_{\text{Planck}}$	PArthENoPE	0.02240 ± 0.00013	0.5
		PRIMAT	0.02228 ± 0.00012	4.5

Table 4.1: Summary of constraints on the Baryon density, $\Omega_b h^2$, from considering several combinations of BBN and CMB data for two possible choices of the nuclear reaction rates. See main text for details.

We can now compare this with the constraints on $\Omega_b h^2$ from the Planck collaboration:

$$\Omega_b h^2 = 0.02242 \pm 0.00014 \tag{4.4}$$

which is obtained using CMB+BAO data. It is clear that, even with the significant improvement due to the precise measurements from the LUNA collaboration and the lower theoretical uncertainty from the method adopted to obtain the PRIMAT rates, the BBN constraints on the baryon density are not really competitive with CMB measurements yet.

While unimportant to any conclusions up to now, the effect of the choice of nuclear reaction rates plays a crucial role now in determining the health of ΛCDM model. The PArthENoPE constraints are in agreement within one sigma with the Planck constraints, implying that the ΛCDM model has withstood another highly non-trivial test. On the other hand, if we adopt the PRIMAT rates, we see that there is a 2.1σ tension with the Standard Model and requiring new physics between the BBN and CMB epochs to be resolved. These results are summarized on Fig. 4.2.

In order to address the overall tension of the ΛCDM model with observations of primordial abundances, we can add a prior for the baryon density, thus constraining it to the values in eq. 4.4 and obtain the best-fit value given the observations for Y_P and $D/H|_P$. The value of $\chi^2_{\min}$ will then give us a measure for the health of the ΛCDM model.

The conclusions range from extremely healthy over slightly concerned to the worst case scenario, with the determination of Y_P by the EMPRESS collaboration and the PRIMAT rates, where the cosmological model is in some serious trouble with $\chi^2_{\min} = 12.3$ corresponding to a $\sim 3.5\sigma$ tension. Thus, while the strong agreement between BBN theory and observation has allowed this theory to establish itself as one of the pillars of Cosmology, the increased precision from the experimental as well as theoretical side is starting to show some cracks in its foundation.

4.2   Neutron Lifetime

We have up to now discussed only the $\Omega_b h^2$ dependence of the final abundances arguing that is the only parameter influencing SBBN predictions. However, this is only partly true, since it is the only *cosmological* parameter, but there are many more that are used as input from nuclear as well as particle physic. This includes, for example, the already extensively discussed reaction rates the masses of the particles involved and the parameters controlling the strength of their interactions. Of this last category, probably the most important one is the neutron lifetime τ_n, that is used to calibrate the weak reaction rates.

Up to now, we have used the value reported by the PDG [11]:

$$\tau_n = (878.4 \pm 0.5)\,\mathrm{s} \tag{4.5}$$

as an input. While this looks like a very precise determination. However, there is a long-standing anomaly concerning the neutron lifetime which has not been resolved to date, see [57, 58, 50] for recent reviews on this topic. Essentially, the anomaly boils down to the following problem. There are two current methods to determine the neutron lifetime, which we will henceforth refer to as the *beam* and *bottle* methods.

As the name suggests, for the beam method one requires a beam of slow neutrons that go into an experimental volume V that is surrounded by strong electromagnetic fields. The neutrons if stable will not be affected by the E and B fields and are counted upon exiting the volume, in order to know how many neutrons are in the volume at any given moment. If they decay, however, they will produce protons, which are then extracted by virtue of the electromagnetic fields and subsequently counted. From the ratio of neutrons inside the volume and the protons detected, one then obtains the neutron lifetime. The results obtained using this method are consistent with each other and give[58]:

$$\tau_n^{\mathrm{beam}} = (888.0 \pm 2.0)\,\mathrm{s} \tag{4.6}$$

The approach of the bottle method, on the other hand, is to use ultra cold neutrons (UCNs) and let them flow into a of a container whose walls have a high potential energy and are thus reflective for neutrons. Due to the form of the container (hence the name bottle), neutrons are trapped by gravity inside the container. Then one allows the neutron to decay for a variable amount of time Δt comparable to τ_n and measures the neutrons remaining inside the bottle upon extraction. This can then be fit to obtain the neutron lifetime. Again, measurements that rely on this method are consistent with each other and give [58]:

$$\tau_n^{\mathrm{bottle}} = (878.4 \pm 0.5)\,\mathrm{s} \tag{4.7}$$

As can be seen, the value reported by the PDG is mainly composed of bottle measurements. Both measurements are consistent with each other and report very small systematic and statistical uncertainties. Nonetheless, they differ by:

$$\Delta\tau_n = (8.6 \pm 2.1)\,\mathrm{s} \tag{4.8}$$

which corresponds to a $\sim 4.1\sigma$ tension between the two determinations. Unless the anomaly turns out to be an indication of new physics, a resolution will most
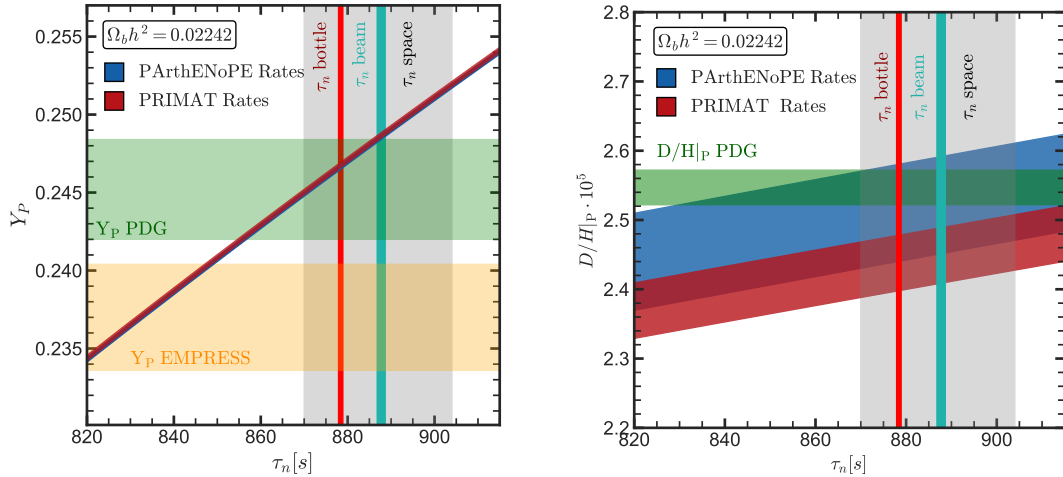
Figure 4.3: 68% CL bands for the Primordial Helium mass fraction, Y_P, (Left) and Deuterium to Hydrogen ratio, $D/H|_P$, (Right) as a function of the neutron lifetime τ_n for $\Omega_b h^2 = 0.02242$ for both choices of nuclear rates. The green bands correspond to the PDG-22 68% CL of Y_P and $D/H|_P$, where as the yellow band corresponds to the EMPRESS prior on Y_P. The vertical bands correspond to the different experimental measurements of τ_n.

likely involve an independent measurement with a different method, completely uncorrelated systematic uncertainties and a similar precision.

In that spirit, recently, space-based determinations of the neutron lifetime have emerged [59, 60], which rely on measuring the flux of neutrons emitted from the surface of an astrophysical body due to interactions between the surface and cosmic rays during flyby missions. From this, one can obtain a measurement with clearly very different systematic errors to laboratory measurements. Combining both measurements using the same technique, [60] finds:

$$\tau_n^{\text{space}} = (883 \pm 17)\,\text{s} \tag{4.9}$$

Which is in agreement with both bottle and beam experiments, but is not competitive with either measurement given its large uncertainties. Thus, the neutron lifetime measurement remains a puzzle that cannot be solved.

In order to assess how significant this tension is for nucleosynthesis, we must first understand how a change in τ_n influences the final Helium and Deuterium abundances. This dependence is shown on Fig. 4.3, with Helium on the left and Deuterium on the right. For Helium we only show the determinatio using the PArthENoPE rates, since the PRIMAT result is virtually identical.

We see that, unlike for the baryon density, Helium is extremely sensitive to the exact value of τ_n. The reason is that almost all neutrons available at the onset of Nucleosynthesis at T_{BBN} are cast into Helium. After neutrons have frozen out, they are essentially free until that happens. Thus, the evolution of their abundance at that time can be described as:

$$n_n \simeq n_n|_{\text{f.o.}} \cdot e^{-\frac{t}{\tau_n}} \tag{4.10}$$

A change in the neutron lifetime therefore has two effects on its abundance at T_{BBN}. First, the weak reaction rates controlling the nucleon freeze-out $\Gamma_{n \leftrightarrow p} \propto \frac{1}{\tau_n}$, so an increase in τ_n implies a decrease in the strength of the weak reactions, which consequently means that freeze-out happens at an earlier time where the neutron abundance is less suppressed. Second, an increase in τ_n implies that neutrons will decay more slowly. Both of these effects are very significant and add up and increase the final Helium abundance, making it exceptionally sensitive to the exact value of the lifetime. More quantitatively, we find:

$$\text{PRIMAT}: \quad Y_P = Y_{P,\text{ref}} \cdot \left(\frac{\tau_n}{\tau_{n,\text{ref}}} \right)^{0.734} \tag{4.11a}$$

$$\text{PArthENoPE}: \quad Y_P = Y_{P,\text{ref}} \cdot \left(\frac{\tau_n}{\tau_{n,\text{ref}}} \right)^{0.741} \tag{4.11b}$$

For deuterium, on the other hand, we see on the right panel of Fig. 4.3 that the dependence on τ_n is somewhat milder, but still positively correlated. The reason is, similarly to Helium, that a larger value of the neutron abundance implies an overall larger reservoir which increases the final abundance. Additionally, we are quoting the ratio of Deuterium over protons. An increase in the initial abundance of neutrons implies an equally large decrease in the final proton abundance, so that D/H increases. Quantitatively we find:

$$\text{PRIMAT}: \quad D/H|_P = D/H|_{P,\text{ref}} \cdot \left(\frac{\tau_n}{\tau_{n,\text{ref}}} \right)^{0.417} \tag{4.12a}$$

$$\text{PArthENoPE}: \quad D/H|_P = D/H|_{P,\text{ref}} \cdot \left(\frac{\tau_n}{\tau_{n,\text{ref}}} \right)^{0.418} \tag{4.12b}$$

While it should not come as a surprise that the final abundances strongly depend on a parameter as crucial as the lifetime of the neutron, the real question is how choosing either the beam or bottle mean will affect the conclusions that can be drawn from BBN. From Eqs. 4.11, 4.12, we can see that a change in τ_n of the size of the discrepancy between both measurements, $\Delta \tau_n = 8.6\,\text{s}$, corresponds to a shift of:

$$\Delta Y_P = 0.0018 \simeq 0.6\sigma_Y$$
$$\Delta D/H|_P = 0.0010 \simeq 0.1\sigma_D$$

for any choice of rates, where σ combines the theoretical and observational uncertainties on the abundance. Thus, given the large observational uncertainty for primordial Helium, a different choice of prior for the neutron lifetime will only mildly affect any conclusions drawn from nucleosynthesis, shifting it by, at most, $0.6\sigma_Y$. For D/H, it is the combination with the large theoretical uncertainty that makes the possible significance of the choice of prior much lower.

Thus, we may conclude that, although a precise determination of the neutron lifetime is of crucial importance for BBN, choosing between either the beam or bottle determination will not critically affect conclusions. Perhaps the most important aspect, though, is to remember that there is a long-standing problem with the neutron lifetime and that, even though generally a theoretical uncertainty of only $\sigma_{Y,\text{th}} = 0.00017$ is reported, at present the theoretical uncertainty is actually higher than that.
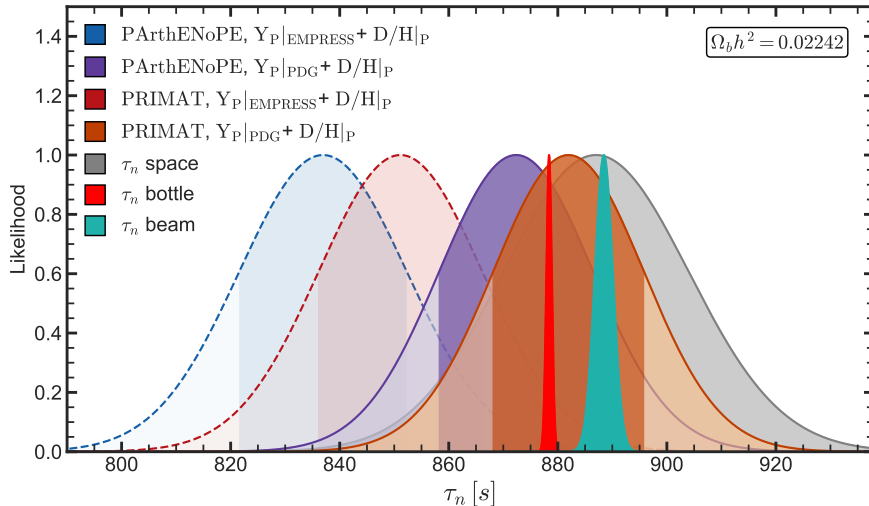
Figure 4.4: Likelihood function for τ_n in seconds from the PDG-22 (solid) and EM-PRESS (dashed) prior on Y_P and the PDG-22 prior on $D/H|_P$ for PRIMAT(red/orange) and PArthENoPE(blue/purple) rates for $\Omega_b h^2 = 0.02242$, as well as from different experiments. See text for further details.

However, instead of complaining about the possible challenges that the neutron lifetime puzzle might pose for Nucleosynthesis, we can also make use of the fact that we have, assuming the CMB prior for the baryon density is correct, two direct measurements whose prediction is very sensitive to and solely depends on the neutron lifetime. Thus, we can obtain from BBN a cosmological measurement of the neutron lifetime that is totally independent from the laboratory measurements and might help solve the puzzle for good.

The resulting likelihood distributions that can be obtained from BBN using the PArthENoPE as well as the PRIMAT rates for both the PDG and the EMPRESS determination of Y_P, along with the likelihoods obtained from beam, bottle and space measurements are shown on Fig. 4.4 and summarized on Table 4.2. Concretely, for the PDG prior on Y_P we find:

$$\tau_n = (870 \pm 14)\,\text{s} \tag{4.13}$$

for both choices of nuclear rates. Given that observations and data broadly agreed using the PDG-22 prior for Y_P and τ_n for the entire range of $\Omega_b h^2$, it should come as no surprise that this value agrees with τ_n^{bottle}, as the average is based on these measurements. On the other hand, it also agrees with τ_n^{beam} within $\sim 1\sigma$. Given the large observational uncertainty on the Helium measurement, this determination is not competitive with neither beam nor bottle measurements, so unfortunately it cannot give a preference for one or the other and does not alleviate the tension. Nonetheless, the sensitivity is comparable with the recent space-based measurements of τ_n, which is remarkable considering how easy it is to obtain this measurement.

Unfortunately, adding a prior on D/H_P does not increase the sensitivity by more than one second, as Helium dominates this determination, given deuteriums lower sensitivity to τ_n, as well as its large theoretical and observational uncertainty. The only thing that changes is that, since PRIMAT rates predict a smaller value for

Bounds on the Neutron Lifetime from BBN				
$\mathbf{Y_P}$	**Data Sets**	**Nuclear Rates**	$\boldsymbol{\tau_n}$	$\boldsymbol{\chi^2_{\min}}$
EMPRESS	Y_P	PArthENoPE	833 ± 16	0
		PRIMAT	832 ± 16	0
	$Y_P + D/H|_P$	PArthENoPE	836 ± 15	1.4
		PRIMAT	851 ± 15	10.4
PDG-22	Y_P	PArthENoPE	870 ± 14	0
		PRIMAT	870 ± 14	0
	$Y_P + D/H|_P$	PArthENoPE	872 ± 14	0.4
		PRIMAT	882 ± 14	5.6

Table 4.2: Summary of constraints on the neutron lifetime, τ_n, from several combinations of BBN data for two possible choices of the nuclear reaction rates. See main text for details.

$D/H|_P$ than measured, the best-fit value for τ_n increases, which only makes the agreement with both methods greater.

Obtaining a precision in the BBN measurement that is comparable with that of beam or bottle experiments requires a dramatic increase in the precision of observations of the Helium abundance. Obtaining a measurement of $\sim 2\,\mathrm{s}$ precision, for example, would require a determination of Helium as low as $\sigma_{Y,\mathrm{obs}} \sim 0.0003$, which would imply an order of magnitude increase in precision that is unthinkable in the foreseeable future as current measurements of Helium are dominated by large systematic uncertainties that are unlikely to go down anytime soon.

However, determinations of the primordial helium abundance by one experiment, like for example that of [18], already report a sensitivity of $\sigma_{Y,\mathrm{obs}} \sim 0.0022$, which would imply an uncertainty of $\sigma_{\tau_n} = 10\,\mathrm{s}$, and if we were to increase the uncertainty further to $\sigma_{Y,\mathrm{obs}} \sim 0.001$, we would obtain $\sigma_{\tau_n} = 4.8\,\mathrm{s}$, which is already smaller than the difference between the beam and bottle methods. Depending on the central value of these determinations, this would have the potential to provide a valuable indication for a cosmologically preferred lifetime.

If instead of using the PDG-22 prior for Y_P we now use that of the EMPRESS collaboration we find:

$$\tau_n = (833 \pm 16)\,\mathrm{s} \tag{4.14}$$

for PArthENoPE rates and a very similar result for PRIMAT rates. These are shown as the dashed lines on Fig. 4.4. As the best-fit value for Y_p reported by EMPRESS is much lower, the neutron lifetime we find is likewise significantly lower, showing again a tension of $\sim 3\sigma$ with observations. However, even though such a low value of the neutron lifetime would, in principle, solve the EMPRESS anomaly, it is severely constrained, not only by the beam and bottle experiments, but by a plethora of other observations.

Seeing as neither the neutron lifetime, nor the baryon density are able to satisfactorily accommodate the low determination of Y_P from EMPRESS, resolving this tension in BBN will require us to go a step further and introduce aspects beyond the respective Standard models of particle physics, as well as cosmology. This is what we will do for the rest of the thesis.

4.3   Effective Number of Neutrino Species

We will now depart from the Standard paradigm of Big Bang Nucleosynthesis and introduce elements of new physics to the theory. This is of interest not only to resolve the tensions we have alluded to in the previous section, but also in itself. Nucleosyntesis is the earliest probe of the Universe available to us at present. The CMB constrains physics at $T \sim \mathcal{O}(0.1\,\mathrm{eV})$, whereas with BBN we can directly probe physics at energies up to $T \sim \mathcal{O}(10\,\mathrm{MeV})$, which is eight orders of magnitude higher than the CMB. In terms of time, with the CMB we can look back to $380\,000\,\mathrm{yr}$ after the Big Bang, while nucleosynthesis gives us a direct insight into physics at only $t \sim \mathcal{O}(10^{-3}\,\mathrm{s})$.

The Standard Model should in principle be valid up to Energies $\sim \mathcal{O}(100\,\mathrm{GeV})$ at least, so any deviations might be an indication of new physics even at such low energies and may serve as a guide-post for BSM physics. On the other hand, many extensions proposed to solve tensions in laboratory physics can have severe impacts on Cosmology at this time, so BBN may help severely constrain these models we would otherwise not be able to reject. Thus, studying the impact of new physics on Nucleosynthesis is of crucial importance.

Just as there are three main epochs of BBN, modifications to it can be likewise put into three categories. First, modifications at late times to the nuclear reaction rate network. These generally require very specific models and will have severe consequences for all nuclei. This type of modifications is generally used to modify the abundance of heavier nuclei like Lithium and Beryllium in order to solve the Lithium problem.

Second, one may also modify the reactions that lead to the neutron to proton freeze-out, either by adding new reactions involving neutrons or protons, modifying the initial abundances of the particles involved, or simply changing the strength of the weak rates. These will affect all abundances, but especially that of Helium.

Last, but definitely not least, even in the absence of any direct interaction with Standard Model particles, the mere presence of new particles (or objects, like for example Primordial Black Holes) will have a direct influence on the energy density at the time of BBN, therefore modifying the Hubble parameter and with it the time-temperature ratio that is of crucial importance to all reactions. This is the modification to the Standard paradigm that is best studied and the one we we will start with.

Aside from the advantage of probing the Universe at an earlier time than the CMB, BBN has another aspect that make it very attractive to study new Physics. It makes very direct and easily falsifiable predictions, namely the primordial abundances which can be directly compared with observations with very simple statistical methods.

This simplicity, while very attractive as it allows to place very stringent constraints that are hard to evade, is also partly its downfall, since there are only two reliable measurements of primordial abundances and we can therefore, out of the plethora of effects that influence nucleosynthesis, only constrain one at a time independently from the CMB or two if we combine BBN and the CMB.

Unlike direct modifications of the neutron to proton ratio, or the nuclear rates,

influencing the background expansion at the time of BBN does not necessarily require any specific type of interactions. The mere presence of exotic particles with a sufficiently large contribution to the Universe's energy density will affect the final abundances in a homogeneous way for a large class of models of new physics.

These models are generally referred to under the umbrella term of *dark radiation*, as most involve the presence of a new particle that is weakly interacting with the Standard model, if at all, with a mass of at most $\mathcal{O}(\text{MeV})$, in order for it to be relativistic or close to it at the epoch of BBN, as otherwise its contribution to ρ_{tot} would be negligible.

Models of dark radiation and many more can be constrained using just one parameter that has already been introduced for Standard BBN, the effective number of neutrinos N_{eff}. While this is considered non-standard nucleosynthesis, the influence of this specific modification has been a topic of intense study for many years now, because of the wide applicability of constraints on this parameter as well as the amount of BSM physics that predict a strong modification to it, hence why we have included it in this section.

From the Standard model, we would expect that $N_{\text{eff}} = 3$. We have already seen that incomplete neutrino decoupling very slightly modifies this relation to be $N_{\text{eff}} = 3.043$. In order to differentiate the Standard Model contribution to N_{eff} from that of dark radiation, it is customary to define:

$$\Delta N_{\text{eff}} = N_{\text{eff}} - N_{\text{eff}}^{\text{SM}} = N_{\text{eff}} - 3.043 \tag{4.15}$$

The question now is how exactly ΔN_{eff} modifies the final Helium and Deuterium abundances. Given that it only modifies the energy density present during BBN, it will mainly affect it through the Hubble rate, which for a radiation dominated Universe can be parametrized in terms of the effective degrees of freedom g_{eff}. The contribution to the degrees of freedom from dark radiation can be written as:

$$g_{\text{eff}}^{e,\text{DR}} = \frac{\rho_{\text{DR}}}{\overline{\rho_\gamma}} = \frac{7}{4}\left(\frac{4}{11}\right)^{\frac{4}{3}} \cdot \Delta N_{\text{eff}} \simeq 0.45 \cdot \Delta N_{\text{eff}} \tag{4.16}$$

Plugging this into eq. 3.17, we find:

$$H = 1.66\sqrt{g_{\text{eff}}^{\text{SM}} + 0.45\Delta N_{\text{eff}}}\,\frac{T^2}{M_{\text{Pl}}} \tag{4.17}$$

During BBN $g_{\text{eff}}^{\text{SM}}$ ranges between $3.36 - 10.75$. Taking the mean value for $g_{\text{eff}}^{\text{SM}} =$, we can assume that $0.45\Delta N_{\text{eff}} \ll g_{\text{eff}}^{\text{SM}}$, so that we can expand the root to find:

$$H = 1.66\sqrt{g_{\text{eff}}^{\text{SM}}}\,\frac{T^2}{M_{\text{Pl}}} \cdot \left(1 + \frac{0.45\Delta N_{\text{eff}}}{2g_{\text{eff}}^{\text{SM}}}\right) \simeq H^{\text{SM}} \cdot (1 + 0.06\Delta N_{\text{eff}}) \tag{4.18}$$

Thus, an increase in ΔN_{eff} implies a relative increase by about $0.06\Delta N_{\text{eff}}$ in the expansion rate, which can be quite sizable. The effect of such an increase in the expansion rate on nucleosynthesis is twofold.

The first is a shift in the time-temperature relation, as $t = \frac{1}{2H(T)}$, such that the same temperature corresponds to a relatively smaller time. The time-temperature relation multiplies all the source terms in the Boltzmann equation and therefore
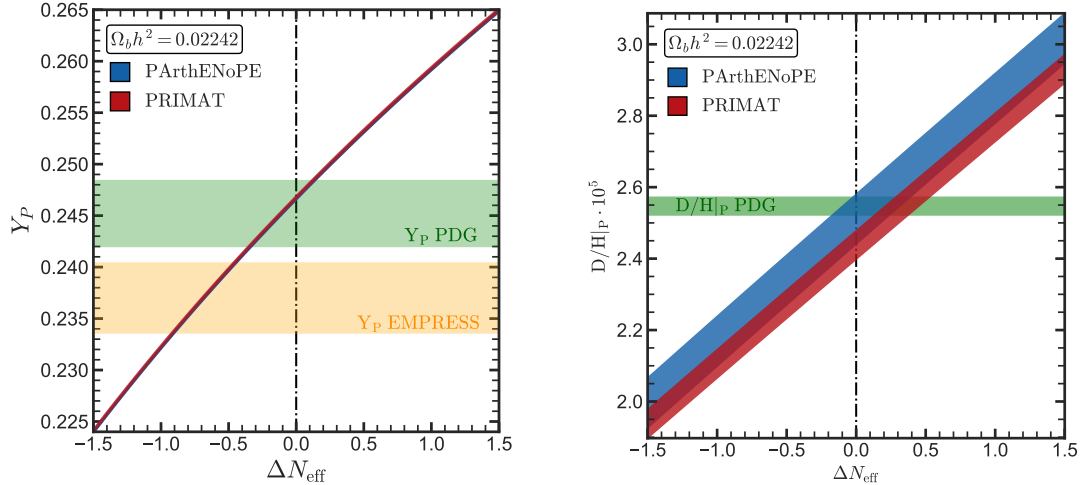
Figure 4.5: Primordial Helium mass fraction, Y_P, (Left) and Deuterium to Hydrogen ratio, $D/H|_P$, (Right) as a function of the additional effective number of neutrino species ΔN_{eff} for $\Omega_b h^2 = 0.02242$ and both choices of nuclear rates. The green bands correspond to the PDG-22 68% CL of Y_P and $D/H|_P$, where as the yellow band corresponds to the EMPRESS prior on Y_P. The vertical bands correspond to the different experimental measurements of τ_n.

influences them in the same manner. As a result, the temperature for the onset of BBN does not change, as this is determined by equating the source term for the DD-reactions and the deuterium photodissociation. Thus, an increase in the expansion rate implies a shorter time-span for free neutrons to decay with τ_n and, consequently, an increase in the neutron to proton ratio at the onset of BBN.

On the other hand, the temperature at which the weak rates freeze-out, determined roughly by the condition that $\frac{\Gamma}{H} \simeq 1$, gets shifted to higher temperatures. Since $\left(\frac{n_n}{n_p}\right)^{\text{eq}} = e^{\frac{-Q}{T}}$, this implies an even higher neutron to proton ratio at the onset of nucleosynthesis which, similarly to the neutron lifetime, increases the abundances of both Helium and Deuterium.

The actual dependence on ΔN_{eff} of the two is shown on Fig. 4.5, with Helium on the left and Deuterium on the right panel. In order to obtain a fit of the same form as for the other parameters, we will recast it in terms of N_{eff} and normalize it to $\Delta N_{\text{eff}}^{\text{SM}}$. The results for both choices of reaction rates are actually identical and we find:

$$Y_P = Y_{P,\text{ref}} \cdot \left(\frac{N_{\text{eff}}}{N_{\text{eff}}^{SM}}\right)^{0.163} \tag{4.19a}$$

$$D/H|_P = D/H|_{P,\text{ref}} \cdot \left(\frac{N_{\text{eff}}}{N_{\text{eff}}^{SM}}\right)^{0.407} \tag{4.19b}$$

Even though the exponents are the same, of course the reference values differ, as can be sen by the offset between the PArthENoPE (blue) and PRIMAT (red) bands on the right panel of Fig. 4.5. We also see that, indeed, both abundances are positively correlated with N_{eff} and are quite sensitive to it, as well. Perhaps counter-intuitively, the Deuterium abundance is actually more sensitive than the Helium abundance to

changes in the Helium abundance.

4.3.1   BBN Constraints on ΔN_{eff}

Unlike the neutron lifetime and the baryon density, the sensitivity of Helium to a non-standard value for N_{eff} actually has the potential to resolve the EMPRESS anomaly. While the prediction for Helium seems to be in agreement with the PDG-22 prior for $\Delta N_{\text{eff}} \approx 0$, resolving the tension with the EMPRESS prior requires a negative value for $\Delta N_{\text{eff}} \approx -0.65$.

This would be fine in princple if not for Deuterium, since a lower value of ΔN_{eff} implies a lower value of D/H. Even though this is not too problematic if we assume PArthENoPE rates, it is severely constrained if we use PRIMAT rates. Despite showing promess, it seems that there is no way to accommodate the measurements as both priors have different preferences for the sign of ΔN_{eff}.

Unlike with Standard Nucleosynthesis, however, this is not necessarily a problem, as we have an additional parameter in $\Omega_b h^2$ we can play with. Allowing this parameter to float is not only helpful to better accommodate the observations, but actually required if we want to be consistent with our analysis since these two parameters are very strongly correlated.

The 1σ and 2σ contours obtained following the methods described in Ch. 2 allowing both ΔN_{eff} and $\Omega_b h^2$ to simultaneously vary are shown on Fig. 4.6. In order not to overload the plot, on the left panel we show the impact of choosing a different prior for Y_P for the PArthENoPE rates, where the EMPRESS prior for Y_P is shown in solid lines and the dashed lines correspond to the PDG-22 value. On the right, the value of Y_P remains that of the EMPRESS collaboration, but the contours obtained using both PArthENoPE (purple/blue) rates and PRIMAT (red/orange) rates are shown. Since both $\Omega_b h^2$ and ΔN_{eff} can be constrained from observations of the CMB, we additionally show the contours one obtains when adding the Planck prior from eq. 2.17, which corresponds to the black-grey contour. The corresponding constraints are also summarized on Table 4.3.

Up to now we have seen that, with the PDG-22 prior on Y_P, there are no tensions between the observations, the ΛCDM model and the standard prediction for both Y_P and D/H with PArthENoPE rates. Thus, the distribution shows no significant preference for a value of $\Delta N_{\text{eff}} \neq 0$ and the Planck 1σ contour is contained at least partly within the 1σ contour for BBN. From this contour, one obtains the following constraints:

$$\Omega_b h^2 = 0.022031 \pm 0.00053\,, \quad [\text{Y}_\text{P} + \text{D/H}|_\text{P} \tag{4.20a}$$
$$N_{\text{eff}} = 2.93 \pm 0.21\,, \qquad\qquad \text{PDG} - 22] \tag{4.20b}$$

Comparing this to eq. 4.3, it is clear that adding an additional parameter has increased the uncertainty on the baryon density, which is to be expected since we have added a new degree of freedom to our fit. Thus, constraints from the CMB still dominate $\Omega_b h^2$. This is evident when looking at the contour including the Planck prior, where the contour very noticeably shrinks in size on the x-axis.

The situation is different regarding N_{eff}. The CMB constrains $N_{\text{eff}} = 2.97 \pm 0.29$. Not only are the constraint on this parameter from BBN are actually stronger than
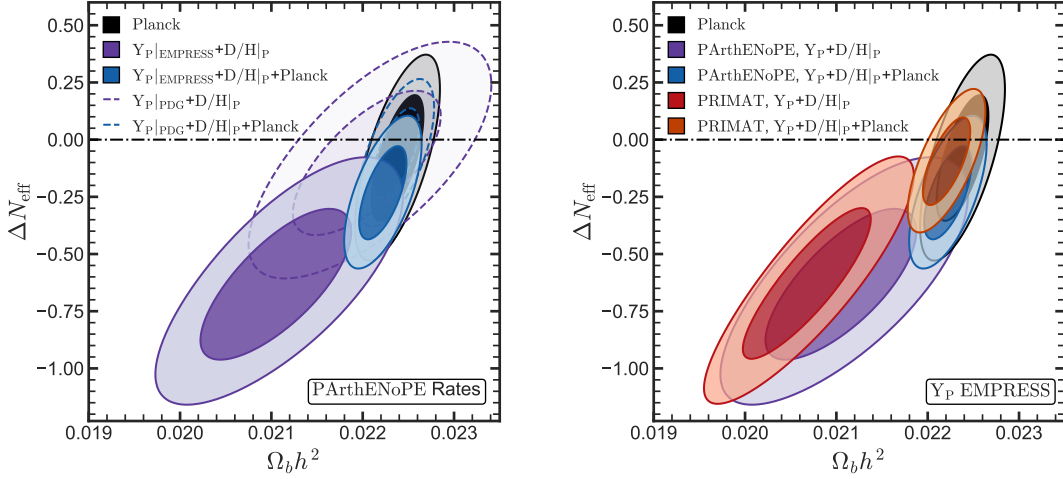
Figure 4.6: **Left:** 1σ and 2σ C.L.s for ΔN_{eff} and $\Omega_b h^2$ for BBN and Planck data, independently and combined, assuming either the EMPRESS (solid) or PDG-22 (dashed) prior on Y_P for PArthENoPE rates. **Right** Same contours using only the EMPRESS prior on Y_P, but adopting also the PRIMAT rates(red/orange).

those from the CMB. Since they are still comparable, though, we expect a noticably increased sensitivity to N_{eff} when adding the Planck prior to our χ^2. More concretely, we find:

$$\Omega_b h^2 = 0.02236 \pm 0.00017\,, \qquad [\text{Y}_\text{P} + \text{D/H}|_\text{P} + \text{CMB} \qquad (4.21\text{a})$$
$$N_{\text{eff}} = 2.98 \pm 0.13\,, \qquad \text{PDG} - 22 + \text{Planck}] \qquad (4.21\text{b})$$

Thus, the sensitivity on N_{eff} increases by ≈ 0.08 when using the Planck prior. This increase is not only due to combining the two independent constraints, but also due to the correlation of N_{eff} with $\Omega_b h^2$. With the central value now pushed closer to 3, any form of extra radiation present at the BBN epoch is severely constrained.

On the other hand, if we instead choose the EMPRESS prior for Y_P, the situation radically changes, we find:

$$\Omega_b h^2 = 0.02103 \pm 0.00054\,, \quad [\text{Y}_\text{P} + \text{D/H}|_\text{P} \qquad (4.22\text{a})$$
$$N_{\text{eff}} = 2.41 \pm 0.22\,, \qquad \text{EMPRESS}] \qquad (4.22\text{b})$$

which differs from eq. 7.20 drastically in the central value of the contours. The most noticeable change is in N_{eff}. Since we can see from Fig. 4.2 that there is no way to obtain such a low value of Y_P with only the baryon density, even though Y_P is less sensitive than $D/H|_\text{P}$ to N_{eff}, it actually dominates the constraints, driving it to a much lower value that, again, differs from the Standard value of $N_{\text{eff}} = 3.043$ by almost 3σ.

As a result of that, $\Omega_b h^2$ gets pushed to lower values in order to compensate for the change in N_{eff}, which increases the tension with the CMB, even for PArthENoPE rates which previously were not in tension with it, albeit only slightly. However, N_{eff} is only a solution since we have permitted $\Omega_b h^2$ to float freely. If instead we add the Planck prior, there is only a small amount of room for $\Omega_b h^2$ to compensate

for negative ΔN_{eff} in $D/H|_P$. The constraints obtained with the Planck prior are:

$$\Omega_b h^2 = 0.02222 \pm 0.00017\,, \quad [\text{Y}_\text{P} + \text{D/H}|_\text{P} + \text{CMB} \tag{4.23a}$$
$$N_{\text{eff}} = 2.81 \pm 0.13\,, \qquad\qquad \text{EMPRESS + Planck}] \tag{4.23b}$$

The resulting constraints, while still pointing towards negative values of ΔN_{eff}, are only in a very mild tension with $\Delta N_{\text{eff}} = 0$. The fit to observational data, though, is worse than without the Planck prior.

Given that the strong correlation between $\Omega_b h^2$ and ΔN_{eff} plays such a crucial role, it is expected that the choice of rates strongly affects the constraints as well. Without a prior on $\Omega_b h^2$, the constraints on N_{eff} are dominated by Y_P, so we do not expect them to change given the choice of rates. On the other hand, the tension between observations and the Standard prediction for BBN needs to be resolved. This adds to the effect of negative ΔN_{eff} and pushes the central value of the fit to lower $\Omega_b h^2$. Additionally, the constraints on $\Omega_b h^2$ get more stringent.

The plot on the right panel of Fig. 4.6 clearly exhibits that behavior, with the red contour not moving at all on the ΔN_{eff}-axis, but shifting to the left and becoming thinner. More quantitatively, for PRIMAT rates and only BBN priors we find:

$$\Omega_b h^2 = 0.02067 \pm 0.00046\,, \quad [\text{Y}_\text{P} + \text{D/H}|_\text{P} \tag{4.24a}$$
$$N_{\text{eff}} = 2.41 \pm 0.22\,, \qquad\qquad \text{EMPRESS}] \tag{4.24b}$$

which agrees with our expectations. Constraining $\Omega_b h^2$ to its CMB value has a similar effect on both parameters as with the PArthENoPE rates, namely increase both towards their standard values. However, in order to account for the additional tension in $\Omega_b h^2$ from this choice of rates, N_{eff} needs to be even higher. Thus, the main effect of including the CMB prior in our fit with PRIMAT rates is to increase N_{eff} slightly. The constraints one finds are:

$$\Omega_b h^2 = 0.02220 \pm 0.00017\,, \quad [\text{Y}_\text{P} + \text{D/H}|_\text{P} + \text{CMB} \tag{4.25a}$$
$$N_{\text{eff}} = 2.95 \pm 0.13\,, \qquad\qquad \text{EMPRESS + Planck}] \tag{4.25b}$$

which is in good agreement with $\Delta N_{\text{eff}} = 0$, but increase the overall tension with observations as evidenced by the higher $\chi^2_{\text{min}} = 12.2$ for this fit.

The same overall behavior of the constraints when choosing a different set of reaction rates is exhibited when using the PDG-22 prior for Y_P. In that case, though, the only tension that needs to be resolved is that in $\Omega_b h^2$. Thus, in the BBN only case we expect values for N_{eff} close to 3, and slightly higher when adding the Planck prior. More concretely, we find:

$$\Omega_b h^2 = 0.02234 \pm 0.00017\,, \quad [\text{Y}_\text{P} + \text{D/H}|_\text{P} + \text{CMB} \tag{4.26a}$$
$$N_{\text{eff}} = 3.09 \pm 0.12\,, \qquad\qquad \text{EMPRESS + Planck}] \tag{4.26b}$$

These constraints, while still in agreement with $\Delta N_{\text{eff}} = 0$, allow values as high as $\Delta N_{\text{eff}} = 0.17$. On the other hand, we have seen that resolving the EMPRESS anomaly with this parameter would require values as low as $\Delta N_{\text{eff}} = -0.85$.

Bounds on the Effective Number of Neutrino species from BBN and CMB Data					
$\mathbf{Y_P}$	**Data Sets**	**Nuclear Rates**	$\mathbf{\Omega_b h^2}$	$\mathbf{N_{eff}}$	$\chi^2_{\min}$
EMPRESS	$Y_P + D/H\vert_P$	PArthENoPE	0.02103 ± 0.00054	2.41 ± 0.22	0
		PRIMAT	0.02067 ± 0.00046	2.41 ± 0.22	0
	$Y_P + D/H\vert_P$ + Planck	PArthENoPE	0.02222 ± 0.00017	2.81 ± 0.13	5.5
		PRIMAT	0.02220 ± 0.00017	2.95 ± 0.13	12.2
PDG-22	$Y_P + D/H\vert_P$	PArthENoPE	0.02201 ± 0.00053	2.93 ± 0.21	0
		PRIMAT	0.02165 ± 0.00044	2.94 ± 0.21	0
	$Y_P + D/H\vert_P$ + Planck	PArthENoPE	0.02236 ± 0.00017	2.98 ± 0.13	0.4
		PRIMAT	0.02234 ± 0.00017	3.09 ± 0.12	4.8

Table 4.3: Summary of constraints on the Baryon density, $\Omega_b h^2$, and the effective number of neutrino species, N_{eff}, from BBN and CMB data, independently and combined, for two possible choices of the nuclear reaction rates. See main text for details.

4.3.2 Light Scalar as Dark Radiation

Regardless of the prior chosen for BBN, the presence of another neutrino species, for example a sterile neutrino, is severely constrained, since a sterile neutrino with a normal mixing angle would increase N_{eff} by 1. In order to understand how even a fractional and small value for $\Delta N_{\text{eff}} < 1$ might still be of interest, we will look concretely at an example of how new Physics might alter it. For simplicity, let us assume the case of a light real scalar particle χ with mass $m_\chi \ll 1\,\text{MeV}$ that only very weakly interacts with the Standard model and does predominantly decay to channels other than electrons and neutrinos. Thus, its only influence on BBN is through its gravitational presence, namely its energy density.

It is produced thermally in the early Universe through the freeze-out mechanism. Given its weak interaction with the SM, it is no longer in equilibrium with the thermal bath of photons. We will assume its decoupling happens at a temperature $T_D \gg 1\,\text{MeV}$. Given that it remains relativistic until BBN, its energy density has the following form:

$$\rho_\chi = \frac{\pi^2}{30} T_\chi^4 = \overline{\rho_\gamma}(T) \cdot \left(\frac{T_\chi}{T}\right)^4 \tag{4.27}$$

The derivation for the temperature ratio is analogous to the case of neutrinos assuming complete decoupling, so that we find:

$$\frac{T_\chi}{T}(T) = \left(\frac{g_{\text{eff}}^{\text{SM}}(T)}{g_{\text{eff}}^{\text{SM}}(T_D)}\right)^{\frac{1}{3}} = \left(\frac{g_{\text{eff}}^{\text{SM}}(T_{\nu,f})}{g_{\text{eff}}^{\text{SM}}(T_D)}\right)^{\frac{1}{3}} \cdot \left(\frac{4}{11}\right)^{\frac{4}{3}} \tag{4.28}$$

which can be directly inserted into the energy density. The energy density in form of radiation at the epoch of BBN now contains contributions from photons, electrons, neutrinos and χ. This can now directly be inserted into the generalized definition of N_{eff} (Eq. 3.47) to find:

$$N_{\text{eff}} = \frac{8}{7} \left(\frac{11}{4}\right)^{\frac{4}{3}} \left(\frac{\rho_\nu + \rho_\chi}{\rho_\gamma}\right)\bigg|_{T_0} \tag{4.29}$$

From this equation, one can easily obtain that:

$$\Delta N_{\text{eff}} = \frac{8}{7}\left(\frac{11}{4}\right)^{\frac{4}{3}}\left(\frac{\rho_\chi}{\rho_\gamma}\right)\Bigg|_{T_0} = \frac{4}{7}\left(\frac{11}{4}\right)^{\frac{4}{3}}\cdot\left(\frac{T_\chi}{T}\right)^4 = \frac{4}{7}\cdot\left(\frac{T_\chi}{T_\nu}\right)^4 \qquad (4.30)$$

The precise contribution from such a particle therefore depends only on the ratio of the photon to χ temperature, which in turn depends on the details of the particle's decoupling which is directly related to the interaction strength of the particle. Thus, by constraining ΔN_{eff}, we can directly constrain $\langle\sigma v\rangle$ and the particle's mass.

Depending on the exact value of $\langle\sigma v\rangle$, the contribution to ΔN_{eff} varies greatly. The smallest contribution it will give is if χ decouples before the electroweak phase transition at $T_D \geq 100\,\text{GeV}$. Then $g_{\text{eff}}^{\text{SM}} = 106.75$, so the minimal contribution to N_{eff} would be $\Delta N_{\text{eff}}^{\text{min}} = 0.02$. One obtains the maximal contribution if $\frac{T_\chi}{T} = \frac{T_\nu}{T}$, yielding $\Delta N_{\text{eff}}^{\text{max}} = 4/7$. The maximal value allowed by the constraints just derived from BBN is $\Delta N_{\text{eff}} = 0.17$, which would imply $\frac{T_\chi}{T} \simeq 0.15$, which places its decoupling close to the QCD phase transition at $T_{\text{QCD}} \simeq 160\,\text{MeV}$. The exact constraints one can extract from this now depend on the dynamics of decoupling for the chosen model. The point, however, is that even a slight deviation from the standard value might be an indication of new physics.

4.3.3 $\Delta N_{\text{eff}} < 0$

A light scalar is just one of many options to increase N_{eff}. However, we have seen that in order to resolve the tension with the EMPRESS anomaly, we require a value for $N_{\text{eff}} < 3$. We have obtained this by blindly varying the parameter without regard for the physical implications. This would be okay if we did not know how many neutrino families there are. However, it is long known that there are at least three species. Depending on their exact interaction with the Standard Model and each other, as well as their masses, this might still not be a problem. For example, if one neutrino were massive enough that it is Boltzmann suppressed, or if it had a mixing angle with other species such that it is not in thermal equilibrium with them, N_{eff} could still be lower than 3.

This is no longer an option, given the measurements on the neutrino mixing parameters and their mass. The formula for the neutrino contribution to N_{eff} , therefore, looks as follows:

$$N_{\text{eff}}^\nu = 3\cdot\frac{8}{7}\left(\frac{11}{4}\right)^{\frac{4}{3}}\cdot\frac{\rho_\nu^1}{\rho_\gamma} \qquad (4.31)$$

where ρ_ν^1 is the contribution to ρ from one neutrino species. Thus, if we want $N_{\text{eff}}^\nu < 3$ we either need to decrease that contribution or reheat the temperature of the photon bath. Both of these modifications are possible, but they require additional interactions with the plasma. This is different from the assumptions under which we have derived the constraints on N_{eff}^ν and, even if we manage to obtain $N_{\text{eff}} < 3$, it is not necessary that this will actually decrease the Helium abundance and solve the EMPRESS anomaly. Models that decrease N_{eff} need to be evaluated on a case to case basis in order to assess how this influences BBN.

One option to obtain $N_{\text{eff}} < 3$ is to increase the photon energy density relative to that of neutrinos. Since neutrino interactions keeping them in thermal equilibrium with photons are efficient until about $\sim 10 - 1\,\text{MeV}$, this class of models generally requires reheating to happen in some form for temperatures below the neutrino decoupling temperature or close to it, but not too close in order not to affect the events of Nucleosynthesis too much. Studying such models with a low reheating temperature would go beyond the scope of this thesis, but the reader is referred to [61, 62] for dedicated studies of this topic.

These studies show that, while a low reheating temperature can be very efficient in decreasing N_{eff}^{ν} to values much lower than 3, they actually increase the final Helium abundance and decrease the Deuterium abundance. Thus, regardless of the choice of nuclear reaction rates, this actually increases the tension for Helium, and for the PRIMAT rates it simultaneously increases the tension with the ΛCDM model coming from Deuterium.

Another class of models that decrease N_{eff} are MeV-scale electrophilic particles, that is, particles with masses $\sim \mathcal{O}(\text{MeV})$ whose predominant annihilation channel is to electron positron pairs. This will naturally have severe consequences on Nucleosynthesis. Dedicated studies ([63, 64] find, similarly to low reheating temperature scenarios, that the Helium abundance actually increases, despite having $\Delta N_{\text{eff}} < 0$. Therefore, even though in principle there are models that can decrease the number of effective neutrino species, none of them actually have the desired effect of reducing the Helium abundance during BBN.

Chapter 5

Time Variation of Fundamental Constants

There is one further possibility that we have not yet considered to obtain $\Delta N_{\text{eff}} < 0$, although it is not clear a priori whether it is more sensible. N_{eff} is used to parametrize changes in the Hubble expansion rate, which is dependent on three things. The first is what we have already studied, namely the total energy density of the Universe. The second is Einstein's theory of relativity, from which the form of the Friedman equation we have solved to obtain the dynamics of the background expansion has been derived. Modified theories of gravity may change the form of this equation. The success of the standard cosmological model up to now constrains these changes to be rather small, but that does not discard them, especially at the early times probed by Nucleosynthesis. Last, but not least, if we do not modify the Friedman equation, then $H \propto \frac{1}{M_{\text{Pl}}} = \sqrt{G_N}$. Thus, a change in the Hubble expansion rate can also be accounted for by a change in Newton's constant G_N.

On the other hand, G_N can be measured in the laboratory to be $G_N = (6.674\,30\pm 0.000\,15)\,\text{m}^3/(\text{kg}\,\text{s}^2)$, that is, with orders of magnitude better accuracy than what can be obtained from BBN. Therefore, G_N is, in principle, not allowed to float freely and these constraints make no sense if interpreted like this. However, we know that many constants have a running with energy due to quantum effects. One is, therefore, left to wonder whether constants may not also vary with time.

The idea is not new and dates back at least as early as 1937, when Dirac proposed his large number hypothesis [65], which implied that G_N should be time dependent. The framework that would allow these constants to vary with time within a consistent field theory was developed shortly after by Jordan [66]. Generally, this requires to promote the constants to be related to dynamical scalar fields and their vacuum expectation value.

5.1   The Gravitational Constant

The specific case of theories where only G_N is time dependent was more closely studied by Brans and Dicke in the context of extensions to General Relativity, leading to the definition of scalar tensor theories of gravity [67]. Such modifications to gravity arise quite naturally in Unified theories, such as Kaluza-Klein and String

theory. Thus, constraints on G_N at the epoch of BBN can be interpreted as constraints on its variation with cosmological time, which in turn may help constrain alternative theories of gravity.

This is not the only way to constrain the time variation of G_N, see for example [68] for an excellent review on these constraints and anything related to time variation of fundamental constants. Constraints from BBN are not only competitive with them, but BBN is the earliest probe of the Universe available to us at the moment. Therefore, it is of paramount importance to constrain the time variation of these "constants" during BBN.

It should be noted that talking about a time variation of a dimensionful quantity is not consistent, since it requires a system of units whose definition is dependent on other constants of nature which may themselves vary with time. Therefore, it only makes sense to talk about time variation of dimensionless constants or, in its absence, of ratios of dimensional constants. Regardless, it is very important to always very precisely explain which constants are promoted to be allowed a time dependence and which are not. Only within that precisely defined metrological system does it make sense to allow a time variation of constants. Concretely, we will focus on a situation where we allow G_N to vary, but all particle physics energy scales like Λ_{QCD} and the Higgs vacuum expectation value v are held fixed at their value today.

With that setup, we can now begin talking about the BBN constraints on time variation of fundamental constants. The nice thing about having used the effective degrees of freedom before is that, instead of having to do a dedicated analysis to answer this question, we can simply recast the constraints on ΔN_{eff} in terms of G_N. In order to do so, let us define

$$\alpha = \frac{\Delta G_N}{G_N^0} \tag{5.1}$$

where G_N^0 is the value we have used up to now for Newton's constant, that is its value as measured today. This allows us to write the Hubble rate as:

$$H = 1.66\sqrt{g_{\text{eff}}^{e,\text{SM}}}T^2 \cdot \sqrt{G_N} = H(T)^{\text{SM}} \cdot \sqrt{1+\alpha} \tag{5.2}$$

from which we obtain the relation:

$$\alpha = \left(\frac{H}{H^{\text{SM}}}\right)^2 - 1 \tag{5.3}$$

If we now parametrize H in terms of ΔN_{eff} , we find that:

$$\alpha = \frac{\Delta G_N}{G_N^0} = \frac{7}{43}\Delta N_{\text{eff}} \tag{5.4}$$

With this equation, we can quite simply obtain the dependence of the abundances as a function of the variation of G_N, which is shown in terms of the ratio $\frac{G_N}{G_N^0}$ on Figure 5.1 for both PArthENoPE and PRIMAT rates, with the left panel showing the dependence of Helium and the right panel that of Deuterium. Since $\frac{\Delta G_N}{G_N^0} \propto \Delta N_{\text{eff}}$, the correlation between G_N and helium and Deuterium is the same, that is, an increase in G_N implies an increase in the Hubble expansion rate, which results in
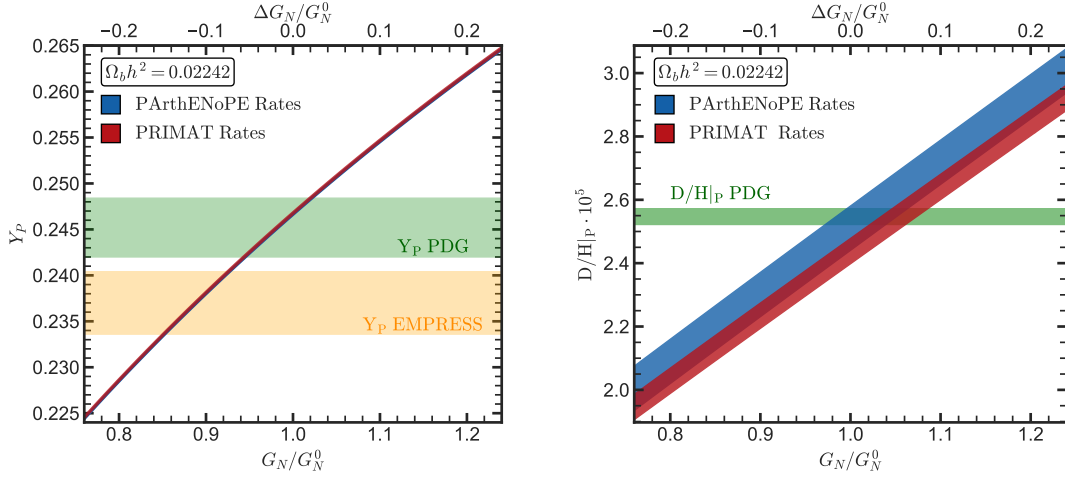
Figure 5.1: Primordial Helium mass fraction, Y_P, (Left) and Deuterium to Hydrogen ratio, $D/H|_P$, (Right) as a function of the ratio between the Gravitational constant at BBN and today $\frac{G_N}{G_N^0}$ for $\Omega_b h^2 = 0.02242$ and both choices of nuclear rates. The green bands correspond to the PDG-22 prior on Y_P and $D/H|_P$, where as the yellow band corresponds to the EMPRESS prior on Y_P.

an increased production of Helium and Deuterium. The exact dependence of the abundances on the variation of Newton's constant can be parametrized as:

$$Y_P = Y_{P,\text{ref}} \cdot \left(\frac{G_N}{G_N^0}\right)^{0.335} \tag{5.5a}$$

$$D/H|_P = D/H|_{P,\text{ref}} \cdot \left(\frac{G_N}{G_N^0}\right)^{0.835} \tag{5.5b}$$

Using Eq. 5.4, we can now recast constraints on ΔN_{eff} in terms of G_N. The results are summarized on Table 5.1 and shown on Fig. 5.2. The most important difference between this figure and Fig.4.6 is the prior used to constrain $\Omega_b h^2$. Simply using the prior for N_{eff} at the epoch of BBN and the epoch of the CMB is not consistent. However, the strong correlation between these two parameters implies that simply using the constraint for $\Omega_b h^2$ from eq. 2.14 will likely overestimate the sensitivity to G_N. Following [69], we will therefore use the slightly more conservative prior on $\Omega_b h^2$

$$\Omega_b h^2 = 0.02236 \pm 0.00030 \tag{5.6}$$

obtained from [70] by allowing G_N to vary in CMB fits and then marginalizing over G_N.

The preference for $N_{\text{eff}} < 3$ obtained from the BBN only constraints with the EMPRESS prior for Y_P with PArthENoPE rates is equivalent to:

$$\frac{\Delta G_N}{G_N^0} = -0.104 \pm 0.035 \tag{5.7}$$

corresponding to a 2.9σ preference for a non-standard value of Newton's constant, relatively lower by almost 10%, at the epoch of BBN. On the other hand, if we use
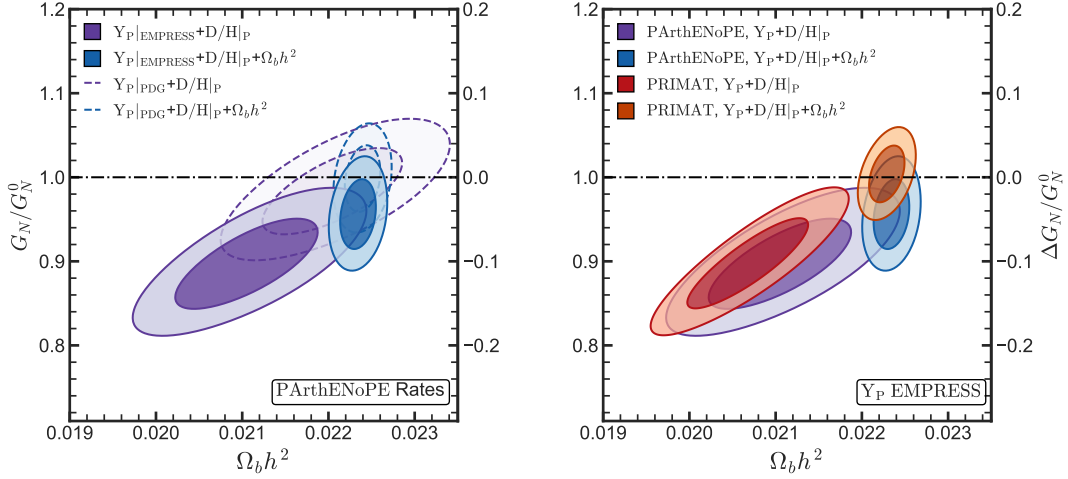
Figure 5.2: **Left:** 1σ and 2σ C.L.s for the ratio of the Gravitational constant at BBN and today $\frac{G_N}{G_N^0}$ and $\Omega_b h^2$ for BBN, assuming either the EMPRESS (solid) or PDG-22 (dashed) prior on Y_P for PArthENoPE rates. An additional conservative CMB prior on $\Omega_b h^2$ (Eq. 5.6, see text for details) is used to increase the sensitivity. **Right** Same contours using only the EMPRESS prior on Y_P, but adopting also the PRIMAT rates(red/orange).

the PDG prior and the PArthENoPE rates, we find:

$$\frac{\Delta G_N}{G_N^0} = -0.019 \pm 0.034 \tag{5.8}$$

which is indeed compatible with $\alpha = 0$.

Since we are allowing $\Omega_b h^2$ to float in this case, there is actually no difference arising from the choice of nuclear rates. This is because the Deuterium abundance essentially fixes the value for $\Omega_b h^2$, while the prior on Y_P is responsible for the constraint on G_N, for which the choice of rates does not play a significant role.

When constraining the baryon density to its CMB value, however, the prediction needs to be fit to data mainly by tuning G_N, which will increase our sensitivity to it. By constraining $\Omega_b h^2$, we are essentially fixing $D/H|_P$ to be within a very small range. Regardless of the prior on Y_P, they require $G_N < G_N^0$, albeit to different degrees. However, this also decreases the deuterium production. Since this cannot be compensated by tuning $\Omega_b h^2$, the deuterium abundance fixes the value of G_N to be close to its value today as well. Thus, regardless of the prior on Y_P, when lifting the degeneracy between $\Omega_b h^2$ and G_N, the preference for $\alpha \neq 0$ decreases and the fit becomes worse as $\chi^2_{\min}$ increases. Naturally, since deuterium now plays the central role in the constraints obtained, the choice of rates will also have a strong effect on the obtained constraints.

Concretely, we find for the EMPRESS prior:

$$\text{PArthENoPE}: \frac{\Delta G_N}{G_N^0} = -0.056 \pm 0.029 \tag{5.9a}$$

$$\text{PRIMAT}: \frac{\Delta G_N}{G_N^0} = -0.023 \pm 0.026 \tag{5.9b}$$

which increases the sensitivity of the constraints by about 20%. Additionally, this still corresponds to a 1.9σ preference for $\frac{\Delta G_N}{G_N^0} \neq 0$ for PArthENoPE rates. On the other hand, there is no preference in the case of PRIMAT rates as they are in agreement with $\frac{\Delta G_N}{G_N^0} = 0$ at $< 1\sigma$. The reason the preference is stronger for PArthENoPE rates is because the prior on $\Omega_b h^2$ is less of a problem for this choice, as they are not in tension with the CMB prior. As a result, the deuterium abundance can be decreased by a larger margin before it generates a tension with the observed abundance. Thus, α can get closer to the value required to solve the Helium tension. However, as evidenced by the large value of $\chi^2_{\min}$, the lack of preference for a non-standard value of G_N should not be mistaken by a reduction of the tension between observations and data.

If instead we use the PDG-22 prior for Y_P, we find:

$$\text{PArthENoPE}: \frac{\Delta G_N}{G_N^0} = -0.007 \pm 0.028 \tag{5.10a}$$

$$\text{PRIMAT}: \frac{\Delta G_N}{G_N^0} = 0.014 \pm 0.025 \tag{5.10b}$$

which shows no preference for $\alpha \neq 0$.

In order to interpret these results as a time variation of G_N and compare them to other measurements, we need to parametrize its time dependence. Following [69], we choose to parametrize it in the simplest way possible as a linear function of time:

$$G_N(t) = G_N^{\text{BBN}} + \dot{G}_N(t - t_{\text{BBN}}) \tag{5.11}$$

The entire time variation is contained in $\dot{G}_N$, which can be simply obtained comparing G_{BBN} with another reference time at which the value of G_N is known. We choose this to be the present time $t_0 = 13.8\,\text{Gyr}$. This weak time variation justifies the assumption that G_N is constant during the relatively short time period of BBN. Using our parametrization of $G_N(t)$, for the PDG-22 prior with a constraint on $\Omega_b h^2$ we find for the logarithmic time variation:

$$\text{PArthENoPE}: \frac{\dot{G}_N}{G_N^0} = (0.5 \pm 2.0) \cdot 10^{-12}\,\text{yr}^{-1} \tag{5.12a}$$

$$\text{PRIMAT}: \frac{\dot{G}_N}{G_N^0} = (-1.0 \pm 1.8) \cdot 10^{-12}\,\text{yr}^{-1} \tag{5.12b}$$

The sensitivity to variations of this constant from BBN is comparable to most other experiments, showing the potential of BBN to obtain powerful constraints on new Physics. The only measurement notably more sensitive is one using data from lunar laser ranging experiments, which reports $\frac{\dot{G}_N}{G_0}\big|_0 = (7.1 \pm 7.6) \cdot 10^{-14}\,\text{yr}^{-1}$ [71].

We obtain the following constraints on the relative time variation:

$$\frac{\dot{G}_N}{G_N^0} = (7.5 \pm 2.6) \cdot 10^{-12}\,\text{yr}^{-1} \tag{5.13}$$

for the BBN only prior the EMPRESS value for Y_P. Thus, within the framework of time dependent fundamental parameters, the EMPRESS anomaly could be interpreted as a 3σ indication that the gravitational constant varies ever so slightly every year, showing a possible deviation from Einstein's theory of relativity.

Constraints on the time variation of the Gravitational Constant from BBN						
$\mathbf{Y_P}$	**Data Sets**	**Nuclear Rates**	$\alpha = \frac{\Delta \mathbf{G_N}}{\mathbf{G_N^0}}$	$\frac{\dot{\mathbf{G}}_{\mathbf{N}}}{\mathbf{G_N^0}} \ [10^{-12}\,\mathrm{yr}^{-1}]$	**Pref $\alpha \neq \mathbf{0}$**	$\chi^2_{\min}$
EMPRESS	$Y_P + D/H\vert_P$	PArthENoPE	-0.104 ± 0.035	7.5 ± 2.6	2.9σ	0
		PRIMAT	-0.104 ± 0.035	7.5 ± 2.6	2.9σ	0
	$Y_P + D/H\vert_P + \Omega_b h^2\vert_{\mathrm{Planck}}$	PArthENoPE	-0.056 ± 0.029	4.1 ± 2.1	1.9σ	4.4
		PRIMAT	-0.023 ± 0.026	1.7 ± 1.9	0.9σ	9.1
PDG-22	$Y_P + D/H\vert_P$	PArthENoPE	-0.019 ± 0.034	1.3 ± 2.5	0.5σ	0
		PRIMAT	-0.017 ± 0.034	1.2 ± 2.5	0.5σ	0
	$Y_P + D/H\vert_P + \Omega_b h^2\vert_{\mathrm{Planck}}$	PArthENoPE	-0.007 ± 0.028	0.5 ± 2.0	0.3σ	0.3
		PRIMAT	0.014 ± 0.025	-1.0 ± 1.8	0.6σ	1.8

Table 5.1: Summary of constraints on the time variation of the Gravitational constant from several combinations of BBN data and two possible choices of the nuclear reaction rates. See main text for details.

However, comparing the required variation with lunar laser ranging constraints, it seems that an interpretation of the EMPRESS anomaly in terms of a time dependent gravitational constant would be ruled out. It should be noted, however, that this measurement has been obtained from an analysis of data taken over a period of 35 years. While relatively long for normal experiments, this measurement has still been taken over a short period of time, whereas the constraints from BBN come from a variation on cosmological time scales. Thus, the parametrization we choose for the time dependence of G_N very strongly influences the constraints obtained.

For example, if instead of a linear parametrization we choose $G_N \propto t^{-x}$, then the resulting constraints are of the order of 10^{-13} and no longer in tension with the lunar laser ranging experiments. Thus, even though for comparison with other literature we still include the limits in terms of $\frac{\dot{G}_N}{G_N}$, both claims of detection as well as that these constraints are ruled out, should be made with caution and constraints on the time variation of fundamental constants on cosmological timescales should be treated as such.

Additionally, while a variation of Newton's constant helps with the EMPRESS anomaly, it does not really solve the possible tensions within the standard model of cosmology, since the prior on $\Omega_b h^2$ worsens the fit with data.

Despite these caveats, the EMPRESS anomaly may indeed have an interpretation in terms of modified theories of gravity. Studying these lies beyond the scope of this thesis, but merits further investigation left for future work.

5.2 Higgs Vacuum Expectation Value

Theories where fundamental constants are allowed to vary, generally require fundamental constants to be related to a scalar field and their Vacuum Expectation Value (vev). To the best of our current knowledge, the only scalar field contained in the standard model is the Higgs field, which acquires a vacuum expectation value leading to the electroweak phase transition during which the fields in the SM become massive. Thus, we have a prime candidate for a fundamental constant which fulfills the requirements to be time dependent. Just as was the case for the gravitational

constant, v is dimensionful. Therefore, we will allow the Higgs vev to vary while keeping the scale of the strong interaction, Λ_{QCD}, fixed, at its value today

Unlike for the Gravitational constant, however, there are far few constraints on this parameter. The few constraints that can be derived mainly come from studying the aftermath of natural nuclear reactors which went critical billions of years ago. An example is the natural nuclear reactor in a uranium mine close to Oklo in the Gabon Republic[72], which went critical about 1.8 Gyr ago, but more have been discovered since. From the abundances of certain isotopes, one can extract key quantities which, among other quantities, depend also on the Higgs vacuum expectation value. However, these require a detailed model of the nuclear reaction rates, which is a very challenging task, making constraints derived from these data on v highly model dependent.

Additionally, one can obtain constraints from precise measurements of long lived α and β decays in ancient meteorites. The resulting constraints are similar to those from the Oklo phenomenon and suffer from the same problems of the model dependence, with additional uncertainty coming from the dating of the meteorites.

On the other hand, the dependence of BBN on the Higgs vev, while still involved, is less model dependent than that of Oklo and meteorite constraints, since modifications to the nuclear reaction rate network play only a secondary role [73]. Additionally, BBN allows us to probe variation of v at the longest time scale possible. With the recent developments in the theoretical description of BBN as well as improvements in the observational abundances, BBN presents itself as one of the key physical processes where variations of the Higgs vev can be tested to high precision.

In principle,the Higgs vev modifies many different parameters of importance for BBN, since it influences the masses of all fermions and sets the scale of the weak rate at the time of BBN, which as we know is of great importance, both for neutrino decoupling and for the neutron to proton freeze-out. Out of these, the most significant modification comes through four parameters, namely Fermi's constant G_F, the electron mass m_e, the nucleon mass difference $Q = m_n - m_p$, and the deuterium binding energy B_D.

In order to obtain the influence of the modification of these parameters through the Higgs vev on the final nuclear abundances, we have written a python code that solves the Boltzmann equations describing the process of nucleosynthesis (Eq. 3.106a) using the reduced network from Fig. 3.4 with the PRIMAT choice of nuclear reaction rates. The effect on the final abundances from variations of v, as we will see, is mainly on the weak rates, which requires that they be recomputed for every new value of the Higgs vev. Calculating them including the long list of corrections detailed in [20] is computationally very expensive. Additionally, making a prediction that is accurate within the theoretical uncertainties of deuterium would require us to include a much more extensive nuclear network.

We need to take both of these effects into account if we want to make predictions at more than 1% precision, which is what we need in order to make correct statements on the compatibility of these scenarios with a time variation of the Higgs vev. However, corrections to the weak rates are of the order of a few percent only already, so we should be able to safely ignore the effect of tiny variations of fundamental constants on these corrections. Additionally, the variation of v does not influence the

rest of the reaction network. It suffices, therefore, to calculate the abundances in the Born approximation, assuming complete neutrino decoupling and with only the small reaction network made up of 12 reactions, where the effect of variations of the fundamental constants is the strongest, and then simply add the effect of each correction as detailed in [20] linearly, that is:

$$Y_P(v) = Y_P^{\text{Born+SN}}(v) + \delta Y_P^{\text{weak rates, FN}} \tag{5.14a}$$

$$D/H|_P = D/H|_P^{\text{Born+SN}}(v) + \delta D/H|_P^{\text{weak rates,FN}} \tag{5.14b}$$

where $\delta Y_P^{\text{weak rates,FN}} = 0.00447$ and $\delta D/H|_P^{\text{weak rates,FN}} = 0.04$. This wil allow for a much faster computation of the final results without compromising on a precise determination of the final abundances.

For Deuterium there is the additional complication that the choice of nuclear rates has a strong effect. Instead of implementing both the PArthENoPE and PRIMAT rates, we adopt a similar method to take this into account, where we modify the deuterium abundance as follows:

$$D/H|_P = D/H|_P^{\text{Born+SN}}(v) + \delta D/H|_P^{\text{weak rates,FN}} + \delta D/H|_P^{\text{nuclear rates}} \tag{5.15}$$

with $\delta D/H|_P^{\text{nuclear rates}} = 0.07$ if we choose the PArthENoPE rates, while, naturally, $\delta D/H|_P^{\text{nuclear rates}} = 0$ for PRIMAT rates.

We have checked that both of these approximmations are actually accurate to better than 0.1% for the parameters studied up to now, namely $\tau_n, \Omega_b h^2, N_{\text{eff}}$,as well as for the neutrino chemical potential ξ_ν we will introduce later. This is supported by the fact that, while the face value of the final abundances does change depending on the choice of rates, the parameters of the fit actually vary only very slightly, if at all. Therefore, we will use this approximation in order to derive BBN constraints on the time variation of the Higgs vev.

5.2.1 Fermi's Constant

The modification of Fermi's constant G_F is perhaps the most obvious parameter that is modified when varying v, since at tree level, is quite simply related to it as:

$$G_F = \frac{1}{\sqrt{2}v^2} \tag{5.16}$$

Thus, it is clear that it will be very sensitive to any change in G_F. The impact of this on Nucleosynthesis is just as easily understood. The weak reaction rates $\Gamma_{n \leftrightarrow p}$ that determine the neutron to proton freeze-out and which are extremely important for Nucleosynthesis in general are $\propto G_F^2$, as we can see from eq. 3.77. This implies that:

$$\frac{\delta \Gamma_{n \leftrightarrow p}}{\Gamma_{n \leftrightarrow p}^0} = 2 \frac{\delta G_F}{G_F^0} \tag{5.17}$$

which is quite a strong dependence. A relative increase in G_F therefore implies an increase in the neutron to proton conversion rates, which pushes the temperature of the neutron to proton decoupling towards lower values, implying a relatively
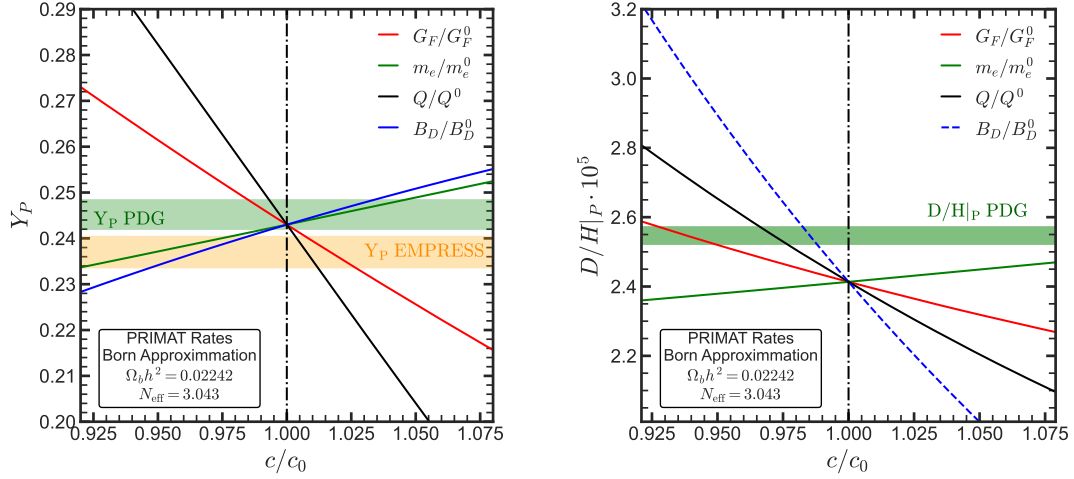
Figure 5.3: Primordial Helium(Left) and Deuterium(Right) abundance as a function of the relative variation of the fundamental constants most affected by a time variation of the Higgs vev, namely Fermi's constant, G_F, the electron mass, m_e, the Deuterium Binding Energy B_D, and the nucleon mass difference, Q. The final abundances have been calculated from the weak rates in the Born approximation and the reduced nuclear network from Fig. 3.4, assuming $N_{\text{eff}} = 3.043$ and $\Omega_b h^2 = 0.02242$ and the PRIMAT nuclear reaction rates.

lower abundance of neutrons at freeze-out. On the other hand, this implies that the neutron lifetime is shorter than the standard value, which has the same effect of reducing the number of free neutrons at the onset of nucleosynthesis, which implies a significant decrease of both the Helium and deuterium abundances.

Additionally, this will also affect the process of neutrino decoupling, which is also governed by the weak rates. However, complete neutrino decoupling will not be affected by this and, since incomplete neutrino decoupling only very weakly affects the outcome of BBN, these effects will most likely be only very weak.

In the Born approximation, the dependence of the primordial abundances as a function of the relative increase in G_F is shown as the solid red line on Fig. 5.3, with the left panel displaying the final Helium and the right panel the Deuterium abundance, confirming what we expected. This dependence can be parametrized as:

$$Y_P = Y_{P,\text{ref}} \cdot \left(\frac{G_F}{G_F^0}\right)^{-1.458} \tag{5.18a}$$

$$D/H|_P = D/H|_{P,\text{ref}} \cdot \left(\frac{G_F}{G_F^0}\right)^{-0.833} \tag{5.18b}$$

We see that the dependence on G_F is quite strong for both nuclei, so slight variations in G_F will have harrowing effects on the final abundances. Additionally, the dependence of Y_P is stronger, which is to be expected given that the Helium abundance is almost completely determined by the neutron abundance at the onset of nucleosynthesis, which is directly related to $\Gamma_{n \leftrightarrow p} \propto G_F^2$.

Since we already know that G_F is not a fundamental parameter, but rather an EFT coupling constant which is related to the Higgs vev, it only makes sense to

vary it as function of the Higgs vev. Given the simple relation between G_F and v, its variation is quite simple to obtain. We define the relative variation of the Higgs vev as:

$$\alpha_v = \frac{\delta v}{v^0} \tag{5.19}$$

such that G_F can be parametrized as follows:

$$G_F/G_F^0 = (1 + \alpha_v)^{-2} \tag{5.20}$$

Thus, an increase in the Higgs vev will lead to a decrease in Fermi's constant, resulting in higher Helium and Deuterium abundances. Inserting this into Eq. 5.18 and expanding around small values of α, we find:

$$Y_P = Y_{P,\text{ref}} \cdot (1 + 2.916\alpha_v) \tag{5.21a}$$

$$D/H|_P = D/H|_{P,\text{ref}} \cdot (1 + 1.666\alpha_v) \tag{5.21b}$$

5.2.2 Electron Mass

The value of the electron mass affects the process of nucleosynthesis in many ways, namely through the electron energy density and pressure, which affects the background thermodynamics. However, in [74] it was found that this effect is subleading and that, for small variations of m_e, the main effect is through the weak rates. While the normalization constant of the weak rates $K \propto m_e^5$, we need to remember that this is only an artifact of choosing to parametrize the phase-space integral in terms of the dimensional constant $\epsilon = \frac{E_e}{m_e}$. Thus, the main effect of m_e on the weak rates is through the overall phase-space of the interaction. An increase in m_e decreases the available phase-space of these reactions, leading to an earlier freeze-out and, consequently, a higher abundance of neutrons at the onset of nucleosynthesis, which implies an increase in the overall abundances of both Helium and deuterium. as can be abstracted from the green line on Fig. 5.3. The parametric dependence of the abundance to changes in the electron mass is found to be:

$$Y_P = Y_{P,\text{ref}} \cdot \left(\frac{m_e}{m_e^0}\right)^{0.484} \tag{5.22a}$$

$$D/H|_P = D/H|_{P,\text{ref}} \cdot \left(\frac{m_e}{m_e^0}\right)^{0.288} \tag{5.22b}$$

As we can see, both abundances only very weakly vary with the electron mass and are positively correlated, as expected.

The dependence on the Higgs vev is, again, quite straightforward, since this is a purely electroweak phenomenon. The electron acquires its mass through the yukawa coupling of the lepton and Higgs doublet, leading to $m_e \propto y_e v$, with y_e the Yukawa coupling of the electron, after electroweak symmetry breaking. We are currently assuming that only the Higgs vev is allowed to vary with time, such that:

$$\frac{\delta m_e}{m_e^0} = \frac{\delta v}{v_0} \tag{5.23}$$

Therefore, by replacing $m_e = m_e^0 \cdot (1 + \alpha_v)$ in our numerical code we obtain the variation of the abundances with the Higgs vev due to its effect on the electron

mass. Given this simple relation between m_e and v, we also know that the effect of varying the vev is the same as that of varying the electron mass, and we can quite simply obtain:

$$Y_P = Y_{P,\text{ref}} \cdot (1 + 0.484\alpha_v) \tag{5.24a}$$

$$D/H|_P = D/H|_{P,\text{ref}} \cdot (1 + 0.288\alpha_v) \tag{5.24b}$$

which is a much weaker dependence than on a variation of Fermi's constant.

5.2.3 Nucleon Mass Difference

Not only leptons obtain their masses through the Higgs mechanism, but all fermions, which naturally includes the quarks that make up the nucleons. Thus, their mass is likewise influenced by changes of the Higgs vev. Slight changes to the absolute value of their masses does not notably affect BBN, but the final abundances are extremely sensitive to their mass difference $Q = m_n - m_p$. It affects the production of nuclei mainly the neutron to proton ratio at freeze-out, which in equilibrium and assuming a negligible chemical potential is given by:

$$\frac{n_n}{n_p} = e^{-\frac{Q}{T}} \tag{5.25}$$

Since both deuterium and Helium are highly sensitive to the neutron to proton ratio at freeze-out, we expect them to be very sensitive to Q. From this equation, we also see that an increase in Q implies a decease of the neutron to proton ratio, which in turn implies a decrease of both the final Helium and Deuterium abundance, as we can also see from the black line on Fig. 5.3. Concretely, we find:

$$Y_P = Y_{P,\text{ref}} \cdot \left(\frac{Q}{Q_0}\right)^{-3.062} \tag{5.26a}$$

$$D/H|_P = D/H|_{P,\text{ref}} \cdot \left(\frac{Q}{Q_0}\right)^{-1.845} \tag{5.26b}$$

Since protons are composite particles bound by the strong force, the relation between the neutron and proton mass difference and the Higgs vev is slightly more complicated, but can be predicted with relatively low uncertainty nonetheless. The mass difference between the nucleons can be traced back to two contributions, namely the difference in the electromagnetic contribution to their self energy, which is proportional to the fine structure constant α_{EM} and Λ_{QCD} and the mass difference between the u and d quarks, which depends on the Yukawa couplings of the up and down quark and the Higgs vev. Following [75], we parametrize both contributions to Q linearly. Additionally, since we only allow the Higgs vev to vary, we find the following relation:

$$\frac{\delta Q}{Q_0} = 1.587 \frac{\delta v}{v_0} \tag{5.27}$$

or equivalently:

$$Q = Q_0 + 2.053 \frac{\delta v}{v_0} \tag{5.28}$$

Therefore, an increase in the Higgs vev will lead to a strong modification of the nucleon mass difference and decrease both the Helium and Deuterium abunance. Especially Helium is extremely sensitive to modifications of this value, and it is actually the strongest effect which will dominate the outcome of any variation. If we insert this into equation 5.26 and expand around $\alpha_v \ll 1$, we find:

$$Y_P = Y_{P,\text{ref}} \cdot (1 - 4.920\alpha_v) \tag{5.29a}$$

$$D/H|_P = D/H|_{P,\text{ref}} \cdot (1 - 2.933\alpha_v) \tag{5.29b}$$

5.2.4 Deuterium Binding Energy

Last, but not least, the deuterium binding energy is also affected by a variation of the Higgs vev through the pion mass. Following Yukawas theory of nuclear interactions, the pion is the particle exchanged during interactions of the nuclear force and, as such, sets the length scale of attractive nuclear forces, as evidenced by the exponential dependence of the attractive Yukawa potential on the exchange particle's mass.

The effect of a variation of the deuterium binding energy on the final abundances is mainly through the deuterium photodissociation rate, which is exponentially suppressed by the binding energy $\propto e^{-\frac{B_D}{T}}$. This reaction regulates the deuterium abundance and determines the onset of nucleosynthesis. This reaction requires the presence of a large amount of highly energetic photons in the Wien tail of the distribution. Once this is no longer the case, it stops being efficient and nucleosynthesis begins.

If the deuterium binding energy increases, the temperature at which this condition is no longer met increases and nucleosynthesis begins earlier, leading to a higher final Helium abundance as less neutrons decay to protons before being cast into Helium. On the other hand, an earlier onset of nucleosynthesis not only implies that the DD-reactions depleting deuterium are efficient for a longer time, but also at higher temperatures where they are stronger, since the higher temperature implies that the Coulomb barrier the nuclei need to tunnel through is smaller. Summarizing, an increased binding energy implies an earlier onset of BBN, leading to a higher value of Y_P and a smaller final abundance of Deuterium, which is also the behavior exhibited by the blue line on Fig.5.3. The functional dependence of BBN on these values can be parametrized as follows:

$$Y_P = Y_{P,\text{ref}} \cdot \left(\frac{B_D}{B_D^0}\right)^{0.687} \tag{5.30a}$$

$$D/H|_P = D/H|_{P,\text{ref}} \cdot \left(\frac{B_D}{B_D^0}\right)^{-3.579} \tag{5.30b}$$

Unlike for the other modifications, the Deuterium binding energy most significantly influences the final abundance of deuterium. This is to be expected, since all of the other modifications mainly modify the outcome of the neutron to proton freeze-out.

Obtaining the dependence of B_D on the Higgs vev requires two ingredients, namely the dependence of B_D on a variation of the pion mass and the sensitivity of the pion mass to changes in v. The latter can be easily obtained to good

approximation from the Gell-Mann-Oakes-Renner relation, which relates the mass of the pion to the u and d quark masses and Λ_{QCD} as follows:

$$m_\pi^2 \propto (m_u + m_d)\Lambda_{QCD} \propto v \tag{5.31}$$

from which we obtain:

$$\frac{\delta m_\pi}{m_\pi} = \frac{1}{2}\frac{\delta v}{v_0} \tag{5.32}$$

The question of how the pion mass influences the binding energy is slightly more involved and requires a dedicated numerical study. These studies find that a linear dependence of the deuterium binding energy on small variations of the pion mass of the kind we are interested in at present, are a good fit to the data. Following [13], we parametrize the dependence as follows:

$$\frac{\delta B_D}{B_D^0} = r \cdot \frac{\delta m_\pi}{m_\pi^0} = \frac{r}{2} \cdot \frac{\delta v}{v_0} \tag{5.33}$$

with $-10 \leq r \leq -6$. There are some caveats to this parametrization, as detailed in [13], but for our purposes and the small variations of the Higgs vev we are interested in, these do not play a major role [74]. For all further calculations, we have chosen the mean, $r = -8$.

Thus, an increase in the Higgs vev leads to a significantly strong modification towards lower values of the Deuterium Binding energy, such that its net effect on nucleosynthesis through B_D is to decrease Helium production and increase the deuterium abundannce. The strong dependence of Deuterium on B_D and the latter's strong variation with the Higgs vev implies that deuterium will be dominated by the effect of a change in the Binding energy, contrary to what was argued in [76, 77]. Expanding around small variations of the Higgs vev we find:

$$Y_P = Y_{P,\text{ref}} \cdot (1 - 2.748\alpha_v) \tag{5.34a}$$

$$D/H|_P = D/H|_{P,\text{ref}} \cdot (1 + 14.316\alpha_v) \tag{5.34b}$$

which confirms how strongly Deuterium depends on the Higgs vev through its binding energy.

To summarize, we find the following dependence on the four main parameters that are affected by a variation of the Higgs vev and that notably influence the outcome of nucleosynthesis:

$$Y_P = Y_{P,\text{ref}} \cdot \left(\frac{G_F}{G_F^0}\right)^{-1.458} \left(\frac{m_e}{m_e^0}\right)^{0.484} \left(\frac{Q}{Q_0}\right)^{-3.086} \left(\frac{B_D}{B_D^0}\right)^{0.687} \tag{5.35a}$$

$$D/H|_P = D/H|_{P,\text{ref}} \cdot \left(\frac{G_F}{G_F^0}\right)^{-0.833} \left(\frac{m_e}{m_e^0}\right)^{0.288} \left(\frac{Q}{Q_0}\right)^{-1.848} \left(\frac{B_D}{B_D^0}\right)^{-3.579} \tag{5.35b}$$

Comparing the effect of a variation in these parameters with others obtained before, we see that the dependence of the final abundances on these parameters is much stronger than on, for example, the effective number of neutrino species, showing how sensitive BBN is to even small variations on fundamental parameters.

In order to obtain the variation of the SM Higgs vev, we need to allow all of these parameters to collectively vary as a function of v. This is done by implementing the changes of Eqs. 5.20, 5.23 , 5.28 and 5.33 in the code used to obtain the final abudnances. However, it should be noted that for other mechanisms which endow the Standard model with a more complex and phenomenologically rich scalar sector, like for example two Higgs doublet models, these variations need may be independent from each other to some extent. Studying the effect of extensions to the scalar sector on primordial nucleosynthesis would lie beyond the scope of this thesis, but is an interesting prospect left for future work.

5.2.5   Variation of the Higgs Vacuum Expectation Value

For now, we will stick to the SM scenario where there is only one Higgs and one vev. In that case, we see that while the effect of every single variation by itself is very strong, they can counteract each other. The actual outcome is the result of a fierce competition between the different effects. Using the linear expansions in terms of α_v of Eqs. 5.21, 5.24, 5.29 and 5.34, we can quantify this competition. For Helium, we find:

$$
\begin{aligned}
\frac{Y_P}{Y_{P,\mathrm{ref}}} &= 1 + \alpha_v \cdot (c_{G_F} + c_{m_e} + c_Q + c_{B_D}) \\
&= 1 + \alpha_v \cdot (2.916 + 0.484 - 4.920 - 2.748) = 1 - 4.2677\alpha_v
\end{aligned}
\tag{5.36}
$$

We see that the effect of Fermi's constant and the Deuterium binding energy on the fina Helium abundance almost cancel each other. The effect of the electron mass is only subdominant and the final abundance is actually mainly dictated by the variation of Q. Therefore, Helium is anticorrelated with a variation of v, since it increases Q which in turn reduces the final Helium abundance. The left panel of Fig. 5.4 shows the Final Helium mass fraction as a function of the relative variation of v. We see that, indeed, this effect dominates and that Y_P and v are negatively correlated with a very strong dependence, such that Y_P is sensitive to variations on the Higgs vev at the order of 1%. This is much stronger than for example on variations of the neutron lifetime or the effective number of neutrino species.

For small variations of v, the Helium abundance can be fit as follows:

$$
Y_P = Y_{P,\mathrm{ref}} \cdot (1 + \alpha_v)^{-4.421}
\tag{5.37}
$$

which is remarkably close to our previous estimate of the exponent -4.2677. Additionally, this negative correlation implies that resolving the EMPRESS anomaly will generally require a value of the Higgs vev that is slightly higher than its value today.

For Deuterium, there is little room for competition between the different effects. The linear expansion in terms of α_v of Eq. 6.15 looks as follows:

$$
\begin{aligned}
\frac{D/H|_P}{D/H|_{P,\mathrm{ref}}} &= 1 + \alpha_v \cdot (c_{G_F} + c_{m_e} + c_Q + c_{B_D}) \\
&= 1 + \alpha_v \cdot (1.666 + 0.288 - 2.932 + 14.316) = 1 + 13.337\alpha_v
\end{aligned}
\tag{5.38}
$$

Thus, the incredibly strong dependence on variations of its binding energy overpowers any other effects modifying the final abundance, leading to a strong sensitivity
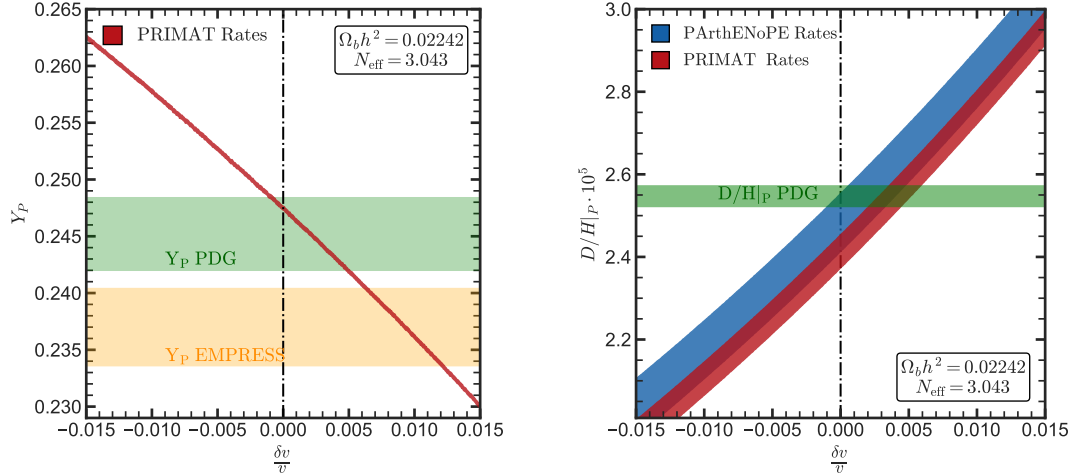
Figure 5.4: Primordial Helium mass fraction, Y_P, (Left) and Deuterium to Hydrogen ratio, $D/H|_P$, (Right) as a function of the relative time variation of the Higgs Vacuum expectation value $\alpha_v = \frac{\delta v}{v^0}$ for $\Omega_b h^2 = 0.02242$ and $N_{\text{eff}} = 3.043$. For Helium we only show the PRIMAT rates, as the results for PArthENoPE rates are identical and for Deuterium we adopt both choices of nuclear rates. The green bands correspond to the PDG-22 prior on Y_P and $D/H|_P$, the yellow band corresponds to the EMPRESS prior.

to variations of the Higgs vev and a positive correlation. This is shown on the right panel of Fig. 5.4. The dependence of the Deuterium abundance on variations of the Higgs vev can be parametrized as follows:

$$D/H|_P = D/H|_{P,\text{ref}} (1 + \alpha_v)^{13.580} \tag{5.39}$$

which is in very good agreement with the linear expansion of eq. 5.38. The strong sensitivity of the Helium and Deuterium abundances to variations of the Higgs vev shows the potential of BBN to precisely constrain its dependence with cosmological time.

5.2.6 Constraints

We will now analyze how scenarios with a time dependent variation of the Higgs vev are constrained by cosmological data. The above results have been derived for a fixed baryon density $\Omega_b h^2 = 0.02242$. While not decisive for the Helium abundance, Deuterium production very strongly depends on it. We saw in Sec. 4.1 that deuterium is actually strongly anti-correlated $\propto (\Omega_b h^2)^{-1.632}$. Therefore, the final deuterium abundance is degenerate with respect to these two parameters, as, in principle, any increase in the Higgs vev at the epoch of BBN can be compensated for with a slightly stronger increase in $\Omega_b h^2$. Therefore, in order to derive constraints on the Higgs vev, we also allow the baryon density to float simultaneously.

Assuming no presence of Dark radiation that is $N_{\text{eff}} = 3.043$, we will constrain α_v independently from BBN using the observational abundances of Helium and Deuterium and subsequently combine these with the Planck prior from eq. 2.16. By running the analysis using both the EMPRESS prior on $Y_P = 0.2370 \pm 0.0034$,
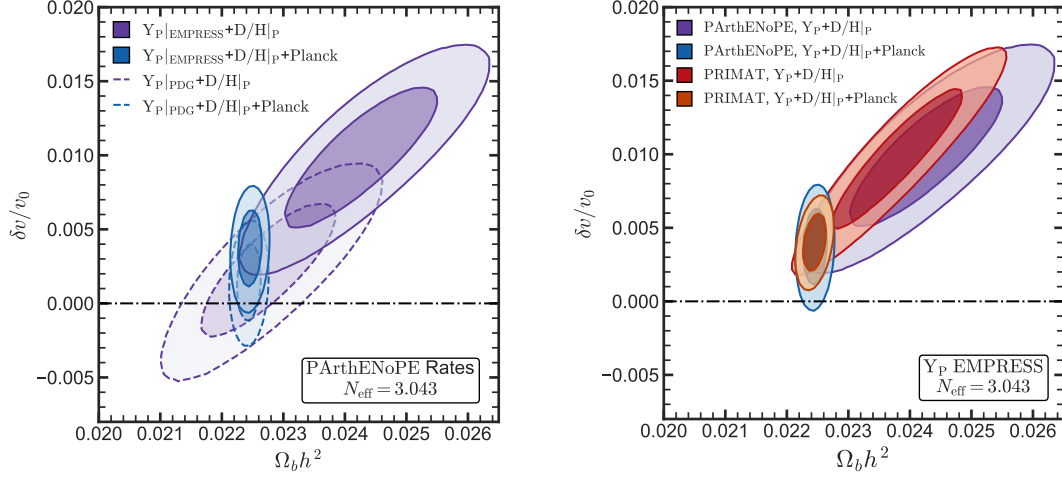
Figure 5.5: **Left:**1σ and 2σ C.L.s for the relative variation of the Higgs vev $\frac{\delta v}{v^0}$ and $\Omega_b h^2$ for BBN and the CMB independently and combined, assuming either the EMPRESS (solid) or PDG-22 (dashed) prior on Y_P for PArthENoPE rates. **Right** Same contours using only the EMPRESS prior on Y_P, but adopting also the PRIMAT rates(red/orange).

as well as the PDG-22 determination $Y_P = 0.245 \pm 0.003$, and two different choices for the nuclear reaction rates, we will additionaly highlight the effect that these two choices have on the constraints and its interpretation in the context of the Standard Model of Cosmology and particle physics.

The resulting constraints are summarized in table 5.2, with the corresponding 1σ and 2σ contours are shown on Fig. 5.5. The left panel shows the effect of the different priors on the constraints using the PRIMAT rates, while on the right panel we vary the choice of nuclear reactions and focus only on the EMPRESS prior on Y_P.

The first thing that becomes apparent when regarding these plots is the strong correlation between the baryon density and a variation of the Higgs vev. Since Y_P only very weakly depends on $\Omega_b h^2$, the contour for the BBN only constraints is essentially determined by the variation of Y_P. The sensitivity of the constraints will be comparable to the precision in the observational determination of Helium $\sigma_{Y_P} \approx 0.003$ for both priors, while the central of both α_v and $\Omega_b h^2$ will depend on the central value adopted.

If we use the EMPRESS prior on Y_P and the PArthENoPE rates, we find:

$$\Omega_b h^2 = 0.02427 \pm 0.00082 \,, \quad [Y_P + D/H|_P \tag{5.40a}$$

$$\frac{\delta v}{v_0} = 0.0100 \pm 0.0032 \,, \qquad \text{EMPRESS}] \tag{5.40b}$$

The lower central value for Y_P implies that the Higgs vev at the epoch of BBN should be higher than its value today by almost 1% at a significance of 3.0σ. Assuming, like for the variation of the Gravitational constant, a linear time dependence $v(t) =$

$v_{\mathrm{BBN}} + \dot{v} \cdot (t - t_{\mathrm{BBN}})$, we find a yearly variation of the Higgs vev:

$$\frac{\dot{v}}{v_0} = (-7.2 \pm 2.3) \cdot 10^{-13}\,\mathrm{yr}^{-1} \tag{5.41}$$

Due to the positive correlation between $\Omega_b h^2$ and α_v, the baryon density likewise gets pushed to higher values compared to the SBBN best-fit value 0.02222 ± 0.00040. Additionally, this strong correlation leads to a loss in sensitivity in the determination of $\Omega_b h^2$. Even with this large uncertainty, this result still implies a 2.2σ tension with the ΛCDM model of cosmology, even for the PArthENoPE set of rates. This is because these rates generally lead to an increased production of deuterium, which given the large value of the Higgs vev required to resolve the tension in Y_P requires even larger values of $\Omega_b h^2$ to compensate.

On the other hand, when choosing the PDG-22 prior on Y_P we find:

$$\Omega_b h^2 = 0.02267 \pm 0.00072\,, \quad [\mathrm{Y_P + D/H|_P} \tag{5.42a}$$

$$\frac{\delta v}{v_0} = 0.0022 \pm 0.0030\,, \qquad \mathrm{PDG - 22}] \tag{5.42b}$$

which is consistent with the ΛCDM model of Cosmology and constrains the time variation of the Higgs vev to be consistent with its value today at $\sim 0.5\%$. However, this is only so because we have allowed the baryon density to freely float, which has nullified the high sensitivity of deuterium to variations in α_v. In order to constrain it, we will use a prior from the Planck CMB data.

It should be noted that, similarly to the case of a time variation of Newton's constant, we need to be careful when using priors from epochs that are separated by a long time like BBN and the CMB. However, this is only important if a variation of the Higgs vev strongly affect the power spectrum of the CMB.

This was investigated in [74] , which found that indeed the CMB is influenced by a variation of the Higgs vev through the electron mass, which affects the thomson scattering cross section as well as the Helium binding energy, but was found to be much smaller than its effect on BBN. We will neglect this effect and assume the prior from Eq. 2.16. Combined with BBN priors and adopting PArthENoPE rates we find:

$$\Omega_b h^2 = 0.02244 \pm 0.00013\,, \quad [\mathrm{Y_P + D/H|_P + CMB} \tag{5.43a}$$

$$\frac{\delta v}{v_0} = 0.0039 \pm 0.0016\,, \qquad \mathrm{EMPRESS + Planck}] \tag{5.43b}$$

Constraining the baryon density, we increase sensitivity to α_v by a factor of two. Even though the central value is much lower than from the BBN only determination, this increased sensitivity implies that data still favor a time variation of the Higgs vev

$$\frac{\dot{v}}{v_0} = (-2.8 \pm 1.2) \cdot 10^{-13}\,\mathrm{yr}^{-1} \tag{5.44}$$

which is different from zero at 2.1σ. However, the overall fit to the data decreases and this determination is inconsistent with the previous determination at 1.7σ, since the central value is much lower because the degeneracy between $\Omega_b h^2$ and α_v in deuterium is broken and α_v cannot be pushed to the high values required by Y_P.

When choosing the PDG-22 determination of Y_P, we find:

$$\Omega_b h^2 = 0.02244 \pm 0.00013\,, \qquad [\text{Y}_\text{P} + \text{D/H}|_\text{P} + \text{CMB} \tag{5.45a}$$

$$\frac{\delta v}{v_0} = 0.0013 \pm 0.0017\,, \qquad \text{PDG} - 22 + \text{Planck}] \tag{5.45b}$$

which is another confirmation of the excellent success of the ΛCDM model of Cosmology. Additionally, this strongly constrains the time variation to be

$$\frac{\dot{v}}{v_0} = (-0.9 \pm 1.2) \cdot 10^{-13}\,\text{yr}^{-1} \tag{5.46}$$

which is consistent with no time variation within the current uncertainties.

We now focus our attention on how the choice of nuclear reaction rates changes these conclusions. For the EMPRESS and CMB independent prior we find:

$$\Omega_b h^2 = 0.02347 \pm 0.00070\,, \quad [\text{Y}_\text{P} + \text{D/H}|_\text{P} \tag{5.47a}$$

$$\frac{\delta v}{v_0} = 0.0096 \pm 0.0031\,, \qquad \text{EMPRESS}] \tag{5.47b}$$

As the BBN only constraints on α_v are dominated by the value of Y_P, we see that the choice of rates does not modify the results too much. If anything, we can gauge from this the importance of the Deuterium abundance for these constraints. On the other hand, since PRIMAT rates underproduce Deuterium, the central value of the baryon density decreases compared to that obtained with PArthENoPE rates to compensate for it, which actually reduces the tension with the ΛCDM model. This differs from the SBBN scenario and the scenarios with a time varying fundamental constant or Dark radiation. However, it does not alleviate the overall tension, at the CMB and BBN determinations of $\Omega_b h^2$ still differ by 1.8σ.

When constraining the baryon density to its Planck value, we find for PRIMAT rates:

$$\Omega_b h^2 = 0.02244 \pm 0.00012\,, \quad [\text{Y}_\text{P} + \text{D/H}|_\text{P} + \text{CMB} \tag{5.48a}$$

$$\frac{\delta v}{v_0} = 0.0039 \pm 0.0012\,, \qquad \text{EMPRESS} + \text{Planck}] \tag{5.48b}$$

Thus, the lower theoretical uncertainty stemming from more stringent data selection criteria implies an increase in the sensitivty by ~ 0.0004 if we adopt this choice, leading to a yearly decrease of the Higgs vev by:

$$\frac{\dot{v}}{v_0} = (-2.8 \pm 0.9) \cdot 10^{-13}\,\text{yr}^{-1} \tag{5.49}$$

which, even though the best fit value does not change is an even stronger indication for a non-zero time variation of the Higgs vev by 3σ. However, the cost of this increased sensitivity is a worse fit to the data.

If we now adopt the PDG-22 prior on Y_P, we find the following BBN only constraints:

$$\Omega_b h^2 = 0.02229 \pm 0.00060\,, \quad [\text{Y}_\text{P} + \text{D/H}|_\text{P} \tag{5.50a}$$

$$\frac{\delta v}{v_0} = 0.0022 \pm 0.0029\,, \qquad \text{PDG} - 22] \tag{5.50b}$$

which shows the same inferred value for α_v, but a significantly lower value of $\Omega_b h^2$, which is actually below the preferred value from Planck measurements of the CMB, which in turn will allow for larger values of α_v. Concretely we find:

$$\Omega_b h^2 = 0.02244 \pm 0.00013\,, \quad [\mathrm{Y_P + D/H|_P + CMB} \tag{5.51a}$$

$$\frac{\delta v}{v_0} = 0.0026 \pm 0.0013\,, \qquad \mathrm{PDG-22 + Planck]} \tag{5.51b}$$

which is consistent with the CMB determination of $\Omega_b h^2$, as well as a negative time variation of a similar magnitude as that inferred from the EMPRESS+Planck prior at 1σ. Concretely, it implies a preference for a non-zero time variation of the Higgs vev

$$\frac{\dot{v}}{v_0} = (-2.8 \pm 0.9) \cdot 10^{-13}\,\mathrm{yr}^{-1} \tag{5.52}$$

with a significance of 2.1σ. A time variation of the Higgs of that magnitude would not only ameliorate the tension coming from the low best-fit value reported by the EMPRESS collaboration, but also that between BBN and the CMB best fits stemming from the different choice of reaction rates.

By deriving these constraints, we have also shown how sensitive BBN is to slight changes in the value of the Higgs vev. For the BBN only constraints, we find that it is susceptible to variations as small as $\sigma_{\alpha_v} = 0.0029$, with constraints limited only by the precision of observations of the Helium abundance, because the Deuterium abundance is degenerate with respect to these two parameters.

Breaking this degeneracy requires input from other cosmological data, namely an independent measurement of the baryon density $\Omega_b h^2$, for example from observations of the CMB. When additionally including this information in our analysis, we find that the sensitivity increases by almost a factor of 3, reaching a sensitivity $\sigma_{\alpha_v} = 0.0012$ that can constrain time variations of the Higgs vev of the order of $1 \cdot 10^{-13}\,\mathrm{yr}^{-1}$, which is more stringent than on the Gravitational constant.

These constraints, regardless of the prior or nuclear reaction rates one chooses, are in agreement with previous constraints. The authors of [74] find $-0.007 \leq \alpha_v \leq 0.02$, while those of [13] report $-0.005 \leq \alpha_v \leq 0.012$ (at 95% confidence). We improve upon these constraints in several ways. First and foremost, we use up to date priors on the observational abundances. This is especially significant for Deuterium, where $10^5 \cdot D/H|_P = 3.0^{+1.0}_{-0.5}$ was used in [74] and $10^5 \cdot D/H|_P = 2.87 \pm 0.22$ in [13]. Additionally, the theoretical prediction of both Helium and Deuterium has seen massive improvements in recent years, especially given the novel determination of the deuterium burning rate by the LUNA collaboration [55], which we have taken into account, allowing for a much more precise determination of α_v.

Nevertheless, there are some caveats which are left for future work. The first is, quite straightforwardly, implementing the modifications coming from a variation of the Higgs vev consistently for all corrections to the weak rates and assuming a much larger network of reactions. Modifications coming from this are expected to be small and not notably affect the conclusions presented here.

Additionally, we have used perhaps an outdated determination of the dependence of the Deuterium Binding Energy on the pion mass, and consequently on the Higgs vev. Given its strong influence, especially on the Deuterium final abundance, this might need to be revisited.

			Constraints on the time variation of the Higgs vev from BBN and CMB data				
$\mathbf{Y_P}$	**Data Sets**	**Nuclear Rates**	$\mathbf{\Omega_b h^2}$	$\mathbf{\alpha_v = \frac{\delta v}{v_0}}$	$\frac{\dot{v}}{v_0}[10^{-13}\mathbf{yr}^{-1}]$	$\mathbf{Pref.\alpha_v \neq 0}$	$\chi^2_{\min}$
EMPRESS	$Y_P + D/H\vert_P$	PArthENoPE	0.02427 ± 0.00082	0.0100 ± 0.0032	-7.2 ± 2.3	3.0σ	0.0
		PRIMAT	0.02374 ± 0.00070	0.0096 ± 0.0031	-6.9 ± 2.3	3.0σ	0.0
	$Y_P + D/H\vert_P + $ Planck	PArthENoPE	0.02244 ± 0.00013	0.0039 ± 0.0016	-2.8 ± 1.2	2.1σ	5.3
		PRIMAT	0.02244 ± 0.00012	0.0039 ± 0.0012	-2.8 ± 0.9	3.0σ	3.8
PDG-22	$Y_P + D/H\vert_P$	PArthENoPE	0.02267 ± 0.00072	0.0022 ± 0.0030	-1.6 ± 2.2	0.8σ	0.0
		PRIMAT	0.02229 ± 0.00060	0.0022 ± 0.0029	-1.6 ± 2.1	0.7σ	0.0
	$Y_P + D/H\vert_P + $ Planck	PArthENoPE	0.02244 ± 0.00013	0.0013 ± 0.0017	-0.9 ± 1.2	0.9σ	0.3
		PRIMAT	0.02244 ± 0.00013	0.0026 ± 0.0013	-1.9 ± 1.0	2.1σ	0.1

Table 5.2: Summary of constraints on the variation of the Higgs vev $\alpha_v = \frac{\delta v}{v^0}$ and $\Omega_b h^2$, as well as the yearly variation of $v(t)$ assuming a linear time dependence from considering BBN and CMB data for two possible choices of the nuclear reaction rates, $N_{\text{eff}} = 3.043$ and $\tau_n = 878.4\,\text{s}$ See main text for details.

Last but not least, when adding the CMB prior, we have neglected the effect a variation of the Higgs vev might have on the power spectrum and simply used a gaussian prior obtained assuming the Higgs vev is constant. We know that this is not actually the case, as the Higgs vev modifies the mass of the electron which affects the process of recombination. While the constraints found in [74] are not competitive with BBN determinations, these are based on very early WMAP data. Updates on constraints of the variation of the electron mass using Planck data find $\frac{\delta m_e}{m_e^0} = 0.0039 \pm 0.0074$ [78], which implies that the CMB is sensitive to variations of the Higgs vev of the order of 1%. Thus, one may expect that this can have a noticeable effect on the combined BBN and CMB constraints derived here.

Given the rather strong indication from EMPRESS data that the Higgs vev is indeed variable with time and the effects this may have on Cosmology, we believe that it is important to study these aspects. Implementing these improvements is left for future work.

Chapter 6

Neutron Dark Decays

We have now explored how a modification to the Hubble expansion rate affects the process of Nucleosynthesis, both from the point of view of dark radiation as well as a time variation of G_N. Aditionally, we have seen how changes to the weak and nuclear reaction rates through a time variation of the Higgs vev affect the final abundances. Now, we will focus our attention on how we can constrain new physics affecting solely the process of the neutron to proton freeze-out through modifications of the weak rates.

The weak rates affect the outcome of nucleosynthesis by determining the neutron to proton ratio at the onset of BBN, as we saw in sec. 3.3.2, in two ways. First, the strength of the interactions $\propto G_F$ determines the moment these reactions freeze-out, which happens for $T_f \simeq 0.8\,\text{MeV}$. In the instant freeze-out approximation, the neutron and proton abundances are in chemical equilibrium until that temperature. Assuming a negligible chemical potential, we find

$$\frac{n_n}{n_p}\bigg|_{T_f} = e^{-\frac{Q}{T_f}} \tag{6.1}$$

The freeze out temperature is determined by the condition that $\frac{\Gamma}{H} \leq 1$. Since $\Gamma \propto G_F^2 T^5$ and $H \propto T^2$, we find that $T_f \propto G_F^{-\frac{2}{3}}$, such that

$$\frac{n_n}{n_p}\bigg|_{T_f} \propto e^{-Q \cdot G_F^{2/3}} \tag{6.2}$$

Therefore, the neutron to proton ratio at freeze-out is exponentially sensitive to the interaction strength of the four point Fermi interaction between neutrons and protons. Once the neutrons have frozen out, they are allowed to decay freely $\propto e^{-\frac{t}{\tau_n}}$ with a lifetime τ_n until nucelosynthesis begins at $T_{\text{BBN}} \simeq 0.073\,\text{MeV}$. Since we are assuming only modifications to the process of nucleon freeze-out, this temperature remains unchanged. Thus, we find:

$$\frac{n_n}{n_p}\bigg|_{T_{\text{BBN}}} \propto e^{-Q \cdot G_F^{2/3}} e^{-\frac{t_{\text{BBN}}}{\tau_n}} \tag{6.3}$$

where, in the last step we have neglected the effect of neutrons decaying to protons,which for the time range of interest here amounts to an effect $\sim 4\%$. Generally,

the neutron lifetime is used to calibrate the weak rate interaction strength from Eq. 3.81, so both of these modifications together are generally regarded as modifications to the value the neutron lifetime, so that:

$$\left.\frac{n_n}{n_p}\right|_{T_{\mathrm{BBN}}} \propto e^{-\frac{Q}{\tau_n^{1/3}}} e^{-\frac{t_{\mathrm{BBN}}}{\tau_n}} \tag{6.4}$$

In the Standard Model, the neutron can only decay to a proton and this parametrization is correct. However, it should be noted that these two contributions in general measure two different things. First, the neutron to proton abundance at freeze-out is determined by the strength of the weak interactions, and the value of the total neutron lifetime influences how many neutrons are left-over from the freeze-out abundance when BBN begins.

This is especially of interest in the context of the neutron lifetime anomaly. As was already explained in Sec.4.2, this boils down to different experimental methods measuring consistently different values for the neutron lifetime with a significance of $\sim 4\sigma$. If we assume this tension not to come from systematic errors that have carried through from one experiment to the other, an explanation of this anomaly requires new physics.

In order to do so, we need to look at the difference between the two experiments. Aside from many technical details, they mainly differ in one very crucial aspect, namely what they actually measure. The beam method measures the amount of protons that are produced by neutrons decaying in a steady stream when passing through an experimental volume V, whereas the bottle method measures the amount of neutrons left inside a trap after a variable amount of time.

Thus, while the bottle method measures directly the total lifetime of the neutrons, the beam method measures it indirectly through protons, which in principle means that both experiments actually measure two different physical quantities, namely the total neutron lifetime τ_n and the branching ratio of decays to protons or, equivalently, the lifetime of the neutron when assuming it only decays to protons, which we will henceforth call τ_{np}. Interestingly, the experiments find that $\tau_{np} > \tau_n$

Within the Standard model, the neutron can only decay to protons, such that $\tau_n = \tau_{np}$. However, these two are not necessarily the same if we include BSM physics. Motivated by this observation, the authors of [12] proposed that both measurements can indeed be reconciled if the neutron has one or more dark decay channels to particles other than protons, such that

$$\tau_n^{\mathrm{bottle}} = \tau_n^{\mathrm{beam}} \times \mathrm{Br(n \to p)} \leq \tau_n^{\mathrm{beam}} \tag{6.5}$$

with a branching ratio

$$\mathrm{Br(n \to p)} \approx 99\% \tag{6.6}$$

or, equivalently, for dark decays:

$$\mathrm{Br(n \to X \neq p)} \approx 1\% \tag{6.7}$$

As we saw in eq. 6.3, the neutron to proton ratio is sensitive to both the interaction strength G_F and the total neutron lifetime. The existence of dark decays of the neutron does not modify the relation between G_F and the neutron lifetime

decaying to protons. Thus, we can still calibrate the weak rates using using τ_{np}. On the other hand, nothing changes in the neutron decay, since here nucleosynthesis is truly only influenced by the total decay rate of the neutron, regardless of its end product. Thus, Eq. 6.3 becomes:

$$\frac{n_n}{n_p}\bigg|_{T_{\text{BBN}}} \propto e^{-\frac{Q}{\tau_{np}^{1/3}}} e^{-\frac{t_{\text{BBN}}}{\tau_n}} \tag{6.8}$$

which shows that the neutron to proton ratio at the onset of nucleosynthesis is exponentially sensitive to both the total neutron lifetime, as well as the lifetime of its decay to protons or the corresponding branching ratio, allowing us to constrain models

We will focus on a simplified scenario where we assume the that $n \to X$, with X some arbitrary decay product X, for example the decay of $n \to \chi\phi$ with a fermion χ and a scalar ϕ as investigated in [79]. In order to remain as model independent as possible, we will look at the scenario where the dark particle's contribution to the energy density of the Universe is negligible and the inverse decays producing neutrons are negligible. This is a crucial assumption that would need to be checked for any given model. For example, the case that the neutron decays to photons is severely constrained by BBN precisely for this reason [80].

Keeping this assumption in mind, the only modification required to the standard picture of nucleosynthesis is to add an additional decay channel for the neutron to some sort of dark sector which we will collectively describe by $X_{\text{Dark}} = \frac{n_{\text{Dark}}}{n_B}$, whose abundance we assume to be negligibly small at the beginning of nucleosynthesis. The Boltzmann equation describing its evolution is:

$$\frac{dX_{\text{Dark}}}{dt} = \Gamma_{n \to \text{Dark}} \cdot X_n = \left(\frac{1}{\tau_n} - \frac{1}{\tau_{np}} \right) X_n \tag{6.9}$$

where we need to make sure that the condition $\tau_{np} > \tau_n$ is always satisfied, such that we do not have the unphysical scenario of a negative decay rate. Additionally, a similar contribution needs to be included in the Boltzmann equation of the neutron, such that

$$\frac{dX_n}{dt} \supset -\Gamma_{n \to \text{Dark}} \cdot X_n \tag{6.10}$$

This modification can now be implemented in state of the art codes for nucleosynthesis in order to obtain the dependence of the final abundances of Helium and Deuterium as a function of both "neutron lifetimes". In this case, we have used the code PRIMAT [20].

Assuming the central value from 4.4 for $\Omega_b h^2$, Fig. 6.1 shows the dependence of the Helium(Left) and Deuterium(Right) abundances on both τ_n(red) and τ_{np} (orange). For the dependence on τ_n, we have chosen to set τ_{np} to the central value of beam experiments $\tau_n^{\text{beam}} = 888.0\,\text{s}$, whereas for the dependence on τ_{np} we have chosen to set the central value of bottle experiments $\tau_n^{\text{bottle}} = 878.4\,\text{s}$. Enforcing the condition that $\tau_{np} > \tau_n$ is the reason that both lines end so abruptly at those values, which correspond to the dash-dotted orange and red lines.

An increased value of τ_{np}, which implies a weaker interaction strength, and consequently, means that the decoupling happens at an earlier time, such that the
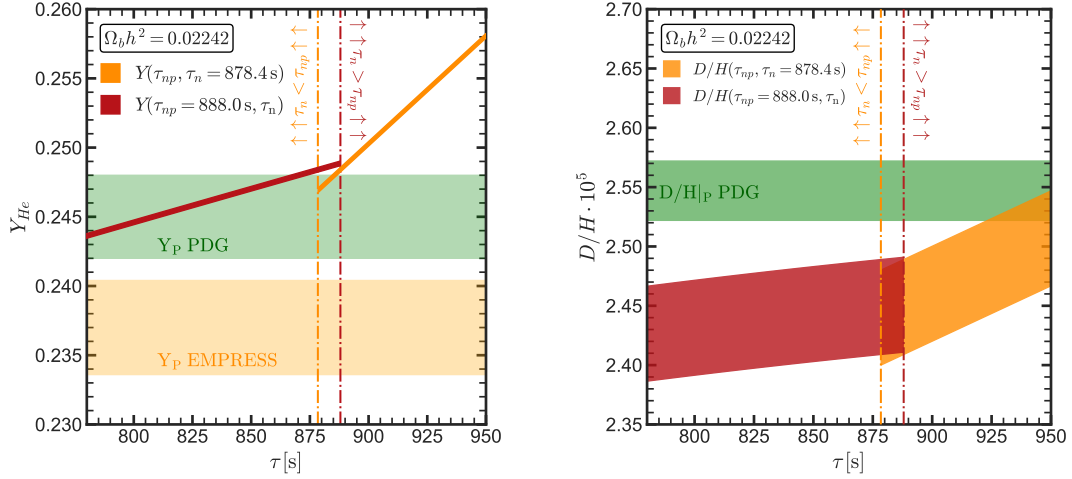
Figure 6.1: 1σ C.L. bands for the primordial Helium mass fraction, Y_P, (Left) and Deuterium to Hydrogen ratio, $D/H|_P$, (Right) for both types of neutron lifetime (see text for details) The red band shows the total neutron lifetime τ_n assuming that its lifetime decaying only to protons is $\tau_{np} = 888.0\,\text{s}$, whereas the orange band is a function of τ_{np}, assuming $\tau_n = 878.4\,\text{s}$. Additionally, $\Omega_b h^2 = 0.02242$ and $N_{\text{eff}} = 3.043$. In both cases we show only the results from PRIMAT rates. The dash-dotted lines separate the physical from the unphysical parameter space because $\tau_{np} > \tau_n$. The green bands correspond to the PDG-22 prior on Y_P and $D/H|_P$, the yellow band corresponds to the EMPRESS prior.

abundance at freeze-out is less suppressed. On the other hand, an increased total neutron lifetime implies that the neutrons will decrease less slowly, which likewise increases the abundance of neutrons at t_{BBN}. An increase in the neutron to proton ratio before BBN begins and that does not affect the reaction network in any other way translates to a slightly smaller increase in the Deuterium abundance. Therefore, an increase in either lifetime correlates with an increase in the production of both nuclei, as can be seen on Fig. 6.1. Concretely, we find that the abundances can be parametrized as follows:

$$Y_P = Y_{P,\text{ref}} \cdot \left(\frac{\tau_n}{\tau_n^0}\right)^{0.171} \left(\frac{\tau_{np}}{\tau_{np}^0}\right)^{0.532} \cdot \Theta(\tau_{np} - \tau_n) \tag{6.11a}$$

$$D/H|_P = D/H|_{P,\text{ref}} \cdot \left(\frac{\tau_n}{\tau_n^0}\right)^{0.069} \left(\frac{\tau_{np}}{\tau_{np}^0}\right)^{0.350} \cdot \Theta(\tau_{np} - \tau_n) \tag{6.11b}$$

where we have used the standard value of the neutron lifetime $\tau_n = 878.4\,\text{s}$ as the reference value for both lifetimes. The theta function simply makes sure that we remain in a physical parameter space. We see from this equation that we recover the standard dependence on the neutron lifetime from Eq. 4.11 in the case of $\tau_n = \tau_{np}$.

Constraints

We have now seen that the production of light nuclei depends on both values of the Neutron lifetime, showing that we can indeed constrain dark baryons with
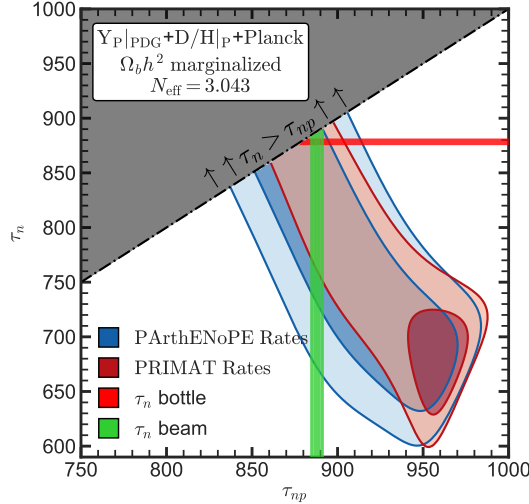
92

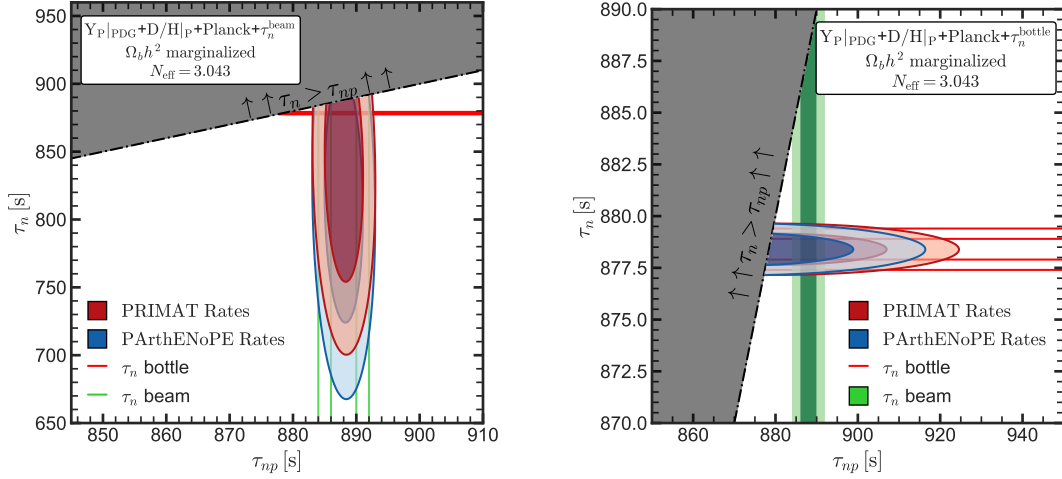Figure 6.2: 1σ and 2σ C.L.s in the (τ_n, τ_{np}) parameter space after marginalizing over $\Omega_b h^2$ for both sets of nuclear rates. We choose the PDG-22 priors on Y_P and $D/H|_P$ combined with a Planck prior to constrain the baryon density assuming $N_{\text{eff}} = 3.043$. The grey region corresponds to the unphysical parameter space where $\tau_n > \tau_{np}$. The green bands corresponds to the 2σ C.L. from beam experiments and the red band to the 6σ C.L. from bottle experiments.

observations of the primordial abundances. However, this also implies that nucleosynthesis now has three parameters, while we can only observe the Helium and Deuterium abundances with a sufficient degree of accuracy, so our parameter space will be degenerate. In order to lift that degeneracy, we will either include a prior on the baryon density from the CMB (Eq. 4.4) or the neutron lifetime from both types of experiment or a combination of these three.

Additionally, we saw in Sec. 4.2 that using the EMPRESS determination of Y_P as a prior leads to a preferred value of τ_n which is drastically different from the Standard value used today, so we came to the conclusion that an interpretation of this anomaly in terms of a non-standard value of τ_n was unlikely. In order to not over-complicate this section by introducing unnecessary sources of tension that we believe are orthogonal to our discussion, we will stick to the PDG-22 prior on Y_P when deriving these constraints.

Even though the dependence of the deuterium abundance on the neutron lifetime will be subdominant, it will fix the value of the baryon density. In order to assess how the choice of nuclear reaction rates will influence the final constraints, we will assume that the effect of the neutron lifetime on the choice of nuclear reaction rates leading to the difference in the production of Deuterium will be negligible, so that we can approximate:

$$D/H|_P^{\text{PArthENoPE}}(\tau_{np}, \tau_n) = D/H|_P^{\text{PRIMAT}}(\tau_{np}, \tau_n) + \delta D/H|_P^{\text{rates}} \qquad (6.12)$$

with $\delta D/H_P^{\text{rates}} = 0.07$.

The 1σ and 2σ contours one obtains when assuming only a prior on the baryon density and marginalizing over it are shown on Fig. 6.2 for both choices of nuclear reaction rates. The black region in the top left corner of the plot indicates

the nonphysical parameter space where the creation rate of dark sector particles is negative.

Even though we have added a prior on $\Omega_b h^2$, one can clearly see that the parameter space remains degenerate in this case, more strongly so for PArthENoPE rates, given that the effect of the neutron lifetimes on both abundances is actually degenerate. The prior on $\Omega_b h^2$ fixes the deuterium abundance at $D/H|_P = 2.52 \cdot 10^{-5}$, while the Helium abundance remains unconstrained, since its standard value is mostly determined by the neutron lifetime. The central value of the observational abundance of Helium is slightly lower than its standard value with $\tau_n = \tau_{np} = 878.4\,\text{s}$, so in order to come closer to that value, one needs to either decrease the value of τ_{np}, which will reduce Y_P more drastically, but only goes so far as $\tau_{np} \geq \tau_n$, or reduce the value of τ_n.

Once we reach the exact value of the observational abundance, any change coming from a further decrease in τ_n can be compensated by a smaller increase in τ_{np}, or vice versa, which explains the shape of the 1σ contour. The range of the contour is only determined by the observational uncertainty on the Helium abundance as well as the slight increase in the theoretical uncertainty coming from allowing the baryon density to float.

While the dependence of Deuterium on the neutron lifetime is much weaker, the degeneracy between the parameters is slightly different. Thus, compensating for a decrease of τ_n, requires a different increase in τ_{np}. While this effect is small, given the overall weak τ dependence and large observational and theoretical uncertaintes of deuterium, at some point the value departs from the observational uncertainty, which is why the 1σ contour ends at $\tau_n \approx 630\,\text{s}$ and $\tau_{np} \approx 970\,\text{s}$ despite the degeneracy of both deuterium and Helium with respect to these parameters. All of this leads to the constraints from BBN with only a prior on the baryon density not being very stringent, with values of both neutron lifetimes allowed that are far from the experimental determinations today.

These experimental constraints are shown on Fig. 6.2, with the green band corresponding to the 2σ contour from beam experiments, which measures τ_{np}, and the red band showing constraints from bottle measurements at the 6σ confidence level in order to make them more visible. The neutron lifetime anomaly arising between the two is visible by the fact that both of these contours do not meet for the standard scenario that $\tau_n = \tau_{np}$ close o to the black dash-dotted line that separates the physical and nonphysical parameter space, but actually meet to the right of it. Nonetheless, the place where they meet is contained within the 1σ contour for PArthENoPE rates, showing that Nucleosynthesis is not in tension with the new physics interpretation of the Neutron Lifetime Anomaly (NLA) proposed in [12].

Additionally, as we saw already in sec. 4.2, SBBN is not in tension with either determination of the neutron lifetime. This can also be abstracted from Fig. 6.2, since the region where the contours corresponding to either technique meet with the dash-dotted line in the parameter space are likewise fully contained in the 1σ contour.

On the other hand, the situation is quite different for the PRIMAT choice of rates, whose 1σ and 2σ contours are shown in red. Unlike for the PArthENoPE rates, the

Figure 6.3: **Left:** 1σ and 2σ C.L.s in the (τ_n, τ_{np}) parameter space after marginalizing over $\Omega_b h^2$ for both sets of nuclear rates. We choose the PDG-22 priors on Y_P and $D/H|_P$ combined with a Planck prior to constrain the baryon density assuming $N_{\text{eff}} = 3.043$ and, most importantly, constraining $\tau_{np} = (888.0 \pm 2.0)\,\text{s}$. **Right:** Same contours as on the left panel, but now constraining the total neutron lifetime to the value measured in bottle experiments $\tau_n = (878.4 \pm 0.5)\,\text{s}$, corresponding to the beam experiments that measure only protons. On both figures, the grey region corresponds to the unphysical parameter space where $\tau_n > \tau_{np}$. The green bands corresponds to the 1σ and 2σ C.L. from beam experiments and the red band to those from bottle experiments.

prior on $\Omega_b h^2$ introduces a tension with the observational deuterium abundance, as it predicts a much lower value. Reconciling theory and observation requires a stark increase in the Deuterium abundance, which can only be achieved by an increase in τ_{np}. However, this very strongly modifies the Helium production as well, which needs to be compensated by a smaller value of τ_n. Accommodating both observations is therefore only possible for a narrow window compared to the case with PArthENoPE rates around $\tau_n = (674.6 \pm 32.0)\,\text{s}$ and $\tau_{np} = (960 \pm 11)\,\text{s}$. In principle, this implies that BBN is in tension with both measurements of the neutron lifetime, which seems rather unlikely for many reasons, not only from the experiments but also from tthe consistency of BBN itself given the large production of dark sector particles that comes from such a low value of τ_n. Most likely this means that we need to first resolve the issues that are causing the 2σ tension within the ΛCDM model before taking 1σ constraints on the neutron lifetimes serious when using PRIMAT rates.

Regardless of the rates, the degeneracy between the two parameters as well as the relatively large uncertainty in the priors for both abundances makes the purely cosmological constraints on this scenario very weak. The only assessment one can make, and even this is only partly true, is that the new physics interpretation of the neutron lifetime is permitted by cosmological observations. In order to improve this, we will now add a prior on the neutron lifetimes themselves which will break the degeneracy.

First, we include a prior on $\tau_{np} = \tau_n^{\text{beam}}(888.0 \pm 2.0)\,\text{s}$ from beam experiments, since these measure only the protons resulting from the neutron decay. The resulting

contours for both choices of nuclear reaction rates are shown on the left panel of Fig.6.3. Indeed this prior lifts the degeneracy , but the low sensitivity of the Helium abundance to τ_n implies that the constraints are not very stringent. Since they are entirely dominated by the determination of Y_P, we can estimate the sensitivity using Eq. 6.11 as $\Delta\tau_n \approx 126$ s given the possible variation of $\Delta Y_P = 0.006$. Numerically, we find:

$$\tau_n = 814^{+61}_{-60}\text{s}, \quad \chi^2_{\min} = 0.3 \qquad [\text{PArthENoPE}] \tag{6.13a}$$

$$\tau_n = 841^{+48}_{-57}\text{s}, \quad \chi^2_{\min} = 4.2 \qquad [\text{PRIMAT}] \tag{6.13b}$$

Both determinations show no significant deviation from neither the bottle nor beam measurements of τ_n, reinforcing our conclusion that there is no tension with neither the new physics nor the systematic interpretation of the NLA. Additionally, the $\chi^2_{\min}$, while close to zero for PArthENoPE rates, is > 1 for PRIMAT rates due to the tension in the baryon density.

Additionally, the sensitivity in the estimate of the neutron lifetime is in keeping with our naive estimate for the lower limits, but especially for the PRIMAT rates the upper limit is slightly smaller. The reason for this becomes apparent when looking at the red contour on the left panel of Fig. 6.3, namely that there are no physical points in the parameter space that can accommodate such a high value of the total neutron lifetime. Thus, the in principle Gaussian contour gets cut-off at the top slightly, giving the resulting constraint. This is not the case for the PArthENoPE rates, since their best-fit value is much lower, given that they have more room to lower the Helium abundance to values closer to 0.245 without increasing the tension with the determination of the deuterium abundance.

We can also constrain the total neutron lifetime to its value as measured in bottle experiments $\tau_n = \tau_n^{\text{bottle}} = (878.4 \pm 0.5)$ s. The resulting 1σ and 2σ contours are shown on the right panel of Fig. 6.3. These constraints, as we can already see from the contour itself, are the most stringent ones for several reasons. The first is that the dependence of Helium on τ_{np} is simply much stronger.. Additionally, the prior on τ_n is so stringent that it is equivalent to not allowing the parameter to float, which further increases the sensitivity. Lastly, this strong constraint implies that $\tau_{np} > 878.4$ s, so the Helium abundance is essentially limited to be $Y_P \geq 0.2469$. Thus, there is essentially a much smaller effective observational uncertainty $\Delta Y_P = 0.001$, leading to a much higher effective sensitivity. Numerically, we find:

$$\tau_{np} = 878.5^{+11.4}_{-0.1}\text{s}, \quad \chi^2_{\min} = 0.6 \qquad [\text{PArthENoPE}] \tag{6.14a}$$

$$\tau_{np} = 879.5^{+18.1}_{-1.1}\text{s}, \quad \chi^2_{\min} = 4.4 \qquad [\text{PRIMAT}] \tag{6.14b}$$

Which is much more sensitive than any of the determinations from before, even for the standard BBN result. Both inferred values of the neutron lifetime are very close to the best fit value from bottle experiments, since the Helium abundance generally prefers lower values of τ_n, τ_{np} in order to accommodate the slightly lower best fit value from observations. As a result, the lower bounds are only determined by the difference between the best fit value for τ_{np} and τ_n.

Likewise, the dominant effect determining the upper bound, rather than the sensitivity in the observational abundances, is the central value of the ellipse, which is determined by the prior on the baryon density through the deuterium observation

and the prior on τ_n working in unison with the condition that $\tau_{np} \geq \tau_n$. For PRIMAT rates, the value of $\Omega_b h^2$ is as close to its lower bound as possible to increase the deuterium production, such that $Y_P \geq 0.2463$, whereas the value of $\Omega_b h^2$ is higher for the PArthENoPE rates, such that $Y_P \geq 0.2469$, which is why the constraint is more stringent for the PArthENoPE rates.

Regardless of the choice of rates, though, the new physics interpretation of the NLA remains in good agreement with the BBN predictions, as well as the interpretation as a systematic error in one of the experiments, as both the bottle and beam measurements are within the 1σ bounds of eq. 6.14. However, especially for the constraint derived using a prior on τ_n, even a slight increase may, depending on the central value of Y_P, actually begin to constrain any scenario involving the dark decay of neutrons.

6.1   General Modifications to the Weak Rates

We have neglected the impact of the EMPRESS anomaly in our discussion of the dark decay of the neutron, so we will now focus our attention on how the EMPRESS anomaly may actually be interpreted as a hint of new physics at the epoch of BBN. We have already looked at modifications of the Hubble expansion of the Universe and a time variation of the fundamental constants, as well as modifications of the SBBN paradigm from the value of the neutron lifetime. Except for the latter, whose modification we have concluded is an unlikely explanation of the EMPRESS anomaly, is that Deuterium is the key element when it comes to constraining these scenarios, whereas the EMPRESS anomaly only concerns Y_P. For the previous scenarios, this implied an increased tension with the Standard Model of Cosmology or, equivalently, when constraining the baryon density to its CMB value, the deuterium abundances sensitivity prevented a production of Helium as low as required by EMPRESS.

In order to ameliorate the EMPRESS anomaly, we therefore need to modify Nucleosynthesis in a way that more strongly affects the production of Helium than of Deuterium. This almost certainly discards any modifications to the nuclear reaction rates, to which in general the Helium abundance is rather insensitive. In light of that, we are left with either a modification of the expansion history, which we have already investigated, and of the weak rates.

In light of that, we will now analyze how modifications to the weak rates affect both the Helium and deuterium abundances and then look, more specifically, at aspects of new physics that may influence these, in order to target the EMPRESS anomaly in a more isolated fashion. First, we need to assess the dependence of the final abundance on these reactions by independently varying the normalization of each of the six weak reactions from Eq. 3.50. The relative variation of Helium (Left) and Deuterium (Right) as a function of the ratio with respect to the Born Approximation of the reaction when using the PRIMAT nuclear reaction rates is shown on Fig. 6.4. The solid lines correspond to the reaction creating protons from neutrons, and the dashed line correspond to the reverse reaction and the green and orange bands indicate the different priors on the observational abundances.

Similarly to modifications of the neutron lifetime, a change in the weak rates will
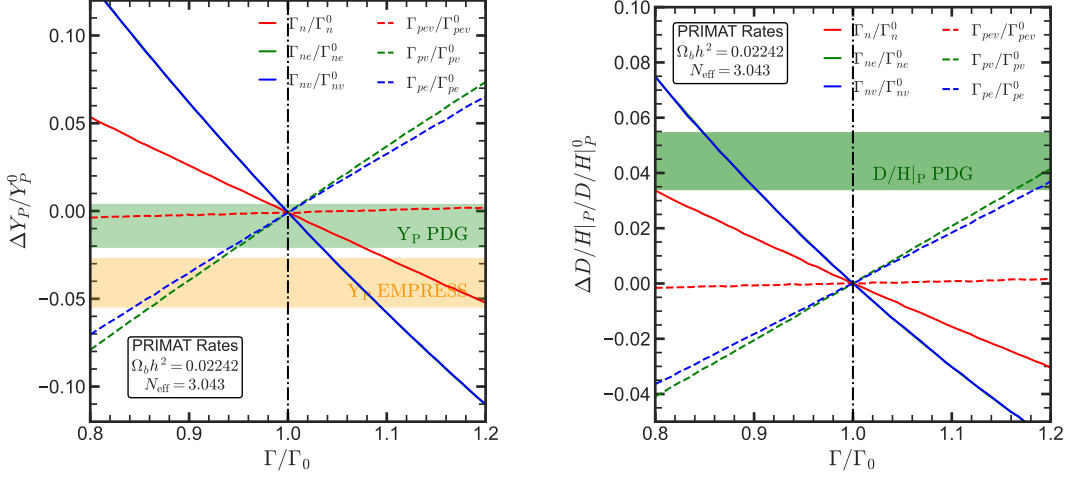
Figure 6.4: Primordial Helium(Left) and Deuterium(Right) abundance as a function of the relative variation of each weak rate interconverting neutrons and protons individually. The final abundances have been calculated from the weak rates in the Born approximation and the reduced nuclear network from Fig. 3.4, assuming $N_{\text{eff}} = 3.043$ and $\Omega_b h^2 = 0.02242$ and the PRIMAT nuclear reaction rates and then corrected using the approximation detailed in Eq. 5.14.

only affect the neutron to proton ratio at the onset of nucleosynthesis. Since all nuclei require at least one neutron, the sum of all abundances is set by the amount of neutrons available in the reservoir when nucleosynthesis begins. An increase (decrease) in the normalization of the reservoir does not change the redistribution if the abundance into nuclei, but increases (decreases) their overall abundance, so modifications to the weak rates will affect the deuterium and Helium production in a similar way but with a weaker effect on Deuterium, which is the behavior exhibited on Fig. 6.4.

Additionally, increasing any of the reactions transforming neutrons into protons will naturally decrease the abundance of neutrons when BBN begins, leading to a smaller Helium abundance, and vice versa for the reverse reaction. Concretely, we find that:

$$Y_P = Y_{P,\text{ref}} \cdot \left(\frac{\Gamma_n}{\Gamma_n^0}\right)^{-0.258} \left(\frac{\Gamma_{ne}}{\Gamma_{ne}^0}\right)^{-0.581} \left(\frac{\Gamma_{nv}}{\Gamma_{nv}^0}\right)^{-0.580} \tag{6.15a}$$
$$\left(\frac{\Gamma_{pev}}{\Gamma_{pev}^0}\right)^{0.014} \left(\frac{\Gamma_{pv}}{\Gamma_{pv}^0}\right)^{0.338} \left(\frac{\Gamma_{pe}}{\Gamma_{pe}^0}\right)^{0.380}$$
$$D/H|_P = D/H|_{P,\text{ref}} \cdot \left(\frac{\Gamma_n}{\Gamma_n^0}\right)^{-0.157} \left(\frac{\Gamma_{ne}}{\Gamma_{ne}^0}\right)^{-0.321} \left(\frac{\Gamma_{nv}}{\Gamma_{nv}^0}\right)^{-0.320} \tag{6.15b}$$
$$\left(\frac{\Gamma_{pev}}{\Gamma_{pev}^0}\right)^{0.008} \left(\frac{\Gamma_{pv}}{\Gamma_{pv}^0}\right)^{0.182} \left(\frac{\Gamma_{pe}}{\Gamma_{pe}^0}\right)^{0.204}$$

which shows precisely this behavior. Additionally, an increase in the neutron to proton conversion more strongly affects the final abundances than the reverse reaction. This is to be expected, since an increase in the neutron lifetime, which corresponds to a decrease of all rates collectively through the normalization, leads to a higher

Helium and Deuterium abundance, which would not be the case of the effect of modifying the proton to neutron conversion were stronger.

From the left panel of Fig. 6.4 we can already see that variations of the weak rates can accommodate the Helium prior from the EMPRESS collaboration if we increase any of the reactions transforming neutrons to protons by a sufficient amount. Since modifying single reactions will require a very specific model, we will focus on variations of the neutron to proton conversion rates as a whole. Not only will this be simpler to do, but actually it has the strongest effect on the final Helium abundance, so that even small variations can explain the Helium anomaly. Concretely, we find that a variation of the weak rates

$$\frac{\Delta\Gamma_{n\to p}}{\Gamma^0_{n\to p}} = 0.03 \pm 0.01 \tag{6.16}$$

that is, an increase in the reaction rates at the percent level, is enough to resolve the EMPRESS anomaly. The question now arises as to how we can achieve such an increase in the weak rates other than a modification of the overall normalization from either a variation of the neutron lifetime or Fermi's constant.

Given that a possible solution to the NLA is the proposition of new particles that interact with the neutron, one is left to wonder whether these particles also have interactions that allow an increase in the neutron to proton conversion rates but without affecting the reverse reaction. One possibility to do this would be to simply adjust the masses of the particles such that the reverse reaction from a proton to a neutron is simply forbidden by energy conservation. This will require the presence of at least two new particles with a mass difference between the two particles to be smaller than the nucleon mass difference Q. Additionally, one of the particles needs to be electromagnetically charged. These requirements severely constrain the scenario and make it perhaps not as attractive as initially thought.

We therefore focus our attention to the weak rates themselves. From Eq. 3.77, we see that aside from the matrix element, contained in the normalization factor K, they only depend on the phase-space distribution of the electrons and neutrinos. Sine the electron phase-space distribution is more constrained, perhaps the simplest way to modify the weak reaction rates is through a modification of the neutrino phase-space distribution.

Without modifying the details of neutrino interactions too much, spectral distortions will play a subdominant role on the final abundances, as shown in [20]. Thus, we will assume that they remain in thermal equilibrium, so that the distribution is generally only dependent on two quantities: the neutrino temperature T_ν and the chemical potential μ_ν.

The temperature can only be modified by changing the details of the neutrino freeze-out, thus altering the ratio of the neutrino to photon temperature. This, as we can see from Eq. 3.49, is equivalent to a modification of N_{eff}, whose effect we have already looked into in Sec.4.3. In this case, the EMPRESS anomaly required $\Delta N_{\text{eff}} < 0$. Aside from perhaps an interpretation as an indication for a time variation of G_N at the epoch of BBN, models that reduce the effective degrees of freedom generally lead to even higher values of Y_P.

Thus, perhaps the simplest way to obtain a value for Helium as low as required by the EMPRESS measurements is to allow for the presence of a large neutrino

chemical potential or, equivalently, a large lepton asymmetry at the epoch of BBN.

Chapter 7

Lepton Asymmetries

The presence of a lepton asymmetry in general at the time of BBN should not come as a surprise, though. The mere fact that we are alive today is an indication that, at least on small scales, there is an asymmetry between matter and antimatter. This leaves us with three options. We are simply living inside a large inhomogeneity as a result of an expected statistical fluctuation, where there is more matter than antimatter, this is simply the way the Universe was created, or, perhaps the most attractive one and the one most in keeping with our current picture of the expanding Universe: there exists some sort of mechanism generating a primordial asymmetry between matter and antimatter in the very early Universe, regardless of its initial state [81].

For the case of baryons, we have already seen that we can constrain the baryon density $\Omega_b h^2$ from observations of the primordial abundances of light elements, although in this context it is customary to use the equivalent baryon to photon ratio η_B. A primordial overabundance of matter over antimatter density $\Delta X = n_X - n_{\overline{X}}$ in principle remains constant as the Universe evolves except for the effect of dilution due to its expansion, but the respective particles actually annihilate if they meet, which they eventually do. Thus, the primordial asymmetry makes itself apparent by the density of particles of that species leftover. This implies:

$$\eta_B \bigg|_{T_{\text{BBN}}} = \frac{n_B}{n_\gamma} \bigg|_{T_{\text{BBN}}} = \frac{n_B - n_{\overline{B}}}{n_\gamma} \bigg|_{T_{\text{BBN}}} \tag{7.1}$$

that is, that we are actually constraining the baryon asymmetry, as it is the same as the baryon density. The current constraints from BBN actually give, for PArthENoPE rates and the EMPRESS prior on Y_P:

$$\eta_B = (6.06 \pm 0.11) \times 10^{-10} \tag{7.2}$$

while the currently most precise determination combining CMB and BAO data finds $\eta_B \equiv (n_B - n_{\overline{B}})/n_\gamma = (6.14 \pm 0.04) \times 10^{-10}$ [82], with a precision $\lesssim 1\%$.

The simplest theories proposed to generate this baryon asymmetry require a CP and B violating out of equilibrium decay of a thermally produced particle. The amount of symmetry violation and initial abundance of said particle is adjusted in

---

This section is based on the publication [24]

such a way to produce just the right amount of asymmetry as required by observations. Given that we have reason to assume the Standard model to be correct up to energies of $\sim 100\,\mathrm{GeV}$, the simplest idea is to generate this asymmetry at energies above the electroweak phase transition in the very early Universe.

At those energies, however, the vacuum structure of the Standard model becomes non-trivial and sphaleron transitions become efficient [83]. Sphalerons are static solutions of the electroweak Equations of motion of the Standard Model which interpolate between vacuum solutions corresponding to different baryon and lepton numbers. These transitions, while they conserve the total $B - L$ number, they actually violate $B + L$ and, therefore, B and L respectively. Thus, sphaleron transitions transfer part of the baryon asymmetry to an asymmetry in the lepton sector. Naively, one would therefore expect that the asymmetry in the lepton sector is of the same magnitude as that in the baryon sector[84, 85, 86, 87].

On the other hand, several scenarios have been constructed where the lepton asymmetries at the time of BBN can be much larger than the baryon asymmetry. In order to evade the constraints from sphalerons, one typically needs these scenarios to produce the lepton asymmetry at temperatures below the sphaleron freeze-out. Different models differ in how they generate the lepton asymmetry, for example via Affleck-Dine leptogenesis [88, 89], decays of topological defects [90], freeze-in leptogenesis [91, 92], resonant-leptogenesis [93, 94] or Q-ball decays [95, 96]. Furthermore, there are scenarios where large lepton asymmetries are generated before sphaleron freeze-out, but in which the total lepton asymmetry in the Universe is zero [97, 98].

Unfortunately, even though there is a very precise determination of the baryon asymmetry implying that it is extremely small, there is no evidence that this is actually the case for the primordial lepton asymmetries, η_{L_α}, with $\alpha = e,\ \mu,\ \tau$. This is mainly because the lepton asymmetry will eventually be stored in neutrinos, as it is the lightest lepton and the only neutral one, which are notoriously hard to detect. Without the possibility of measuring the cosmic neutrino background, we need to obtain constraints on the asymmetry stored in the lepton sector indirectly. Aside from the constraint explored in [99] which is only valid for very high temperatures $T > 10^6\,\mathrm{GeV}$, the most stringent constraints on a lepton asymmetry actually come from its effect on the primordial Helium abundance, again showing the potential of BBN to constrain new physics.

7.1 Implications of a Primordial Lepton Asymmetry for BBN and the CMB

The primordial lepton asymmetry is normally parametrized by the neutrino chemical potential, μ_ν. At energies above $\mathcal{O}(10\,\mathrm{MeV})$, the neutrinos are kept in chemical equilibrium through the reactions in Eq. 3.33, which implies that:

$$\mu_\nu = -\mu_{\overline{\nu}} \tag{7.3}$$

so that the phase-space distributions $f_{\overline{\nu}}(E_{\overline{\nu}}, T_{\overline{\nu}}, \mu_{\overline{\nu}}) = f_\nu(E_\nu, T_\nu, -\mu_\nu)$, which significantly simplifies matters. Since the chemical potential, just like the energy, gets

red-shifted as the Universe expands, it is customary to define the comoving chemical potential

$$\xi_\nu = \frac{\mu_\nu}{T_\nu} \tag{7.4}$$

We define the lepton asymmetry for each flavor just as we have defined the baryon asymmetry:

$$\eta_{L_\alpha} \equiv \frac{n_{\nu_\alpha} - n_{\bar{\nu}_\alpha}}{n_\gamma} \tag{7.5}$$

Inserting the neutrino phase-space density into Eq. A.3 and expanding around small values of the chemical potential, we find [13]:

$$\begin{aligned} \eta_{L_\alpha} \equiv \frac{n_{\nu_\alpha} - n_{\bar{\nu}_\alpha}}{n_\gamma} &= \frac{1}{12\zeta(3)} \left[\frac{T_{\nu_\alpha}}{T_\gamma} \right]^3 \left(\pi^2 \xi_{\nu_\alpha} + \xi_{\nu_\alpha}^3 \right) , \\ &\simeq 0.25\, \xi_{\nu_\alpha} \left[1 + \xi_{\nu_\alpha}^2/\pi^2 \right] , \end{aligned} \tag{7.6}$$

where $\zeta(3) \simeq 1.20206$. In the last step, we have used the value of T_γ/T_ν expected from neutrino decoupling in the Standard Model [100]. This relation explains why the chemical potential can be used to parametrize the asymmetry, so we will now use the two interchangeably.

The implications of a nonzero lepton asymmetry in BBN and the CMB have been studied in the past (for reviews, see *e.g.* [101, 13, 20, 102]), but we will outline the most important modifications to the paradigm described in Ch. 3.

The first modification is to the expansion history through the energy density. Up to now, we have assumed that $\rho_\nu = \rho_{\bar{\nu}}$ and taken this into account simply by multiplying ρ_ν by a factor 2. The presence of a chemical potential actually increases the energy stored in the form of neutrinos regardless of the sign of ξ_ν, so that $\rho_\nu + \rho_{\bar{\nu}} \geq 2\rho_\nu$. We can parametrize this increase in terms of the effective number of neutrino species ΔN_{eff} by simply inserting the neutrino phase-space density into the definition of ΔN_{eff}. Unlike for the lepton asymmetry, we can actually obtain an exact closed form solution of the integral. We find:

$$\Delta N_{\text{eff}} = \sum_\alpha^{e,\mu,\tau} \left[\frac{30}{7} \left(\frac{\xi_\alpha}{\pi} \right)^2 + \frac{15}{7} \left(\frac{\xi_\alpha}{\pi} \right)^4 \right] , \tag{7.7}$$

This modification is independent of the neutrino flavour and of its sign, always leading to $\Delta N_{\text{eff}} \geq 0$. Since neutrinos oscillate between different flavours when free-streaming, one expects $|\xi_{\nu_e}| \simeq |\xi_{\nu_\mu}| \simeq |\xi_{\nu_\tau}|$ [103, 104, 105, 106]. Therefore, and in view of the current constraints on the electron lepton asymmetry, $|\xi_{\nu_e}| \lesssim 0.1$, the modification on ΔN_{eff} due to a nonzero chemical potential is expected to be $\Delta N_{\text{eff}} \lesssim 0.01$. In order to obtain predictions accurate at the percent level for Y_P from nucleosynthesis, we will take this effect into account when calculating $Y_P(\xi_\nu)$. This would in principle already leave an imprint in the CMB through N_{eff} by itself, but given the current sensitivity of experiments, we will neglect this contribution and focus only on the impact of the nonzero lepton asymmetry on Y_P.

The effect of ξ_ν on nucleosynthesis actually does depends critically upon its flavor. A non-zero lepton asymmetry will mainly modify SBBN through the weak rates,

which only involve neutrinos of the electron flavour. This is not because the reaction with other flavours is forbidden, it is just extremely suppressed because of the large mass of muons and tauons. Thus, when referring to ξ_{ν_e} in the context of BBN, we generally mean only ξ_{ν_e}, but as we have already seen it is expected that these are equilibrated through neutrino oscillations.

A non-zero chemical potential will not really affect the free neutron decay, but its main effect will be on the two body reactions. It will increase the neutron to proton conversion through $n + \nu \to p + e^-$ and decrease the proton conversion through $p + \bar{\nu} \to n + e^+$. Thus, a lepton asymmetry has precisely the desired modification of the weak rates we pointed out in the last section.

Assuming neutrons and protons are kept in chemical equilibrium through the above reactions, we find for the chemical potentials $\xi_p - \xi_n = \xi_{\nu_e}$. Before, we assumed $\xi_{\nu_e} = 0$, leading to the equilibrium neutron to proton ratio $\propto e^{-\frac{Q}{T}}$ we have used up to now. In the presence of a non-negligible chemical potential, we find:

$$\left. \frac{n_n}{n_p} \right|_{\text{eq.}} = e^{-\frac{Q}{T} + \xi_n - \xi_p} = e^{-\frac{Q}{T}} \cdot e^{-\xi_{\nu_e}} \tag{7.8}$$

Thus, a positive value of the neutron chemical potential will lower the equilibrium value of the neutron to proton ratio, ultimately lowering its value at freeze-out, thereby reducing all abundances. From this criterion, we can already gather that a decrease of Y_P as required by EMPRESS corresponds to $\xi_{\nu_e} \sim 0.04$. In order to have a more quantitative measure, we need to re-derive the weak reaction rates governing the nucleon freeze-out including a neutrino chemical potential. These modifications are actually rather simple in the Born Approximation and we can find a similarly compact form for the reaction rates. The derivation of the reaction rate for the process $n + \nu \to p + e^-$ actually also holds up to Eq. 3.74 for the case of a neutrino chemical potential, so we find:

$$\Gamma_{n\nu \to pe} = K \int_q^\infty d\epsilon \, \epsilon \, (\epsilon - q)^2 \sqrt{\epsilon^2 - 1} \cdot f_\nu(\epsilon - q, \xi_{\nu_e}) f_e(-\epsilon) \tag{7.9}$$

For the other rates, the we have an antineutrino in the final state. In this case, we can derive the following relation assuming a FD distribution:

$$1 - f_\nu(E_\nu, \xi_{\bar{\nu}}) = f_\nu(-E_\nu, -\xi_{\bar{\nu}}) \tag{7.10}$$

Using the fact that $\xi_{\nu_e} = -\xi_{\bar{\nu}}$, we see that the energy relations in the Pauli-blocking factors for the two reactions remain the same and we simply need to add the dependency of the chemical potential with a positive sign in both cases. Thus, similarly as with eq. 3.77, we can define the total sum of all reactions converting neutrons to protons, finding:

$$\Gamma_{n \to p} = K \int_1^\infty d\epsilon \, \epsilon \sqrt{\epsilon^2 - 1} \left[(\epsilon - q)^2 f_\nu(\epsilon - q, \xi_{\nu_e}) f_e(-\epsilon) \right.$$
$$\left. (\epsilon + q)^2 f_\nu(-(\epsilon + q), \xi_{\nu_e}) f_e(\epsilon) \right] \tag{7.11}$$

Since an increase in ξ_{ν_e} implies an increase in the phase-space distribution f_ν, a positive chemical potential will have the desired effect of increasing the reaction
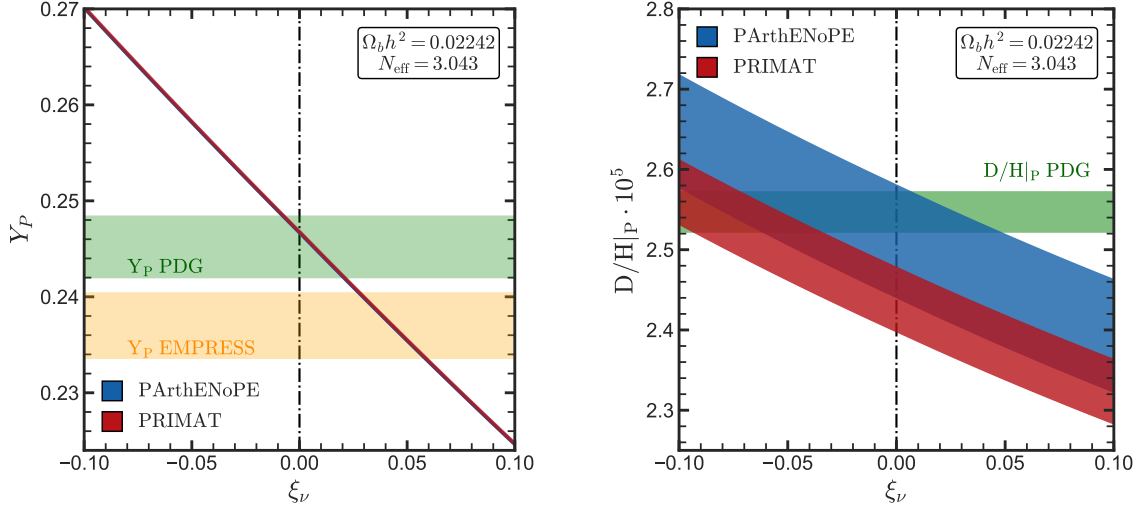
Figure 7.1: Primordial Helium mass fraction, Y_P, (Left) and Deuterium to Hydrogen ratio, $D/H|_P$, (Right) as a function of the electron neutrino chemical potential ξ_{ν_e} for $\Omega_b h^2 = 0.02242$ and $N_{\text{eff}} = 3.043$ for both choices of nuclear rates. The green bands correspond to the PDG-22 prior on Y_P and $D/H|_P$, the yellow band corresponds to the EMPRESS prior.

rate in this direction, confirming what we have already established. From this it is quite simple to obtain the reverse reaction rate. For the $p + e \rightarrow n + \nu$ reaction, the neutrino is now a final state, such that the phase-space density becomes $f_\nu(-E_\nu, -\xi_{\nu_e})$. Similarly, the antineutrinos from the other two equations are now initial states, so that the phase-space density becomes $f_\nu(E_\nu, -\xi_{\nu_e})$. The kinematic relations defining the energy are not affected, so that we find that, just as in the case for negligible potential, the relation between forward and backward reaction is actually quite simple, namely:

$$\Gamma_{p \rightarrow n}(q, \xi_{\nu_e}) = \Gamma_{n \rightarrow p}(-q, -\xi_{\nu_e}) \tag{7.12}$$

This implies, that an increase in the chemical potential will have a positive effect on the neutron conversion rate and the inverse effect on the proton conversion rate, thus further decreasing the final abundance of Helium as desired.

The corrections to the weak rates can also be modified to allow for a non-standard value of the neutrino chemical potential, as is shown in [13, 20]. Modifications from a large chemical potential to the weak rates, as well as the increase in the neutrino energy density from Eq.7.7, have been implemented in state of the art codes. For the remainder of this section, we will use `PArthENoPE-v3.0` [42, 43, 44]. For both choices of nuclear reaction rates, the dependence of Helium(left) and Deuterium (Right) as a function of the lepton asymmetry in the electron flavour is shown on Fig. 7.1

From this figure, we can clearly see how strong the impact of a non-zero lepton asymmetry is, especially on the Helium abundance, even for small variations of ξ_{ν_e}. As we expected, a positive value of ξ_{ν_e} corresponds to a decrease in Y_P. More concretely, it leads to a shift in the primordial helium abundance of [20]:

$$Y_{\text{P}}(\xi_{\nu_e}) \simeq Y_{\text{P}}|_{\text{ref}} \cdot (1 + \xi_{\nu_e})^{-0.92} , \tag{7.13}$$

where $Y_P|_{\text{ref}} = 0.2469$ refers to the primordial helium abundance in the standard BBN scenario. Naturally, a nonzero lepton asymmetry also affects the abundances of the rest of the light elements, albeit less strongly. For deuterium the effect is [20]:

$$\text{D/H}|_P(\xi_{\nu_e}) \simeq \text{D/H}|_{P,\,\text{ref}} \cdot (1 + \xi_{\nu_e})^{-0.50} \ . \tag{7.14}$$

where, again, $\text{D/H}|_{P,\,\text{ref}}$ refers to the value of the primordial deuterium abundance for a zero lepton asymmetry. Since the effect of ξ_{ν_e} on deuterium is mainly through the weak rates, the choice of rates does not modify the dependence of $D/H|_P$, but the reference value does significantly change. From Fig. 7.1, we can already gather that the choice of rates can have a strong influence. However, given the strong sensitivity of Deuterium to the baryon density, $\text{D/H}|_P \propto (\Omega_b h^2)^{-1.6}$, the sensitivity to ξ_{ν_e} from $\text{D/H}|_P$ is lost unless $\Omega_b h^2$ is given as an input by other methods. In the absence of such a prior, the larger value in ξ_{ν_e} may be compensated for by a lower value of $\Omega_b h^2$.

7.2 Current constraints

We will now analyze how BBN and CMB data can constrain the electron neutrino chemical potential for two possible cosmological scenarios, namely when we assume a standard expansion history during BBN such that $N_{\text{eff}} = N_{\text{eff}}^{\text{SM}} + \Delta N_{\text{eff}}(\xi_{\nu_e}) = 3.044 + \Delta N_{\text{eff}}(\xi_{\nu_e})$[1] , or when N_{eff} differs from the SM expectation, corresponding to a non-standard expansion history by allowing N_{eff} to float.

The resulting constraints are summarized in Figs. 7.2 and 7.3 for cosmological scenarios with a standard and non-standard expansion history, respectively, as well as on Table 7.1.

In Fig. 7.2 we show the 1 and 2σ confidence regions for ξ_{ν_e} and $\Omega_b h^2$, fixing $N_{\text{eff}} = N_{\text{eff}}^{\text{SM}} = 3.044$ and for the PArthENoPE choice of rates for different priors on Y_P. The grey contour corresponds to constraints coming from CMB data only, whereas the purple contours show the BBN only constraints. We see quite clearly that, while CMB data dominates the constraints on the baryon density, current constraints on the (electron) lepton asymmetry ξ_{ν_e} are dominated by BBN data. Given the strong dependence of $D/H|_P$ on $\Omega_b h^2$, in the absence of a prior for this parameter, the prior on $D/H|_P$ will fix the value of the baryon density, such that the constraints on ξ_{ν_e} are dominated by Y_P. As a result, the correlation between he baryon density and ξ_{ν_e} is almost non-existent, as we can see from the marginal tilt in the purple contour.

As we can also abstract from the figure, the importance of the choice of prior on Y_P cannot be understated. The new EMPRESS result points to a positive lepton asymmetry,

$$\xi_{\nu_e} = 0.043 \pm 0.015 \quad [\text{EMPRESS}] \,, \tag{7.15}$$

which is different from zero with a $\sim 3\sigma$ significance. Instead, if one adopts the PDG-22 recommended value, one obtains:

$$\xi_{\nu_e} = 0.008 \pm 0.013 \quad [\text{PDG}-22] \,, \tag{7.16}$$

---

[1]In this section we use $N_{\text{eff}}^{\text{SM}} = 3.044$ since these results were obtained before the publication of [46]. However, a modification of $\Delta N_{\text{eff}} = 0.001$ will not affect any of the conclusions.
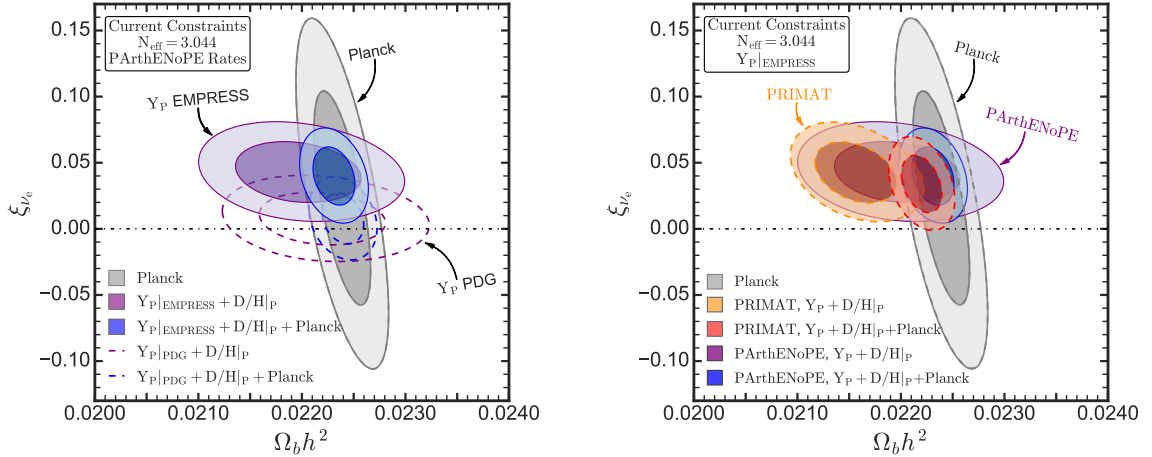
Figure 7.2: 1 and 2σ C.L. regions for ξ_{ν_e} and $\Omega_b h^2$ from nucleosynthesis data, CMB data, and their combination for a cosmological scenario without dark radiation (*i.e.* assuming $N_{\rm eff} = N_{\rm eff}^{\rm SM} = 3.044$). The left panel compares the favored regions for two determinations of the helium abundance (EMPRESS survey and the PDG-21 recommended value) adopting the PArthENoPE nuclear rates, while the right panel compares the favored regions for two choices of the nuclear reaction rates (PArthENoPE or PRIMAT) adopting the EMPRESS measurement of the helium abundance.

showing no preference for a nonzero lepton asymmetry. The combination with the Planck data does not alter significantly the conclusions for the lepton asymmetry, although it reduces the allowed range for $\Omega_b h^2$. For PArthENoPE rates this does not pose a problem and the overall fit to data is quite good regardless of the prior.

On the right panel of Fig. 7.2 we show how the choice of nuclear reaction rates affects the constraints. This plot shows the 1σ and 2σ contours from BBN and CMB data independently and combined for both the PArthENoPE (purple/blue) and PRIMAT(orange/red) nuclear rates. This figure quite clearly shows that The EMPRESS hint for a nonzero lepton asymmetry is fairly insensitive to the choice of the nuclear reaction rates, with the contours only very marginally shifting along the ξ_{ν_e}-axis. This was to be expected, given that the constraints on ξ_{ν_e} come solely from Helium and are mostly uncorrelated with $\Omega_b h^2$.

Additionally, the lack of correlation also implies that we expect to see a shift in the baryon density constraints from BBN only similar to that found in the SBBN case, namely that the reconstructed value of $\Omega_b h^2$ is slightly lower when adopting the PRIMAT rates than for the PArthENoPE rates. This also worsens the overall fit to data when combining BBN and CMB priors, as can be seen by the difference in the respective $\chi^2_{\rm min}$ values.

We now allow the effective number of neutrino species to float. This implies that we now have a three-dimensional parameter space, but only two reliable measurements for the primordial abundances, so our parameter space is degenerate. Therefore, just as in the case of the dark decays, we require some form of input to lift the degeneracy between parameters. We choose two different priors in this case. First, in order to assume as little as possible from the CMB we will only take the
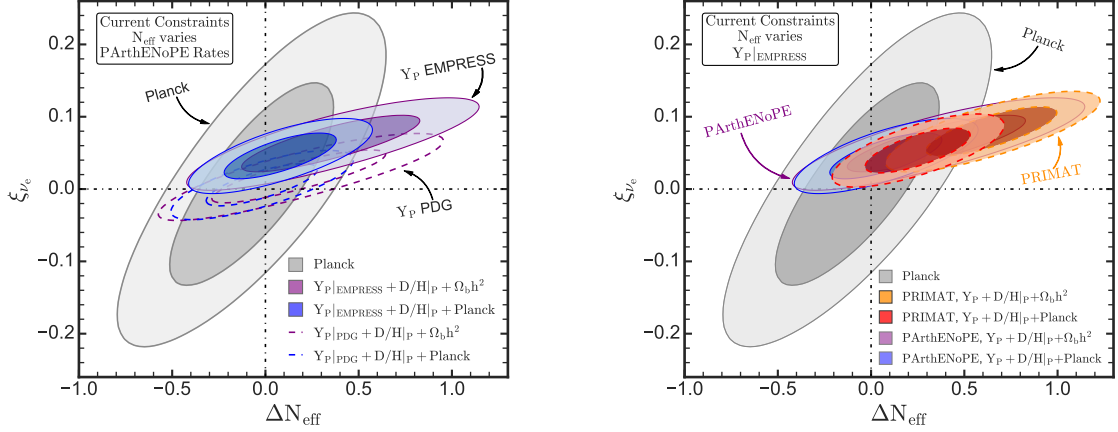
Figure 7.3: Same as Fig. 7.2, in the plane of ξ_{ν_e} and ΔN_{eff}, without making assumptions on the dark radiation content in the Universe.

prior on the baryon density. However, this is not entirely consistent since the effect of the baryon density, N_{eff}, and Y_P on the CMB power spectrum is correlated. Thus, we will use the full Gaussian prior from Eq. 2.17 that takes this into account.

In Fig. 7.3 we show the 1 and 2σ confidence regions for ξ_{ν_e} and ΔN_{eff}, corresponding to a scenario with a non-standard expansion history after marginalizing over the baryon density.

The left panel shows the importance of the choice of prior on Y_P. From the grey contour corresponding to CMB data only, we can abstract that also in this cosmological scenario, the determination of ξ_{ν_e} is dominated by BBN data.

Additionally, we have seen in Sec. 4.3 that Helium production is positively correlated with N_{eff}, As can be seen by the elongated shape of the purple ellipse, this implies that N_{eff} and ξ_{ν_e} are degenerate. With only a prior on $\Omega_b h^2$, the degeneracy is only broken because of the slightly different correlation of both parameters for the deuterium abundance. The degeneracy implies that slightly higher values for both parameters are allowed at the cost of some sensitivity. Concretely, for the EMPRESS prior we find

$$\xi_{\nu_e} = 0.063 \pm 0.026\,, \quad [Y_P + D/H|_P + \Omega_b h^2 \tag{7.17a}$$

$$N_{\text{eff}} = 3.39 \pm 0.31\,, \qquad \text{EMPRESS} + \text{Planck}] \tag{7.17b}$$

with a 2.4σ preference for a non-zero value of the chemical potential. On the other hand, for the PDG-22 prior we find:

$$\xi_{\nu_e} = 0.018 \pm 0.024\,, \quad [Y_P + D/H|_P + \Omega_b h^2 \tag{7.18a}$$

$$N_{\text{eff}} = 3.21 \pm 0.31\,. \qquad \text{PDG}-22 + \text{Planck}] \tag{7.18b}$$

with no preference for a non-zero chemical potential. However, in both cases the degeneracy between the two parameters allows for much larger values of N_{eff} than in the standard scenario, which may ease the tension between some scenarios including dark radiation and BBN.

Planck measurements of N_{eff} break the positively correlated degeneracy between ξ_{ν_e} and ΔN_{eff}, thereby reducing slightly the allowed range of ξ_{ν_e}, so that the preferred

values of ξ_{ν_e} and N_{eff}, using the EMPRESS determination of Y_{P}, are:

$$\xi_{\nu_e} = 0.046 \pm 0.021 \,, \quad [\text{Y}_{\text{P}} + \text{D/H}|_{\text{P}} + \text{CMB} \tag{7.19a}$$

$$N_{\text{eff}} = 3.12 \pm 0.20 \,, \qquad \text{EMPRESS} + \text{Planck}] \tag{7.19b}$$

which amounts to a 2.2σ preference for a nonzero lepton asymmetry. If one adopts, instead, the PDG-22 recommended value, one finds:

$$\xi_{\nu_e} = 0.006 \pm 0.019 \,, \quad [\text{Y}_{\text{P}} + \text{D/H}|_{\text{P}} + \text{CMB} \tag{7.20a}$$

$$N_{\text{eff}} = 3.03 \pm 0.20 \,. \qquad \text{PDG}{-}21 + \text{Planck}] \tag{7.20b}$$

yielding no preference for a nonzero lepton asymmetry.

Since also in this case Y_P dominates the constraints on ξ_{ν_e}, the conclusions on this parameter do not depend strongly on the choice of the nuclear reaction rates, as shown in the right panel of Fig. 7.3. On the other hand, the preferred values for ΔN_{eff} can vary sizably depending on this choice. The PRIMAT rates already under-produce Deuterium assuming the Planck value for $\Omega_b h^2$, a situation which is only worsened when allowing for a positive neutrino chemical potential, which further suppresses the Deuterium production. This has to be compensated for by an increase in N_{eff}, leading to a shift of the best-fit value of the orange contour on the right panel of Fig. 7.3 towards greater ΔN_{eff}.

This effect is largest when only adding a prior on the baryon density. In this case, using PRIMAT rates and the EMPRESS determination of Y_{P} we find:

$$\xi_{\nu_e} = 0.079 \pm 0.026 \,, \quad [\text{Y}_{\text{P}} + \text{D/H}|_{\text{P}} + \Omega_{\text{b}} \text{h}^2 \tag{7.21a}$$

$$N_{\text{eff}} = 3.68 \pm 0.23 \,, \qquad \text{EMPRESS} + \text{Planck}] \tag{7.21b}$$

which shows a 3.5σ preference for a large leptons asymmetry and, additionally, is only mildly in tension with the presence of a sterile neutrino during BBN, a scenario which is largely ruled out from other observations. For the PDG-22 recommended value,

$$\xi_{\nu_e} = 0.034 \pm 0.020 \,, \quad [\text{Y}_{\text{P}} + \text{D/H}|_{\text{P}} + \Omega_{\text{b}} \text{h}^2 \tag{7.22a}$$

$$N_{\text{eff}} = 3.50 \pm 0.22 \,. \qquad \text{PDG}{-}22 + \text{Planck}] \tag{7.22b}$$

The strong correlation between N_{eff} and ξ_{ν_e} leads to a 1.7σ preference for a non-zero lepton asymmetry, even with the comparatively larger value of Y_P from the PDG-22 determination. These should be compared to Eq. (7.17) and Eq. (7.18), respectively.

However, when constraining the effective number of neutrinos from observations of the CMB, such high values of N_{eff} are no longer allowed, and this preference vanishes, while the goodness of fit worsens due to the $\sim 2\sigma$ tension coming from the PRIMAT rates. More concretely, we find

$$\xi_{\nu_e} = 0.052 \pm 0.020 \,, \quad [\text{Y}_{\text{P}} + \text{D/H}|_{\text{P}} + \text{CMB} \tag{7.23a}$$

$$N_{\text{eff}} = 3.29 \pm 0.19 \,, \qquad \text{EMPRESS} + \text{Planck}] \tag{7.23b}$$

with a 2.6σ preference for a non-zero lepton asymmetry, while for the PDG-22 recommended value, the

$$\xi_{\nu_e} = 0.014 \pm 0.018 \,, \quad [\text{Y}_{\text{P}} + \text{D/H}|_{\text{P}} + \text{CMB} \tag{7.24a}$$

$$N_{\text{eff}} = 3.19 \pm 0.18 \,. \qquad \text{PDG}{-}22 + \text{Planck}] \tag{7.24b}$$

	Bounds and Sensitivities on the Primordial Lepton Asymmetries from BBN and CMB data					
Y_P	Data Sets	Nuclear Rates	ξ_{ν_e}	N_{eff}	Pref $\xi_{\nu_e} \neq 0$	$\chi^2_{\min}$
CMB	Planck	PArthENoPE	0.022 ± 0.053	3.044	0.4σ	0
		PRIMAT	0.022 ± 0.053	3.044	0.4σ	0
		PArthENoPE	0.004 ± 0.092	2.97 ± 0.29	0.0σ	0
		PRIMAT	0.002 ± 0.094	2.94 ± 0.29	0.0σ	0
EMPRESS $Y_P = 0.2370(34)$	$\mathbf{Y_P + D/H|_P}$	PArthENoPE	0.043 ± 0.015	3.044	2.9σ	0
		PRIMAT	0.042 ± 0.015	3.044	2.9σ	0
	$Y_P + D/H|_P + \Omega_b h^2|_{\mathrm{Planck}}$	PArthENoPE	0.040 ± 0.015	3.044	2.7σ	1.2
		PRIMAT	0.030 ± 0.014	3.044	2.1σ	8.1
	$Y_P + D/H|_P + \mathrm{Planck}$	PArthENoPE	0.040 ± 0.014	3.044	2.8σ	1
		PRIMAT	0.034 ± 0.014	3.044	2.4σ	7.3
	$Y_P + D/H|_P + \Omega_b h^2|_{\mathrm{Planck}}$	PArthENoPE	0.063 ± 0.026	3.39 ± 0.31	2.4σ	0
		PRIMAT	0.079 ± 0.023	3.68 ± 0.23	3.5σ	0
	$\mathbf{Y_P + D/H|_P + Planck}$	PArthENoPE	0.046 ± 0.021	3.12 ± 0.20	2.2σ	0.9
		PRIMAT	0.052 ± 0.020	3.29 ± 0.19	2.6σ	5.6
PDG-22 $Y_P = 0.245(3)$	$\mathbf{Y_P + D/H|_P}$	PArthENoPE	0.008 ± 0.013	3.044	0.6σ	0
		PRIMAT	0.007 ± 0.013	3.044	0.6σ	0
	$Y_P + D/H|_P + \Omega_b h^2|_{\mathrm{Planck}}$	PArthENoPE	0.006 ± 0.013	3.044	0.5σ	0.3
		PRIMAT	0.000 ± 0.013	3.044	0.0σ	4.4
	$Y_P + D/H|_P + \mathrm{Planck}$	PArthENoPE	0.008 ± 0.013	3.044	0.6σ	0.4
		PRIMAT	0.004 ± 0.013	3.044	0.3σ	4.9
	$Y_P + D/H|_P + \Omega_b h^2|_{\mathrm{Planck}}$	PArthENoPE	0.018 ± 0.024	3.21 ± 0.31	0.7σ	0
		PRIMAT	0.034 ± 0.020	3.50 ± 0.22	1.7σ	0
	$\mathbf{Y_P + D/H|_P + Planck}$	PArthENoPE	0.006 ± 0.019	3.03 ± 0.20	0.3σ	0.5
		PRIMAT	0.014 ± 0.018	3.19 ± 0.18	0.8σ	4.3
Forecasted Constraints	**Simons Observatory** $(Y_P = 0.2370)$	PArthENoPE	0.044 ± 0.015	3.044	2.9σ	-
		PArthENoPE	0.051 ± 0.035	3.13 ± 0.11	1.4σ	-
	CMB-S4 $(Y_P = 0.2370)$	PArthENoPE	0.044 ± 0.010	3.044	4.2σ	-
		PArthENoPE	0.051 ± 0.023	3.13 ± 0.08	2.1σ	-
	Simons Observatory + EMPRESS	PArthENoPE	0.043 ± 0.010	3.044	4.4σ	-
		PArthENoPE	0.047 ± 0.016	3.12 ± 0.07	2.9σ	-
	CMB-S4 + EMPRESS	PArthENoPE	0.043 ± 0.008	3.044	5.3σ	-
		PArthENoPE	0.045 ± 0.014	3.12 ± 0.06	3.3σ	-
	Simons Observatory + Y_P SM	PArthENoPE	-0.001 ± 0.010	3.044	0.0σ	-
		PArthENoPE	0.001 ± 0.015	3.05 ± 0.07	0.1σ	-
	CMB-S4 + Y_P SM	PArthENoPE	0.000 ± 0.008	3.044	0.0σ	-
		PArthENoPE	0.001 ± 0.013	3.05 ± 0.06	0.0σ	-

Table 7.1: Summary of constraints or forecasts on the primordial (electron) lepton asymmetry, ξ_{ν_e}, from considering several combinations of BBN and CMB data, for cosmological scenarios without or with dark radiation, and for two possible choices of the nuclear reaction rates. See main text for details.

which is in agreement within current observations with $\xi_{\nu_e} = 0$ and $N_{\mathrm{eff}}^{\mathrm{SM}}$. These should be compared to Eq. (7.19) and Eq. (7.20), respectively.

It is noteworthy that if one requires ΔN_{eff} to be positive, as occurs in most models of dark radiation, then the preference for a positive lepton asymmetry further increases, as negative values of ξ_{ν_e} cannot be compensated for by a negative value of ΔN_{eff}. As we have seen, except for a scenario with a time variation of the gravitational constant, the few cosmological settings that feature $\Delta N_{\mathrm{eff}} < 0$, notably MeV-scale reheating [61, 62] and scenarios with MeV-scale electrophilic particles [64, 63], actually modify the expansion history in a different and highly non-trivial way instead of simply parametrically reducing as we have assumed here. Therefore, they actually lead to a higher Y_P, see [107, 108] and would thus enhance the tension with the EMPRESS measurement.

7.3 Forecasts for the Simons Observatory and CMB-S4

The sensitivity of current cosmological probes to a primordial lepton asymmetry is limited by two factors. First, the observational uncertainty on Y_P from astrophysical observations dominates the sensitivity to ξ_{ν_e} for a standard expansion history of the Universe. Since these measurements are constrained mostly by systematic uncertainties which are unlikely to be improved in the near future, an independent from a different source will be extremely important. Additionally, in the case of allowing for a non-standard expansion history of the Universe, then the sensitivity is additionally influenced by the positive correlation between N_{eff} and ξ_{ν_e}.

In light of that, future CMB observations will be instrumental to further probe the hint for a nonzero lepton asymmetry from EMPRESS. Not only will they provide an independent and precise measurement of Y_P, but these experiments have been specifically designed to yield an unprecedented sensitivity to N_{eff}. Thus they fulfill both requirements to significantly increase the sensitivity in the case of a standard and non-standard expansion history.

In this section we consider specifically the prospects for detecting a nonzero primordial asymmetry with the upcoming Simons Observatory and the projected CMB-S4. We will follow a similar method in our statistical analysis, so we will first need an estimate of the Gaussian covariance matrix of these observations. Additionally, in order not to over-complicate matters and not to combine measurements which are on tension, as this will lead to non-sensical results, we will use only the PArthENoPE rates for this section, as these show good agreement with currrent CMB observations.

For the Simons Observatory, we take the baseline covariance matrix to the relevant parameters of our analysis Y_P, N_{eff} and $\Omega_b h^2$ [109]. Once marginalized over the rest of cosmological parameters, they read [63]:

$$\text{Simons Observatory}$$
$$\sigma(\Omega_b h^2) = 0.000073\,, \tag{7.25a}$$
$$\sigma(Y_P) = 0.0066\,, \tag{7.25b}$$
$$\sigma(N_{\text{eff}}) = 0.11\,, \tag{7.25c}$$
$$\rho(\Omega_b h^2,\, Y_P) = 0.33\,, \tag{7.25d}$$
$$\rho(\Omega_b h^2,\, N_{\text{eff}}) = 0.072\,, \tag{7.25e}$$
$$\rho(N_{\text{eff}},\, Y_P) = -0.86\,. \tag{7.25f}$$

For CMB-S4, we use the results from the Fisher matrix forecast performed in [63] which is in very good agreement with the results reported by the collaboration [110, 111]. The relevant parameters read:

$$\text{CMB}-\text{S4}$$
$$\sigma(\Omega_b h^2) = 0.000047\,, \tag{7.26a}$$
$$\sigma(Y_P) = 0.0043\,, \tag{7.26b}$$
$$\sigma(N_{\text{eff}}) = 0.081\,, \tag{7.26c}$$
$$\rho(\Omega_b h^2,\, Y_P) = 0.22\,, \tag{7.26d}$$

$$\rho(\Omega_b h^2, N_{\text{eff}}) = 0.25 \,, \tag{7.26e}$$

$$\rho(N_{\text{eff}}, Y_{\text{P}}) = -0.84 \,. \tag{7.26f}$$

While for the covariance matrix we can make more or less correct or, at least conservative, estimates, the best fit value will only be determined once the actual experiments take data. The best we can do is to make some well-motivated assumptions on possible central values of all three parameters that suit the purpose of our analysis. Our main goal is to see how future measurements will be able to discard or support the EMPRESS hint for a lepton asymmetry. There is also a third possibility that the new determination does neither one nor the other, but that is not what we are concerned with here.

For Y_{P}, we will therefore consider two possibilities, either $Y_{\text{P}} = Y_{\text{P}}|_{\text{SBBN}} = 0.2469$ or $Y_{\text{P}} = Y_{\text{P}}|_{\text{EMPRESS}} = 0.2370$, corresponding to a scenario where the helium abundance coincides with the standard BBN prediction, thus constraining the EMPRESS hint for a large lepton asymmetry, or when it is lower as hinted by EMPRESS, which will increase the significance of the hint. For both, we consider also a direct astrophysical determination with an error bar of 0.003 which matches the precision of current determinations, since it is unlikely that these will significantly change in the future as systematic errors already dominate these measurements.

For the central value of the baryon density we will take $\Omega_b h^2 = 0.02242$, as favored by Planck CMB observations, see Eq. (2.14), since this is in good agreement alos with the BN prediction with PArthENoPE rates.

Finally, for N_{eff} we will either choose $N_{\text{eff}}^{\text{SM}} = 3.044$, as expected in the Standard Model, or the central value inferred from the current full analysis of BBN and CMB data using PArthENoPE rates, namely $N_{\text{eff}} = 3.12$, see Eq. (7.19b).

In Fig. 7.4 we present the results of our forecast. In the upper panels, we show the sensitivity to ξ_{ν_e} from the Simons Observatory (left) or CMB-S4 (right) as a function of $\Omega_b h^2$ for a scenario with a fixed $N_{\text{eff}} = 3.044$. We compare this sensitivity to the one obtained from current CMB+BBN data. The green contours correspond to the BBN independent constraints, while the yellow contours correspond to the combination with current measurements of the primordial abundances.

The green contours should, therefore, be compared with the grey contour on Fig. 7.2, which already shows how significant an improvement this is. After the Simons observatory is done taking data, CMB only constraints on the neutrino chemical potential will be competitive with current independent and combined BBN constraints.

Furthermore, even though the conservative projection of the uncertainty of the measurement of Y_P from CMB-S4 is larger than current observations, its unprecedented sensitivity to the baryon density actually implies that the CMB only constraints from this experiments will actually improve the sensitivity with respect to current combined constraints. More concretely, our forecast sensitivity to the lepton asymmetry for each experiments reads:

$$\sigma(\xi_{\nu_e})|_{N_{\text{eff}}=3.044} \simeq 0.015 \,, \quad \text{[Simons Obs.]} \tag{7.27a}$$

$$\sigma(\xi_{\nu_e})|_{N_{\text{eff}}=3.044} \simeq 0.010 \,. \quad \text{[CMB}-\text{S4]} \tag{7.27b}$$

which should be compared to $\sigma(\xi_{\nu_e})|_{N_{\text{eff}}=3.044} = 0.0015$ as obtained from current experiments.
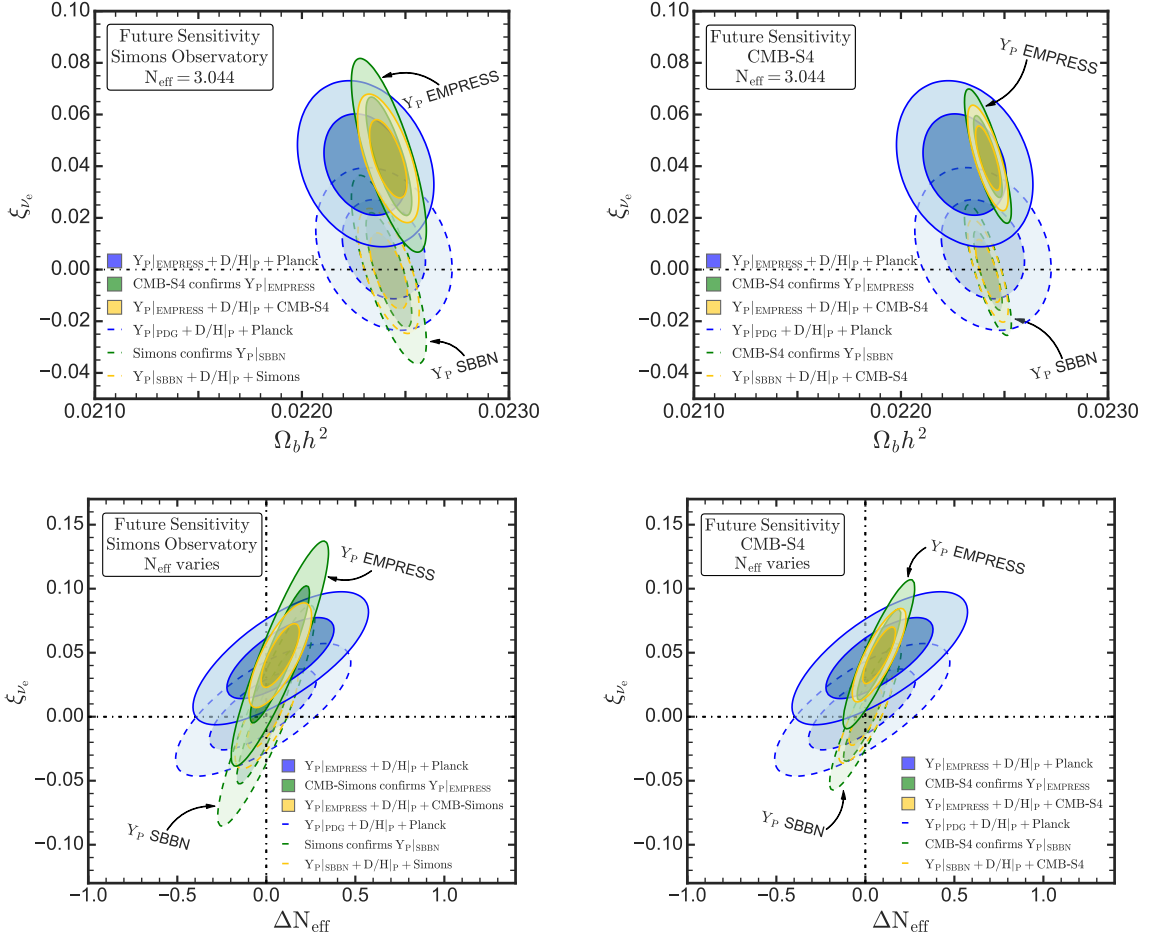
Figure 7.4: 1 and 2σ C.L. forecast regions for ξ_{ν_e} and $\Omega_b h^2$ for a scenario without dark radiation (top panels), or ξ_{ν_e} and ΔN_{eff} for a scenario without making assumptions on the amount of dark radiation (bottom panels) from nucleosynthesis data, the upcoming Simons Observatory (left panels) or the projected CMB-S4 (right panels), and their combination.

More importantly, if the true value of the helium abundance correspond to the EMPRESS determination of $Y_P = 0.2370$, and the Universe does not contain substantial amounts of dark radiation, $N_{\text{eff}} = 3.044$, then the combination of EM-PRESS and the Simons Observatory would increase the significance for a nonzero lepton asymmetry, to $\sim 4.4\sigma$, and the combination with CMB-S4 to $\sim 5.3\sigma$ (see Table 7.1). While the projected sensitivity is independent of the central value we have chosen, the significance of the prediction for a non-zero lepton asymmetry should be taken as best-case scenarios, as they naturally very strongly depend on the central value. Instead, they should be interpreted as best case-scenarios.

In the lower panels of Fig. 7.4, we allow N_{eff} to vary. As expected, the reach of the Simons Observatory and of CMB-S4 worsen when relaxing the assumptions on the cosmological scenario. We obtain for the sensitivity of these scenarios independently
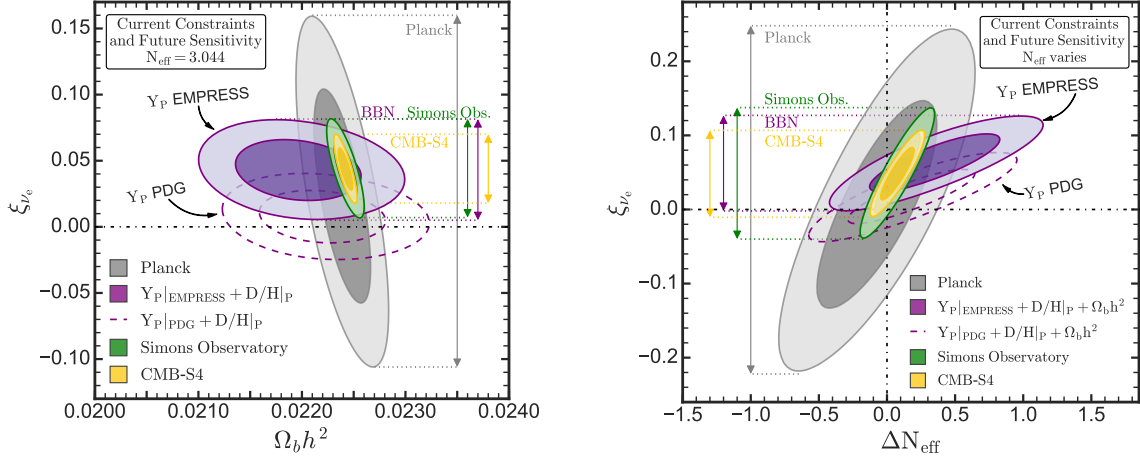
Figure 7.5: Summary of current and forecast 1- and 2-σ allowed regions for ξ_{ν_e} and $\Omega_b h^2$ in a scenario without dark radiation (left panel), or ξ_{ν_e} and ΔN_{eff} in a scenario without making assumptions on the amount of dark radiation (right panel) from nucleosynthesis data (EMPRESS survey or PDG-21 recommended value) and CMB data (Planck, Simons Observatory or CMB-S4).

of BBN:

$$\sigma(\xi_{\nu_e}) \simeq 0.04 \,, \quad [\text{Simons Obs.}] \tag{7.28a}$$

$$\sigma(N_{\text{eff}}) \simeq 0.11 \,, \quad [\text{Simons Obs.}] \tag{7.28b}$$

$$\sigma(\xi_{\nu_e}) \simeq 0.02 \,, \quad [\text{CMB-S4}] \tag{7.28c}$$

$$\sigma(N_{\text{eff}}) \simeq 0.08 \,. \quad [\text{CMB-S4}] \tag{7.28d}$$

which should be compared to the $\sigma(\xi_{\nu_e}) = 0.020$ that can be reached with current experiments. This is still better than the sensitivity obtained independently from the Simons Observatory. On the other hand, CMB-S4 will reach a similar sensitivity as current combined measurements, even if we allow N_{eff} to float. This should not be surprising, since the unprecedented sensitivity of this experiment to N_{eff} implies that this is almost equivalent to actually keeping N_{eff} fixed.

For both experiments, though, we can definitely say that the sensitivity is at the very least comparable to current experiments, so that the combination of EMPRESS with CMB experiments will significantly narrow down the allowed ranges for ξ_{ν_e} and ΔN_{eff}, thereby strengthening the case for a nonzero lepton asymmetry, should the EMPRESS hint be correct. Concretely, combining current BBN an dfuture CMB data we find

$$\xi_{\nu_e} = 0.047 \pm 0.016 \,, \quad [\text{EMPRESS + SimonsObs.}] \tag{7.29a}$$

$$N_{\text{eff}} = 3.12 \pm 0.07 \,, \quad [\text{EMPRESS + SimonsObs.}] \tag{7.29b}$$

$$\xi_{\nu_e} = 0.045 \pm 0.014 \,, \quad [\text{EMPRESS + CMB-S4}] \tag{7.29c}$$

$$N_{\text{eff}} = 3.12 \pm 0.06 \,. \quad [\text{EMPRESS + CMB-S4}] \tag{7.29d}$$

which improves significantly upon the current sensitivity. Regarding the possible significance of the anomaly, within this cosmological scenario, the EMPRESS hint for a non-zero lepton asymmetry is at 2σ significance, whereas the combination of EMPRESS data with the Simons Observatory or CMB-S4 would increase the

significance to $\sim 3\sigma$. However, given the strong sensitivity of both experiments to N_{eff} and its streong positive correlation with ξ_{ν_e}, the central value of N_{eff} will be extremely important determining the significance of the EMPRESS anomaly should it persist.

Lastly, we have not really mentioned Deuterium throughout this section, even though in principle it is also quite sensitive to ξ_{ν_e}, so it may also play a significant role in determining the significance of the EMPRESS hint. Unlike the case for Helium, the current measurement is limited by statistics, and it is expected to improve substantially in the near future with the advent of 30m class optical/near-infrared telescopes [112]. Perhaps more importantly, though, the current uncertainty is actually dominated by uncertainty in the theoretical prediction for $D/H|_P$ coming from the $d + d \to n + {}^3\mathrm{He}$ and $d + d \to p + {}^3\mathrm{H}$ reaction rates. Additionally, since the most stringent constraints actually rely on a combination of CMB and BBN data, resolving the possible tension between BBN and the CMB, which we have ignored up to now in this discussion, is imperative. Therefore, in order to provide a competitive probe of the lepton asymmetry, it is mandatory to measure more precisely these reactions, or improve the theoretical modeling [52].

7.4 Conclusions

The recent measurement of the primordial helium abundance by EMPRESS could be an indication for a nonzero lepton asymmetry in the electron neutrino flavor. Motivated by this new measurement, we have performed a global analysis of the primordial lepton asymmetries using both BBN and CMB data. Our main results are summarized in Fig. 7.5, which shows the current constraints on the lepton asymmetry (parametrized by the neutrino chemical potential ξ_{ν_e}) and its correlation with the baryon asymmetry ($\Omega_b h^2$) and with the amount of dark radiation in the Universe (parametrized by the extra contributions to the effective number of neutrino species, ΔN_{eff}); quantitative results are reported in Table 7.1.

The constraints on the lepton asymmetry are currently dominated by the helium abundance, so that they are naturally strongly dependent on the prior chosen on Y_P, while the choice of nuclear reaction rates only mildly affects the results. We find a $\sim 3\sigma$ preference for nonzero lepton asymmetry when using the EMPRESS data, while with the PDG-22 recommended value the preference vanishes (see Fig. 7.2 and Table 7.1). These conclusions are broadly in agreement with other recent works analyzing the implications of the EMPRESS measurements on the cosmological parameters [10, 113].

Finally, we have also performed a forecast of the sensitivity to the lepton asymmetry from the upcoming Simons Observatory and the future CMB-S4. As can be already seen by Fig. 7.5, Simons Observatory will reach, independently, a sensitivity comparable to the current BBN constraints, while CMB-S4 has the potential of improving upon them. Should the Simons Observatory confirm the EMPRESS result, the CMB data from the Simons Observatory, combined with the results from EMPRESS, will strengthen the hint for a nonzero lepton asymmetry to $\sim 3\sigma$ if we allow for a non-standard background evolution, and $\sim 4\sigma$ if $N_{\mathrm{eff}} = N_{\mathrm{eff}}^{\mathrm{SM}}$. With the future CMB-S4 data, the significance would be $\sim 3\sigma$ and $\sim 5\sigma$ for the different

scenarios respectively

If confirmed, this result would hint toward new physics generating a large lepton asymmetry that is not converted to a correspondingly large baryon asymmetry by sphaleron processes. The construction of possible models and their possible signals deserves, in our opinion, further investigation.

Chapter 8

Conclusion

From its rocky start in the early 1940s, as a controversial and slightly neglected idea, primordial nucleosynthesis has seen some impressive advances with time, both from a theoretical as well as an experimental point of view and has established itself as one of the pillars of modern Cosmology. Now, Nucleosynthesis has entered the era of precision cosmology and as such has become one of the most powerful probes of the early Universe, opening up a window into the Universe just three minutes after its conception.

While, overall, one can definitely say that BBN has withstood the test of time, in this era of precision cosmology, just as in other branches of cosmology, possible cracks in its foundation are starting to show. Aside from the long-standing Lithium problem, which we have simply ignored throughout this thesis, recent measurements of the $d+p \rightarrow {}^3He + \gamma$ rate by the LUNA collaboration [55] have exposed a possible $\sim 2\sigma$ tension between the baryon density abstracted from measurements of the CMB and BBN, when they should be equal according to the ΛCDM model. Additionally, the novel determination of the primordial Helium abundance by the EMPRESS collaboration is in about a 3σ tension with the Standard Model. This would imply that for every observational abundance we can constrain there is a significant tension between prediction and observation. On the other hand, different determinations of Y_P show no tension with the SBBN prediction of Y_P and the tension with the Deuterium abundance leading to the smaller predicted value of $\Omega_b h^2$ vanishes if one interpolates the experimental rates differently.

A resolution of this tension will only come with either new measurements of the Helium abundance either confirming or rejecting the EMPRESS result and with new experimental data on the DD-reactions that dominate the error budget of the Deuterium abundance. Thus, while saying that BBN is in trouble may be a bit of an overstatement, we also need to be careful when championing the remarkable agreement between theory and data of the primordial abundances of light nuclei given its fragility.

More importantly, though, as we hope to have shown with this thesis, in neither of the two cases, the importance of BBN as a probe of new physics is undermined in any way. If the EMPRESS value for Y_P and the choice of nuclear reaction rates from PRIMAT turn out to be confirmed, this may be interpreted as a hint of new physics at play at the epoch of BBN, guiding further development in the areas of Cosmology and Particle Physics, whereas if the PDG-22 determination and the rates adopted

117

in ParthENoPE turn out to be correct, then BBN can constrain those same aspects of new physics.

Throughout this thesis, we have attempted to do both, by highlighting the effects the seemingly trivial choice of prior on Y_P and nuclear reaction rates has on the conclusions, while still performing exhaustive global analyses using different sets of BBN and CMB data, both independently and combined.

We have focused on three scenarios. First, we have allowed for a non-standard expansion history of the Universe parametrized by $\Delta N_{\text{eff}} \neq 0$. In this case, the choice of nuclear reaction only very mildly affects the constraints, while the prior on Y_P significantly changes the conclusions. Regardless of the combination between CMB and BBN data, with the PDG-22 value we find good agreement with $N_{\text{eff}} = N_{\text{eff}}^{\text{SM}}$. For the EMPRESS prior, on the other hand, we find $N_{\text{eff}} = 2.41 \pm 0.22$, which is about 3σ lower than the Standard model value and slightly in tension with the CMB determination. While some models leading to ΔN_{eff} exist, they actually increase the primordial abundance of Helium, actually worsening the tension with the Standard model. We find that the simplest interpretation of this is actually as a 3σ indication of a time variation of the Gravitational constant $\frac{\Delta G_N}{G_N^0} = -0.104 \pm 0.035$ or, assuming a linear time dependence for $G_N(t)$, $\frac{\dot{G_N}}{G_N^0} = (7.5 \pm 2.6) \times 10^{-12} \text{yr}$.

We then studied the time variation of the Higgs vacuum expectation value and its effect on BBN. Both Helium and Deuterium are positively correlated with a relative variation of v, more strongly so for Deuterium than for Helium. However, given a degeneracy between the baryon density and the Higgs vev for Deuterium, the sensitivity from BBN on this parameter is entirely dominated by the prior on Y_P. Thus, we find $\frac{\delta v}{v_0} = 0.0096 \pm 0.0031$ for the EMPRESS prior on Y_P regardless of the choice of nuclear rates and a similar sensitivity but no preference for $\frac{\delta v}{v_0} \neq 0$ for PDG rates. When assuming a prior on $\Omega_b h^2$, the degeneracy for Deuterium breaks and it is now this abundance that dominates the constraints. Interestingly, given the strong dependence of the Deuterium abundance on $\frac{\delta v}{v_0}$, even for the PDG-22 value for Y_P the tension coming from the choice of PRIMAT rates translates into a 2.1σ preference for $\frac{\delta v}{v_0} = -1.9 \pm 1.0$. However, since this constraint is now driven by the Deuterium abundance, the preference vanishes for ParthENoPE rates. Regardless, this may be a hint that both the PRIMAT tension as well es the EMPRESS anomaly are an artifact of a time variation of the Higgs vev.

Departing from the topic of the time variation of fundamental constants, we have also studied how BBN can be used to perhaps resolve the Neutron Lifetime Anomaly. First, the strong sensitivity of the Helium abundance to τ_n and the increased precision in the Helium determination allows one to make an indirect measurement of τ_n from BBN data, yielding $(870 \pm 14)\,\text{s}$ for the PDG-22 prior, which is comparable to space determinations of τ_n, although it does not provide any significant preference for one or the other. For the EMPRESS prior on Y_P we find a value lower by about 3σ than both determinations, which seems an unlikely explanation of the EMPRESS anomaly. The error on τ_n is entirely dominated by the uncertainty in Y_P, so increasing the precision in the BBN measurement of τ_n requires increasing the precision in Y_P, making it unlikely that the BBN measurement of τ_n will become comparable with the most precise determinations to date.

However, we can also directly constrain the BSM physics interpretation propsosed

in [12]. They remark that the NLA could be explained if the neutron decayed to protons, with a lifetime we call τ_{np}, and additionally had a small branching ratio $\sim 1\%$ to some dark sector particles, that leads to a slightly smaller total neutron lifetime τ_n. While more stringent constraints can be derived, we show that BBN is in principle sensitive to both types of neutron lifetime, providing essentially a model independent constraint on this scenario.

Given the large observational uncertainty on Helium and the fact that Deuterium and Helium are degenerate with respect to τ_n and τ_{np}, we find that BBN in principle agrees both with the SM and BSM interpretations of the NLS, although the constraints are far from being competitive. The most stringent constraints are obtained from PArthENoPE rates by adding a prior on $\tau_n = \tau_n^{\text{bottle}} = (878.4 \pm 0.5)\,\text{s}$, for which we find $\tau_{np} = 878.5^{+11.4}_{-0.1}\text{s}$, which still agrees both with the SM as well as the dark neutron decay interpretation of the anomaly. However, in this case, depending on the central value of Y_P, even with slight improvements in the observational determination of Y_P, we can begin to constrain the BSM physics interpretation of the NLA.

Last, but definitely not least, having explored several other options, we come to the conclusion that a modification of the weak rates is perhaps the simplest way to reduce the Helium abundance without influencing strongly the Deuterium abundance. Therefore, we propose the presence of a large lepton asymmetry at the time of BBN as the most likely explanation of the EMPRESS anomaly and again perform an exhaustive analysis of the effect of a non-zero lepton asymmetry on BBN and the CMB, both for the case of a standard, $N_{\text{eff}} = N_{\text{eff}}^{\text{SM}}$, as well as a non-standard, $N_{\text{eff}} \neq N_{\text{eff}}^{\text{SM}}$, expansion history of the Universe.

The constraints on ξ_{ν_e} are dominated by the Helium abundance and, therefore, very strongly dependent on the prior chosen for Y_P, but rather insensitive to the choice of nuclear reaction rates, although the other parameters allowed to simultaneously vary are slightly affected by it. The significance for a non-zero chemical potential is $\sim 3\sigma$ when keeping N_{eff} fixed and $\sim 2\sigma$ when allowing N_{eff} to float for the EMPRESS prior on Y_P. On the other hand, with the PDG-22 prior on Y_P we find no preference for such a large lepton asymmetry.

Furthermore, we have performed a forecast of the sensitivity of future experiments improving observations of the CMB, namely the Simons Observatory and the CMB-S4. Assuming $N_{\text{eff}} = N_{\text{eff}}^{\text{SM}}$, we find that the Simons Observatory independently will provide a sensitivity that is comparable to the current senstivity from BBN only. CMB-S4 on the other hand will actually improve the sensitivity by $\sim 30\%$. We find that these experiments, if they were to confirm the EMPRESS results, have the potential to increase preference for a non-zero chemical potential to 4σ for the Simons Observatory and 5σ for the case of CMB-S4. The improvement for the case of $N_{\text{eff}} \neq N_{\text{eff}}^{\text{SM}}$ is less striking. Nonetheless, both experiments will provide powerful independent determinations of Y_P dominated by different systematics. If they were to confirm the EMPRESS results, this would be a strong indication of the presence of a large lepton asymmetry during BBN.

All in all, hopefully this thesis has shown the potential of BBN as a cosmological probe to constrain a plethora of different elements of new physics and provide hints to be used as guideposts for future developments.

Appendix A

Equilibrium Thermodynamics

A.1 Phase Space Distribution

The great accomplishment of statistical mechanics is to make a connection between a statistical description of the microscopic processes in a thermodynamic system, the microstates, and the quantities that describe it completely, the macrostate. This approach has proven useful and astonishingly accurate at modeling many complex systems under relatively simple assumptions and deriving valid results for the macroscopic observables.

Each microstate is described by a vector in the phase space Γ of all particles and amounts to a specific macrostate. Many microstates can yield the same macrostate. The key to describing any thermodynamic system and its development is to know how the probability for each microstate is distributed in the phase space, in order to determine which macrostate is most likely to happen.

This is described by the phase-space distribution $f(q, p)$, where $q = (q_1, ..., q_N)$ and $p = (p_1, ..., p_N)$ stand for the generalized coordinates and momenta of all particles. All thermodynamic quantities can be abstracted from it, requiring the limit of a large number of particles which we can safely say is fulfilled.

Thus, we can assume for the phase space distribution of a particle in equilibrium in the early Universe the phase space distribution of a single particle in an ideal gas, significantly reducing the degrees of freedom and the complexity of the problem. In the most general sense, that is, taking quantum and relativistic effects into account, one can write the phase space distribution as:

$$f(q, p) = \frac{1}{e^{\beta(E-\mu)} \pm 1} \tag{A.1}$$

where $\beta = \frac{1}{k_B T}$, E is the energy of the particle for a given microstate and μ is the chemical potential of the particle. There is a distinction between an ideal gas of bosons and fermions. The plus stands for fermions and the minus for bosons. For simplicity reasons, it will not always be clarified which sign stands for bosons and which for fermions. Unless explicitly stated otherwise, if a double sign like $\pm$ is used in an equation, the sign above will stand for fermions, the one below for bosons.

This slight difference has an enormous impact on the overall behaviour of such a gas, as can be seen from figure A.1. For bosons the distribution diverges to infinity
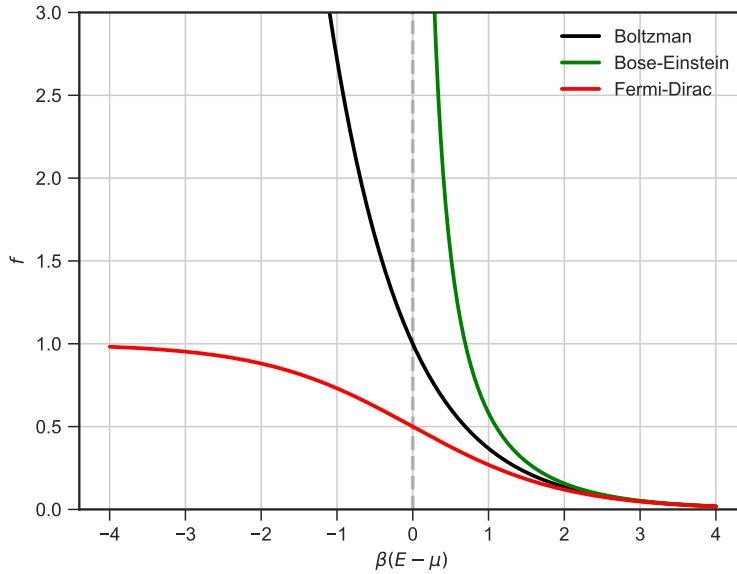
Figure A.1: Bose-Einstein, Fermi-Dirac and Boltzmann distributions as a function of $x = \beta(E - \mu)$. For $x > 2$ all three distributions show the same behavior, whereas they have very different limits for $x \ll 1$.

as $\beta(E - \mu)$ approaches 0, a behavior which leads to Bose-Einstein condensation at low temperatures, whereas for fermions the Pauli exclusion principle forces the distribution to remain below one.

A further distribution which is also very important in this context is the Boltzmann distribution:

$$f(q, p) = e^{-\beta(E-\mu)} \tag{A.2}$$

Both the Bose-Einstein and the Fermi-Dirac distribution converge to the Boltzmann distribution in the limit of either low particle density or high temperature (see fig. A.1). This approximation greatly simplifies the equations and, in most cases, approximating the Fermi-Dirac and Bose-Einstein distribution as a Boltzmann distribution, thus neglecting the difference between the nature of these particles and the quantum effects arising from it, is remarkably accurate.

A.2 Non-relativistic Particles

We can now proceed to calculate some quantities that we will need very often throughout the thesis, starting with the particle density. We will neglect the chemical potential in this section, as this will allow us to obtain closed form solutions. The phase space distributions from eq. A.1 and A.2 are not probability density functions, as they are not normalized to one. They are normalized to yield the total number of particles in the system N if integrated over phase space. Thus, only integrating over momentum space should lead to the distribution of particles in position space,

also known as the particle number density. We can therefore write:

$$n = \frac{g_i}{(2\pi)^3} \int d^3\vec{p}\, f(|\vec{p}|) \tag{A.3}$$

The factor $\frac{g_i}{(2\pi)^3}$ accounts for the fact that we have assumed that the distribution of possible microstates in the phase space is continuous and the factor g accounts for the internal degrees of freedom of the particle, that is, the fact that each eigenstate may be degenerate, for example, due to multiple possible spin configurations.

In the non-relativistic limit, the kinetic energy $E = \frac{|\vec{p}|^2}{2m} = \frac{3}{2}T$ is much smaller than the rest mass, so that in the non-relativistic limit $m/T \gg 1$. Thus, the energy momentum relation can be approximated as:

$$E = \sqrt{m^2 + |\vec{p}|^2} = m\sqrt{1 + \frac{|\vec{p}|^2}{m^2}} \approx m + \frac{|\vec{p}|^2}{2m} \tag{A.4}$$

Furthermore, in the non-relativistic limit, the phase space densities of both fermions and bosons can be approximated by the same Boltzmann distribution. Thus, the integral for the particle density results in:

$$n_{nr} = \frac{g_i}{(2\pi)^3} \int d^3\vec{p}\, e^{-\beta\left(m + \frac{|\vec{p}|^2}{2m}\right)} = e^{-\frac{m}{T}} \frac{g_i}{(2\pi)^3} \int d^3\vec{p}\, e^{-\frac{\beta}{2m}(p_x^2 + p_y^2 + p_z^2)}$$

$$\Rightarrow \boxed{n_{nr} = g_i \left(\frac{mT}{2\pi}\right)^{\frac{3}{2}} e^{-\frac{m}{T}}} \tag{A.5}$$

The energy density is defined in a similar manner by multiplying the integrand with the energy of a particle and integrating over momentum space:

$$\rho = \frac{g_i}{(2\pi)^3} \int d^3\vec{p}\, E(\vec{p}) f(\vec{p}) \tag{A.6}$$

Again, in the non-relativistic limit this can be evaluated analytically:

$$\rho_{nr} = \frac{g_i}{(2\pi)^3} \int d^3\vec{p}\, \left(m + \frac{|\vec{p}|^2}{2m}\right) e^{-\beta\left(m + \frac{|\vec{p}|^2}{2m}\right)} \tag{A.7}$$

$$\Leftrightarrow \rho_{nr} = m\frac{g_i}{(2\pi)^3} \int d^3\vec{p}\, e^{-\beta\left(m + \frac{|\vec{p}|^2}{2m}\right)} + \frac{e^{-\frac{m}{T}}}{2m} \frac{g_i}{2\pi^2} \int d|\vec{p}||\vec{p}|^4 e^{\frac{-\beta}{2m}|\vec{p}|^2}$$

where we have gone into spherical coordinates and integrated over the solid angle $d\Omega$, which results in a factor of 4π. With the integral

$$\int_0^\infty x^4 e^{-ax^2} = \frac{3\sqrt{\pi}}{8a^{5/2}} \tag{A.8}$$

from [114] and the definition for the particle density from A.5, this equation can be further simplified to:

$$\rho_{nr} = m \cdot n_{nr} + \frac{3T}{2m} g_i \left(\frac{mT}{2\pi} \right)^{3/2} e^{-\frac{m}{T}}$$

(A.9)

$$\Leftrightarrow \rho_{nr} = m \cdot n_{nr} \left(1 + \frac{3}{2} \frac{T}{m} \right)$$

Remembering that we are in the non-relativistic limit $\frac{m}{T} \gg 1$, eq. A.9 can be further simplified to give the formula:

$$\boxed{\rho_{nr} = m \cdot n_{nr}}$$

(A.10)

A.3   Relativistic Particles

However, not all particles are non-relativistic and we cannot always neglect quantum relativistic effects. Therefore, the particle and energy densities have to be calculated for the distributions in eq. A.1. We can not use A.4 anymore, but have to employ the full energy momentum relation

$$E^2 = |\vec{p}|^2 + m^2$$

(A.11)

The phase-space distribution from eq. A.1 only depends on the absolute value of momentum, so we will use spherical coordinates and rewrite the integral over $|\vec{p}|$ as an integral over energy. The differential of the absolute value of momentum is substituted by:

$$|\vec{p}|^2 d|\vec{p}| = \sqrt{E^2 - m^2} E dE$$

(A.12)

Thus, after performing the integral over the solid angle, eq A.3 for a boson or fermion takes on the form:

$$n_r = \frac{g_i}{(2\pi)^3} \cdot 4\pi \int_m^\infty dE \, \frac{E\sqrt{E^2 - m^2}}{e^{\beta E} \pm 1}$$

(A.13)

We can now introduce the dimensionless variables $x = \frac{m}{T}$ and $z = \frac{E}{T}$, so that:

$$n_r = \frac{g_i}{2\pi^2} T^3 \int_x^\infty dz \, \frac{z\sqrt{z^2 - x^2}}{e^z \pm 1}$$

(A.14)

For the Energy density, a similar result is obtained just by multiplying the integrand from eq. A.13 with E and then performing the variable change. This yields:

$$\rho_r = \frac{g_i}{2\pi^2} T^4 \int_x^\infty dz \, \frac{z^2\sqrt{z^2 - x^2}}{e^z \pm 1}$$

(A.15)

Unfortunately, these integrals are not always analytically solvable, but have to be evaluated numerically. In the ultra-relativistic limit we have $\frac{m}{T} = x \ll 1$, so that

the integrals from equations A.14 and A.15 can be approximated as:

$$n_r = \frac{g_i}{2\pi^2} T^3 \int_0^\infty dz \, \frac{z^2}{e^z \pm 1} \tag{A.16}$$

$$\rho_r = \frac{g_i}{2\pi^2} T^4 \int_0^\infty dz \, \frac{z^3}{e^z \pm 1} \tag{A.17}$$

The integrals on the right hand side arise very often in statistical mechanics and can be solved with the Γ and ζ functions. The integrals are introduced in, for example, ref. [115]. For bosons, the relevant integral is:

$$\int_0^\infty dx \frac{x^{s-1}}{e^x - 1} = \Gamma(s)\zeta(s) \tag{A.18}$$

For fermions, the result is slightly different:

$$\int_0^\infty dx \frac{x^{s-1}}{e^x + 1} = \Gamma(s) \left(1 - 2^{1-s}\right) \zeta(s) \tag{A.19}$$

With the further definition that

$$\Gamma(n) = (n-1)! \qquad \forall \, n \, \in \mathbb{N} \tag{A.20}$$

and

$$\zeta(2) = \frac{\pi^2}{6} \quad , \qquad \zeta(4) = \frac{\pi^4}{90} \tag{A.21}$$

the particle density of a boson in the relativistic limit can be written as:

$$\boxed{\begin{aligned} n_r &= \frac{g_i}{2\pi^2} T^3 \zeta(3)\Gamma(3) = \frac{\zeta(3)}{\pi^2} g_i T^3 \\ \rho_r &= \frac{g_i}{2\pi^2} T^4 \zeta(4)\Gamma(4) = \frac{\pi^2}{30} g_i T^4 \end{aligned}} \tag{A.22}$$

For fermions, the only difference is a factor $1 - 2^{1-s}$, which results in:

$$\boxed{\begin{aligned} n_r &= \frac{g_i}{2\pi^2} T^3 \left(1 - 2^{1-3}\right) \zeta(3)\Gamma(3) = \frac{3}{4}\frac{\zeta(3)}{\pi^2} g_i T^3 \\ \rho_r &= \frac{g_i}{2\pi^2} T^4 \left(1 - 2^{1-3}\right) \zeta(4)\Gamma(4) = \frac{7}{8}\frac{\pi^2}{30} g_i T^4 \end{aligned}} \tag{A.23}$$

A.4   Equations of State

Also of interest is the pressure of the gas, mainly for the calculations of the Entropy as we will see later. However, instead of deriving it the same way the energy density has been derived, the very important concept of equations of state for Cosmology will be introduced. An equation of state is an equation which relates state variables in equilibrium. The best example of such an equation is the ideal gas equation:

$$pV = NT \tag{A.24}$$

However, what is generally meant by an equation of state in the context of cosmology is an equation which relates energy density to pressure, namely:

$$w = \frac{p}{\rho} \tag{A.25}$$

where w is any real number.

For non-relativistic particles, this factor is relatively easy to compute, because the ideal gas equation A.24 holds in the non-relativistic limit. Rearranging eq. A.24, we obtain:

$$p = T\frac{N}{V} = Tn_{nr} = \frac{T}{m}\rho_{nr} \tag{A.26}$$

Therefore, as we are in the non-relativistic limit $\frac{T}{m} \ll 1$:

$$w = \frac{p}{\rho_{nr}} = \frac{T}{m} \approx 0 \tag{A.27}$$

Thus, for non-relativistic particles:

$$\boxed{w = 0} \tag{A.28}$$

To calculate the same relation for a relativistic gas, it is useful to introduce the grand canonical potential and the grand canonical partition function for bosons and fermions

$$\Phi(V, T, \mu) = -T \ln Z \tag{A.29}$$

with the grand canonical partition function Z for bosons and fermions

$$Z = \begin{cases} \displaystyle\prod_r \frac{1}{1 - e^{-\beta(E_r - \mu)}} & \text{for bosons} \\[4mm] \displaystyle\prod_r \left(1 + e^{-\beta(E_r - \mu)}\right) & \text{for fermions} \end{cases} \tag{A.30}$$

where r runs over all possible energy states of the system. The grand canonical potential is the quantity from which all thermodynamic observables can be derived for a system whose natural variables are volume, temperature and chemical potential. As it is a potential, it has to be an extensive quantity. However, the only extensive quantity it depends on is the volume. Therefore, $\Phi \propto V$. From the differential of the grand canonical potential

$$d\Phi = -SdT - pdV - Nd\mu \tag{A.31}$$

it follows that

$$\Phi = -pV = -T \ln Z \tag{A.32}$$

In order to derive the relativistic equation of state, all that is left now is to calculate the right hand side of A.32. To that end, we will assume again that the eigenstates

of the system are so dense in the phase-space that we can approximate the sum over all eigenstates by an integral. Thus:

$$\frac{pV}{T} = \ln Z = \pm \sum_r \ln \left(1 \pm e^{-\beta(E_r - \mu)}\right) \tag{A.33}$$

$$\approx \pm \frac{g_i \cdot V}{2\pi^2} \int d|\vec{p}| |\vec{p}|^2 \ln \left(1 \pm e^{(-\beta(E_r - \mu))}\right)$$

The V on the right-hand side of the equation comes from the integration over the spatial coordinates and cancels out with the Volume on the left hand side of the equation. We can now partially integrate this term. The derivative with respect to momentum of the logarithm in the integrand is:

$$\pm \frac{\partial}{\partial|\vec{p}|} \left(\ln\left(1 \pm e^{-\beta(E_r - \mu)}\right)\right) = -\frac{\beta e^{-\beta(E_r - \mu)}}{1 \pm e^{-\beta(E_r - \mu)}} \frac{\partial E}{\partial|\vec{p}|}$$

$$= -\frac{1}{T} \frac{1}{e^{\beta(E_r - \mu)} \pm 1} \frac{\partial E}{\partial|\vec{p}|} = -\frac{1}{T} f \frac{\partial E}{\partial|\vec{p}|} \tag{A.34}$$

Thus, by multiplying eq. A.33 with T on both sides after performing the partial integration step, the temperature cancels out. The boundary term vanishes because the phase space distribution approaches 0 as p approaches infinity, so eq. A.33 reduces to:

$$p = \frac{1}{3} \frac{g_i}{2\pi^2} \int d|\vec{p}| \frac{|\vec{p}|^3}{e^{\beta(E - \mu)} \pm 1} \frac{\partial E}{\partial|\vec{p}|}$$

From the energy momentum relation we know that $\frac{\partial E}{\partial|\vec{p}|} = \frac{E}{|\vec{p}|}$, so the final result is:

$$p = \frac{1}{3} \frac{g_i}{2\pi^2} \int d|\vec{p}| \frac{|\vec{p}|^2 E}{e^{\beta(E - \mu)} \pm 1} = \frac{1}{3}\rho \tag{A.35}$$

The equation of state for relativistic particles takes on the form:

$$\boxed{\frac{p}{\rho} = \frac{1}{3}} \tag{A.36}$$

A.5 Entropy

We now have all the tools at hand to introduce yet another very important quantity, the entropy, or rather the entropy density. To that end, we will recall the first law of thermodynamics in its differential form. While generally μ is very significant, we will, as we have done up to now, assume its contribution is negligible and we assume there are no further generalized forces. Thus:

$$dE = TdS - pdV \Rightarrow dS = \frac{p}{T}dV + \frac{1}{T}dE \tag{A.37}$$

From the differential for Φ (eq. A.31), the definition for the entropy in the grand canonical ensemble can be abstracted:

$$S(V, T) = -\frac{\partial \Phi}{\partial T}\bigg|_{V,\mu} \tag{A.38}$$

With equations A.30 and A.32, this can be evaluated to:

$$S(V,T) = -\frac{\partial}{\partial T}\left(-T\ln Z\right)\bigg|_V = \ln Z + T\frac{\partial \ln Z}{\partial T}\bigg|_V = \frac{p(T)V}{T} + T\frac{\partial \ln Z}{\partial T}\bigg|_V \quad (A.39)$$

Let us have a closer look at $\frac{\partial \ln Z}{\partial T}$. Our starting point for $\ln Z$ will be eq. A.33. As the boundaries do not depend on the temperature, the derivative can be applied before integrating:

$$\frac{\partial \ln Z}{\partial T}\bigg|_V = \pm\frac{g_i \cdot V}{2\pi^2}\int d|\vec{p}||\vec{p}|^2 \frac{\partial}{\partial T}\left(\ln\left(1 \pm e^{-\beta E}\right)\right) \quad (A.40)$$

The derivative in the integrand evaluates to:

$$\pm\frac{\partial}{\partial T}\left(\ln\left(1 \pm e^{-\beta E}\right)\right) = \frac{1}{T^2}\frac{E}{e^{\beta E} \pm 1} \quad (A.41)$$

so that

$$\frac{\partial \ln Z}{\partial T}\bigg|_V = \frac{V}{T^2}\frac{g_i}{2\pi^2}\int d|\vec{p}||\vec{p}|^2 \frac{E}{e^{\beta E} \pm 1} = \frac{V}{T^2}\rho(T) \quad (A.42)$$

In the last equation we have simply used the definition of the energy density from eq. A.6. Inserting it all into equation A.39:

$$S(V,T) = \frac{V}{T}\left(\rho(T) + p(T)\right) \quad (A.43)$$

or, defining the entropy density as $\frac{\partial S}{\partial V}\big|_T$:

$$\boxed{s = \frac{1}{T}\left(\rho(T) + p(T)\right) = \frac{(1+w)}{T}\rho(T)} \quad (A.44)$$

While we have used the relativistic phase space distribution, the same relation holds in the non-relativistic limit, remembering that in that case $\beta E \gg 1$, so that the logarithm in equation A.33 can be approximated for $x \ll 1$ as:

$$\ln\left(1 + x\right) \approx x \quad (A.45)$$

Thus, equation A.44 holds for all cases.

It is interesting to see how the entropy density evolves with time, more concretely, we will see that in a co-moving volume Entropy is conserved. Even though the necessary equations for such an analysis will be introduced later on in section B, the derivation is more suitable at this point.

Essentially, we will look at how the entropy evolves with time in a cube of time-dependent side-length $a(t)$. Thus, our volume is just $V = a^3$. The density and pressure change according to eq. B.8, which can be cast into the form:

$$\frac{dp}{dt}a^3 = \frac{dp}{dT}\frac{dT}{dt}a^3 = \frac{d}{dt}\left(a^3(p+\rho)\right) \quad (A.46)$$

We will now try to derive $\frac{dp}{dT}$. We will start with the differential for the entropy written, unusually, in terms of the energy density as:

$$dS = \frac{1}{T}d(\rho V) + \frac{p}{T}dV = \frac{V}{T}\frac{d\rho(T)}{dT}dT + \frac{1}{T}\left(\rho(T) + p(T)\right)dV$$

Thus, the derivatives of entropy with respect to V and T take on the following form:

$$\frac{\partial S}{\partial T}\bigg|_V = \frac{V}{T}\frac{\mathrm{d}\rho(T)}{\mathrm{d}T} \qquad \frac{\partial S}{\partial V}\bigg|_T = \frac{1}{T}\left(\rho(T) + p(T)\right)$$

Assuming that entropy is a smooth function and we can change the order in which we apply the derivatives, we can set

$$\frac{\partial^2 S}{\partial V \partial T} = \frac{\partial^2 S}{\partial T \partial V}$$

This yields:

$$\frac{\partial}{\partial V}\left(\frac{V}{T}\frac{\mathrm{d}\rho(T)}{\mathrm{d}T}\right) = \frac{\partial}{\partial T}\left(\frac{1}{T}\left(\rho(T) + p(T)\right)\right)$$

$$\Leftrightarrow \frac{1}{T}\frac{\mathrm{d}\rho(T)}{\mathrm{d}T} = -\frac{1}{T^2}\left(\rho(T) + p(T)\right) + \frac{1}{T}\frac{\mathrm{d}\rho(T)}{\mathrm{d}T} + \frac{1}{T}\frac{\mathrm{d}p(T)}{\mathrm{d}T} \tag{A.47}$$

Thus:

$$\frac{\mathrm{d}p(T)}{\mathrm{d}T} = \frac{1}{T}\left(\rho(T) + p(T)\right) \tag{A.48}$$

This can be inserted into equation A.46:

$$\frac{a^3}{T}\left(\rho(T) + p(T)\right)\frac{\mathrm{d}T}{\mathrm{d}t} = \frac{\mathrm{d}}{\mathrm{d}t}\left(a^3(p + \rho)\right)$$

$$\Leftrightarrow \frac{a^3}{T^2}\left(\rho(T) + p(T)\right)\frac{\mathrm{d}T}{\mathrm{d}t} = \frac{1}{T}\frac{\mathrm{d}}{\mathrm{d}t}\left(a^3(p + \rho)\right)$$

$$\Leftrightarrow -\frac{\mathrm{d}}{\mathrm{d}t}\left(\frac{1}{T}\right)\cdot\left(\rho(T) + p(T)\right) = \frac{1}{T}\frac{\mathrm{d}}{\mathrm{d}t}\left(a^3(p + \rho)\right)$$

which can be rewritten as:

$$\boxed{\frac{\mathrm{d}}{\mathrm{d}t}\left(\frac{a^3}{T}\left(\rho(T) + p(T)\right)\right) = 0} \tag{A.49}$$

Remembering that $V = a^3$ and comparing this to eq. A.53 we see that the entropy inside a co-moving volume is conserved.

A.6 Effective Degrees of Freedom

Up until now, all the results are valid for an ideal gas made up of a single particle species. However, the Universe is comprised of many different particle species, so, using the results derived up to this point, we will proceed to find a description of the total energy and entropy density in the Universe.

While, generally, mixing two gases of different particle species gives rise to very interesting effects and such a system is not easy to describe, in our model of the Universe, the procedure is very straightforward. The only ingredients for such a

recipe are the formulas derived for the densities of a specific particle and a precise knowledge of the particle species in equilibrium at any given point, the moment a particle species decouples from equilibrium and its temperature after this moment.

Knowing this, the total energy density, for example, is just the sum of the energy densities of all species i, or:

$$\rho_{tot} = \sum_i \rho_i = \sum_i \frac{g_i}{2\pi^2} T_i^4 \int_{x_i}^\infty dz_i \ \frac{z_i^2 \sqrt{z_i^2 - x_i^2}}{e^{z_i} \pm 1} \tag{A.50}$$

Here, we have already accounted for the different temperatures the particles might have. For particles in thermal equilibrium, these are all the same, as they interact. After a species decouples, it does not interact with the particles still in equilibrium on average, so its temperature might differ from that of photons. This is what happens, for example, with neutrinos and photons. The internal temperature of neutrinos is lower than that of photons by a factor $\left(\frac{4}{11}\right)^{1/3}$

For massless particles we have already seen that the integral in A.50 can be solved analytically, so that the total energy density is just $\propto T_i^4$. In fact, in the ultra-relativistic limit, each particle's contribution to the total energy density is just dependent on its internal degrees of freedom, this being the most a particle can contribute.

For massless particles, as the solution of the integral is not dependent on temperature, the relative contribution of one degree of freedom does not change. However, for massive particles, the contribution to the total energy density decreases with temperature, and, as they slow down and stop being relativistic, even gets exponentially suppressed by the Boltzmann factor. The effective contribution of one degree of freedom of a massive particle as a function of temperature is shown on figure A.2.
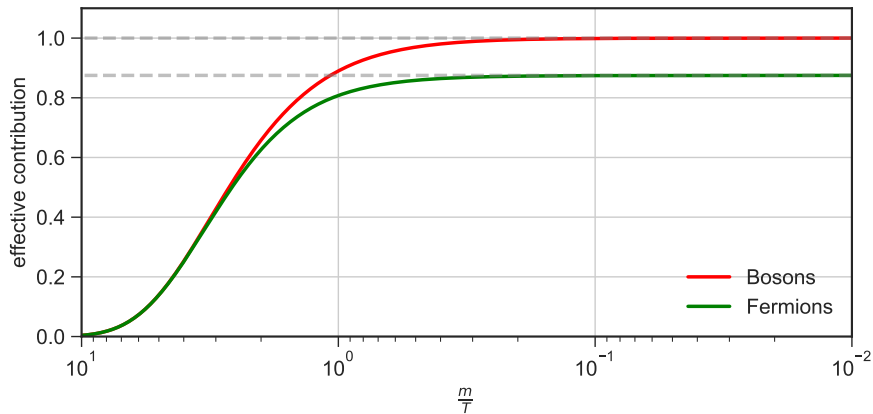
Figure A.2: Effective contribution of a degree of freedom of a massive particle as a function of the ratio of mass to temperature $x = m/T$, both for bosons and fermions. The gray lines show the constant value for a massless particle.

This leads to the idea that one may parametrize the energy density in a form similar to eq. A.22, but with the internal degrees of freedom g_i containing the information of how much each degree of freedom contributes at a given temperature relative to its maximal contribution, that is parametrizing the temperature depen-

dence which differs from the simple Stefan Boltzmann law $\propto T^4$ by introducing the effective degrees of freedom of the universe.

Taking the temperature of a photon as a reference, $T_\gamma := T$, as it stays in equilibrium the longest and always contributes fully to the energy density, we can write:

$$\rho_{tot} = \frac{\pi^2}{30} g_{eff}(T) \cdot T^4 \tag{A.51}$$

where g_{eff} is defined as:

$$g_{eff} = \sum_i \rho_i = \sum_i \frac{\pi^4}{15} g_i \left(\frac{T_i}{T}\right)^4 \int_{x_i}^\infty dz_i \frac{z_i^2 \sqrt{z_i^2 - x_i^2}}{e^{z_i} \pm 1} \tag{A.52}$$

Essentially the only thing we have done compared to A.50 is to factor out the energy density of a photon with one degree of freedom, but the idea behind this small manipulation is the important part. As non-relativistic particles barely contribute to the total energy density, the exact temperature dependence of the total energy density does not differ greatly from $\propto T^4$, except for some moments where it changes very fast due to a particle becoming non-relativistic as the Universe cools down. The idea is to simplify the temperature dependence of the energy density from eq. A.6 by introducing the effective degrees of freedom, which essentially contain all of the information on the particle content and evolution of the Universe. The evolution of this parameter as a function of temperature is shown on figure A.3a.
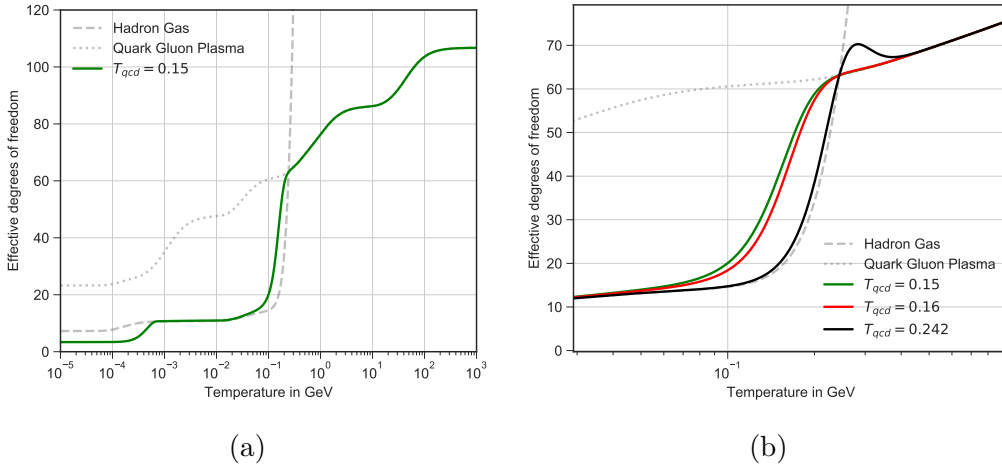
Figure A.3: Effective degrees of freedom for the energy density. Figure A.3a shows the calculation according to eq. A.56 and a value for the QCD phase transition $T_{QCD} = 150\,\text{MeV}$. Figure A.3b shows a close-up on the region of the phase transition for different values for T_{QCD} and the effective degrees of freedom for the quark gluon plasma and the hadron gas respectively

A similar treatment can be applied to the entropy density, so that:

$$s = \sum_i \frac{1}{T_i} \left(\rho_i(T) + p_i(T)\right) = \sum_i \frac{(1 + w_i)}{T_i} \rho_i(T) \tag{A.53}$$

In equation A.50 we have assumed the relativistic phase-space distribution for all particles. Thus, $w_i = \frac{1}{3}$. While for non-relativistic particles this is not the correct

equation of state, they contribute so little that this effect is negligible. Thus, the total entropy density can be written in a similar form to the energy density:

$$\boxed{s_{tot} = \frac{2\pi^2}{45} g_{eff}^s T^3} \tag{A.54}$$

with the effective entropy degrees of freedom defined as:

$$g_{eff}^s = \sum_i \rho_i = \sum_i \frac{\pi^4}{15} g_i \left(\frac{T_i}{T}\right)^3 \int_{x_i}^{\infty} dz_i \frac{z_i^2 \sqrt{z_i^2 - x_i^2}}{e^{z_i} \pm 1} \tag{A.55}$$

The only difference with respect to A.52 is that $\frac{T_i}{T}$ goes with the power of three instead of four. Therefore, while the particle's temperature does not differ from the photon temperature, the energy and entropy degrees of freedom are approximately the same. They only differ noticeably after neutrino decoupling, as the effective temperature of the neutrinos is smaller than that of photons by a factor $(4/11)^{\frac{1}{3}}$. Therefore, unless explicitly stated otherwise, it has been assumed that these are equal.

The only thing left is to clarify the particle content of the Universe at any given moment contributing to the effective degrees of freedom. We will start at high temperatures and assume only the particle content of the Standard Model. Some sort of Dark Matter particle will definitely play a role for high temperatures as well, but under the assumption that the particle is non-relativistic before freeze-out, its contribution can be neglected. We will refrain from making any assumptions to the contribution long before freeze-out, as it would be a wild guess at best.

Therefore, for high temperatures, we have 28 degrees of freedom from bosons and 90 from fermions. From A.23 we know that fermions contribute less to the energy density by a factor of 7/8. This puts the total number up to $28 + 7/8 \cdot 90 = 106.75$. With this we can calculate, according to eq. A.52, the effective degrees of freedom as a function of temperature.

However, there is one event in the evolution of the Universe which very significantly changes the number of degrees of freedom: the phase transition from a quark-gluon-plasma to a hadron gas at around $T \approx 160\,\text{MeV}$. After the transition, quarks and gluons are confined into hadrons and we can no longer assume they are free, separate particles. Essentially what this means is that the particles in equilibrium, which interact with leptons and photons, which contribute to the effective degrees of freedom, are no longer quarks and gluons, but rather all possible hadrons. Most of them are very heavy compared to the temperature and contribute only very little to them, an exception in this case are pions. However, due to the almost exponentially increasing number of hadrons and excited hadron states, even though they are non-relativistic, the effective degrees of freedom are extremely high and increase very rapidly. This strong increase in the degrees of freedom can be observed on figure A.3a, where the effective degrees of freedom of the hadron gas phase are shwon in gray dashed lines. For a list of all the hadrons taken into account to calculate g_{eff} see [116].

One further information that is extremely important is the order of the phase transition. It is a cross-over transition, meaning that the entropy and energy densities have to be, at least, steady and differentiable. To that end, we have smoothed

out the effective degrees of freedom during the phase transition with a $\tanh x$ function, taking advantage of the fact that it very rapidly changes from -1 to 1. Thus, figure A.3a in fact shows:

$$g_{eff}(T) = g_{eff}^{hg}(T) + \frac{1 + \tanh\left((a \cdot (T - T_{QCD}))\right)}{2}\left(g_{eff}^{qgp}(T) - g_{eff}^{hg}(T)\right) \qquad \text{(A.56)}$$

where the superscripts hg and qgp indicate that these are effective degrees of freedom in the hadron gas and quark-gluon-plasma phase respectively. The factor a controls how fast the transition occurs. The value chosen for T_{QCD} has a significant effect during the phase transition, so it is important especially for the low mass regime for our calculations later on. Figure A.3b shows g_{eff} for different temperatures of the phase transition. The value used for all numerical calculations is $150\,\text{MeV}$.

Appendix B

Standard Cosmology

In recent years, the amount of experimental techniques available to astrophysicists has increased greatly, allowing for the first time to really put cosmological models to the test with precise measurements at all scale, from the galactic to the cosmological scale.

While these have disproved many theories and might actually have raised more questions than they have answered, some very important and general assumptions have, up to now, stood the test of time and are becoming the solid foundation upon which future improvements and ideas in Cosmology will most likely have to be based on, a Standard Model in Cosmology in a way.

The exact definition of a Standard Model of Cosmology is hard to give, mainly because it changes very rapidly with time due to recent experiments and there is not an overall consensus in most details as there might be on the Standard Model of Particle Physics.

However, cosmologists agree on a set of guidelines a cosmological model should follow given the huge amount of experimental data pointing towards this conclusion. These guidelines will be our focus now.

The first and most important idea is that of an isotropic and homogeneous Universe. This is originally based upon the Copernican Principle, which states that Humanity and Earth do not occupy a privileged point in space. Actually the opposite, we are nothing more than a small grain of sand in a vastly immense desert we call Universe and there is nothing special about our grain of sand for the underlying laws of physics. Therefore, these should behave the same at any point in space and in every direction we look. Any other assumption would dispute the Copernican Principle.

While philosophycally speaking this is a logical argument, physics needs experimental proof of such assumptions. The biggest proof is the Cosmic Microwave Background Radiation (CMB), which shows a completely homogeneous and isotropic distribution except for some minimal density fluctuations which arise from quantum fluctuations before inflation.

The CMB is actually one of the most important sources of information, because it offers the possibility of measuring some crucial cosmological parameters to remarkably great accuracy, like the overall energy density of the Universe, as well as the abundance of the different components that make up the Universe.

Surprisingly, most of the energy density does not come from the matter we know and which surround us. In fact, according to measurements by the WMAP collaboration ([117]), only 4.5% of the energy density is made of baryonic matter. The most important contribution, about 72.9%, stems from some unknown form of energy known as Dark energy. And, last but not least, about 22.6% is made up of Dark Matter, which will be the main focus of this thesis.

The final assumption is that Einstein's General Relativity (GR) describes the interactions of particles at a large scale, while the Standard Model (SM) or rather a Quantum Field Theory describing the particle content of the Universe (this includes possible extensions to the SM) describes the interactions at the smallest scale. It should be noted that of course a more general approach which includes and extends both of these theories is also needed, especially for an accurate description of the very early Universe, but there is no evidence as to which of the possible theories is true.

Therefore, to our best knowledge, the equations governing the evolution of the Universe are Einstein's field equations([118]):

$$R_{\mu\nu} - \frac{1}{2}g_{\mu\nu}R = -8\pi G_N T_{\mu\nu} \tag{B.1}$$

where $R_{\mu\nu}$ is the Ricci tensor, the Riemannian curvature tensor contracted with the metric $g_{\mu\nu}$, R is the Ricci scalar, $T_{\mu\nu}$ is the energy momentum tensor and G_N is Newton's gravitational constant. Thus, the content of this set of differential equations is clear: the geometry of the Universe, described by the curvature tensor, is essentially defined by its energy content. This information is contained in the energy momentum tensor.

We will make use of the first assumption made about the Universe being homogeneous and isotropic in order to considerably simplify the calculation of these equations. With this assumption, the metric describing the Universe can be assumed to be the Friedmann-Lemaître-Robertson-Walker(FLRW)-metric. A line element in the FLRW metric in spherical coordinates has the form [118]:

$$ds^2 = dt^2 - a(t)^2 \left(\frac{dr^2}{1 - kr^2} + r^2 d\theta + r^2 \sin^2\theta d\phi^2 \right) \tag{B.2}$$

$a(t)$ is the scale factor of the Universe and k is an integer valued variable which indicates the curvature of the Universe. The possible values for k are:

$$k = \begin{cases} 1 & \text{closed} \\ 0 & \text{flat} \\ -1 & \text{open} \end{cases} \tag{B.3}$$

The line element from 3.1 doesn't have any mixed elements, therefore the metric tensor defined as

$$ds^2 = g_{\mu\nu}dx^\mu dx^\nu$$

has to be diagonal. In fact its exact form can be extracted from eq. 3.1:

$$g_{\mu\nu} = \begin{pmatrix} 1 & 0 & 0 & 0 \\ 0 & \frac{-a(t)^2}{1-kr^2} & 0 & 0 \\ 0 & 0 & -a(t)^2 r^2 & 0 \\ 0 & 0 & 0 & -a(t)^2 r^2 \sin^2\theta \end{pmatrix} \tag{B.4}$$

The energy momentum tensor also simplifies greatly as it takes on the following diagonal form [119]:

$$T_{\mu\nu} = \begin{pmatrix} \rho & 0 & 0 & 0 \\ 0 & -p & 0 & 0 \\ 0 & 0 & -p & 0 \\ 0 & 0 & 0 & -p \end{pmatrix} = \begin{pmatrix} \rho & 0 & 0 & 0 \\ 0 & -w\rho & 0 & 0 \\ 0 & 0 & -w\rho & 0 \\ 0 & 0 & 0 & -w\rho \end{pmatrix} \tag{B.5}$$

where ρ stand for the energy density and p for the pressure.

With this information, following ref. [118], the equations describing the evolution of the scale parameter can be obtained:

$$\left(\frac{\dot{a}(t)}{a(t)}\right)^2 + \frac{k}{a(t)^2} = \frac{8\pi G_N}{3}\rho \tag{B.6}$$

$$\frac{2\ddot{a}(t)}{a(t)} + \left(\frac{\dot{a}(t)}{a(t)}\right)^2 + \frac{k}{a(t)^2} = -8\pi G_N p \tag{B.7}$$

Furthermore, using the conservation of the energy momentum tensor, following [118], a third very important equation can be derived:

$$a^3 \frac{\mathrm{d}p}{\mathrm{d}t} = \frac{\mathrm{d}}{\mathrm{d}t}\left(a^3\left(\rho + p\right)\right) \tag{B.8}$$

Out of these three equations only two are linearly independent. Usually, B.6 and B.8 are used, as it is easier to work with them. However, B.7 is also important, for example in order to derive the time dependence of the scale parameter.

Equation B.6, the Friedmann equation, is probably the most known out of the three. It is useful to introduce the Hubble parameter defined as:

$$H(t) = \frac{\dot{a}(t)}{a(t)} \tag{B.9}$$

Its value today is extremely important as we shall see later on, but it is also a great puzzle. It can be abstracted from measurements of the CMB. The WMAP collaboration ([117]) found the value:

$$H_0 = (70.2 \pm 1.4)\,\mathrm{km/(s\,Mpc)} \tag{B.10}$$

However, the Hubble parameter can be measured by a myriad other ways. The problem is that the results from different measurements do not seem to agree on an exact value, which is becoming ever more problematic with the uncertainties becoming smaller and smaller. They all agree on the order of magnitude of the

parameter. Thus, in order to avoid uncertainties from the this value, it is useful to parametrize the Hubble parameter as:

$$H_0 = h \cdot 100 \, \text{km}/(\text{s Mpc}) \tag{B.11}$$

where the reduced Hubble parameter ranges from $h \approx 0.6 - 0.8$.

With the Hubble parameter defined, the Friedmann equation can be cast into the more familiar form:

$$\boxed{H(t)^2 + \frac{k}{a(t)^2} = \frac{8\pi G_N}{3} \rho} \tag{B.12}$$

Equation B.12 describes the dynamics of the Universe. With it, the geometric form of the Universe can be calculated, whether it is flat, positively curved, like a sphere, or negatively curved. It predicted the expansion of the Universe before the measurements by Hubble could confirm it. The answer to the age old question of the age of the Universe, or rather the time it has been expanding for, can also be calculated with the Friedmann equation. Needless to say, it is extremely significant. From B.3 we know that for a flat Universe $k = 0$. In that case, the Friedmann equation yields:

$$(H(t))^2 = \frac{8\pi G_N}{3} \rho \tag{B.13}$$

This allows us to introduce the critical density ρ_c:

$$\rho_c = \frac{3 \left(H(t) \right)^2}{8\pi G_N} \tag{B.14}$$

It is useful to normalize the Friedmann equation with the critical density. The density parameter is defined as:

$$\Omega = \sum_i \Omega_i = \sum_i \frac{\rho_i}{\rho_c} \tag{B.15}$$

where the summation over i runs over all the components contributing to the energy density. Generally, these are grouped by the different equations of state into a matter, radiation and vacuum component, as these evolve with time and temperature differently, as we shall see later on. Also, even though this is not really a particle component, Ω_k can also be introduced to describe the term dependant on the value of k:

$$\Omega_k = -\frac{k}{H^2 R^2} \tag{B.16}$$

With B.15 we can therefore rewrite the Friedmann equation B.12 as:

$$-\Omega_k = \frac{k}{H^2 a^2} = \Omega - 1 \tag{B.17}$$

From B.17, it is clear to see:

- if $\Omega > 1$, that is, if the total density is greater than the critical density, then $k > 1$ and the Universe is closed.

- if $\Omega < 1$, that is, if the total density is smaller than the critical density, then $k < 1$ and the Universe is open.

It is important to note that the different components in B.15 evolve with time differently. In order to derive said time-dependence, we will start at eq. B.8. We will perform this analysis for a generic particle with the equation of state $\rho = wp$, so that it is valid for all three components.

Applying the time derivative on the right-hand side of B.8 yields:

$$\dot{p}a^3 = \dot{p}a^3 + \dot{\rho}a^3 + 3H(\rho + p)a^3 \tag{B.18}$$

The derivative of the pressure with respect to time cancels out. Using the equation of state, eq. B.18 can be cast into the form:

$$\dot{\rho} + 3H(\rho + P) = \dot{\rho} + 3H(1 + w) \cdot \rho = 0$$

$$\Leftrightarrow \frac{\dot{\rho}}{\rho} = -3H(1 + w)$$

This is a differential equation which can be solved upon integration. We will integrate from a time t up to present time t_0:

$$\int_t^{t_0} dt' \frac{\dot{\rho}}{\rho} = \int_{\rho(t)}^{\rho_0} d\rho' \frac{1}{\rho'} = \int_t^{t_0} dt' - 3H(t')(1 + w)$$

$$\Rightarrow \ln \frac{\rho_0}{\rho(t)} = -3(1 + w) \ln \frac{a(t_0)}{a(t)}$$

or equivalently:

$$\rho(t) = \rho_0 \cdot \left(\frac{a(t_0)}{a(t)} \right)^{3(1+w)} \tag{B.19}$$

Given that the Universe expands as described by the Friedmann equation, the wavelength of light travelling through space will become redshifted, because the wavelength increases as space itself is being created. The relative deviation from its emission wavelength can be parametrized by the redshift parameter z defined by the relation:

$$1 + z = \frac{a(t_0)}{a(t)} \tag{B.20}$$

With this parameter, equation B.19 reads:

$$\boxed{\rho(z) = \rho_0 \cdot (1 + z)^{3(1+w)}} \tag{B.21}$$

This leads to the following dependencies:

- for radiation $w = \frac{1}{3}$ (A.36), so that $\rho \propto (1 + z)^4 \propto a^{-4}$

- from A.28 we know $w = 0$ for matter (non-relativistic particles). Thus $\rho \propto (1 + z)^3 \propto a^{-3}$

- While the equation of state for vacuum energy has not been derived, we define vacuum energy as an inherent property of space, so that it can not change with time. Thus, equation B.21 tells us that $w = -1$

- For Ω_k this analysis was not necessary, as we can see directly from B.12 that $\Omega_k \propto (1 + z)^2 \propto a^{-2}$

With this information and normalizing the Friedmann equation with the value of the critical density today, it is possible to write the Friedmann equation in terms of the redshift parameter z as:

$$\frac{H^2(z)}{H_0^2} = \Omega_{vac} + \Omega_k(1+z)^2 + \Omega_m(1+z)^3 + \Omega_r(1+z)^4 \tag{B.22}$$

Equation B.12, inserting the energy density in terms of the temperature directly gives us an expression for $H(T)$. Equation B.22 fulfills the same need, but in terms of the redshift parameter z. However, one crucial dependency is still missing, namely $H(t)$. To that end, we will subtract eq. B.6 from B.7. to obtain:

$$\frac{\ddot{a}}{a} = -\frac{4\pi G_N}{3}\left(\rho + 3p\right) = -\frac{4\pi G_N}{3}\rho\left(1 + 3w\right) \tag{B.23}$$

The case where $w = -1$ is slightly different, as ρ is constant, which results in an exponentially increasing scale factor. This is the case for the inflation phase of the early Universe. We are however more interested in the processes after inflation, so we will take $w \neq -1$, so that $1 + w \neq 0$.

To solve this equation, the first ansatz that comes to mind is a power law ansatz $R = c_1 t^\alpha$, where c_1 is just a constant dependent on the initial conditions of the problem. However, as we are interested in the Hubble parameter, this constant cancels out and it is not necessary to further specify it. Inserting this ansatz into eq. B.23 and using B.19 to write the energy density as $\rho = c_2 \cdot R^{-3(1+w)}$ yields:

$$\frac{1}{c_1 t^\alpha}\frac{\mathrm{d}^2 c_1 t^\alpha}{\mathrm{d}t^2} = -\frac{4\pi G_N}{3}\left(1 + 3w\right)c_2 \cdot R^{-3(1+w)}$$

$$\Leftrightarrow \frac{\alpha(\alpha-1)c_1 t^{\alpha-2}}{c_1 t^\alpha} = -\frac{4\pi G_N}{3}\left(1 + 3w\right)c_2 R^{-3(1+w)}$$

Solving this equation for R results in:

$$a(t) = -\frac{4\pi G_N(1+3w)}{3\alpha(\alpha-1)}t^{\frac{2}{3(1+w)}} \tag{B.24}$$

Therefore, the time dependence of the scale parameter is:

$$\boxed{a(t) \propto t^{\frac{2}{3(1+w)}}} \tag{B.25}$$

Using the equations of state for matter (A.28) and radiation (A.36), the scale parameter goes as:

$$a(t) \propto \begin{cases} t^{\frac{1}{2}} & \text{for radiation} \\ t^{\frac{2}{3}} & \text{for matter} \end{cases} \tag{B.26}$$

so that the Hubble parameter as a function of time may be written as:

$$H(t) = \begin{cases} \frac{1}{2t} & \text{for radiation} \\ \frac{2}{3t} & \text{for matter} \end{cases} \tag{B.27}$$

This equation, along with B.12 allows us to find a relation between the temperature of the Universe and the time since its creation. As the Universe is radiation dominated for the most part of the development in the early Universe, it is a good approximation to assume that this, in fact, is the only contribution to the total energy density. The curvature parameter is also assumed to be negligible. The Friedmann equation simplifies to:

$$H^2 = \frac{8\pi G_N}{3}\rho_r = \frac{8\pi^3 G_N}{90}g_{eff}(T) \cdot T^4 \tag{B.28}$$

Thus, in a radiation dominated universe, the Hubble parameter takes on the simple form:

$$\boxed{H(T) = \sqrt{\frac{8\pi^3}{90}} \cdot \sqrt{G_N \cdot g_{eff}}T^2 = 1.66\sqrt{g_{eff}}\frac{T^2}{m_{Pl}}} \tag{B.29}$$

where we have introduced the Planck mass:

$$m_{Pl} = \frac{1}{\sqrt{G_N}} = 1.221 \cdot 10^{19}\,\text{GeV} \tag{B.30}$$

Setting B.29 equal to $H(t) = \frac{1}{2t}$ and solving for time, we obtain the relation between time and temperature:

$$t = \frac{1}{2 \cdot 1.66}\frac{m_{Pl}}{g_{eff}T^2} = 0.3\frac{m_{Pl}}{\sqrt{g_{eff}}T^2} \tag{B.31}$$

This is a very important relation, as we will generally use temperature to express the evolution of the Early Universe, as most changes happen in the first seconds of the Universe, which is small compared to the 13.7 billion years of its history. However, the orders of magnitude the Universe changes in temperature in those few seconds and the consequences this has make it a more suitable to describe the evolution of the Early Universe.

Appendix C

Boltzmann Equation

The Boltzmann equation describes the time evolution of the phase-space distribution and, thus, of all observables that can be derived from it $(n, \rho, ...)$. In its most general form, the Boltzmann equation can be written as follows:

$$\widehat{\mathbf{L}}f(x,p) = \widehat{\mathbf{C}}f(x,p) \tag{C.1}$$

f is the phase-space distribution. The operator on the left-hand side is the Liouville operator, which describes the time-dependence of f. The operator on the right-hand side is the Collision operator. Essentially, what this equation is telling us, is that the change in time of the phase-space distribution of a particle is given by its collisions and interactions with other particles.

C.1 The Liouville Operator

Let us first have a look at the left-hand side of the equation. The relativistic form of the Liouville operator for a particle of mass m is nothing more than the total derivative of f with respect to proper time τ multiplied by said mass. As for the rest of the thesis, we will use Einstein's summation convention of summing over repeated indices, where one is covariant and the other contravariant. Using the chain rule we can now write this as:

$$\widehat{\mathbf{L}}f(x,p) = m\frac{\mathrm{d}f(x,p)}{\mathrm{d}\tau} = m\frac{\partial f(x,p)}{\partial x^\mu}\frac{\mathrm{d}x^\mu}{\mathrm{d}\tau} + m\frac{\partial f(x,p)}{\partial v^\mu}\frac{\mathrm{d}v^\mu}{\mathrm{d}\tau}$$

With four-velocity and four-momentum defined as:

$$p^\mu = mv^\mu \tag{C.2}$$

$$v^\mu = \frac{\mathrm{d}x^\mu}{\mathrm{d}\tau} \tag{C.3}$$

we get the following equation:

$$m\frac{\mathrm{d}f(x,p)}{\mathrm{d}\tau} = m\frac{\partial f(x,p)}{\partial x^\mu}v^\mu + m^2\frac{\partial f(x,p)}{\partial p^\mu}\frac{\mathrm{d}^2x^\mu}{\mathrm{d}\tau^2}$$

which is equivalent to:

$$m\frac{\mathrm{d}f(x,p)}{\mathrm{d}\tau} = \frac{\partial f(x,p)}{\partial x^\mu}p^\mu - \frac{\partial f(x,p)}{\partial p^\mu}\Gamma^\mu{}_{\sigma\nu}p^\sigma p^\nu \tag{C.4}$$

In this last step we have used Einstein's geodesic equation ([118])

$$\frac{\mathrm{d}^2 x^\mu}{\mathrm{d}\tau^2} + \Gamma^\mu{}_{\sigma\nu} \frac{\mathrm{d}x^\sigma}{\mathrm{d}\tau} \frac{\mathrm{d}x^\nu}{\mathrm{d}\tau} = 0 \tag{C.5}$$

where the Christoffel Symbols $\Gamma^\mu{}_{\sigma\nu}$ are defined with the space-time metric tensor $g^{\mu\nu}$ as:

$$\Gamma^\mu{}_{\sigma\nu} = \frac{g^{\rho\mu}}{2} \left(\frac{\partial g_{\nu\rho}}{\partial x^\sigma} + \frac{\partial g_{\sigma\rho}}{\partial x^\nu} - \frac{\partial g_{\nu\sigma}}{\partial x^\rho} \right) \tag{C.6}$$

The geodesic equation can be interpreted as a kind of force equation analogous to Newton's second law. It describes the motion of a particle freely moving in a gravitational field. The most important part about this equation is that it relates the motion of the particle to a purely geometrical quantity, the Christoffel Symbols. This means that the motion of a particle is just influenced by how the masses surrounding it have curved space-time.

Thus, before we go any further, we have to make some assumptions as to how the Universe looks at a very large scale. These are also core assumptions of the Standard Model of Cosmology, namely isotropy and homogeneity. For our calculation this means two things:

- The phase-space density has to be invariant under translations and rotations in space. Therefore $f(x, p) = f(|\vec{p}|, t)$ or equivalently $f = f(E, t)$ and all derivatives apart from the ones with respect to x^0 and p^0 are zero. This leaves us with:
$$m \frac{\mathrm{d}f(E, t)}{\mathrm{d}\tau} = \frac{\partial f(E, t)}{\partial x^0} p^0 - \frac{\partial f(E, t)}{\partial p^0} \Gamma^0{}_{\sigma\nu} p^\sigma p^\nu \tag{C.7}$$

- We can assume that the FLRW metric from eq. 3.1 describes the Universe.

We can now calculate the Christoffel Symbols according to equation C.6. As we only need $\Gamma^0{}_{\sigma\nu}$, the formula simplifies to:

$$\Gamma^0{}_{\sigma\nu} = \frac{g^{\rho 0}}{2} \left(\frac{\partial g_{\nu\rho}}{\partial x^\sigma} + \frac{\partial g_{\sigma\rho}}{\partial x^\nu} - \frac{\partial g_{\nu\sigma}}{\partial x^\rho} \right) \tag{C.8}$$

The metric tensor is diagonal, so only the elements where $\rho = 0$ are unequal to zero.

$$\Rightarrow \Gamma^0{}_{\sigma\nu} = \frac{g^{00}}{2} \left(\frac{\partial g_{\nu 0}}{\partial x^\sigma} + \frac{\partial g_{\sigma 0}}{\partial x^\nu} - \frac{\partial g_{\nu\sigma}}{\partial x^0} \right) \tag{C.9}$$

The same argument holds now for ν and σ. Furthermore, as $g_{00} = 1$, all derivatives of that element of the metric tensor vanish and we are left with:

$$\Gamma^0{}_{\sigma\nu} = -\frac{1}{2} \left(\frac{\partial g_{\nu\sigma}}{\partial x^0} \right) \tag{C.10}$$

The only term in the metric tensor with an explicit time-dependence is the scale factor $a(t)$. From eq. 3.1 we can see that the elements dependent on $a(t)$ are

$g_{ii} \propto a(t)^2$, for $i = 1, 2, 3$. Thus, all non-zero derivatives of the metric tensor with respect to $x^0 = t$ are of the form:

$$\frac{\partial g_{ii}}{\partial t} = \frac{\partial}{\partial t}$$

$$\Leftrightarrow \frac{\partial g_{ii}}{\partial t} = \text{const.} \cdot 2a(t)\dot{a}(t)$$

$$\Leftrightarrow \frac{\partial g_{ii}}{\partial t} = 2\frac{\dot{a}(t)}{a(t)} \cdot g_{ii}$$

Inserting this into eq. C.10 yields:

$$\Gamma^0{}_{\mu\nu} = \begin{cases} 0 & \text{if } \mu, \nu = 0 \\ -\frac{\dot{a}(t)}{a(t)} g_{\mu\nu} & \text{otherwise} \end{cases} \tag{C.11}$$

We can now insert this into equation C.7 to get:

$$m\frac{\mathrm{d}f(E,t)}{\mathrm{d}\tau} = E\frac{\partial f(E,t)}{\partial t} + \frac{\partial f(E,t)}{\partial E}\frac{\dot{a}(t)}{a(t)} \cdot \left(g_{11}p^1p^1 + g_{22}p^2p^2 + g_{33}p^3p^3\right) \tag{C.12}$$

The metric tensor is diagonal and, just as with the Minkowski metric in special relativity, the general metric tensor for the absolute value of a three dimensional vector in curved space is encoded in the spatial components g_{ii} of the metric tensor, albeit a different sign. Thus:

$$g_{ii}p^ip^i = -|\vec{p}|^2 \tag{C.13}$$

so that eq. C.12 is equivalent to:

$$\widehat{\mathbf{L}}f(E,t) = E\frac{\partial f(E,t)}{\partial t} - \frac{\dot{a}(t)}{a(t)}|\vec{p}|^2\frac{\partial f(E,t)}{\partial E} \tag{C.14}$$

Coming back to the task at hand, which is to derive from the Boltzmann equation the time evolution of the particle density, we will now take the collision term back into account. We will divide by E on both sides and then integrate the whole equation over the momentum of a particle with mass m, energy E, momentum $\vec{p}$ and degrees of freedom g:

$$\frac{g}{(2\pi)^3}\int d^3\vec{p}\left(\frac{\partial f(E,t)}{\partial t} - \frac{\dot{a}(t)}{a(t)}\frac{|\vec{p}|^2}{E}\frac{\partial f(E,t)}{\partial E}\right) = \frac{g}{(2\pi)^3}\int\frac{d^3\vec{p}}{E}\widehat{\mathbf{C}}f(E,t) \tag{C.15}$$

As the bounds of the integral do not depend on t, we can apply the time derivative on the integral after having integrated over the phase space distribution. This allows us, with the definition of the particle number density from eq. A.3, to write:

$$\frac{g}{(2\pi)^3}\int d^3\vec{p}\,\frac{\partial f(E,t)}{\partial t} = \frac{\partial}{\partial t}\frac{g}{(2\pi)^3}\int d^3\vec{p}f(E,t) = \frac{\partial n}{\partial t} \tag{C.16}$$

For the second term on the left-hand side of eq. C.15 we can employ the relativistic energy momentum relation to express the absolute value of momentum in terms of energy $|\vec{p}| = \sqrt{E^2 - m^2}$. This allow us to write:

$$\frac{1}{E}\frac{\partial f}{\partial E} = \frac{1}{E}\frac{\partial f}{\partial|\vec{p}|}\frac{\partial|\vec{p}|}{\partial E} = \frac{1}{E}\frac{\partial f}{\partial|\vec{p}|}\frac{E}{\sqrt{E^2 - m^2}} = \frac{1}{|\vec{p}|}\frac{\partial f}{\partial|\vec{p}|}$$

$$\Leftrightarrow \frac{1}{E}\frac{\partial f}{\partial E} = \frac{1}{|\vec{p}|}\frac{\partial f}{\partial|\vec{p}|} \tag{C.17}$$

Inserting this into equation C.15 yields:

$$-\frac{g}{(2\pi)^3}\int d^3\vec{p}\,\frac{\dot{a}(t)}{a(t)}\frac{|\vec{p}|^2}{E}\frac{\partial f(E,t)}{\partial E} = -\frac{g}{(2\pi)^3}\int d^3\vec{p}\,\frac{\dot{a}(t)}{a(t)}|\vec{p}|\frac{\partial f(E,t)}{\partial|\vec{p}|}$$

This can be rewritten using spherical coordinates:

$$-\frac{\dot{a}(t)}{a(t)}\frac{g}{(2\pi)^3}\int d\Omega \int d|\vec{p}|\,|\vec{p}|^3\frac{\partial f(E,t)}{\partial|\vec{p}|} \tag{C.18}$$

The integral over the absolute value of momentum can be partially integrated. The boundary conditions disappear, because f approaches 0 as $|\vec{p}|$ tends to infinity and $|\vec{p}|$ is 0 at the origin, whereas the phase-space distribution has a constant value. Thus, eq. C.18 is equivalent to:

$$3\frac{\dot{a}(t)}{a(t)}\frac{g}{(2\pi)^3}\int d\Omega \int d|\vec{p}|\,|\vec{p}|^2 f(E,t) = 3\frac{\dot{a}(t)}{a(t)}\frac{g}{(2\pi)^3}\int d\vec{p}\,|\vec{p}|^2 f(E,t)$$
$$= 3\frac{\dot{a}(t)}{a(t)}n \tag{C.19}$$

We can insert equations C.16 and C.19 back into C.15. If we also use the Hubble Parameter from eq. B.9, eq. C.15 now has the following form:

$$\boxed{\dot{n} + 3Hn = \frac{g}{(2\pi)^3}\int \frac{d^3\vec{p}}{E}\,\widehat{\mathbf{C}}f(E,t)} \tag{C.20}$$

C.2   The Collision Term

We will now have a closer look at the right hand side of eq. C.20. It contains the collision term. Instead of deriving this term, we will motivate its dependencies. A more thorough derivation yielding the same results is also possible from the BBGKY hierarchy [51].

The collision term describes the interactions of particles that affect kinetic equilibrium. Therefore, the first step is determining which reactions actually change the phase-space distribution of the particle we are interested in. In general, the reaction is of the form:

$$a + b + ... \longleftrightarrow j + k + ... \tag{C.21}$$

Though the general case is analogous, we will assume that only two types of particles are colliding for simplicity reasons, namely a and b and turning into i and j. For Big Bang Nucleosynthesis these reactions would be the weak force reactions turning neutrons into protons. For WIMP Dark matter this would be the annihilation of particle and anti-particle to produce a pair of Standard Model particles. In the following derivation the subscript on the variables will imply that this quantity describes this particle only.

Having established this, let us now have a look at the Collision Term and what it is comprised of. We are interested in determining the density n_a for particle a. The collision term describes the likelihood of a collision yielding a specific final result.

Thus, of course, it has to be proportional to the absolute value of the transitional matrix element squared:

$$\frac{g_a}{(2\pi)^3} \int \frac{d^3\vec{p}_a}{E_a} \, \widehat{\mathbf{C}} f_a(E_a, t) \propto |M_{i\to f}|^2$$

This matrix element has to be summed over all possible combinations of the initial and final spins of the particles.

Furthermore, because particles are interacting in the Early Universe, not in a controlled system as in an experiment, energy and momentum are not fixed. Actually, depending on the temperature, these quantities follow a distribution, the phase-space distribution f that has been used up to this point. Therefore, the integrand has to be proportional to the phase-space distribution of the particles in the initial state of the reaction, which for now will be taken to be a and b:

$$\frac{g_a}{(2\pi)^3} \int \frac{d^3\vec{p}_a}{E_a} \, \widehat{\mathbf{C}} f_a(E_a, t) \propto f_a f_b (1 \pm f_j)(1 \pm f_k)|M_{i\to f}|^2$$

where the $\propto 1 \pm f_{i,j}$ accounts for the quantum effects of stimulated emission for bosons and Pauli-blocking for Fermions.

Additionally, even though energy and momentum are distributed according to f, the reactions must always obey energy and momentum conservation. This can be achieved by integrating over a delta function which enforces said law of conservation:

$$\frac{g_a}{(2\pi)^3} \int \frac{d^3\vec{p}_a}{E_a} \, \widehat{\mathbf{C}} f_a(E_a, t) \propto f_a f_b (1 \pm f_j)(1 \pm f_k)|M_{i\to f}|^2 (2\pi)^4 \delta^4(p_a + p_b - p_j - p_k)$$

All that is left now is to integrate over the lorentz-invariant phase space

$$d\Pi_s = \frac{g_s}{(2\pi)^3} \frac{d^3\vec{p}_s}{2E_s} \tag{C.22}$$

of the particles taking part in the reaction, so that the resulting collision term for the reaction $a + b \to j + k$:

$$\frac{g_a}{(2\pi)^3} \int \frac{d^3\vec{p}_a}{E_a} \, \widehat{\mathbf{C}} f_a(E_a, t) = -(2\pi)^4 \int d\Pi_a \int d\Pi_b \int d\Pi_j \int d\Pi_k$$
$$\cdot \, \delta^4(p_a + p_b - p_j - p_k)|M_{i\to f}|^2 f_a f_b (1 \pm f_j)(1 \pm f_k) \tag{C.23}$$

The minus sign indicates that this reaction diminishes the total number of particles a, as they are annihilating with b to j and k.

What we have not accounted for yet is the fact that the particles j, k can react back to a and b, thus increasing their particle density. This can easily be helped, as the only thing we need to do is add the same terms from eq. C.23, but as the particles we are starting with are j and k and the reaction goes from the final to the initial state, we have to swap the indices and modify the matrix element if CP is not conserved.

The resulting collision term which accounts for both directions of the reaction is:

$$\frac{g_a}{(2\pi)^3} \int \frac{d^3\vec{p}_a}{E_a} \, \widehat{\mathbf{C}} f_a(E_a, t) = -(2\pi)^4 \int d\Pi_a \int d\Pi_b \int d\Pi_j \int d\Pi_k \, \delta^4(p_a + p_b - p_j - p_k)$$
$$\cdot \left(f_a f_b (1 \pm f_j)(1 \pm f_k)|M_{i \to f}|^2 - f_j f_k (1 \pm f_a)(1 \pm f_b)|M_{f \to i}|^2 \right) \quad \text{(C.24)}$$

From this equation, it is apparent that the evolution of the phase space density of particle a is coupled to that of particles b, j, k. Thus, in general, the Boltzmann equation is a system of partial differential equations, one for each particle taking part in the reaction. This is the form of the Boltzmann equation from which we will derive the equation governing the nucleon freeze-out.

For the case of nuclear reactions, we will further simplify the term in eq. C.24 by making some simplifying assumptions. First, we will assume that the particles are in kinetic equilibrium. Thus, their phase-space density has equilibrium form. For massive particles, like nuclei, this is the Boltzmann distribution. In that case, $f \ll 1$, so that $1 \pm f \approx 1$.

The second assumption we make is that CP symmetry is conserved. Concretely for our process this means that the matrix element is the same regardless of the direction in which the reaction is happening, because if CP is conserved, then so is T because of the CPT theorem.

First discovered in Kaon Oscillations, it is known that CP symmetry is not conserved in the Standard model. However, the symmetry breaking phase in the CKM matrix is so small that the effect is barely noticeable and, for our considerations, CP can be assumed to be approximately conserved. Both assumptions allow us to write the collision term from eq. C.24 into the form:

$$\frac{g_a}{(2\pi)^3} \int \frac{d^3\vec{p}_a}{E_a} \, \widehat{\mathbf{C}} f_a(E_a, t) = -\int d\Pi_a \int d\Pi_b \, (f_a f_b - f_j f_k)$$
$$\cdot \int d\Pi_j \int d\Pi_k (2\pi)^4 |M_{i \to f}|^2 \delta^4(p_a + p_b - p_j - p_k) \quad \text{(C.25)}$$

We will now set the left hand side of equation C.25 equal to the time dependence of the particle density of particle a (eq. C.20). We can compare this to the general definition for the cross section given by the Lorentz-invariant version of Fermi's Golden Rule (see e.g. [118]):

$$\sigma_{a+b \to j+k} = \int d\Pi_j \int d\Pi_k (2\pi)^4 \frac{|M_{i \to f}|^2 \delta^4(p_a + p_b - p_j - p_k)}{4\sqrt{(p_a \cdot p_b)^2 - m_a^2 m_b^2}} \quad \text{(C.26)}$$

Apart from the factor $\left(4\sqrt{(p_a \cdot p_b)^2 - m_a^2 m_b^2} \right)^{-1}$, this is identical with what we find in equation C.25. If we multiply equation C.26 with the inverse of this term on both sides we can insert this directly into eq. C.25 to obtain:

$$\dot{n}_a + 3H n_a = -\int d^3\vec{p}_a \int d^3\vec{p}_b \frac{g_a g_b \sqrt{(p_a \cdot p_b)^2 - m_a^2 m_b^2}}{E_a E_b} \sigma \, (f_a f_b - f_j f_k) \quad \text{(C.27)}$$

The factor 4 cancels out with the factors $\frac{1}{2}$ of the phase-space from eq. C.22. We will now define the Møller velocity as in [120]:

$$v_{mol} = \frac{g_a g_b \sqrt{(p_a \cdot p_b)^2 - m_a^2 m_b^2}}{E_a E_b} \tag{C.28}$$

As the Møller velocity is the only velocity we will use, we will not carry the subscript all the time and just call it v. This now yields the slightly more simple formula for the collision term:

$$\dot{n}_a + 3Hn_a = -\int d^3\vec{p}_a \int d^3\vec{p}_b \, \sigma v \left(f_a f_b - f_j f_k \right) \tag{C.29}$$

The phase space distribution is normalized to yield N if integrated over the phase space. In order to interpret the phase space distributions correctly as probability density functions, it is necessary to normalize them to one. The expectation value of an operator A for a general phase space distribution f on the phase space Γ then looks as follows:

$$\langle A \rangle = \frac{\int d\Gamma A f}{\int d\Gamma f}$$

In our case, we have a phase space distribution f which is the product of f_a and f_b or f_j and f_k, which are assumed to be independent, and the combined phase space is the dot product of the phase space for particles a and b. By convention, we will use the equilibrium distribution without a chemical potential, which for a pair of nuclei yields :

$$\langle A \rangle = \frac{\int d\Gamma A e^{-\frac{E_a}{T}} e^{-\frac{E_b}{T}}}{\int d\Gamma e^{-\frac{E_a}{T}} e^{-\frac{E_b}{T}}}$$

The phase space distribution is independent of the position, so the integral over position space just yields the volume both in the numerator and the denominator. If we take A to be the cross section times the Møller velocity, its expectation value can be written as:

$$\langle \sigma v \rangle = \frac{\int d^3\vec{p}_a \int d^3\vec{p}_b \, \sigma v f_a^{eq} f_b^{eq}}{\int d^3\vec{p}_a \int d^3\vec{p}_b \, f_a^{eq} f_b^{eq}} \tag{C.30}$$

With the definition of the particle density from eq. A.3, this may be rewritten as:

$$\langle \sigma v \rangle = \frac{\int d^3\vec{p}_a \int d^3\vec{p}_b \, \sigma v f_a^{eq} f_b^{eq}}{n_a^{eq} n_b^{eq}} \tag{C.31}$$

$$\Leftrightarrow \langle \sigma v \rangle \, n_a^{eq} n_b^{eq} = \int d^3\vec{p}_a \int d^3\vec{p}_b \, \sigma v f_a^{eq} f_b^{eq} \tag{C.32}$$

Looking at the right hand side of eq. C.29 more closely, it is clear to see that the latter expression of the above equation has exactly the same form, except for the use of the equilibrium phase-space distribution instead of the normal distribution with a chemical potential. Given the simple form of the Boltzmann distribution, we can simply write:

$$e^{\frac{\mu}{T}} = \frac{n}{n^{eq}} \tag{C.33}$$

so that eq. C.29 may be written as:

$$\dot{n}_a + 3H(t)n_a = -\langle\sigma v\rangle\left(n_a n_b - \frac{n_a^{eq}n_b^{eq}}{n_j^{eq}n_k^{eq}}n_j n_k\right) \tag{C.34}$$

This is the form of the Boltzmann equation we will use for the nuclear reaction rates. This form, although in order to solve it numerically we will modify it a little bit, is very useful to understand the underlying physics and to reason why the equation should look like this.

C.3 Physical Interpretation
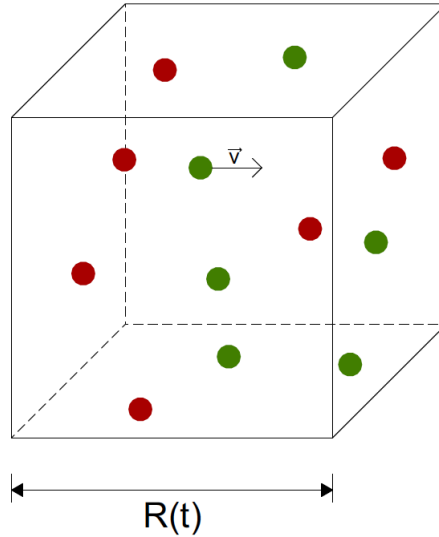
Figure C.1: Particle interactions in a co-moving volume in the early Universe modelled as particles interacting inside an expanding cube of side length $a(t)$

With that in mind, let us look at the evolution of a set of particles in a co-moving volume. That is, let us make a model of our Universe, as in figure C.1, by assuming a cube with time-dependant side length $a(t)$, which corresponds to the scale parameter, in which we have a gas of different particles at temperature T. At first, we will not allow them to interact with each other. Thus, the total number of particles remains constant. The number of particles of type a in the cube is given by

$$N_a(t) = n_a \cdot a(t)^3 \tag{C.35}$$

Therefore:

$$\frac{\mathrm{d}N_a}{\mathrm{d}t} = a(t)^3\dot{n}_a + 3a(t)^2\dot{a}(t)n_a = a(t)^3\left(\dot{n}_a + 3H(t)n_a\right) = 0 \tag{C.36}$$

However, if we allow the particles to interact with each other, they will be destroyed or created the same way they do in the Early Universe. Therefore, the

change in time of the particle number will be determined by the rate at which particles get created or destroyed. The time dependence will be equal to the difference in the reaction rate Γ. This also explains why, in equilibrium, the particle density remains constant.

$$\frac{\mathrm{d}N_a}{\mathrm{d}t} = \Gamma_{\text{prod.}} - \Gamma_{\text{destr.}} \tag{C.37}$$

Now, in our cube Universe, we will have the same reactions as in eq. C.21. We will assume that particles a and b are moving about with a certain velocity v and colliding head on with each other, the same for particles j and k.

The reaction rate is given by the amount of collisions which result in the desired end-products. This is where the cross-section becomes important, as it describes the effective surface upon which every reaction yields the desired end products. It is a measure of how effective the collisions are in producing the particles we want. Thus, the rate is proportional to the quotient between the total surface $a(t)^2$ and the effective surface of scattering.

$$\Gamma \propto \frac{\sigma}{a(t)^2} \tag{C.38}$$

The amount of collisions is, of course, proportional to the number of particles in the cube of both types. The more particle in a co-moving volume, the more likely a reaction.

$$\Gamma \propto N_a N_b \tag{C.39}$$

All that is left now is to divide the number of reactions by the time Δt it takes for one interaction to happen. Assuming they are colliding head on, the maximal time for a collision to happen is the time it takes one particle to travel from one end of the cube to the other.

$$\Delta t = \frac{a(t)}{v} \tag{C.40}$$

Piecing all the pieces of the puzzle together we obtain the reaction rate:

$$\Gamma = N_a N_b \cdot \frac{\sigma}{a(t)^2} \cdot \frac{1}{\Delta t} = \frac{n_a a(t)^3 n_b a(t)^3 \sigma v}{a(t)^3} = a(t)^3 \sigma v n_a n_b \tag{C.41}$$

The production rate is proportional to the density of j and k, while the annihilation rate is proportional to the density of a and b. Additionally, we will assume that the chemical potential of the particles is negligible, such that there is no preferred direction of the reaction and $\langle \sigma_{tot} v \rangle$ is the same in both directions. [1] Inserting this result for the reaction rates and C.36 into equation C.37 yields

$$a(t)^3 \left(\dot{n}_a + 3H(t)n_a \right) = a(t)^3 \sigma v \left(n_j n_k - n_a n_b \right) \tag{C.42}$$

Or the more familiar form:

$$\dot{n}_a + 3H(t)n_a = -\sigma v \left(n_a n_b - n_j n_k \right) \tag{C.43}$$

---

[1]This amounts to setting $\frac{n_a^{eq} n_b^{eq}}{n_j^{eq} n_k^{eq}} = 1$

which is identical to C.34, albeit the thermal averaging of the cross section times velocity.

Thus, the Boltzmann equation in the form C.34 has the features we would have expected from it. It describes the time dependence of the number of particles in the universe and states that it is equal to the difference in the production and destruction rate.

Bibliography

[1] Thomas S. Kuhn. *The Structure of Scientific Revolutions*. Chicago: University of Chicago Press, 1962.

[2] Jens Erler and Matthias Schott. "Electroweak Precision Tests of the Standard Model after the Discovery of the Higgs Boson". In: *Prog. Part. Nucl. Phys.* 106 (2019), pp. 68–119. DOI: 10.1016/j.ppnp.2019.02.007. arXiv: 1902.05142 [hep-ph].

[3] Georges Aad et al. "Observation of a new particle in the search for the Standard Model Higgs boson with the ATLAS detector at the LHC". In: *Phys. Lett. B* 716 (2012), pp. 1–29. DOI: 10.1016/j.physletb.2012.08.020. arXiv: 1207.7214 [hep-ex].

[4] N. Aghanim et al. "Planck 2018 results. I. Overview and the cosmological legacy of Planck". In: *Astron. Astrophys.* 641 (2020), A1. DOI: 10.1051/0004-6361/201833880. arXiv: 1807.06205 [astro-ph.CO].

[5] Alessandra D'Alise et al. "Standard model anomalies: lepton flavour non-universality, g − 2 and W-mass". In: *JHEP* 08 (2022), p. 125. DOI: 10.1007/JHEP08(2022)125. arXiv: 2204.03686 [hep-ph].

[6] Nathaniel Craig. "Naturalness: A Snowmass White Paper". In: *Snowmass 2021*. May 2022. arXiv: 2205.05708 [hep-ph].

[7] Eleonora Di Valentino et al. "In the realm of the Hubble tension—a review of solutions". In: *Class. Quant. Grav.* 38.15 (2021), p. 153001. DOI: 10.1088/1361-6382/ac086d. arXiv: 2103.01183 [astro-ph.CO].

[8] Catherine Heymans et al. "KiDS-1000 Cosmology: Multi-probe weak gravitational lensing and spectroscopic galaxy clustering constraints". In: *Astron. Astrophys.* 646 (2021), A140. DOI: 10.1051/0004-6361/202039063. arXiv: 2007.15632 [astro-ph.CO].

[9] Brian D. Fields. "The Primordial Lithium Problem". In: *Annual Review of Nuclear and Particle Science* 61.1 (Nov. 2011), pp. 47–68. DOI: 10.1146/annurev-nucl-102010-130445. arXiv: 1203.3551 [astro-ph.CO].

[10] Akinori Matsumoto et al. "EMPRESS. VIII. A New Determination of Primordial He Abundance with Extremely Metal-poor Galaxies: A Suggestion of the Lepton Asymmetry and Implications for the Hubble Tension". In: *Astrophys. J.* 941.2 (2022), p. 167. DOI: 10.3847/1538-4357/ac9ea1. arXiv: 2203.09617 [astro-ph.CO].

[11] R. L. Workman et al. "Review of Particle Physics". In: *PTEP* 2022 (2022), p. 083C01. DOI: 10.1093/ptep/ptac097.

[12] Bartosz Fornal and Benjamín Grinstein. "Dark Matter Interpretation of the Neutron Decay Anomaly". In: *Phys. Rev. Lett.* 120 (19 May 2018), p. 191801. DOI: 10.1103/PhysRevLett.120.191801. URL: https://link.aps.org/doi/10.1103/PhysRevLett.120.191801.

[13] Fabio Iocco et al. "Primordial Nucleosynthesis: from precision cosmology to fundamental physics". In: *Phys. Rept.* 472 (2009), pp. 1–76. DOI: 10.1016/j.physrep.2009.02.002. arXiv: 0809.0631 [astro-ph].

[14] Erik Aver et al. "Improving helium abundance determinations with Leo P as a case study". In: *JCAP* 03 (2021), p. 027. DOI: 10.1088/1475-7516/2021/03/027. arXiv: 2010.04180 [astro-ph.CO].

[15] Vital Fernández et al. "A Bayesian direct method implementation to fit emission line spectra: Application to the primordial He abundance determination". In: *Mon. Not. Roy. Astron. Soc.* 487.3 (2019), pp. 3221–3238. DOI: 10.1093/mnras/stz1433. arXiv: 1905.09215 [astro-ph.GA].

[16] Tiffany Hsyu et al. "The PHLEK Survey: A New Determination of the Primordial Helium Abundance". In: *Astrophys. J.* 896.1, 77 (June 2020), p. 77. DOI: 10.3847/1538-4357/ab91af. arXiv: 2005.12290 [astro-ph.GA].

[17] Mabel Valerdi, Antonio Peimbert, and Manuel Peimbert. "Chemical abundances in seven metal-poor H II regions and a determination of the primordial helium abundance". In: *Mon. Not. Roy. Astron. Soc.* 505.3 (Aug. 2021), pp. 3624–3634. DOI: 10.1093/mnras/stab1543. arXiv: 2105.12260 [astro-ph.GA].

[18] O. A. Kurichin et al. "A new determination of the primordial helium abundance using the analyses of H II region spectra from SDSS". In: *Mon. Not. Roy. Astron. Soc.* 502.2 (2021), pp. 3045–3056. DOI: 10.1093/mnras/stab215. arXiv: 2101.09127 [astro-ph.CO].

[19] Y. I. Izotov, T. X. Thuan, and N. G. Guseva. "A new determination of the primordial He abundance using the He i $\lambda 10830$ Å emission line: cosmological implications". In: *Mon. Not. Roy. Astron. Soc.* 445.1 (2014), pp. 778–793. DOI: 10.1093/mnras/stu1771. arXiv: 1408.6953 [astro-ph.CO].

[20] Cyril Pitrou et al. "Precision big bang nucleosynthesis with improved Helium-4 predictions". In: *Phys. Rept.* 754 (2018), pp. 1–66. DOI: 10.1016/j.physrep.2018.04.005. arXiv: 1801.08023 [astro-ph.CO].

[21] Ryan Cooke and Michele Fumagalli. "Measurement of the primordial helium abundance from the intergalactic medium". In: *Nature Astron.* 2.12 (2018), pp. 957–961. DOI: 10.1038/s41550-018-0584-z. arXiv: 1810.06561 [astro-ph.CO].

[22] https://pla.esac.esa.int/.

[23] Nashwan Sabti. "New Physics Through the Eyes of Big-Bang Nucleosynthesis". PhD thesis. King's Coll. London, 2022.

[24] Miguel Escudero, Alejandro Ibarra, and Victor Maura. "Primordial lepton asymmetries in the precision cosmology era: Current status and future sensitivities from BBN and the CMB". In: *Phys. Rev. D* 107.3 (2023), p. 035024. DOI: 10.1103/PhysRevD.107.035024. arXiv: 2208.03201 [hep-ph].

[25]   Ryan Cooke et al. "Precision measures of the primordial abundance of deuterium". In: *Astrophys. J.* 781.1 (2014), p. 31. DOI: `10.1088/0004-637X/781/1/31`. arXiv: `1308.3240 [astro-ph.CO]`.

[26]   Ryan J. Cooke, Max Pettini, and Charles C. Steidel. "One Percent Determination of the Primordial Deuterium Abundance". In: *Astrophys. J.* 855.2 (2018), p. 102. DOI: `10.3847/1538-4357/aaab53`. arXiv: `1710.11129 [astro-ph.CO]`.

[27]   F. Spite and M. Spite. "Abundance of lithium in unevolved halo stars and old disk stars: Interpretation and consequences". In: *Astron. Astrophys.* 115 (1982), pp. 357–366.

[28]   R. L. Workman et al. "Review of Particle Physics". In: *PTEP* 2022 (2022), p. 083C01. DOI: `10.1093/ptep/ptac097`.

[29]   Ofelia Pisanti et al. "Primordial Deuterium after LUNA: concordances and error budget". In: *JCAP* 04 (2021), p. 020. DOI: `10.1088/1475-7516/2021/04/020`. arXiv: `2011.11537 [astro-ph.CO]`.

[30]   Cyril Pitrou et al. "A new tension in the cosmological model from primordial deuterium?" In: *Mon. Not. Roy. Astron. Soc.* 502.2 (2021), pp. 2474–2481. DOI: `10.1093/mnras/stab135`. arXiv: `2011.11320 [astro-ph.CO]`.

[31]   R. A. Alpher, H. Bethe, and G. Gamow. "The origin of chemical elements". In: *Phys. Rev.* 73 (1948), pp. 803–804. DOI: `10.1103/PhysRev.73.803`.

[32]   Phillip James Edwin Peebles. "Discovery of the Hot Big Bang: What happened in 1948". In: *Eur. Phys. J. H* 39 (2014), pp. 205–223. DOI: `10.1140/epjh/e2014-50002-y`. arXiv: `1310.2146 [physics.hist-ph]`.

[33]   G. Gamow. "Expanding universe and the origin of elements". In: *Phys. Rev.* 70 (1946), pp. 572–573. DOI: `10.1103/PhysRev.70.572.2`.

[34]   Ralph A. Alpher and Robert C. Herman. "On the Relative Abundance of the Elements". In: *Phys. Rev.* 74 (12 Dec. 1948), pp. 1737–1742. DOI: `10.1103/PhysRev.74.1737`. URL: `https://link.aps.org/doi/10.1103/PhysRev.74.1737`.

[35]   G. Gamow. "The Evolution of the Universe". In: *Nature* 162.4122 (1948), pp. 680–682. DOI: `10.1038/162680a0`.

[36]   Arno A. Penzias and Robert Woodrow Wilson. "A Measurement of excess antenna temperature at 4080-Mc/s". In: *Astrophys. J.* 142 (1965), pp. 419–421. DOI: `10.1086/148307`.

[37]   C. Hayashi. "Proton-Neutron Concentration Ratio in the Expanding Universe at the Stages preceding the Formation of the Elements". In: *Prog. Theor. Phys.* 5.2 (1950), pp. 224–235. DOI: `10.1143/ptp/5.2.224`.

[38]   Ralph A. Alpher and Robert Herman. "Evolution of the Universe". In: *Nature* 162.4124 (1948), pp. 774–775. DOI: `10.1038/162774b0`.

[39]   Ralph A. Alpher, James W. Follin, and Robert C. Herman. "Physical Conditions in the Initial Stages of the Expanding Universe". In: *Phys. Rev.* 92 (6 Dec. 1953), pp. 1347–1361. DOI: `10.1103/PhysRev.92.1347`. URL: `https://link.aps.org/doi/10.1103/PhysRev.92.1347`.

[40] Robert V. Wagoner, William A. Fowler, and Fred Hoyle. "On the Synthesis of elements at very high temperatures". In: *Astrophys. J.* 148 (1967), pp. 3–49. DOI: 10.1086/149126.

[41] E. Grohs et al. "Neutrino energy transport in weak decoupling and big bang nucleosynthesis". In: *Physical Review D* 93.8 (Apr. 2016). DOI: 10.1103/physrevd.93.083522. URL: https://doi.org/10.1103%2Fphysrevd.93.083522.

[42] O. Pisanti et al. "PArthENoPE: Public Algorithm Evaluating the Nucleosynthesis of Primordial Elements". In: *Comput. Phys. Commun.* 178 (2008), pp. 956–971. DOI: 10.1016/j.cpc.2008.02.015. arXiv: 0705.0290 [astro-ph].

[43] R. Consiglio et al. "PArthENoPE reloaded". In: *Comput. Phys. Commun.* 233 (2018), pp. 237–242. DOI: 10.1016/j.cpc.2018.06.022. arXiv: 1712.04378 [astro-ph.CO].

[44] S. Gariazzo et al. "PArthENoPE revolutions". In: *Comput. Phys. Commun.* 271 (2022), p. 108205. DOI: 10.1016/j.cpc.2021.108205. arXiv: 2103.05027 [astro-ph.IM].

[45] Brian D. Fields et al. "Big-Bang Nucleosynthesis after Planck". In: *JCAP* 03 (2020). [Erratum: JCAP 11, E02 (2020)], p. 010. DOI: 10.1088/1475-7516/2020/03/010. arXiv: 1912.01132 [astro-ph.CO].

[46] Mattia Cielo et al. "Neff in the Standard Model at NLO is 3.043". In: (June 2023). arXiv: 2306.05460 [hep-ph].

[47] Brian D. Fields, Scott Dodelson, and Michael S. Turner. "Effect of neutrino heating on primordial nucleosynthesis". In: *Phys. Rev. D* 47 (10 May 1993), pp. 4309–4314. DOI: 10.1103/PhysRevD.47.4309. URL: https://link.aps.org/doi/10.1103/PhysRevD.47.4309.

[48] Christian Fidler and Cyril Pitrou. "Kinetic theory of fermions in curved spacetime". In: *Journal of Cosmology and Astroparticle Physics* 2017.06 (June 2017), pp. 013–013. DOI: 10.1088/1475-7516/2017/06/013. URL: https://doi.org/10.1088%2F1475-7516%2F2017%2F06%2F013.

[49] Robert E. Lopez, Michael S. Turner, and Geza Gyuk. "Effect of finite nucleon mass on primordial nucleosynthesis". In: *Phys. Rev. D* 56 (6 Sept. 1997), pp. 3191–3197. DOI: 10.1103/PhysRevD.56.3191. URL: https://link.aps.org/doi/10.1103/PhysRevD.56.3191.

[50] Tammi Chowdhury and Seyda Ipek. "Neutron Lifetime Anomaly and Big Bang Nucleosynthesis". In: (Oct. 2022). arXiv: 2210.12031 [hep-ph].

[51] David Tong. *Lectures on Kinetic Theory.* 2012. URL: https://www.damtp.cam.ac.uk/user/tong/kintheory/kintheory.pdf.

[52] Cyril Pitrou et al. "Resolving conclusions about the early Universe requires accurate nuclear measurements". In: *Nature Rev. Phys.* 3.4 (2021), pp. 231–232. DOI: 10.1038/s42254-021-00294-6. arXiv: 2104.11148 [astro-ph.CO].

[53] Tsung-Han Yeh et al. "Probing physics beyond the standard model: limits from BBN and the CMB independently and combined". In: *JCAP* 10 (2022), p. 046. DOI: 10.1088/1475-7516/2022/10/046. arXiv: 2207.13133 [astro-ph.CO].

[54] A. Tumino et al. "NEW DETERMINATION OF THE 2H(d,p)3H AND 2H(d,n)3He REACTION RATES AT ASTROPHYSICAL ENERGIES". In: *The Astrophysical Journal* 785.2 (Apr. 2014), p. 96. DOI: 10.1088/0004-637X/785/2/96. URL: https://dx.doi.org/10.1088/0004-637X/785/2/96.

[55] V. Mossa et al. "The baryon density of the Universe from an improved rate of deuterium burning". In: *Nature* 587.7833 (2020), pp. 210–213. DOI: 10.1038/s41586-020-2878-4.

[56] N. Aghanim et al. "Planck 2018 results. VI. Cosmological parameters". In: (July 2018). arXiv: 1807.06209 [astro-ph.CO].

[57] Tsung-Han Yeh, Keith A. Olive, and Brian D. Fields. "The Neutron Mean Life and Big Bang Nucleosynthesis". In: *Universe* 9.4 (2023), p. 183. DOI: 10.3390/universe9040183. arXiv: 2303.04140 [astro-ph.CO].

[58] Andrzej Czarnecki, William J. Marciano, and Alberto Sirlin. "Neutron Lifetime and Axial Coupling Connection". In: *Phys. Rev. Lett.* 120.20 (2018), p. 202002. DOI: 10.1103/PhysRevLett.120.202002. arXiv: 1802.01804 [hep-ph].

[59] Jack T. Wilson et al. "Space-based measurement of the neutron lifetime using data from the neutron spectrometer on NASA's MESSENGER mission". In: *Phys. Rev. Res.* 2 (2 June 2020), p. 023316. DOI: 10.1103/PhysRevResearch.2.023316. URL: https://link.aps.org/doi/10.1103/PhysRevResearch.2.023316.

[60] Jack T. Wilson et al. "Measurement of the free neutron lifetime using the neutron spectrometer on NASA's Lunar Prospector mission". In: *Phys. Rev. C* 104 (4 Oct. 2021), p. 045501. DOI: 10.1103/PhysRevC.104.045501. URL: https://link.aps.org/doi/10.1103/PhysRevC.104.045501.

[61] P. F. de Salas et al. "Bounds on very low reheating scenarios after Planck". In: *Phys. Rev. D* 92.12 (2015), p. 123534. DOI: 10.1103/PhysRevD.92.123534. arXiv: 1511.00672 [astro-ph.CO].

[62] Takuya Hasegawa et al. "MeV-scale reheating temperature and thermalization of oscillating neutrinos by radiative and hadronic decays of massive particles". In: *JCAP* 12 (2019), p. 012. DOI: 10.1088/1475-7516/2019/12/012. arXiv: 1908.10189 [hep-ph].

[63] Nashwan Sabti et al. "Refined Bounds on MeV-scale Thermal Dark Sectors from BBN and the CMB". In: *JCAP* 01 (2020), p. 004. DOI: 10.1088/1475-7516/2020/01/004. arXiv: 1910.01649 [hep-ph].

[64] Kenneth M. Nollett and Gary Steigman. "BBN And The CMB Constrain Light, Electromagnetically Coupled WIMPs". In: *Phys. Rev. D* 89.8 (2014), p. 083508. DOI: 10.1103/PhysRevD.89.083508. arXiv: 1312.5725 [astro-ph.CO].

[65] P. A. M. Dirac. "The Cosmological Constants". In: *Nature* 139.3512 (Feb. 1937), p. 323. DOI: 10.1038/139323a0.

[66] Peter Jordan. "Die physikalischen Weltkonstanten". In: *Naturwissenschaften* 25 (1937), pp. 513–517. URL: https://api.semanticscholar.org/CorpusID:33800056.

[67] C. Brans and R. H. Dicke. "Mach's Principle and a Relativistic Theory of Gravitation". In: *Phys. Rev.* 124 (3 Nov. 1961), pp. 925–935. DOI: 10.1103/PhysRev.124.925. URL: https://link.aps.org/doi/10.1103/PhysRev.124.925.

[68] Jean-Philippe Uzan. "Varying Constants, Gravitation and Cosmology". In: *Living Rev. Rel.* 14 (2011), p. 2. DOI: 10.12942/lrr-2011-2. arXiv: 1009.5514 [astro-ph.CO].

[69] James Alvey et al. "Improved BBN Constraints on the Variation of the Gravitational Constant". In: *Eur. Phys. J. C* 80.2 (2020), p. 148. DOI: 10.1140/epjc/s10052-020-7727-y. arXiv: 1910.10730 [astro-ph.CO].

[70] Yang Bai, Jordi Salvado, and Ben A. Stefanek. "Cosmological Constraints on the Gravitational Interactions of Matter and Dark Matter". In: *JCAP* 10 (2015), p. 029. DOI: 10.1088/1475-7516/2015/10/029. arXiv: 1505.04789 [hep-ph].

[71] F. Hofmann and J. Müller. "Relativistic tests with lunar laser ranging". In: *Classical and Quantum Gravity* 35.3, 035015 (Feb. 2018), p. 035015. DOI: 10.1088/1361-6382/aa8f7a.

[72] Laurent Pourcelot. "Les reacteurs de fission naturels du gabon. Contribution a l'etude des conditions de stabilite d'un site naturel de stockage de dechets radioactifs (2 ga)". 1997STR13007. PhD thesis. 1997, 223 P. URL: http://www.theses.fr/1997STR13007.

[73] Alain Coc et al. "The variation of fundamental constants and the role of A=5 and A=8 nuclei on primordial nucleosynthesis". In: *Phys. Rev. D* 86 (2012), p. 043529. DOI: 10.1103/PhysRevD.86.043529. arXiv: 1206.1139 [astro-ph.CO].

[74] Jaiyul Yoo and Robert J. Scherrer. "Big bang nucleosynthesis and cosmic microwave background constraints on the time variation of the Higgs vacuum expectation value". In: *Phys. Rev. D* 67 (2003), p. 043517. DOI: 10.1103/PhysRevD.67.043517. arXiv: astro-ph/0211545.

[75] Kazuhide Ichikawa and M. Kawasaki. "Constraining the variation of the coupling constants with big bang nucleosynthesis". In: *Physical Review D* 65.12 (June 2002). DOI: 10.1103/physrevd.65.123511. URL: https://doi.org/10.1103%2Fphysrevd.65.123511.

[76] V. V. Dixit and Marc Sher. "Variation of the Fermi constant and primordial nucleosynthesis". In: *Phys. Rev. D* 37 (4 Feb. 1988), pp. 1097–1098. DOI: 10.1103/PhysRevD.37.1097. URL: https://link.aps.org/doi/10.1103/PhysRevD.37.1097.

[77] Robert J. Scherrer and David N. Spergel. "How constant is the Fermi coupling constant?" In: *Phys. Rev. D* 47 (10 May 1993), pp. 4774–4777. DOI: 10. 1103/PhysRevD.47.4774. URL: https://link.aps.org/doi/10.1103/PhysRevD.47.4774.

[78] Luke Hart and Jens Chluba. "New constraints on time-dependent variations of fundamental constants using Planck data". In: *Mon. Not. Roy. Astron. Soc.* 474.2 (2018), pp. 1850–1861. DOI: 10.1093/mnras/stx2783. arXiv: 1705.03925 [astro-ph.CO].

[79] Bartosz Fornal. "Neutron Dark Decay". In: (June 2023). arXiv: 2306.11349 [hep-ph].

[80] David McKeen, Maxim Pospelov, and Nirmal Raj. "Cosmological and astrophysical probes of dark baryons". In: *Phys. Rev. D* 103.11 (2021), p. 115002. DOI: 10.1103/PhysRevD.103.115002. arXiv: 2012.09865 [hep-ph].

[81] Valery A. Rubakov and Dmitry S. Gorbunov. *Introduction to the Theory of the Early Universe: Hot big bang theory*. Singapore: World Scientific, 2017. ISBN: 978-981-320-987-9, 978-981-320-988-6, 978-981-322-005-8. DOI: 10.1142/10447.

[82] N. Aghanim et al. "Planck 2018 results. VI. Cosmological parameters". In: *Astron. Astrophys.* 641 (2020), A6. DOI: 10.1051/0004-6361/201833910. arXiv: 1807.06209 [astro-ph.CO].

[83] Michela D'Onofrio, Kari Rummukainen, and Anders Tranberg. "Sphaleron Rate in the Minimal Standard Model". In: *Phys. Rev. Lett.* 113.14 (2014), p. 141602. DOI: 10.1103/PhysRevLett.113.141602. arXiv: 1404.3565 [hep-ph].

[84] V. A. Kuzmin, V. A. Rubakov, and M. E. Shaposhnikov. "On the Anomalous Electroweak Baryon Number Nonconservation in the Early Universe". In: *Phys. Lett. B* 155 (1985), p. 36. DOI: 10.1016/0370-2693(85)91028-7.

[85] S. Yu. Khlebnikov and M. E. Shaposhnikov. "The Statistical Theory of Anomalous Fermion Number Nonconservation". In: *Nucl. Phys. B* 308 (1988), pp. 885–912. DOI: 10.1016/0550-3213(88)90133-2.

[86] Jeffrey A. Harvey and Michael S. Turner. "Cosmological baryon and lepton number in the presence of electroweak fermion number violation". In: *Phys. Rev. D* 42 (1990), pp. 3344–3349. DOI: 10.1103/PhysRevD.42.3344.

[87] Herbert K. Dreiner and Graham G. Ross. "Sphaleron erasure of primordial baryogenesis". In: *Nucl. Phys. B* 410 (1993), pp. 188–216. DOI: 10.1016/0550-3213(93)90579-E. arXiv: hep-ph/9207221.

[88] Alberto Casas, Wai Yan Cheng, and Graciela Gelmini. "Generation of large lepton asymmetries". In: *Nucl. Phys. B* 538 (1999), pp. 297–308. DOI: 10.1016/S0550-3213(98)00606-3. arXiv: hep-ph/9709289.

[89] A. D. Dolgov and D. P. Kirilova. "ON PARTICLE CREATION BY A TIME DEPENDENT SCALAR FIELD". In: *Sov. J. Nucl. Phys.* 51 (1990), pp. 172–177.

[90] Borut Bajc, Antonio Riotto, and Goran Senjanovic. "Large lepton number of the universe and the fate of topological defects". In: *Phys. Rev. Lett.* 81 (1998), pp. 1355–1358. DOI: 10.1103/PhysRevLett.81.1355. arXiv: hep-ph/9710415.

[91] Takehiko Asaka and Mikhail Shaposhnikov. "The νMSM, dark matter and baryon asymmetry of the universe". In: *Phys. Lett. B* 620 (2005), pp. 17–26. DOI: 10.1016/j.physletb.2005.06.020. arXiv: hep-ph/0505013.

[92] Takehiko Asaka, Steve Blanchet, and Mikhail Shaposhnikov. "The nuMSM, dark matter and neutrino masses". In: *Phys. Lett. B* 631 (2005), pp. 151–156. DOI: 10.1016/j.physletb.2005.09.070. arXiv: hep-ph/0503065.

[93] Apostolos Pilaftsis and Thomas E. J. Underwood. "Resonant leptogenesis". In: *Nucl. Phys. B* 692 (2004), pp. 303–345. DOI: 10.1016/j.nuclphysb.2004.05.029. arXiv: hep-ph/0309342.

[94] Debasish Borah and Arnab Dasgupta. "Large Neutrino Asymmetry from TeV Scale Leptogenesis in the Light of Helium Anomaly". In: (June 2022). arXiv: 2206.14722 [hep-ph].

[95] M. Kawasaki, Fuminobu Takahashi, and Masahide Yamaguchi. "Large lepton asymmetry from Q balls". In: *Phys. Rev. D* 66 (2002), p. 043516. DOI: 10.1103/PhysRevD.66.043516. arXiv: hep-ph/0205101.

[96] Masahiro Kawasaki and Kai Murai. "Lepton asymmetric universe". In: *JCAP* 08.08 (2022), p. 041. DOI: 10.1088/1475-7516/2022/08/041. arXiv: 2203.09713 [hep-ph].

[97] John March-Russell, Hitoshi Murayama, and Antonio Riotto. "The Small observed baryon asymmetry from a large lepton asymmetry". In: *JHEP* 11 (1999), p. 015. DOI: 10.1088/1126-6708/1999/11/015. arXiv: hep-ph/9908396.

[98] Kyohei Mukaida, Kai Schmitz, and Masaki Yamada. "Baryon Asymmetry of the Universe from Lepton Flavor Violation". In: *Phys. Rev. Lett.* 129.1 (2022), p. 011803. DOI: 10.1103/PhysRevLett.129.011803. arXiv: 2111.03082 [hep-ph].

[99] Valerie Domcke et al. "A new constraint on primordial lepton flavour asymmetries". In: (Aug. 2022). arXiv: 2208.03237 [hep-ph].

[100] Miguel Escudero Abenza. "Precision early universe thermodynamics made simple: $N_{\rm eff}$ and neutrino decoupling in the Standard Model and beyond". In: *JCAP* 05 (2020), p. 048. DOI: 10.1088/1475-7516/2020/05/048. arXiv: 2001.04466 [hep-ph].

[101] Subir Sarkar. "Big bang nucleosynthesis and physics beyond the standard model". In: *Rept. Prog. Phys.* 59 (1996), pp. 1493–1610. DOI: 10.1088/0034-4885/59/12/001. arXiv: hep-ph/9602260.

[102] Julien Lesgourgues et al. *Neutrino Cosmology*. Cambridge University Press, Feb. 2013. ISBN: 978-1-108-70501-1, 978-1-139-60341-6.

[103] A. D. Dolgov et al. "Cosmological bounds on neutrino degeneracy improved by flavor oscillations". In: *Nucl. Phys. B* 632 (2002), pp. 363–382. DOI: 10.1016/S0550-3213(02)00274-2. arXiv: hep-ph/0201287.

[104] Yvonne Y. Y. Wong. "Analytical treatment of neutrino asymmetry equilibration from flavor oscillations in the early universe". In: *Phys. Rev. D* 66 (2002), p. 025015. DOI: 10.1103/PhysRevD.66.025015. arXiv: hep-ph/0203180.

[105] Kevork N. Abazajian, John F. Beacom, and Nicole F. Bell. "Stringent Constraints on Cosmological Neutrino Antineutrino Asymmetries from Synchronized Flavor Transformation". In: *Phys. Rev. D* 66 (2002), p. 013008. DOI: 10.1103/PhysRevD.66.013008. arXiv: astro-ph/0203442.

[106] Julien Froustey and Cyril Pitrou. "Primordial neutrino asymmetry evolution with full mean-field effects and collisions". In: *JCAP* 03.03 (2022), p. 065. DOI: 10.1088/1475-7516/2022/03/065. arXiv: 2110.11889 [hep-ph].

[107] Kazuhide Ichikawa, Masahiro Kawasaki, and Fuminobu Takahashi. "The Oscillation effects on thermalization of the neutrinos in the Universe with low reheating temperature". In: *Phys. Rev. D* 72 (2005), p. 043522. DOI: 10.1103/PhysRevD.72.043522. arXiv: astro-ph/0505395.

[108] Edward W. Kolb, Michael S. Turner, and Terrence P. Walker. "The Effect of Interacting Particles on Primordial Nucleosynthesis". In: *Phys. Rev. D* 34 (1986), p. 2197. DOI: 10.1103/PhysRevD.34.2197.

[109] Peter Ade et al. "The Simons Observatory: Science goals and forecasts". In: *JCAP* 02 (2019), p. 056. DOI: 10.1088/1475-7516/2019/02/056. arXiv: 1808.07445 [astro-ph.CO].

[110] Kevork N. Abazajian et al. "CMB-S4 Science Book, First Edition". In: (Oct. 2016). arXiv: 1610.02743 [astro-ph.CO].

[111] Kevork Abazajian et al. "CMB-S4 Science Case, Reference Design, and Project Plan". In: (July 2019). arXiv: 1907.04473 [astro-ph.IM].

[112] Evan B. Grohs et al. "Big Bang Nucleosynthesis and Neutrino Cosmology". In: (Apr. 2019). arXiv: 1903.09187 [astro-ph.CO].

[113] Anne-Katherine Burns, Tim M. P. Tait, and Mauro Valli. "Indications for a Nonzero Lepton Asymmetry in the Early Universe". In: (June 2022). arXiv: 2206.00693 [hep-ph].

[114] Milton Abramowitz and Irene A. Stegun. *Handbook of Mathematical Functions with Formulas, Graphs, and Mathematical Tables*. Dover, 1964.

[115] David Tong. *Lectures on Statistical Physics*. 2012. URL: http://www.damtp.cam.ac.uk/user/tong/statphys.html.

[116] Lars Husdal. "On Effective Degrees of Freedom in the Early Universe". In: *Galaxies* 4.4 (2016), p. 78. DOI: 10.3390/galaxies4040078. arXiv: 1609.04979 [astro-ph.CO].

[117] E. Komatsu et al. "Seven-Year Wilkinson Microwave Anisotropy Probe (WMAP) Observations: Cosmological Interpretation". In: *Astrophys. J. Suppl.* 192 (2011), p. 18. DOI: 10.1088/0067-0049/192/2/18. arXiv: 1001.4538 [astro-ph.CO].

[118] Lars Bergström and Ariel Goobar. *Cosmology and Particle Astrophysics*. Wiley, 2007.

[119] Edward W. Kolb and Michael S. Turner. *The Early Universe*. Addison-Wesley Publishing Company, 2004.

[120]   Mariangela Lisanti. "Lectures on Dark Matter Physics". In: *Theoretical Advanced Study Institute in Elementary Particle Physics: New Frontiers in Fields and Strings*. 2017, pp. 399–446. DOI: 10.1142/9789813149441_0007. arXiv: 1603.03797 [hep-ph].